

Development of Passive LTCC Components with Improved Characteristics for Microwave Front-End Applications

DISSERTATION

durchgeführt von Dipl.-Ing. Roman KRAVCHENKO

zur Erlangung des akademischen Grades eines
Doktors der technischen Wissenschaften

Doktoratsstudium der Technischen Wissenschaften
im Rahmen der Doktoratsschule
"Elektrotechnik"



Technische Universität Graz

in Zusammenarbeit mit



TDK-EPC

EPCOS OHG (Group Company of TDK-EPC) Deutschlandsberg

Betreuer / Begutachter:

Ao.Univ.-Prof. Dr. Erich LEITGEB, Institut für Breitbandkommunikation

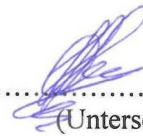
Ao.Univ.-Prof. Dr. Klaus REICHMANN, Institut für Chemische Technologie von Materialien

Graz, im April 2011

EIDESSTATTLICHE ERKLÄRUNG

Ich erkläre an Eides statt, dass ich die vorliegende Arbeit selbstständig verfasst, andere als die angegebenen Quellen/Hilfsmittel nicht benutzt und die den benutzten Quellen wörtlich und inhaltlich entnommenen Stellen als solche kenntlich gemacht habe.

Graz, am 24.03.11



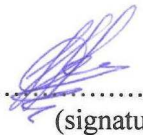
.....
(Unterschrift)

Englische Fassung:

STATUTORY DECLARATION

I declare that I have authored this thesis independently, that I have not used other than the declared sources / resources and that I have explicitly marked all material which has been quoted either literally or by content from the used sources.

24.03.11
.....
date



.....
(signature)

Abstract

Nowadays communication technique is supporting different standards and provides a wide spectrum of service. A common multi-frequency transceiver incorporates front-end part, which main function is to separate / combine frequency channels. This work focuses on development of the improved key passive components included in the front-end part. These components are filters and dividers (frequency and power).

LTCC technology has been chosen for production of the components providing size miniaturization that is very important for hand-held devices especially. New solutions allowing the further size minimization were proposed. The idea is to minimize a number of elements in the structure providing the best achievable performance.

First of all, a new transversal / recursive passive filter with bandpass characteristics is presented. The lumped elements structure represents an equivalent circuit of a ring resonator with perturbations. Due to optimizing, the simple and easy tuned filter was designed.

A new power divider realized with coupled transmission line (CTL) sections was developed for function with ultra-wideband (UWB) signals. The splitter is matched in the frequency range of 3.1 – 10.6 GHz.

Multiplexing of contiguous frequency bands was improved using the proposed multiplexing circuit based on CTL sections providing quasi-balun function. Performance of the multiplexer is confined only within the bandwidth of the quasi-balun.

The theoretical calculations agree with the practical results. The components were produced using LTCC technology, tested and found an application in actual projects.

Keywords – analog integrated circuits, circuit analysis, circuit synthesis, circuit simulation, coupled transmission lines, dielectric materials, distributed parameter circuits, frequency division multiplexing, RF communication, impedance matching, microwave circuits, LTCC, passive circuits, power combiners, power dividers, RLC circuits, transversal filters, ultra-wideband communication.

Kurzfassung

Derzeitige Kommunikationstechnik unterstützt verschiedene Standards und deckt viele Anwendungsbereiche ab. Der front-end Abschnitt eines Multifrequenz-Transceivers verbindet bzw. teilt Frequenzkanäle zur weiteren Verarbeitung. Diese Arbeit konzentriert sich auf Entwicklung von verbesserten passiven Komponenten, die im front-end Teil eingesetzt werden, wie z. B. Filter und Teiler (Frequenz und Leistung).

Die LTCC Technologie wurde für die Produktion der Komponenten ausgewählt, weil diese zur Miniaturisierung der Bauteilgröße beiträgt, was für den Einsatz in tragbaren Geräten von besonderem Augenmerk ist. Es wurden neue Konzepte vorgeschlagen, die eine weitere Miniaturisierung fördern, ohne dabei die Performance zu vernachlässigen.

Im ersten Teil wird ein neuer passiver transversal / rekursiver Bandpassfilter vorgestellt. Die dabei zum Einsatz kommende lumped Element Struktur ist eine äquivalente Schaltung von Ringresonator mit Inhomogenitäten. Nach der Optimierung wurde der leicht kontrollierte Filter mit einfacher Struktur entwickelt.

Der zweite Teil beschäftigt sich mit einem neuen Leistungsteiler, der mit den gekoppelten Leitungen realisiert wurde. Als Einsatzgebiet wurde UWB spezifiziert, somit erfolgte die Anpassung des Leistungsteilers im Frequenzbereich von 3.1 bis 10.6 GHz.

Abschließend befasst sich diese Arbeit mit der Entwicklung eines Multiplexers, welcher die Funktion eines Quasi-Baluns aufweist, und mit gekoppelten Leitungen realisiert wurde. Dabei wirkt nur die Bandbreite des Quasi-Baluns begrenzend auf die Gesamtperformance des Multiplexers.

Die theoretischen Kalkulationen stimmen mit den praktischen Ergebnissen überein. Diese Komponenten wurden mit LTCC Technologie produziert, getestet und in aktuellen Projekten verwendet.

Schlagwörter – analog integrierte Schaltung, Analysis von Schaltungen, Synthesis von Schaltungen, Simulationen von Schaltungen, gekoppelte Leitungen, dielektrische Materialien, Schaltungen mit distributive Parameters, Frequenz Division Multiplexing, HF Kommunikationen, Anpassung von Impedanz, Hochfrequenz Schaltungen, LTCC, passive Schaltungen, Leistungsaddierer, Leistungsteiler, RLC Schaltungen, transversal Filters, ultra-breitband Kommunikation.

Acknowledgements

I would like to thank all people who in direct or indirect way support me during my investigations and writing this work

First of all, great thanks to Epcos OHG company in Deutschlandsberg, where I have been working since 2005, and my supervisor Prof. Erich Leitgeb from TU Graz (IBK) for giving me an opportunity to write this PhD thesis.

Thanks a lot to Prof. Erich Leitgeb also for wise support and guidance of this research work, for useful technical discussions and help in all my university activities.

I would like also to thank Prof. Klaus Reichmann for kindly consent to supervise my work from technological side and helpful discussions about technological problems and production of the samples.

A lot of complicated and interesting projects at MLIP department, which realization gave me a lot of materials, new ideas and which were extremely useful background for this work, are appreciated. Additional thanks to Prof. Gernot Kubin, Prof. Klaus Witrissal and their colleagues from SPSC Laboratory (TU Graz) for cooperation in the context of modern project on UWB that open way for implementation of some of my investigation in this new field.

I regard my colleagues from MLIP department, my chiefs Dipl. Ing. Manfred Stadler and Dr. Werner Salz for warm and friendly atmosphere, where I've managed to finalize my work. I also appreciate careful spelling corrections of Dipl. Ing. Florian Rak - my colleague and a friend of mine.

Special thanks to Dr. Igor Kartashev, which contribution into my work is highly evaluated, for all our scientific and not only scientific discussions, helpful advises, encouraging and problem solutions. This man is the one who pushed me to write this thesis and I really appreciate it.

I'll always remember National Technical University of Ukraine "KPI" in Kiev I graduated from in 2001, where I have spent six of the best years in my life, as well as my former Master thesis supervisor Ass. Prof. Alexander Mihailovich Kuprij.

Of course, many thanks to my friends those were always happy about my progress.

Finally, I want to thank my family - mother Valentina for kindness, father Vasiliy for believing in me, brother Ivan for supporting me in difficult situations, sister Olga for opening my eyes on some things and beloved Tatiana for revival of me.

Acronyms

3D	three-dimensional
ADC	analog-to-digital converter
B	balun
BalMPX	balanced multiplexer
BalTPX	balanced triplexer
BPF	bandpass filter
BSF	bandstop filter
BT	bluetooth
C	capacitance
CCW	counter-clockwise
CTL	coupled transmission lines
CW	clockwise
DBS	digital broadcast satellite
DC	direct current
DPX	diplexer
DPS	dual power sampler
DSP	digital signal processing
DVB-H	digital video broadcasting handheld
ED	energy detector
ESD	electrostatic discharge
F	filter
FDMA	frequency division multiple access
FEM	front-end module
GPS	global positioning system
GSM	global system for mobile communications
HF	high frequency
HPF	highpass filter
IC	integrated circuit
IL	insertion loss
L	inductance
LH	left-handed
LNA	low-noise amplifier
LNB	low-noise block converter
LPF	lowpass filter
LTCC	low temperature co-fired ceramic
M	matching
MMIC	monolithic microwave integrated circuit
NF	notch filter
NOFDM	noncoherent orthogonal frequency division multiplexing
PA	power amplifier
PCB	printed circuit board
PD	power divider
PM	power monitor
qB	quasi-balun

RF	radio frequency
RH	right-handed
RL	return loss
RX	receive
S	switch
S-parameters	scattering parameters
SAT	satellite
SAW	surface acoustic wave
SCD	single cable distribution
SCR	satellite channel router
SIR	step-impedance resonator
SMD	surface mounted device
TEM	transverse electromagnetic
TL	transmission line
TPX	triplexer
TV	television
TX	transmit
UMTS	universal mobile telecommunication system
UWB	ultra-wideband
VGA	variable gain amplifier
WiMAX	worldwide interoperability for microwave access
WLAN	wireless local area network
WPAN	wireless personal area network
Y-parameters	conductivity parameters

Table of Contents

Abstract

Acknowledgements

Acronyms

1. Introduction	1
1.1 Front-End Signal Processing	2
1.2 Motivation	3
1.3 Outline	4
2. LTCC Technology.	6
2.1 Lumped Elements Realization	8
2.2 Integration of HF Components Using LTCC	10
2.3 References to Chapter 2	11
3. A New Transversal / Recursive Filter	12
3.1 Transversal / Recursive Filter Concept	13
3.2 Analysis of the Simplest Configuration	15
3.2.1 Directional Structure	16
3.2.2 Circular Structure	21
3.3 Synthesis Procedure of the Filter	28
3.4 Practical Realization	29
3.5 Results on the Filter Design	33
3.6 References to Chapter 3	34
4. A New Ultra-Wideband Power Divider	36
4.1 Power Divider Concept	37
4.2 Implementation of the Splitter	38
4.2.1 Matching Procedure	40
4.2.2 Frequency Response	42
4.2.3 Increasing the Bandwidth	45
4.2.4 Final Matching Procedure	51
4.2.4.1 Matching with Implanted Losses	52
4.2.4.2 Lumped Element Matching	52
4.2.4.3 Transmission Line Matching	57

4.3 Realization Using LTCC	60
4.4 Results on UWB Power Divider	68
4.5 References to Chapter 4	69
5. A New Multiplexing Circuit	71
5.1 Multiplexer Concept	73
5.2 Multiplexing Using the Ideal Balun	75
5.3 New Approach	78
5.4 3D Implementation	83
5.4.1 Structure Optimization	85
5.4.2 Performance Using the Ideal Basement	89
5.4.3 LTCC Realization	92
5.5 Results on the Multiplexing Circuit	95
5.6 References to Chapter 5	95
6. Several Applications of the Designed Components	99
6.1 Single Cable Distribution	99
6.2 NOFDM UWB Receiver	107
6.3 Universal Balun	110
6.4 References to Chapter 6	114
7. Conclusion	117
7.1 Summary.....	117
7.2 Future work	118
Appendix A: LTCC Components	120
A.1: Design Process	120
A.2: Production	121
A.3: Measurements	123
Appendix B: S-parameters for the Power Divider	125
Appendix C: S-parameters for the Multiplexing Circuit	128
Appendix D: Broadside-Coupled Striplines	130
D.1: Absolute Relations	130
D.2: Relative Relations	132

1. Introduction

Nowadays, our life could not be imaged without world-wide web providing different communication types between people. This web is not the same as well known abbreviation “www” that has been using for a long time for designation of one of the services communicated via the Internet. The web has all rights to be named “wwIw” (world-wide information web), because it contains all available services providing any information flow. The communications are realized via the Internet, mobile nets, GPS (global positioning system), TV broadcasting and other hard-wire or wireless networks. Anybody can access desired data or establish connection to the other one by using specialized devices. Handheld devices are the most attractive, because almost everyone wants to be always online and have every time unlimited access to the wwIw or even be a part of the wwIw. For example, a mobile phone is the most widely distributed device of such type. The history of mobile phones development shows increasing of their functionality and decreasing of them in size. These two processes are discrepant and they became possible mostly due to the technology improvement. Mobile phones have full wireless access to the wwIw, thus the increased functionality leads to more complex system realization, particularly to high frequency (HF) signal processing. The HF signal processing takes place in the front-end part of the equipment and represents a point of interests in this work.

Frequency response of the widely distributed wireless standards is depicted in Fig.1.1, where there are the several ones mentioned above like DVB-H (digital video broadcasting handheld) (UHF: 470 – 862 MHz), GSM (global system for mobile communications) (824 – 894 MHz, 880 – 960 MHz, 1710 – 1880 MHz, 1850 – 1990 MHz), GPS (1.57542 GHz), UMTS (1920 – 1980 MHz, 2110 – 2170 MHz), BT IEEE 802.15.1 (2402 – 2480 MHz) and WLAN IEEE 802.11n (wireless local area network) (2.4 – 2.4835 GHz, 5.15 – 5.725 GHz). Additionally, WiMAX (worldwide interoperability for microwave access) IEEE 802.16m (2.3 - 2.69 GHz, 3.3 – 3.8 GHz, 5.15 – 5.875 GHz) and UWB (ultra-wideband) IEEE 802.15.4a (3.1 – 10.6 GHz) standards are shown. WiMAX is used for relative high speed (up to 100 Mbit/s for mobile users) broadband internet connection on high distances (maximum range of 50 km), but it can operate either at higher bitrates or over longer distances, but not both. In contrary, UWB provides extra-high speed communication (up to 1 Gbit/s) over short range (maximum of 5 m).

Modern equipment, which is going to be a good candidate for establishing a valuable contact between a human and the wwIw, must support as much standards as possible. Nevertheless, simple single-standard devices found implementation in specific applications, too.

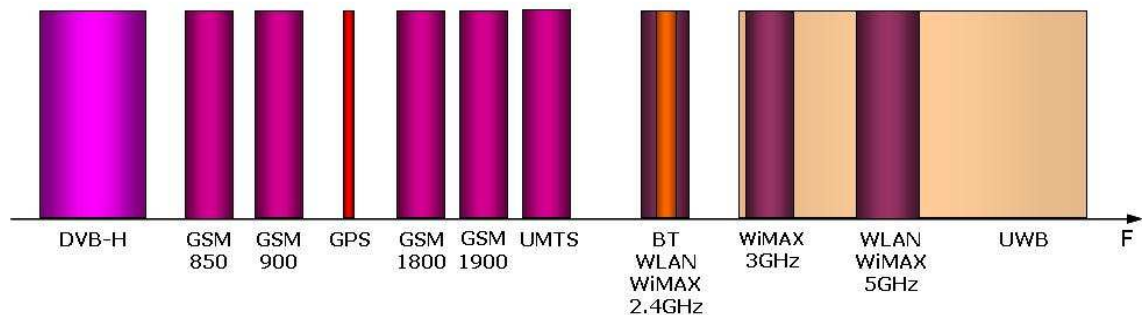


Figure 1.1: Wireless standards: frequency response

1.1 Front-End Signal Processing

For example, in order to provide indoor wireless Internet network, devices supporting only WLAN are needed. A typical WLAN architecture describing such process is presented in Fig.1.2. An access point (AP) is a central part of the wireless network that provides wired to the wireless bridging function and switching function between clients. Access for AP to an external global network is realized by broadband technology. Internal information flows are distributed between the clients, where each of them must have either embedded or external adapter providing connection with the wireless network. A block diagram of a front-end part of the adapter operating with both WLAN frequency bands is shown in Fig.1.3. Two antennas used for transmitting / receiving a signal are matched with the system input impedance by matching circuits (M). ESD (electrostatic discharge) protection device protects integrated circuits (IC) like a switch (S), a low-noise amplifier (LNA) and a power amplifier (PA) from ESD damage. The switch commutates the antennas with receive (RX) and transmit (TX) part. TX part contains a power monitor (PM) registering power of the transmitted signal. Diplexers (DPX) in both paths separate 2 GHz and 5GHz channels, which are filters by bandpass filters (BPF). Lowpass filters (LPF) in TX path suppress harmonics coming from PA. Baluns (B) transform a single-ended signal into the balanced one in order to be compatible with chipsets having balanced inputs. This is a common block diagram; therefore, not all components must be included. M, ESD and B are optional depending on system requirements. The front-end part can be realized as a single components solution as well as an integrated variant – a front-end module (FEM).

Thus, main task of the front-end part is to separate both working frequency bands and receive / transmit paths. The passive elements involved in this function are filters and dividers (frequency (multiplexer) and power (splitter)). These are the key components, which investigation put into this work.

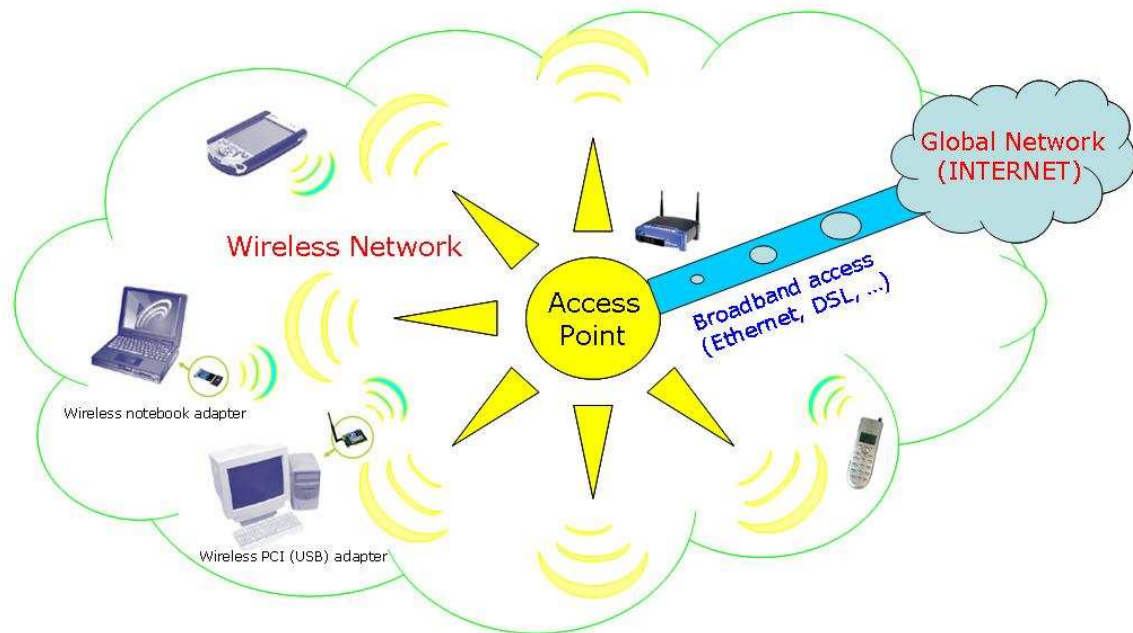


Figure 1.2: WLAN architecture

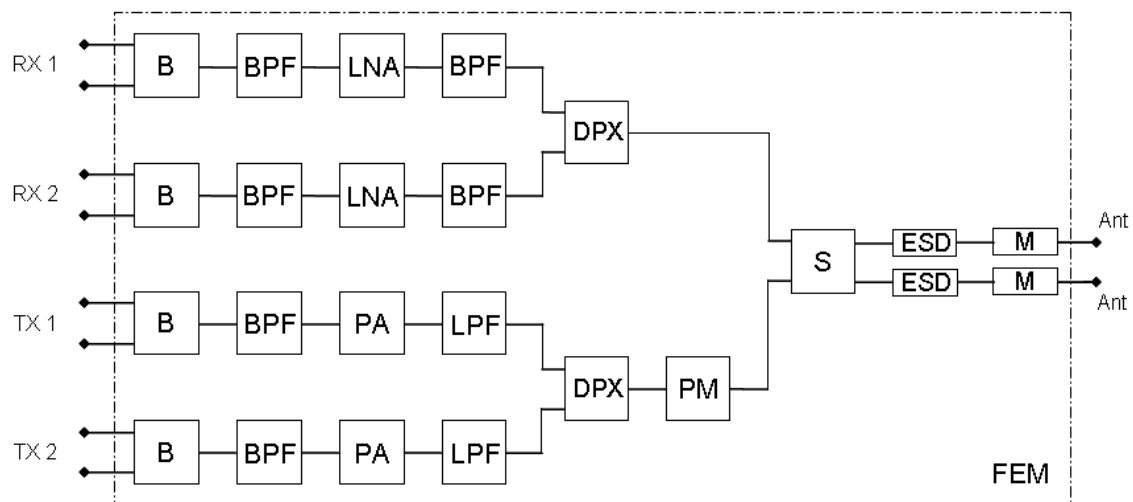


Figure 1.3: A common front-end block diagram

1.2 Motivation

As it was said above, continuous tendency in evolution of handheld communication devices shows increasing of functionality and decreasing of size. This process is possible mostly due to efficient technology development. LTCC (low temperature co-fired ceramic)

technology described in the next topic has been used in our company for producing passive microwave components. Providing high values of dielectric permittivity and three-dimensional multilayer disposition of structures, the technology makes it possible to develop small-size components. Generally, the design process assumes taking already known circuit solution and implementing them into LTCC piece. This process is standard and effective enough, but not in all cases. Simply thinking, one can produce a component as small as possible by just taking as high value of dielectric constant as needed. But it can not be a magic, every technology has its own limits. For example, either it's not possible to realize two-layer structures (Wilkinson power divider, ring resonator with perturbations...) inside small piece of LTCC or there is no sense to use multilayer technology for such structure realization. On the other hand, circuit solutions being able to realized in multiplayer structure can be relative easy integrated in LTCC, but limits on performance of every circuit exist anyway. Moreover, performance degradation is observed by switching from discrete solution to the integrated one and it happens mostly due to higher losses and parasitics. Thus, LTCC technology provides effective integration of passive components, but with the certain limitations in performance and size.

What could be done if size or performance of a designed component still doesn't meet requirements? New system solutions must be found that meet the target of this work – intelligent miniaturization that lies in the minimization of elements number in the structure providing the best achievable performance. For example, the lumped element transversal / recursive bandpass filter proposed in the work is an equivalent of a ring resonator with perturbations fit for multilayer structure and optimized for size and performance. Another example is the new coupled line power divider, which compact structure provides function with UWB signals. The last designed structure described in this work is the multiplexer operating with contiguous bands. This simple structure allows refusing from difficult and big circuit solutions.

1.3 Outline

The present work is split into several parts. The first topic refers to LTCC technology used for the components realization. A new transversal / recursive filter concept has been presented in the second topic. The filter is the bandpass one, which structure solution results in a compact design with sufficient performance. In the third topic, a new coupled transmission line power divider providing function in ultra-wideband frequency range is presented. The simplest structure of the power divider let to enlarge the working bandwidth extremely in comparison with the existing solutions. The next topic is dedicated to a multiplexing circuit deigned to improve performance of the split frequency channels

containing contiguous bands. Typical problems of the contiguous bands splitting are solved due to using special schematic of the multiplexer. Corresponding analysis, calculations and practical investigations are attached to each of the topics. The final part of the work contains information about practical applications of the designed components. All components together or a part of them can be implemented into front-end signal processing part. Several running projects are shortly presented. Conclusion and future work finalize this thesis.

2. LTCC Technology

LTCC (low temperature co-fired ceramic) technology [1] was used for designing the components described in this work. This is one of the progressive multilayer technologies for production of RF (radio frequency) and microwave components. The ceramic itself is based on combination of ceramic and metal layers, therefore it is suitable for passive components realization. 3-dimensional structures can be realized inside the ceramic, while both passive and active components can be mounted on the top of the components, thus forming a hybrid structure. Simplified component cut view is shown in Fig. 2.1. Depending on the configuration, passive inner structures occupy several layers, where connections between them are provided by vias. The connections could be followed to the top of the component, where either SMD (surface mounted device) components can be soldered or other external components can be mounted using wire bond or flip chip technologies. In case of using the external active elements operating with high power levels (e.g. amplifiers), thermal vias have to be implemented inside the ceramic providing a thermal balance. LTCC components are typically soldered on a PCB (printed circuit board).

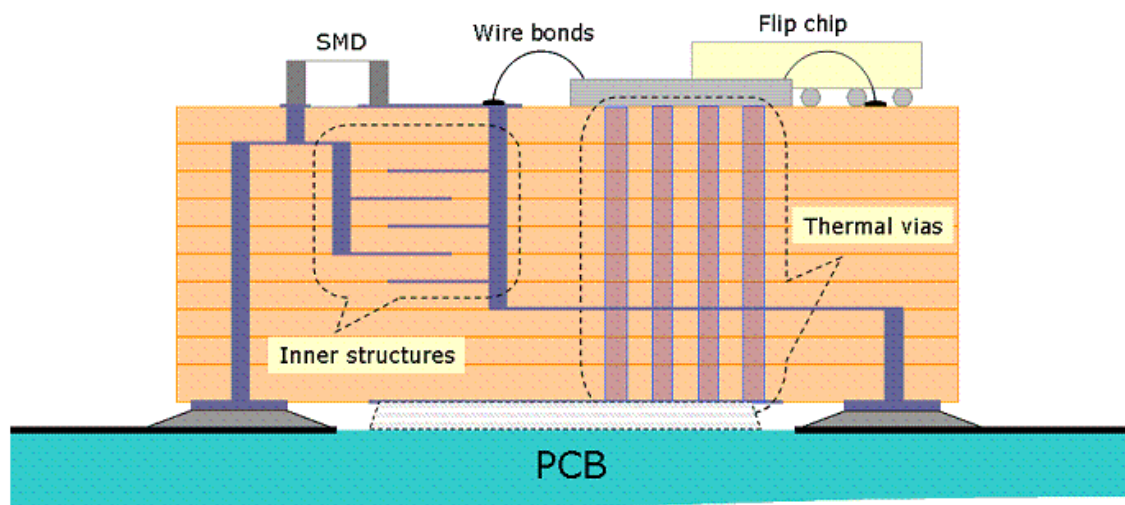


Figure 2.1: LTCC component: generalized cut view

LTCC technology could be implemented for a variety of components beginning with simple couplers and finalizing in complicated systems like front-end modules (FEMs). Such components are the next generation after the solution realized by single SMDs soldered on PCB, thus contributing to the miniaturization process. Detailed material characterization and practical examples are given in [2].

Production process of LTCC components consists of several steps; it is shown in Fig. 2.2 and described in [3]. There is no sense to talk about it one more time. It should be

mentioned that the last step (characterization) means not only optical inspection, HF measurements of the produced component have to be done.

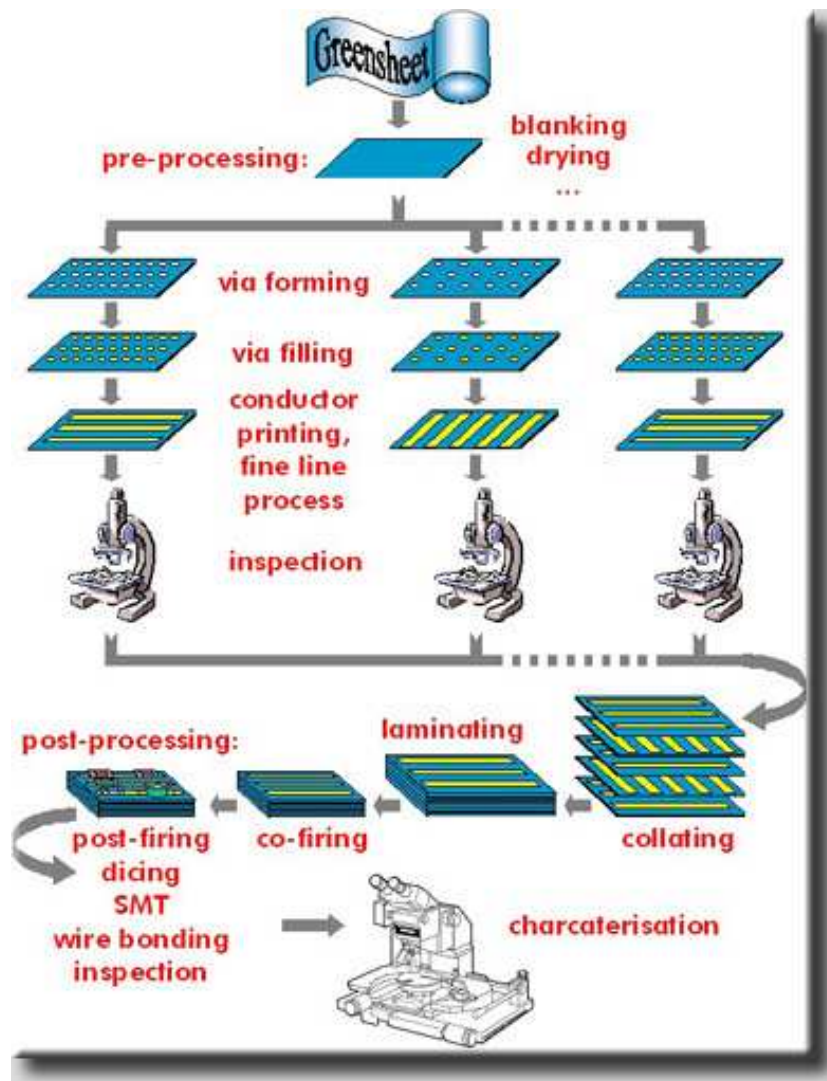


Figure 2.2: LTCC processing (from [3])

LTCC technology possesses a lot of advantages, like low resistive and dielectric loss, good thermal conductivity, high working temperature, high integration density, possibility of 3D circuits integration, robust against mechanical and thermal stress, very good hermetic property of the substrate, low material and production costs and really applied mass production methods. Production errors relate to disadvantages of the technology (misalignment, shrinkage, realization precision ...).

There are two different standard technological processes for LTCC production being used in EPCOS: shrinkage and zero-shrinkage. The shrinkage technology is simpler (cheaper) than the second one and it's used for single passive components, while the zero-shrinkage technology makes both-side metallization possible (therefore external components are able to be mounted on the top of the structure) and it's used for complex components like modules. Standard ceramic material for the non-shrinkage process is

DuPont Green Tape™ 951 with the following parameters: dielectric constant $\epsilon_r = 7.8$, loss tangent $\delta = 0.003$ (the parameters are measured at 3 GHz) and fired thickness – 50 μm (possible are 30 and 100 also). An inner structure is built by a silver paste with thickness $t = 10 \mu\text{m}$ and conductivity $\sigma = 5 \cdot 10^7 \text{ S/m}$. More detailed information about DuPont material is given in [4]. The shrinkage process uses ceramics with several values of the dielectric constant (7.8, 18 and 82), where the ceramic with low value is optimal for LC structures, the high-epsilon ceramic – for transmission line (TL) structures and the middle value – for combinations of them, especially for structures possessing large capacitors.

2.1 Lumped Elements Realization

Some of typical examples of lumped elements realization in LTCC are shown in Fig. 2.3. Two or more layers are needed for the realization. Elements occupying two layers are simple, while elements comprised of more layers are smaller and have more parasitics. By designing, an optimum between size and performance has to be found depending on requirements on the designed component characteristics.

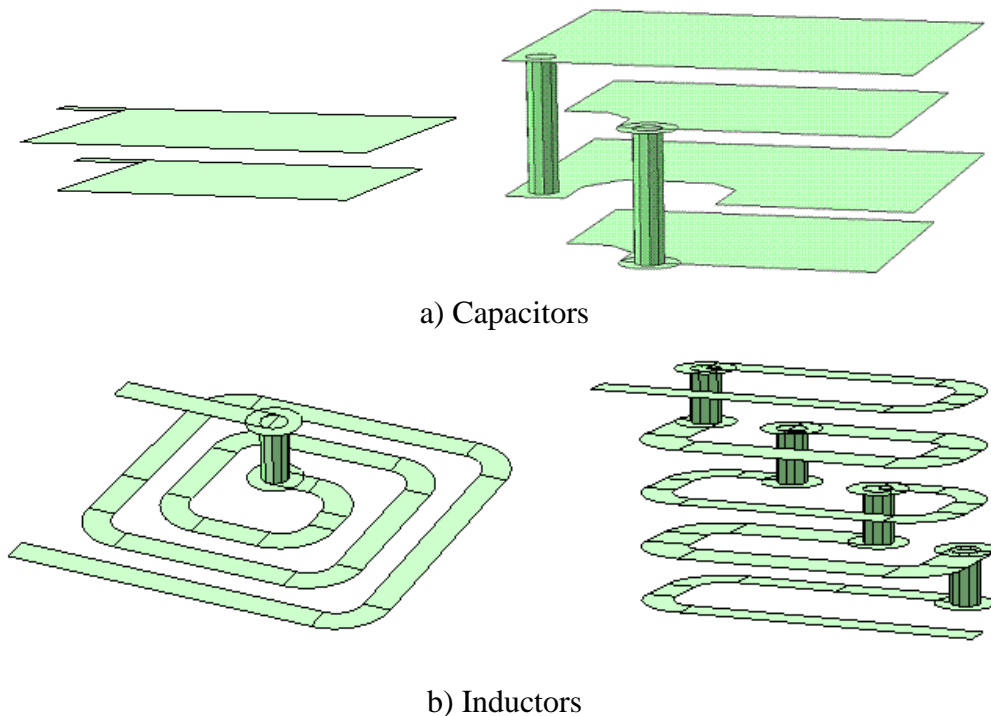
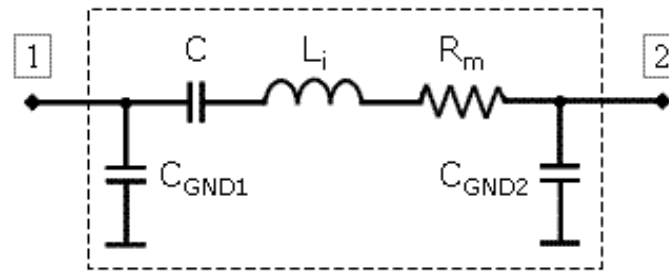


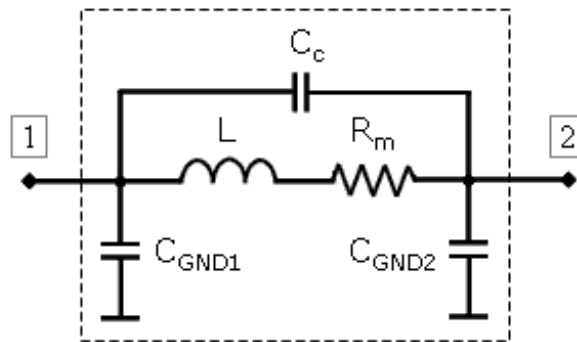
Figure 2.3: Examples of 3D realizations of elements in LTCC (drawn using [5])

Equivalent circuits of the lumped elements realized in LTCC are shown in Fig. 2.4, where all parasitics (coupling to ground (C_{GND}), coupling between coils (C_c), and inductance of interconnections (L_i)) are depicted excluding coupling between the elements inside the structure. Additionally to the original element values (L and C), the losses in the

materials are depicted (R_m). The parasitic couplings to other neighbor structures have not been taken into consideration. Two depicted nodes (1 and 2) correspond to the output nodes of the elements. The parasitics have an impact on the performance of the designed structure mainly due to altering the original schematic; therefore, they must be taken into account during the design process. The fact that the element values of the parasitics are individual for each of the LC structures brings difficulties into design procedure.



a) Capacitor



b) Inductor

Figure 2.4: Equivalent circuits of L and C elements realized in LTCC

An algorithm describing a design process of the LTCC components is depicted in Appendix A. Requirements on a component are usual described in specification, which would be firstly tested on realization ability. If all values are realistic, the next step “preliminary simulations” would be to create a schematic solution providing full compliance with the specification. On this step, a solution considering type of realization (lumped elements, TL or combined) has to be found. After obtaining the optimal solution, schematic will be implemented in 3D LTCC realization and optimized until it will work accordingly to the preliminary simulations. On this step, selection on the ceramic type has to be done (dielectric permittivity), components configuration and their placement have to be fixed. Afterwards, the structure will be proved on stability to the production tolerances. If critical elements exist, necessarily corrections have to be done with the following re-simulations, until the design is ready for being transferred to the production line. The ready components have to be measured and the measurements results must be run through the verification. If the problems or inconsistency between measurement and simulation results

occur, corresponding corrections on the simulations have to be done and the 3D simulations have to be done on more time. After the final successful production, certain paper work on the results documentation should be done.

A number of explanatory figures are placed in Appendix A, where ready produced and cut panel containing LTCC components is shown as well as single components. Additionally, inner structures of the components can be seen on the cut planes. There are two possibilities to measure the components using network analyzer: by pressing on test jig and by soldering on PCB, these methods are also depicted in the appendix. The first method is quicker, while the second one is more precise. Four-port network analyzer is used for simple structure up to single-ended triplexer, while a network analyzer with switch can measure more complicated structures containing more than four ports, like a balanced triplexer.

This part shortly outlined LTCC technology used for production of the components described in this work. More detailed information can be achieved from well known open sources.

2.2 Integration of HF Components Using LTCC

This work contains investigations on key components in the front-end frequency signal processing supported frequency division multiple access (FDMA), described in the chapter 1.1. These components are filter, frequency divider and power divider, which are the parts of different front-end modules (FEMs); some of these components are depicted in the Fig. 1.3. The components could be realized like single components as well as like the integrated ones into FEMs. Based on the realization principles described in the chapter 2.1, the components have been successfully integrated using LTCC technology.

The transversal / recursive bandpass filter has been realized with lumped elements. The effect of the parasitics shown in the Fig. 2.4 can be neglected because of small element values needed for the filter realization that could be one of the advantages of the filter. The realization of the frequency and power dividers are simplified in case of parasitics, because they are built of coupled transmission line sections, which can be quite easily implemented in 3D multilayer structure using distributed elements. Only the design rules could be a problem for very precise realization of the even- and odd-mode line impedance values.

Next three chapters show development of the improved components using mathematical methods and physical model. At the end of each chapter, ready to use LTCC models are proposed. The last chapter contains information about the projects, in which the components have found an implementation. The components have been integrated into the modules, thus the requirements on high level integration have been fulfilled.

2.3 References to Chapter 2

- [1] Y. Imanaka, Multilayered Low Temperature Cofired Ceramics (LTCC) Technology, Ed. Springer Berlin, Mai 2005.
- [2] L. Devlin, G. Pearson, J. Pittock, “RF and Microwave Component Development in LTCC,” *Proceedings on IMAPS Nordic Conference*, Oslo, Mar. 2001, pp.96-110.
- [3] LTCC website. [Online]. Available: http://www.ltcc.de/en/whatis_pro.php
- [4] DuPont Microcircuit Materials: 951 Green Tape. DuPont. [Online]. Available: http://www2.dupont.com/MCM/en_US/assets/downloads/prodinfo/951LTCCGreenTape.pdf.
- [5] Sonnet Software Inc. v.12.52, 2010.

3. A New Transversal / Recursive Filter

LTCC technology has been successfully used in microwave applications for integration of both single passive components and complex components comprised of the single ones, like a module. Filter structures are widely distributed due to a variety of its functionality based on frequency characteristics. Common filters can be mainly classified by realization on transmission line (TL) filters, lumped element filters or combination of these concepts. It depends on operating frequency, ceramic features and frequency characteristics. Common bandpass filters (BPF) represent resonator filters itself or combination of lowpass (LPF) and highpass (HPF) filters, thus provide transmission in the passband simultaneously with rejection of unwanted bands out of the passband. LTCC has been found as the optimal technology for miniaturization and producing such type of the filters.

Another filter type is the transversal / recursive one. Block diagrams of the typical filter are shown in Fig. 3.1. This type is usually used in digital signal processing (DSP) and surface acoustic wave (SAW) structures. Due to a large structure size and poor performance (high losses) DSP filters didn't find wide implementation in microwave filter design. Additional problems with the realization of negative filter coefficients made the use of LTCC technology in the filter fabrication impossible. Some work has been done to combine the transversal / recursive filters with active elements in order to improve the performance and make the filters realizable with MMIC technology [1] - [3]. Nevertheless, it didn't make a big progress in comparison with standard passive LTCC filters. The most critical parameters are size and simplicity of realization.

Some work has been done on designing the transversal filters without active elements in order to provide its compatibility with the passive planar technology. It was the TL filters based on coupler structures [4], [5] or coupled resonators [6] – [8]. The main problem of the filters is too large size (more than 15 mm in one direction), while its implementation in the wireless applications is confined with frequency 6 GHz. Standard size of the filtering components to be used in these application is about 2.0 x 1.5 mm². Moreover, LTCC advantages (multilayer distribution) are not fully used and sometimes it is more reasonable to build a design on printed circuit board (PCB).

A new lumped element transversal filter presented below uses all opportunity of LTCC utilizing the size of 1.9 x 1.0 mm². It provides the low transmission losses with the

good rejection characteristics; it's simple in design and is comprised of any active elements. The solution is patented in [9].

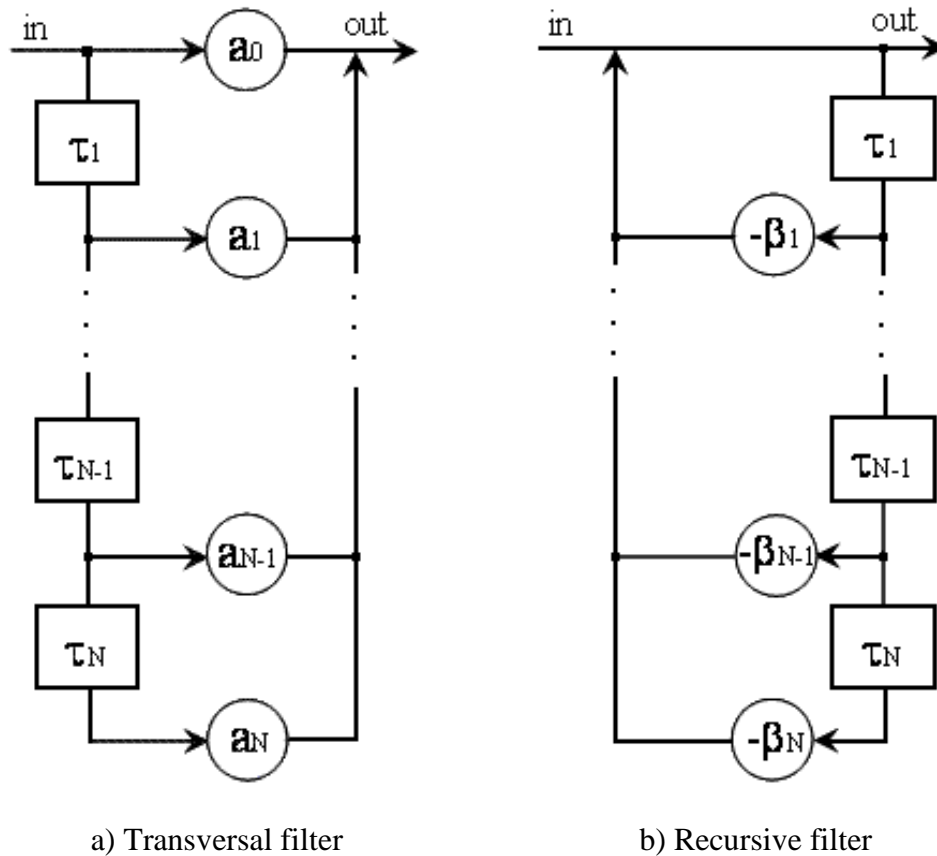


Figure 3.1: Block diagrams of transversal / recursive filters

3.1 Transversal / Recursive Filter Concept

The new filter concept is based on combination of the standard transversal and recursive filters properties. A block diagram of the filter (Fig. 3.2) contains the same delay and attenuation blocks. The main aim of the development was to provide implementation ability of this filter type using LTCC technology, thus all of the blocks are passive. Moreover the blocks are reciprocal; they provide bidirectional signal propagation. This is a distinguishing feature of the filter from the standard ones (Fig. 3.1) and is significant for functionality of the filter. Such filter topology assumes the use of the attenuation blocks together with the delay blocks in one arm.

In general, there are several passes ($N+1$) connected in parallel which form N -order filter. The simplest case is 1st-order filter which contains only two passes connected in parallel. Such filter represents itself a lumped element analog of a ring resonator with perturbations while N -order filter implements a 3D ring resonator filter.

Reciprocity of the passes makes synthesis and analysis procedures more complicated especially for the filters with order more than 1. All interconnections with feedbacks have to be taken into account in this case.

For example, in case of single-directional propagation an output signal in time domain will be like:

$$y(t) = \sum_{n=0}^N a_n x(t - \tau_n) \quad (3-1)$$

where $y(t)$ – output signal, $x(t)$ – input signal, a_n - transmission coefficient for n-channel and τ_n - delay for n-channel. The transfer function in frequency domain will look like:

$$S_{21}(f) = \sum_{n=0}^N a_n e^{-j2\pi f\tau_n} \quad (3-2)$$

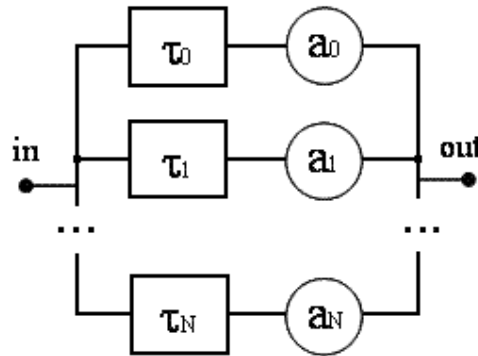


Figure 3.2: New N-order transversal / recursive filter

Considering reciprocity of the proposed circuit, two circular signals are able to propagate through each of the passes, while presenting the circuit with a number of parallel rings these signals will be the clockwise (CW) and the counter-clockwise (CCW) ones. They become excited at the common input, combine by transmitting and reflection from the input and the output of each pass and finally form the output signal by it's interpolating at the output side. A value of the output signal depends on amplitude and phase of the outcoming CW and CCW signals. A variety of filtering characteristics can be obtained by playing with notches. It is clear that the notches will be produced by cancellation of those signals at the output side, which are equal in amplitude and opposite in phase. Thus complex magnitude of the output signal can be calculated with the following equation:

$$\dot{U}_{out} = \Sigma \dot{U}_{inc(CW)} + \Sigma \dot{U}_{inc(CCW)} + \Sigma \dot{U}_{ref(CW)} + \Sigma \dot{U}_{ref(CCW)} \quad (3-3)$$

where $\dot{U}_{inc(CW)}$ – complex amplitude of the incident CW signal upon output, $\dot{U}_{inc(CCW)}$ – complex amplitude of the incident CCW signal upon output, $\dot{U}_{ref(CW)}$ – complex

amplitude of the reflected CW signal from output, $\dot{U}_{\text{ref(CCW)}}$ – complex amplitude of the reflected CCW signal from output.

It's not so clear from the equation (3-3), but it will be shown below that the rejection performance which is formed by the number and position of notches depends not only on the filter order, but also on complexity of the passes. So, in order to improve the rejection characteristics, the filter could be prolonged in both direction – either including the additional parallel passes or making the existing ones more complicated.

Advantage of the filter is high selectivity due to the structure properties achieving without using the resonance circuits with high Q-factor. The filter is distinguished in comparison with other filters [4] – [8] because of refusing from resonators and couplers to combine all passes. This type of filter design interrelates with a design of the ring resonators with perturbations [10]. Duality of the filter occurs in its representation like a lumped element circuit which is equivalent to the ring resonator filter with perturbations on the one hand and the quasi-transversal / recursive filter on the other hand.

3.2 Analysis of the Simplest Configuration

Let's consider a simplest configuration of the proposed filter (1st-order filter). The filter contains two passes, which are comprised of arbitrary selected constituents. In our case, the constituents are selected like T-networks (lowpass in one pass and highpass in the other one). The overall structure is shown in Fig. 3.3. Such typical structure was taken in this chapter in order to simplify the analysis procedure.

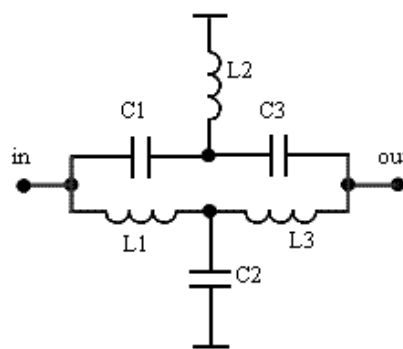


Figure 3.3: 1st-order lumped element transversal / recursive filter

The depicted circuit functions under two conditions. Depending on the element values ratio, either direct signals or the circular ones take part in the performance creation. Actually both passes are reciprocal, therefore the circular signals are always existing; the difference lies only in propagation conditions. Each of the two passes provides different frequency response. There are frequency regions in which both chains transmit the signal

(of course with defined attenuations), or one chain passes the signal through while the other one rejects, and vice versa.

In case of transmission ability of both channels, the circular signals exist and play prior role in functionality of the filter in comparison with the direct signals. In this case the circular currents are nothing but the single-direction currents which are running in opposite directions. Proposed T-networks represent itself LC-equivalent of the left-handled (LH) and the right-handled (RH) lines and the whole structure is a lumped element equivalent circuit of the ring resonator filter with perturbations.

3.2.1 Directional Structure

One way directional currents occur during the propagation only through a single channel, while the other one includes a lot of losses for the signal. The existing circular currents are high suppressed and therefore too weak to influence the filter performance. The use of the direct currents to form notches is not a new idea and it's widely used. For example, structures with interconnections between the output and the input [11] use the same principle. The design procedure is very simple, because two passes are untied and can be calculated separately with the following combination together. Firstly, bandpass filter with the required characteristics has to be designed and then an additional interconnection between the output and the input (cross coupling or circuit element) will be implanted in order to get one or at the most two additional notches. These notches are formed with the directional signals – the signals which propagate in two directions (original BPF and interconnection element). The signals are excited at the input, divided into two parts and finally combined at the output side. The interconnections transmission has to be selected in such a way that the signal with defined frequency appears at the output with the same amplitude as the basic incoming signal (through the original BPF) and opposite in phase. Thus an additional notch appears inside the filter characteristics.

A bandstop filter patented in [12] uses the same principle. It looks like proposed filter but its functionality is based on the direct signal transmission. Therefore the performance of this filter has bandstop character instead of the bandpass one. Two passes provide pure lowpass filter and highpass filter characteristics. The notch appears at the point where the waves observed at the output are equal in amplitude and opposite in phase. This is a typical example of the filter functionality based on the direct signal transmission. A schematic realization of the filter with real element values is depicted in Fig. 3.4a. The analysis of the circuit seems to be simple due to independent functionality of two parallel passes. For these purposes, the filter is divided into two subcircuits, as it is shown in Fig. 3.4b, to be analyzed with its following combination. The original circuit is terminated on

50 Ohm loads; therefore the subcircuits have to be simulated with 100 Ohm environment. Expected simulated LPF (S_{65}, φ_{65}) and HPF (S_{43}, φ_{43}) characteristics of the subcircuits are shown in Fig. 3.5a. The most interesting frequency point locates at 9 GHz, where transfer functions of the subcircuits are equal in amplitude and opposite in phase. Zero transmission appears at the frequency point after the connection of the subcircuits in parallel due to cancelation of the signals at the output.

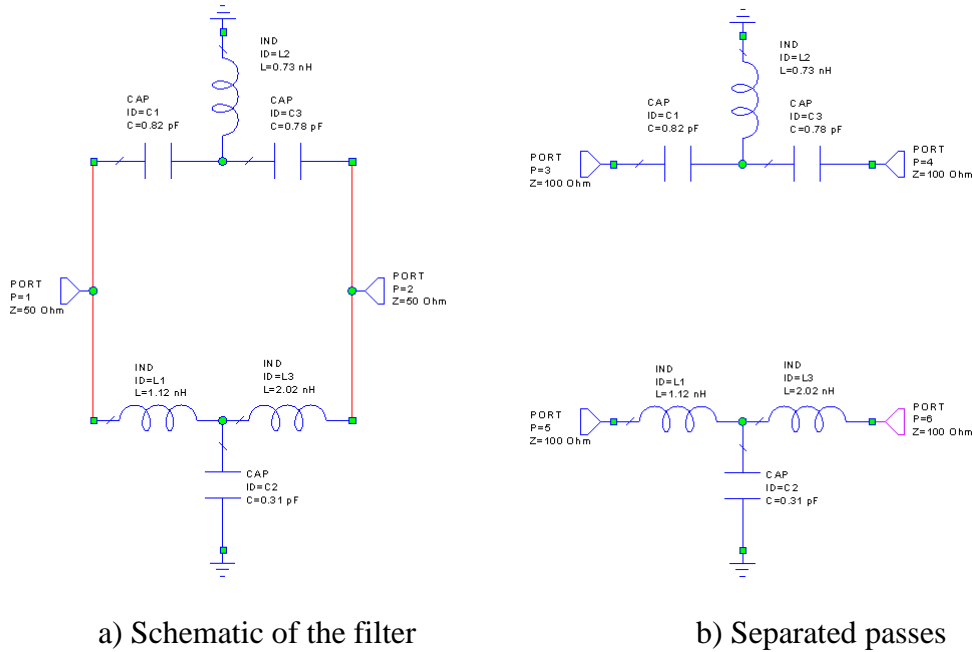


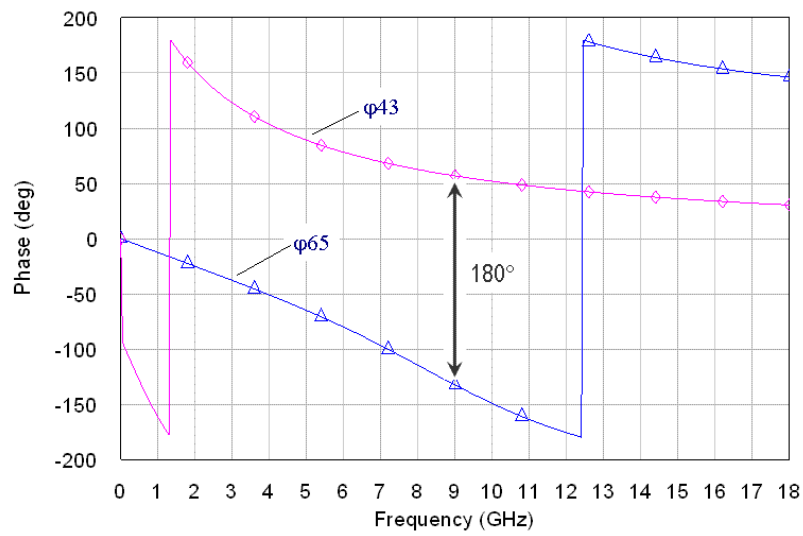
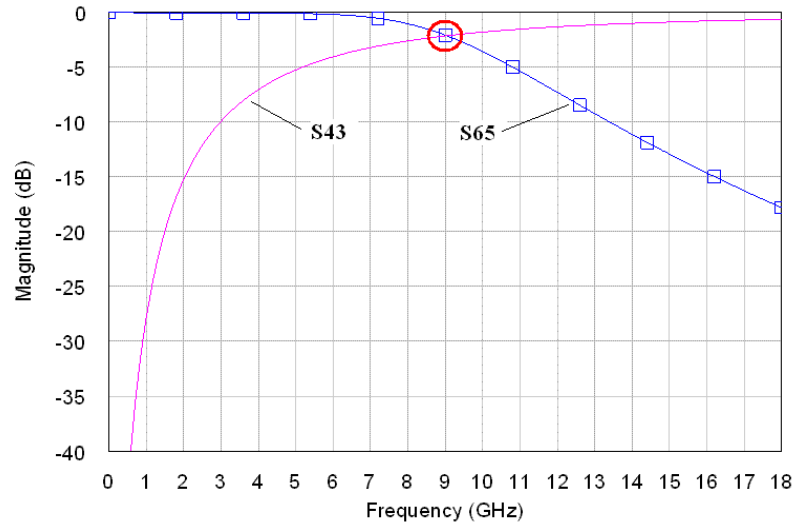
Figure 3.4: A simple directional signal filter (simulated using Microwave Office [14])

It is obvious from the subsection's function that only one frequency point exists where the transmission characteristics are crossing. Thus maximum achievable number of the zero transmissions is only one, therefore such type of the filter is named as notch filter (NF) or bandstop filter (BSF).

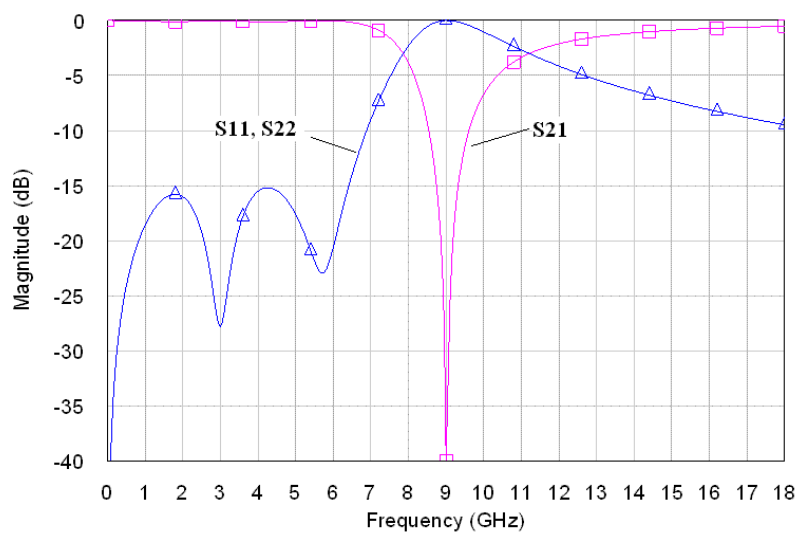
Let's provide more carefully analysis of the mentioned structure in order to achieve its full potential functional ability. To get the whole overview of the filter function the transmission function has to be calculated. It is easy to operate with parallel interconnections using Y-parameters, thus each of the passes - in this case only two passes - has to be represented with Y-parameters, as it shown in Fig. 3.6. Afterwards all obtained Y-matrices sum together in the single Y-matrix, which describes the overall circuit. Finally S-matrix can be derived from the Y-matrix using the transformation equations. It's assumed in the analysis that all elements are ideal and without losses.

The Y-matrices of the separates passes look correspondingly:

$$[Y_1] = \frac{j}{\omega(\omega^2 L_1 L_3 C_2 - L_1 - L_3)} \begin{bmatrix} 1 - \omega^2 L_3 C_2 & 1 \\ 1 & 1 - \omega^2 L_1 C_2 \end{bmatrix} \quad (3-4)$$



a) Transmission amplitude and phase of the structure from Fig. 3.b



b) Notch performance of the structure from Fig. 3.a

Figure 3.5: Partially characteristics of the structures from the Fig. 3.4 (simulated using Microwave Office [14])

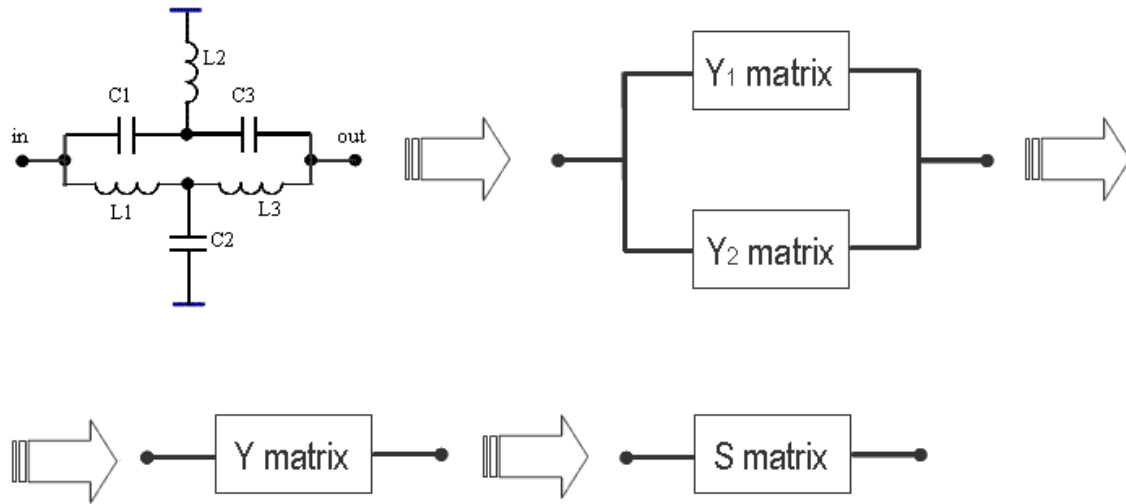


Figure 3.6: Matrix transformation

$$[Y_2] = \frac{j\omega^3 L_2 C_1 C_3}{\omega^2 L_3 (C_1 + C_3) - 1} \begin{bmatrix} 1 - \frac{1}{\omega^2 L_2 C_3} & 1 \\ 1 & 1 - \frac{1}{\omega^2 L_2 C_1} \end{bmatrix} \quad (3-5)$$

The Y-matrix of the complete circuit as a sum of the separate matrices is:

$$[Y] = \begin{bmatrix} \frac{j\omega C_1 (1 - \omega^2 C_3 L_2)}{1 - \omega^2 L_2 (C_1 + C_3)} - \frac{j}{\omega(L_1 + \frac{L_3}{1 - \omega^2 C_2 L_3})} & \frac{j(-1 + \omega^2 L_2 (C_3 + C_1 (1 + \omega^2 C_3 (\omega^2 C_2 L_1 L_3 - (L_1 + L_3))))))}{\omega(\omega^2 L_2 (C_1 + C_3) - 1)(L_1 (\omega^2 C_2 L_3 - 1) - L_3)} \\ \frac{j(-1 + \omega^2 L_2 (C_3 + C_1 (1 + \omega^2 C_3 (\omega^2 C_2 L_1 L_3 - (L_1 + L_3))))))}{\omega(\omega^2 L_2 (C_1 + C_3) - 1)(L_1 (\omega^2 C_2 L_3 - 1) - L_3)} & \frac{j\omega C_2 (1 - \omega^2 C_3 L_3)}{1 - \omega^2 L_3 (C_2 + C_3)} - \frac{j}{\omega(L_1 + \frac{L_2}{1 - \omega^2 C_1 L_2})} \end{bmatrix} \quad (3-6)$$

The obtained Y-matrix is quite enormous to be fully transformed into the S-matrix, therefore only S_{21} parameter will be taken into consideration, which corresponds to the transmission function. Calculated transmission using transformation equation from [13] is:

$$S_{21} = -\frac{2 \cdot Y_{21} \cdot Y_0}{(Y_{11} + Y_0)(Y_{22} + Y_0) - Y_{12} \cdot Y_{21}} = -2 \cdot Y_0 \frac{(-1 + \omega^2 L_2 (C_3 + C_1 (1 + C_3 \omega^2 (-L_1 - L_3 + C_2 L_1 L_3 \omega^2))))}{(-2 \cdot Y_0 - j\omega(C_3 + Y_0^2 (L_1 + L_3))) + Y_0 \omega^2 C_3 (L_1 + 2L_2 + L_3) + jY_0^2 \omega^3 L_2 C_3 (L_1 + L_3) + \omega C_2 (Y_0 \omega L_1 - j)(1 + jY_0 \omega L_3 - \omega^2 C_3 (L_2 + L_3 + jY_0 \omega L_2 L_3)) + \omega C_1 (-j + \omega Y_0 (L_1 + 2L_2 + L_3) + jY_0^2 \omega^2 L_2 (L_1 + L_3) + Y_0 \omega L_1 - \omega^2 C_3 (L_1 + L_3) (2Y_0 \omega L_2 - j) + \omega^2 C_2 (-L_2 (Y_0 \omega L_3 + j(\omega^2 L_3 C_3 - 1)) + L_1 (j(j - Y_0 \omega L_2) (Y_0 \omega L_3 - j) + \omega^2 C_3 (2Y_0 \omega L_2 L_3 - j(L_2 + L_3))))))} \equiv \frac{S_{21T}}{S_{21D}} \quad (3-7)$$

The equation represents itself a common fraction with the single variable ω (radial frequency) and seven unknown parameters to be set up. These parameters are Y_0 – input /

output load impedance and L, C – circuit element values. If the unknown parameters are determined, then frequency response of the transmission function could be calculated.

Let's evaluate a schematic of the notch filter showed in Fig. 3.4a. The notch position can be estimated considering following statement:

$$S_{21} \equiv 0 \quad (3-8)$$

Based on fraction properties, the equation (3-8) can be solved by splitting into two equations:

$$\begin{cases} S_{21T} = 0 \\ S_{21D} \neq 0 \end{cases} \quad (3-9)$$

A fraction is equal to zero if a term of the fraction is equal to zero and its denominator is not equal to zero. Thus assuming that the denominator of the equation (3-7) is not equal to zero; the notch determination process is enclosed within finding a solution for the following equation:

$$\begin{aligned} S_{21T} &= 2 \cdot Y_0 (1 - \omega^2 L_2 (C_3 + C_1 (1 + C_3 \omega^2 (-L_1 - L_3 + C_2 L_1 L_3 \omega^2)))) = \\ &= \omega^6 2Y_0 L_1 L_2 L_3 C_1 C_2 C_3 - \omega^4 L_2 C_1 C_3 (L_1 + L_3) + \omega^2 L_2 (C_1 + C_3) - 2Y_0 \equiv 0 \end{aligned} \quad (3-10)$$

Element values of the BSF are listed below:

$$\begin{aligned} C_1 &= 0.82 \text{ pF} & L_1 &= 1.12 \text{ nH} \\ C_2 &= 0.31 \text{ pF} & L_2 &= 0.73 \text{ nH} \\ C_3 &= 0.78 \text{ pF} & L_3 &= 2.02 \text{ nH} \end{aligned}$$

By substituting these values into the equation (3-10), the following equation with one undefined variable (frequency) can be achieved:

$$1.3 \cdot 10^{-63} \cdot \omega^6 - 4.7 \cdot 10^{-42} \cdot \omega^4 + 2.1 \cdot 10^{-21} \cdot \omega^2 - 1 = 0 \quad (3-11)$$

Solutions of the equation have to be zero-transmission frequencies. As the equation order is 6, the six roots are expected accordingly. Moreover, due to the parity power of the variable (radial frequency) only pairs of the roots with equal value and both signs (plus and minus) correspond to the equation. Solutions of the equation with following transformation into linear frequencies are shown below:

$$\begin{aligned} f_{1,2} &= \frac{\omega_{1,2}}{2\pi} = \pm 9 \text{ GHz} \\ f_{3,4} &= \frac{\omega_{3,4}}{2\pi} = (2.98 \pm j \cdot 1.19) \text{ GHz} \\ f_{5,6} &= \frac{\omega_{5,6}}{2\pi} = (-2.98 \pm j \cdot 1.19) \text{ GHz} \end{aligned}$$

These solutions represent zeros of the polynom (3-7). Mathematically, a position of the real notch will be determined with the frequency:

$$f_{\text{notch}} = 9 \text{ GHz}$$

The denominator of the equation (3-4) at frequency 9 GHz is equal - 315 + j-346930 and it's not equal to zero as assumed.

The result obtained above means that the filter in Fig. 3.4a with the proposed element values provides only single notch response and therefore it's arranged to the BSF community. But as the equation (3-7) shows and it was written above also, the maximum potential number of the equation solutions is six, which are combined into three pairs. Therefore the maximum achievable number of the notches from the depicted structure is three. At the same time Fig. 3.5 proves appearance of single zero-transmission only. There is only one frequency point at which the transmission is equal in amplitude and opposite in phase. Why does the limitation occur on the performance of the circuit? This limitation is put on the filter due to the unidirectional transmission of the currents with different frequencies. Thus such conception of the filter designing doesn't provide full deployment of the filter potential possibilities.

3.2.2 Circular structure

As an alternative the novel transversal / recursive filter based on omnidirectional propagation which uses the whole circuit potential is proposed in this work. In order to simplify analysis procedure, the simplest 1st-order transversal / recursive filter is taken into consideration. A structure of the filter is same as the one of the BSF described above (Fig. 3.3), thus both S-parameter (3-7) and notches criterion (3-9) are actual for analysis. There is only one difference – the element values are altered. The main task now is to put into the equation (3-7) such LC values that all solutions will not contain complex values. Afterwards 3 notches appear in the filter performance automatically. The filter analysis becomes more complex because of the bandpass characteristics. The transmission and the bandstop performances have to be supported with the same element values. So the functional criterion for the transversal / recursive BPF has to be like following:

$$\left\{ \begin{array}{l} \text{at } \omega \text{ notches} \\ \text{at } \omega \text{ passband} \end{array} \right. \left\{ \begin{array}{l} S_{21T} = 0 \\ S_{21D} \neq 0 \\ S_{21} \geq 1/\sqrt{2} \\ S_{11} \leq 1/10 \end{array} \right. \quad (3-12)$$

The optimal solution for the proposed structure would be to provide the transmission at the required passband with the corresponding attenuation by the notches on both sides of the passband. The criterion (3-12) is comprised of four equations and six unknown elements (L_1, L_2, L_3, C_1, C_2 and C_3), while the system impedance (or conductivity Y_0) has

to be given as a standard for each implementation personally. Thus, a variety of solutions exists, which is represented in different notch positions with corresponding to the defined passband transmission.

Two ways exist to solve the system equation. Both of them are based on the unknown element values reduction. The first one is to assign two unknown elements with arbitrary values and solve the system with four equations and four unknown parameters. The second one is to put a restriction on the schematic by assigning symmetry on the passes:

$$\begin{cases} C_1 = C_3 \\ L_1 = L_3 \end{cases} \quad (3-13)$$

Such way reduces a number of the unknowns to four also. The second solution is not as flexible as the first one, because it provides only one type of the rejection performance solution for the assigned passband. It's not possible to change notch positions without any impact on the passband characteristic. Nevertheless, as it will be shown below, this solution is most likely the best one.

Another possibility to reduce complexity of the system (3-12) is based on a well known issue that the transmission occurs by providing the sufficient matching. In other words, the equations 3 and 4 in the system (3-12) have the same meaning and the given system can be exchanged with the following one:

$$\begin{cases} \text{at } \omega \text{ notches} & \begin{cases} S_{21T} = 0 \\ S_{21D} \neq 0 \end{cases} \\ \text{at } \omega \text{ passband} & \begin{cases} S_{21} \geq 1/\sqrt{2} \end{cases} \end{cases} \quad (3-14)$$

Now the system (3-13) represents much more flexible field of solutions, because there are three equations and six unknown elements. It results in a range of bandpass characteristics. But this system has to be carefully used assuming passband ripples, which behavior and magnitude can be random.

Let's start with the solving process on the third equation from (3-13) which corresponds for transmission in passband. The same dividing on term and denominator of the fraction as in (3-7) will be implemented and the equation will take the following form:

$$\sqrt{2} \cdot S_{21T} \geq S_{21D} \quad (3-15)$$

In order to detect only the borders of the passband equation (3-13) is transformed into:

$$\sqrt{2} \cdot S_{21T} = S_{21D} \quad (3-16)$$

By substituting these variables from the (3-7) the following equation can be achieved:

$$\begin{aligned}
& 2\sqrt{2} \cdot Y_0(1 - \omega^2 L_2(C_3 + C_1(1 + C_3 \omega^2(-L_1 - L_3 + C_2 L_1 L_3 \omega^2)))) = 2 \cdot Y_0 - j \omega(C_3 \\
& + Y_0^2(L_1 + L_3)) + Y_0 \omega^2 C_3(L_1 + 2L_2 + L_3) + j Y_0^2 \omega^3 L_2 C_3(L_1 + L_3) + \omega C_2(Y_0 \omega L_1 - \\
& j)(1 + j Y_0 \omega L_3 - \omega^2 C_3(L_2 + L_3 + j Y_0 \omega L_2 L_3)) + \omega C_1(-j + \omega Y_0(L_1 + 2L_2 + L_3) + j \\
& Y_0^2 \omega^2 L_2(L_1 + L_3) + Y_0 \omega L_1 - \omega^2 C_3(L_1 + L_3)(2 Y_0 \omega L_2 - j) + \omega^2 C_2(-L_2(Y_0 \omega L_3 + j \\
& (\omega^2 L_3 C_3 - 1)) + L_1(j(j - Y_0 \omega L_2)(Y_0 \omega L_3 - j) + \omega^2 C_3(2 Y_0 \omega L_2 L_3 - j(L_2 + L_3))))))
\end{aligned} \quad (3-17)$$

Reduction of the equation to the equal items, like a frequency with equal power gives us the following equation:

$$\begin{aligned}
& -\omega^6 \cdot 2(1 + \sqrt{2}) Y_0 L_1 L_2 L_3 C_1 C_2 C_3 - j \omega^5 C_2(C_1 C_3(L_1 L_2 + L_2 L_3 + L_1 L_3) + Y_0^2 L_1 L_2 \\
& L_3(C_1 - C_2 C_3)) + \omega^4 Y_0((1 + 2\sqrt{2}) L_2 C_1 C_3(L_1 + L_3) + C_1 C_2(L_1 L_2 + L_2 L_3 + L_1 L_3) \\
& - C_2 C_3(-L_1 L_2 + L_2 L_3 - L_1 L_3)) - \omega^3(Y_0 C_1^2(2L_1 + 2L_2 + L_3) + j(Y_0^2((C_1 + C_3)(L_1 \\
& L_2 + L_2 L_3) + L_1 L_3 C_2) + C_1 C_2(L_1 + L_2) + C_2 C_3(L_2 + L_3) + C_1 C_3(L_1 + L_3))) - \omega^2 \\
& Y_0(2\sqrt{2} \cdot L_2(C_1 + C_3) + C_2(L_1 + L_3) + C_3(L_1 + 2L_2 + L_3)) + j \omega(C_1 + C_2 + C_3 + \\
& Y_0^2(L_1 + L_3)) + 2(1 + \sqrt{2}) Y_0 = 0
\end{aligned} \quad (3-18)$$

Using the condition (3-13), the obtained equation transforms into the next simpler one:

$$\begin{aligned}
& 2(1 + \sqrt{2}) \omega^6 Y_0 L_1^2 L_2 C_1^2 C_2 - j \omega^5 L_1 C_1 C_2(C_1(L_1 + 2L_2) + 2Y_0^2 L_1 L_2) - \omega^4 Y_0 L_1 C_1 \\
& (4L_2 C_2 + 2L_1 C_2 + 2(2 + \sqrt{2}) L_2 C_1) + j \omega^3(2L_2 C_1 C_2 + 2L_1 C_1(C_1 + C_2) + Y_0^2 L_1 \\
& (L_1 C_2 + 4L_2 C_1)) + 2\omega^2 Y_0(L_1 C_2 + (2 + \sqrt{2}) L_2 C_1 + 2L_1 C_1) - j \omega(2C_1 + C_2 + 2Y_0^2 \\
& L_1) - 2(1 + \sqrt{2}) Y_0 = 0
\end{aligned} \quad (3-19)$$

Left side of the equation can be observed as a complex value with the following form:

$$A + jB = 0 \quad (3-20)$$

This issue simplifies the solution process, because it can be separated into two parts, where both real and imaginary part must be equal to zero:

$$A = 0 \quad (3-21)$$

$$B = 0$$

where

$$\begin{aligned}
A = & 2(1 + \sqrt{2}) \omega^6 Y_0 L_1^2 L_2 C_1^2 C_2 - \omega^4 Y_0 L_1 C_1(4L_2 C_2 + 2L_1 C_2 + 2(2 + \sqrt{2}) L_2 C_1) + \\
& + 2\omega^2 Y_0(L_1 C_2 + (2 + \sqrt{2}) L_2 C_1 + 2L_1 C_1) - 2(1 + \sqrt{2}) Y_0
\end{aligned} \quad (3-22)$$

$$\begin{aligned}
B = & j \omega^5 L_1 C_1 C_2(C_1(L_1 + 2L_2) + 2Y_0^2 L_1 L_2) - j \omega^3(2L_2 C_1 C_2 + 2L_1 C_1(C_1 + C_2) + \\
& Y_0^2 L_1(L_1 C_2 + 4L_2 C_1)) + j \omega(2C_1 + C_2 + 2Y_0^2 L_1)
\end{aligned} \quad (3-23)$$

Let's exchange the frequency variable in the equation (3-22) with a parameter p like it shown below:

$$p = \omega^2 \quad (3-24)$$

Such exchange procedure makes it possible to reduce an order of the equation to number four:

$$2(1 + \sqrt{2})p^4 Y_0 L_1^2 L_2 C_1^2 C_2 - p^2 Y_0 L_1 C_1 (4L_2 C_2 + 2L_1 C_2 + 2(2 + \sqrt{2})L_2 C_1) + 2p Y_0 (L_1 C_2 + (2 + \sqrt{2})L_2 C_1 + 2L_1 C_1) - 2(1 + \sqrt{2})Y_0 = 0 \quad (3-25)$$

The equation for B (3-23) is split into two equations and meets automatically the first solution – zero frequency:

$$\begin{cases} \omega = 0 \\ \omega^4 L_1 C_1 C_2 (C_1 (L_1 + 2L_2) + 2Y_0^2 L_1 L_2) - \omega^2 (2L_2 C_1 C_2 + 2L_1 C_1 (C_1 + C_2) + Y_0^2 L_1 (L_1 C_2 + 4L_2 C_1)) + (2C_1 + C_2 + 2Y_0^2 L_1) = 0 \end{cases} \quad (3-26)$$

The same exchange procedure as the one implemented in (3-24) has to be done using parameter q:

$$q = \omega^2 \quad (3-27)$$

Finally, the equation order is reduced to number two, that simplifies the calculation procedure:

$$q^2 L_1 C_1 C_2 (C_1 (L_1 + 2L_2) + 2Y_0^2 L_1 L_2) - q (2L_2 C_1 C_2 + 2L_1 C_1 (C_1 + C_2) + Y_0^2 L_1 (L_1 C_2 + 4L_2 C_1)) + (2C_1 + C_2 + 2Y_0^2 L_1) = 0 \quad (3-28)$$

In order to solve the equation, the discriminant has to be calculated with the followed equation:

$$D = (2L_2 C_1 C_2 + 2L_1 C_1 (C_1 + C_2) + Y_0^2 L_1 (L_1 C_2 + 4L_2 C_1))^2 - 4L_1 C_1 C_2 (C_1 (L_1 + 2L_2) + 2Y_0^2 L_1 L_2) (2C_1 + C_2 + 2Y_0^2 L_1) \quad (3-29)$$

And the solution for q will be:

$$q = \frac{(2L_2 C_1 C_2 + 2L_1 C_1 (C_1 + C_2) + Y_0^2 L_1 (L_1 C_2 + 4L_2 C_1)) \pm \sqrt{D}}{2}$$

Frequency to be found can be calculated with the equation, derived from (3-27):

$$\omega = \sqrt{q} \quad (3-30)$$

Thus, the criterion for the solutions considering only real values has to be as the followed one:

$$\begin{cases} D \geq 0 \\ q \geq 0 \end{cases} \quad (3-31)$$

Based on combination of this passband criterion (3-31) together with the notches criterion (3-9) all element values can be found. The typical values for WLAN / WiMAX 5 GHz passband filter are shown below:

$$\begin{aligned} C_1 &= 4.78 \text{ pF} & L_1 &= 0.14 \text{ nH} \\ C_2 &= 2.52 \text{ pF} & L_2 &= 0.47 \text{ nH} \\ C_3 &= 4.78 \text{ pF} & L_3 &= 0.14 \text{ nH} \end{aligned} \quad (3-32)$$

The passband boundaries can be achieved by substituting the values in (3-26). The circuit provides a transmission at DC automatically and the calculated passband is confined with frequencies:

$$\begin{aligned} f_1 &= 4.35 \text{ GHz} \\ f_2 &= 6.25 \text{ GHz} \end{aligned} \quad (3-33)$$

The positions of notch frequencies could be derived from the equation (3-10) and they are:

$$\begin{aligned} f_1 &= 2.6 \text{ GHz} \\ f_2 &= 7.4 \text{ GHz} \\ f_3 &= 9.0 \text{ GHz} \end{aligned} \quad (3-34)$$

Characteristics of the filter with assigned elements are depicted in Fig. 3.8b. As it's shown, the transmission exists at DC and at 5 GHz band. The notches are situated from the both sides of the passband.

An advantage of the filter based on the circular currents functionality is obvious in comparison with the standard filter, which function is defined using direct currents. Both filters are built using the same schematic, nevertheless, one of them is BSF and the another one is BPF. The BSF provides rejection at the frequency band with center frequency 9 GHz, while a suppression of the BPF is not confined only with the same band at 9 GHz. The suppression is gained with the additional notches at 2.6 GHz and 7.4 GHz with the corresponding transmission at 5 GHz WLAN / WiMAX band. Thus, the new filter uses all of the proposed schematic potential possibilities. The BSF needs additional filtering in order to reach the bandpass characteristics, which results in size increasing of the component. Therefore, the miniaturization process implemented in the new filter is not a result of the technological process implementation, a rational use of the schematic based on a new conception is assumed as a basis.

The performed analysis operates with the mathematical apparatus, which doesn't provide an overview of the physical processes inside the filter. Therefore it's not clear what type of the currents exists inside the structure. Why did the assumption about the circular currents occur? In order to analyze this issue, the following procedure was used.

The complete 1st-order transversal / recursive filter with the element values obtained in (3-32) is used a structure for the analysis. Two current types are running inside the filter – clockwise and counterclockwise currents. It is reasonable to investigate the currents flow at the output and their interactions with each other that is finalized in the filter performance. At the output node, currents are split into four parts – incident CW, incident CCW, reflected CW and reflected CCW, as it shown in Fig. 3.7a. Detecting these currents is not a trivial task. A directional coupler should be the best device to define the direction and the value of the current flowing in this direction. Unfortunately, the coupler put into the circuit would have an influence on the performance, therefore a device is needed which doesn't

bring any disturbance into the circuit. Such device doesn't exist in reality; therefore the ideal element was implemented into the structure. As it's shown in Fig. 3.7b, the additional ideal device named "Dual Power Sampler" (DPS) is connected in series with each pass to monitor the current flows.

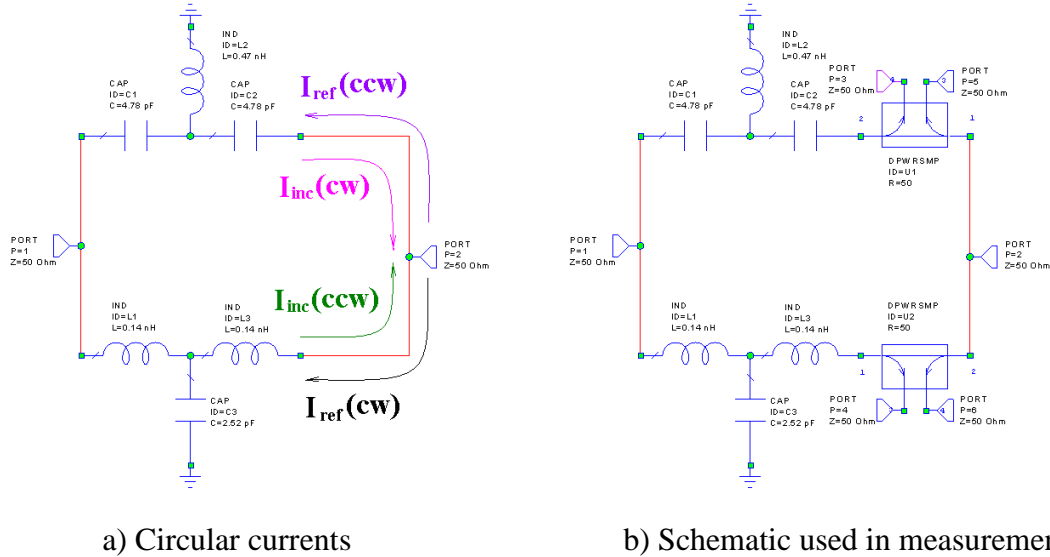
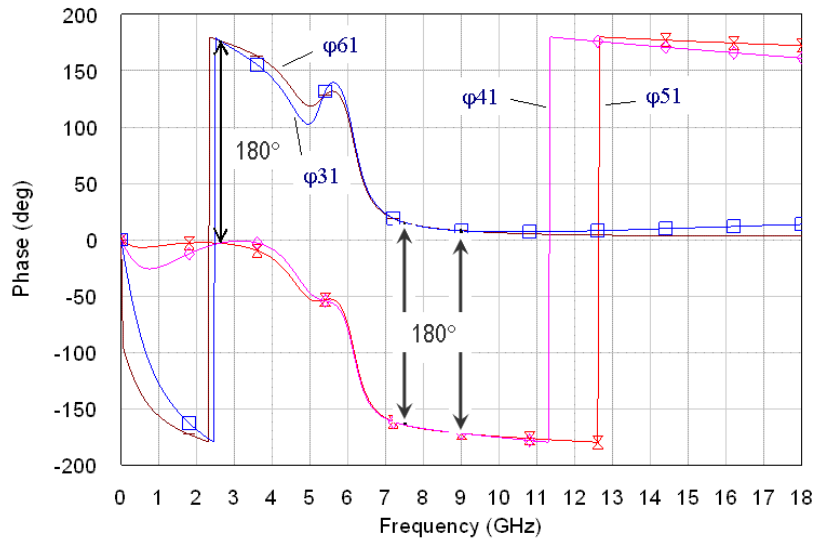
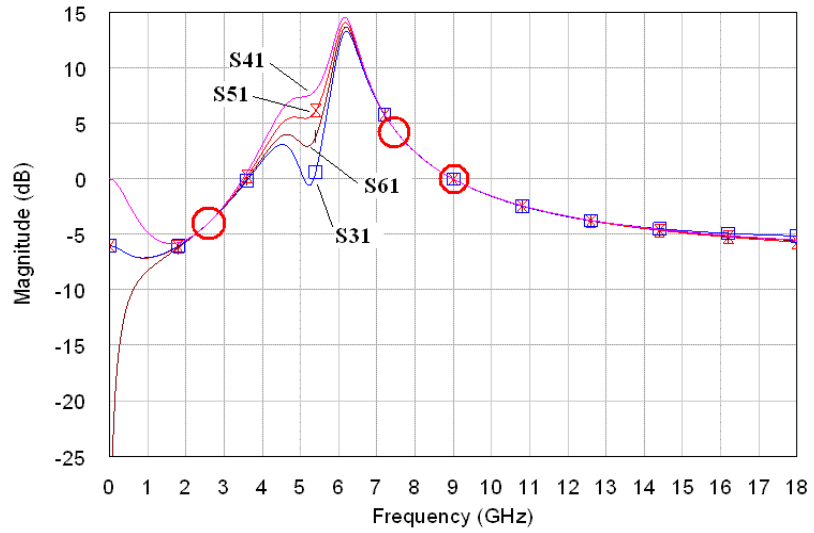


Figure 3.7: Circulating currents analysis (simulated using Microwave Office [14])

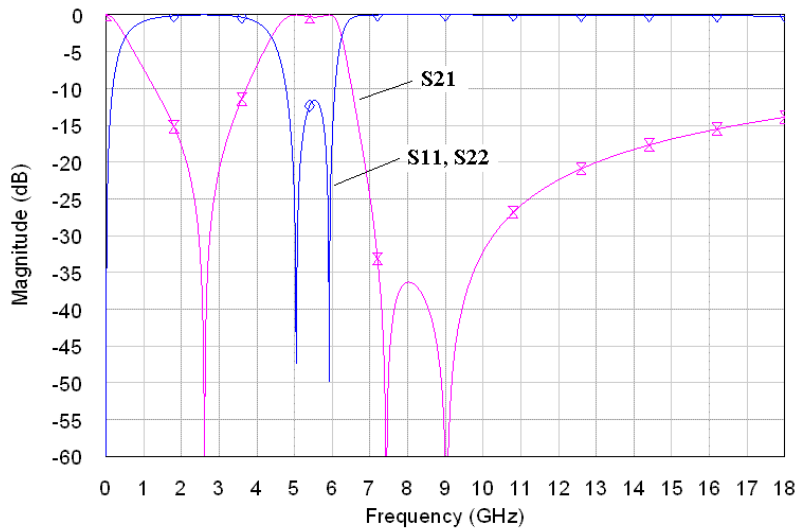
DPS implies two lossless and frequency independent directional couplers. The S-matrix of DPS is:

$$[S]_{DPS} = \begin{bmatrix} 0 & 1 & 0 & 0 \\ 1 & 0 & 0 & 0 \\ 1 & 0 & 0 & 0 \\ 0 & 1 & 0 & 0 \end{bmatrix} \quad (3-35)$$

The sampler is full compatible with the set task, because it passes a signal through without losses and reflections, simultaneously couples the signal for measurement without losses, too. The currents cyclically rotate inside the structure and each of the power samplers counts the sum of all signals transmitted through it in selected direction. Thus the system can be tested without disturbances on its functionality. The signals circulate inside the circuit and each port (3, 4, 5 and 6) gathers power of the signal flowing in corresponding direction. For example, port 3 counts all reflected from the output CCW signals, port 4 counts all incident CCW signals, etc. The results of the counting (magnitude and phase of the excited in port 1 signals) are depicted in Fig. 3.8a. The magnitude values lie above the 0 dB level, because the countless number of summing signals is flowing through the DPS. Superposition of these signals at the output node gives resulting output signal (Fig. 3.8b). The notches appear at that frequency points where signals are equal in amplitude and opposite in phase. Three zero transmissions at frequencies 2.6, 7.4 and 9 GHz (the same ones as calculated before (3-34)) build the rejection characteristic of the filter. There is a wide frequency range from 7 to 18 GHz with roughly equality of the



a) Counted circular signals



b) Superposition of the circular signals at the output node

Figure 3.8: Characteristics of the structure from the Fig. 3.7b (simulated using [14])

circular current amplitudes and with close to 180 degree phase difference. This frequency range is distinguished with the high suppression (more than 15 dB) providing good 2nd harmonic rejection (more than 20 dB) and sufficient higher harmonics rejection.

Thus the simple measuring technique has proved an existing of the circular currents inside the structure and their contribution into the system functionality.

3.3 Synthesis Procedure of the Filter

The analysis procedure described above assumes that the values of all lumped elements in the filter circuit are known and number of the notches and its positions were proved based on these data. It's reasonable for the practical realization also vice-versa procedure – synthesis. The procedure is based on finding the circuit parameters (L, C element values) corresponding to the given frequency specification. It consists of several steps. Firstly, a number of the notches has to be defined accordingly to the specified rejection characteristics. Afterwards, corresponding schematic has to be built, which transmission criterion (3-9) covers this number of the transmission zeros (N). Based on the calculated S-parameters, the system equation (3-14) has to be solved. The solution of the equations will be the frequency points which depend on the circuit element values. These frequencies are the passband boundaries (P) and the notch positions (N). Thus, the new equations system is achieved and it's comprised of $W = P + N$ frequency dependent equations with M lumped element variables inside that must be found. There are three possible cases. The first one occurs if $M < W$, in such situation there is no freedom for appropriate solution, because of not sufficient number of the variables. Physically, the notch frequencies are interdependent and it's not possible to put all of them on fix defined positions. Second variant would happen if $M = W$, it means that only one solution for the element variables exists assuming the given frequencies. The inequality $M > W$ is typical for the third case. It provides freedom by choosing the element values. A number of the element values could be assigned until the condition $M = W$ becomes true. Afterwards, the procedure used in the second case will be implemented.

Optimal solution would be the second case, because it gives a network with a minimum number of the required lumped elements, which can solve the problem. Let's consider the case described in the analysis. The task is to build a filter that provides characteristics shown in Fig. 3.8b. Accordingly to a number of the notches, which is equal to 3, we have to provide a network which will satisfy following requirements given in (3-10) – the equation must have a frequency powered maximum with six. Thus, the complexity of the circuit will be increasing until the following requirements will be met:

$$F(\omega^{2N}) = 0 \quad (3-36)$$

where N - is the number of the notches defined above.

Thus the first part of the final equation system, which solutions correspond to the notch positions, is obtained and it has the following form:

$$\begin{cases} \omega_1 = F(L_1, L_2, \dots, L_A, C_1, C_2, \dots, C_B) \\ \omega_2 = F(L_1, L_2, \dots, L_A, C_1, C_2, \dots, C_B) \\ \dots \\ \omega_N = F(L_1, L_2, \dots, L_A, C_1, C_2, \dots, C_B) \end{cases} \quad (3-37)$$

where A – is a number of inductances (L) in the circuit; B – is a number of capacitors (C) in the circuit.

In addition, boundary of the passband can be found by solving the following equation system:

$$\begin{cases} \omega_{N+1} = F(L_1, L_2, \dots, L_A, C_1, C_2, \dots, C_B) \\ \omega_{N+2} = F(L_1, L_2, \dots, L_A, C_1, C_2, \dots, C_B) \end{cases} \quad (3-38)$$

The equation systems (3-37) and (3-38) must be combined and solved together in order to get complete solution for the elements providing defined filter performance. This final equation system would be:

$$\begin{cases} \omega_1 = F(L_1, L_2, \dots, L_A, C_1, C_2, \dots, C_B) \\ \omega_2 = F(L_1, L_2, \dots, L_A, C_1, C_2, \dots, C_B) \\ \dots \\ \omega_N = F(L_1, L_2, \dots, L_A, C_1, C_2, \dots, C_B) \\ \omega_{N+1} = F(L_1, L_2, \dots, L_A, C_1, C_2, \dots, C_B) \\ \omega_{N+2} = F(L_1, L_2, \dots, L_A, C_1, C_2, \dots, C_B) \end{cases} \quad (3-39)$$

If all frequencies are defined, the last step will be finding the unknown circuit lumped elements.

3.4 Practical Realization

The simplest 1st-order transversal / recursive filter described above proves implementation possibility of the filters using the circular currents. It's not used in practice to provide DC transmission through the filter. The easiest way to avoid the DC transmission is to put into the both passes DC-blocking circuits. Another weakness of the filter prototype lies in a small attenuation far from the passband on both sides. It is obvious that three notches are not able to form wide enough attenuation bands, for example, from DC to 4 GHz and from 7 to 18 GHz simultaneously. In order to get a filter with better performance, an additional improvement has to be done - using either higher order filter or more complicated passes. Let's realize the second conception – to put the additional T-networks into each of the passes as it shown in Fig. 3.9.

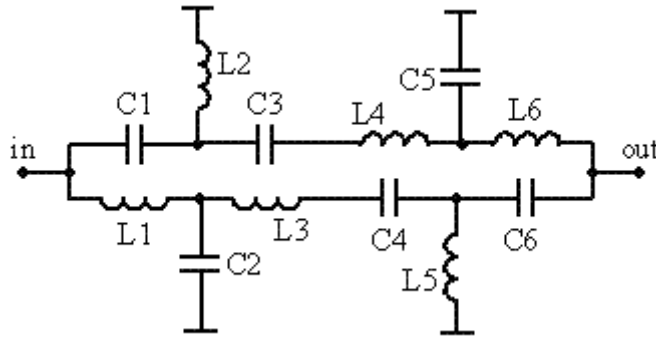


Figure 3.9: 1st-order lumped-element transversal / recursive filter with improved characteristics

Such filter configuration automatically excludes DC transmission and doubles potential number of the transmission zeros. It could be seen from the equation (3-10) for the simplest 1st-order filter that the frequency variable is powered by 6. An analogous equation for the filter proposed in Fig. 3.9 will contain frequency in power 12, which corresponds to the maximum number of the possible notches equal to 6. This number of the notches is already enough to produce sufficient passband characteristics. An example of the filter performance for the WLAN / WiMAX 5 GHz band is shown in Fig. 3.10. The filter was simulated with the ideal lumped elements without losses. In comparison with simple 1st-order filter which characteristics are shown in Fig. 3.8b, the improved one provides much better suppression from both sides of the passband. The higher order harmonics are suppressed more than 25 dB and WLAN / WiMAX low bands together with cellular bands are rejected more than 30 dB.

Thus the transversal / recursive filter with order number 1 is already able to satisfy BPF requirements. For some special implementation, it could be not enough steep slope providing rejection close to the passband. This is the case when the filter with higher order has to be used, because the better steepness can be achieved only by including the additional parallel pass.

The relative passband covered by the filter (Fig. 3.10) in this case is about 20 %. But the filter functionality is not confined with it. In general, it can be used for enormous variety of implementations. For instance, realized relative passband can achieve 100 % and more. This issue could be useful for ultra-wideband (UWB) applications. Such filter was simulated (Fig. 3.11a) and its characteristics are shown in Fig. 3.11b. Transmission band of the filter lies inside standard UWB band – from 3.1 GHz to 10.6 GHz. The filter structure now contains not just the simple LPF and HPF T-chains like in the previous design, now a different combination optimized for this special solution is used. The simulation is based also with ideal LC-elements without losses.

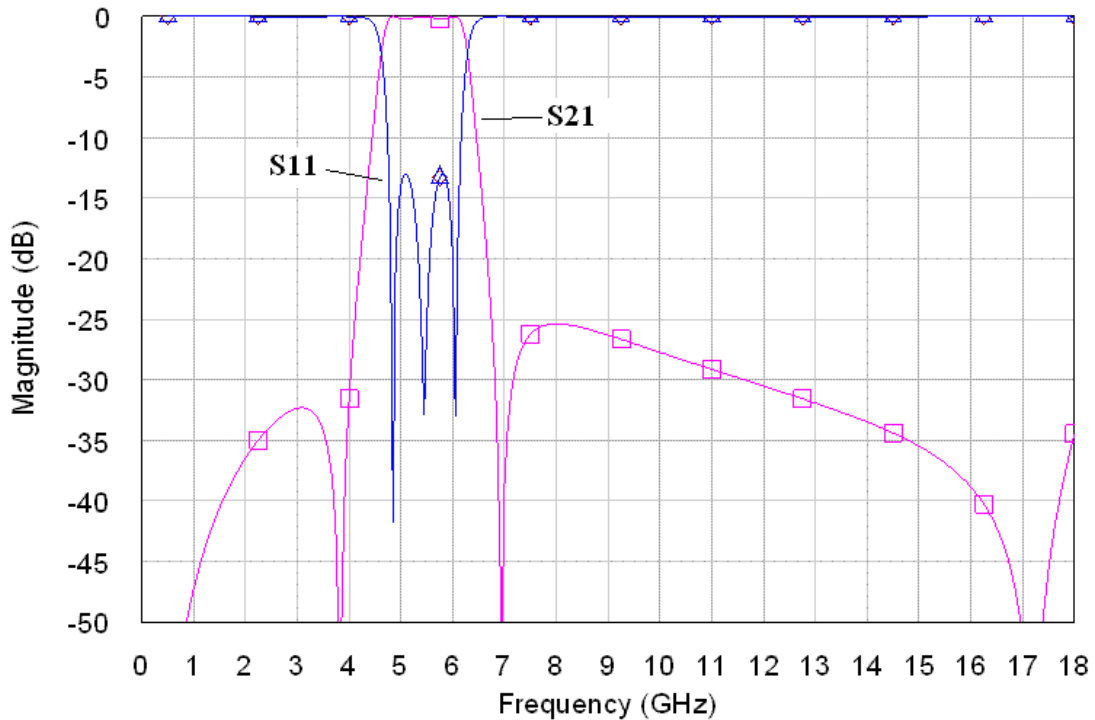
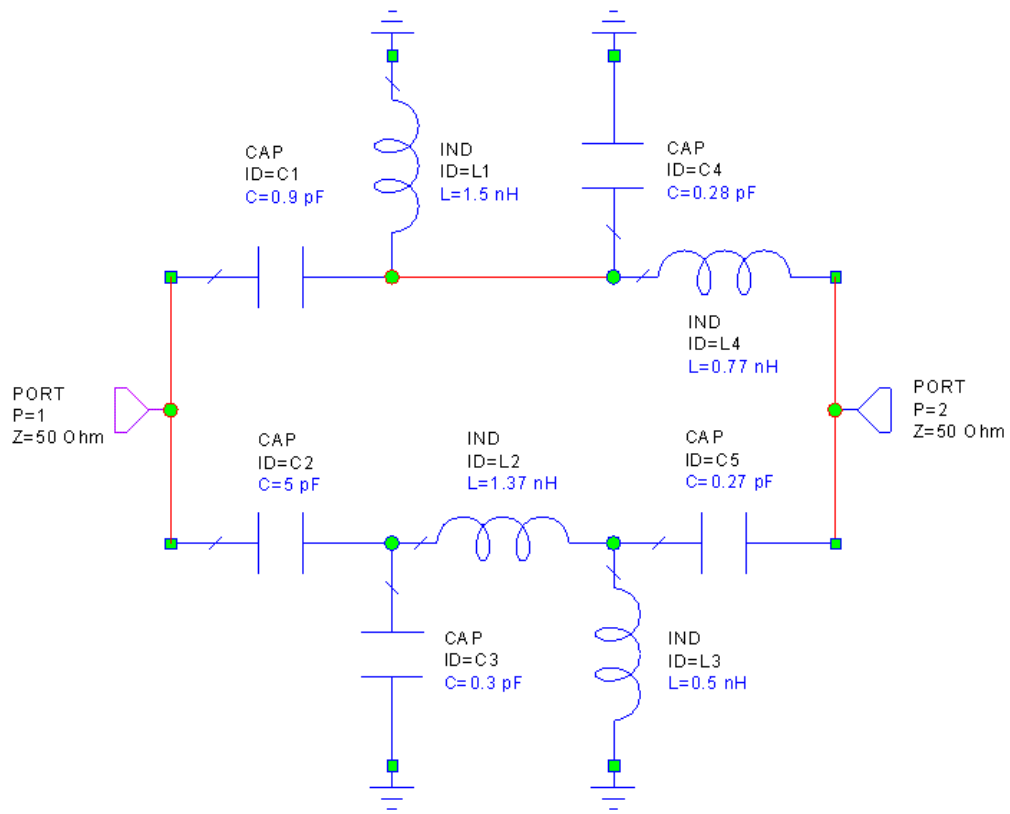


Figure 3.10: Characteristics of the improved 1st-order transversal / recursive filter (simulated using Microwave Office[14])

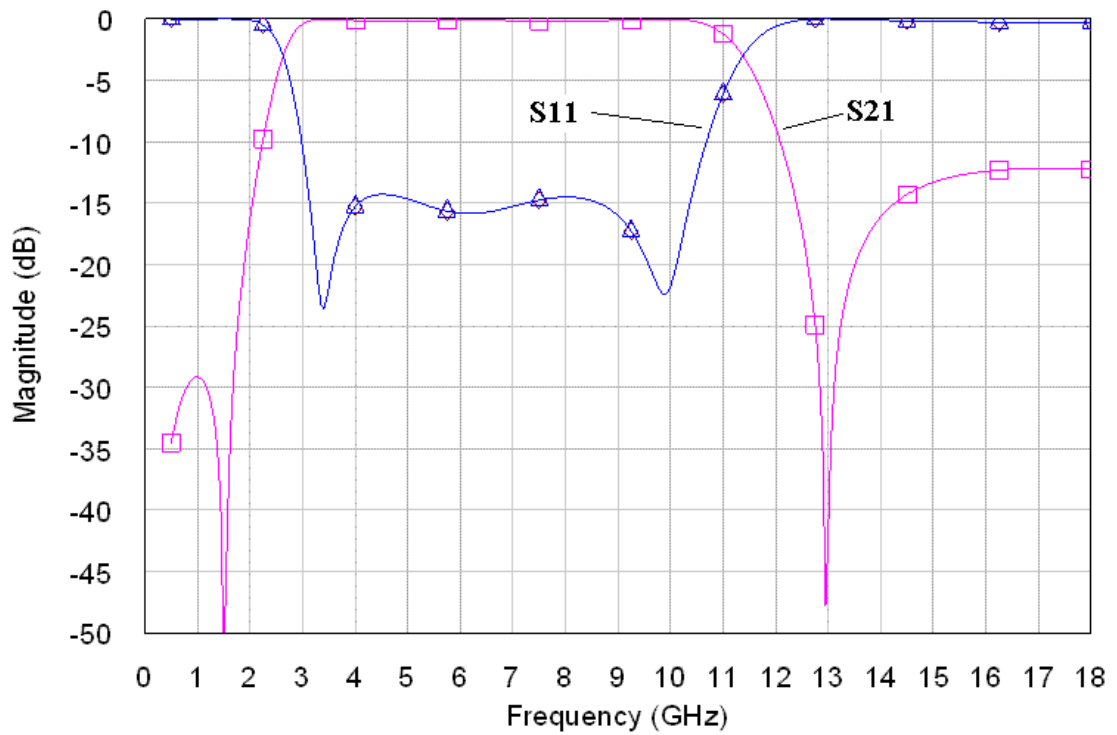
The WLAN / WiMAX filter depicted in Fig. 3.9 has been implemented using LTCC technology. The LTCC substrate parameters are: $\epsilon_r = 7.8$, $\tan\delta = 0.003$, $\sigma = 3 \cdot 10^7$ S/m, layer thickness = 50 μm . 3D view of the structure is shown in Fig. 3.12. Component size is 1.9 x 1.0 x 0.8 mm³, which is typical for BPFs using this frequency band.

Two types of the filter were fabricated and measured. A comparison of the simulations done by Sonnet [15] with the measurements is shown in Fig. 3.13. The first variant of the filter was optimized for better low frequency suppression (Fig. 3.13a) and the second one provides better harmonic rejection characteristics (Fig. 3.13b). Each of the filter characteristics operates with 6 notches – maximal achievable number of zero transmissions in this structure. Five notches implemented in variant 1 are situated inside 18 GHz band and the last one lies at higher frequencies. Characteristics of the filter in variant 2 possess all six notches inside 18 GHz band, though the last notch which positioned near from 16 GHz is not strong pronounced. Assuming such wideband suppression, the insertion loss of the filter is lower than 1.5 dB.

The low frequency characteristics and the passband one are good agreed with simulations due to avoidance of parasitic effects at these frequencies. Parasitic effects (mostly like intercouplings) appear on higher frequencies and slightly change the performance. Nevertheless, it doesn't make a big influence on overall appearance.



a) Schematic



b) Transmission characteristics

Figure 3.11: UWB 1st-order transversal / recursive filter (simulated using Microwave Office [14])

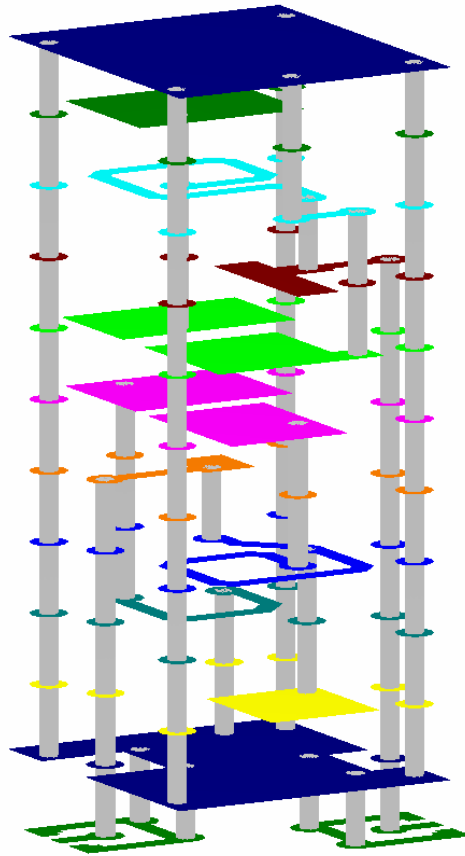


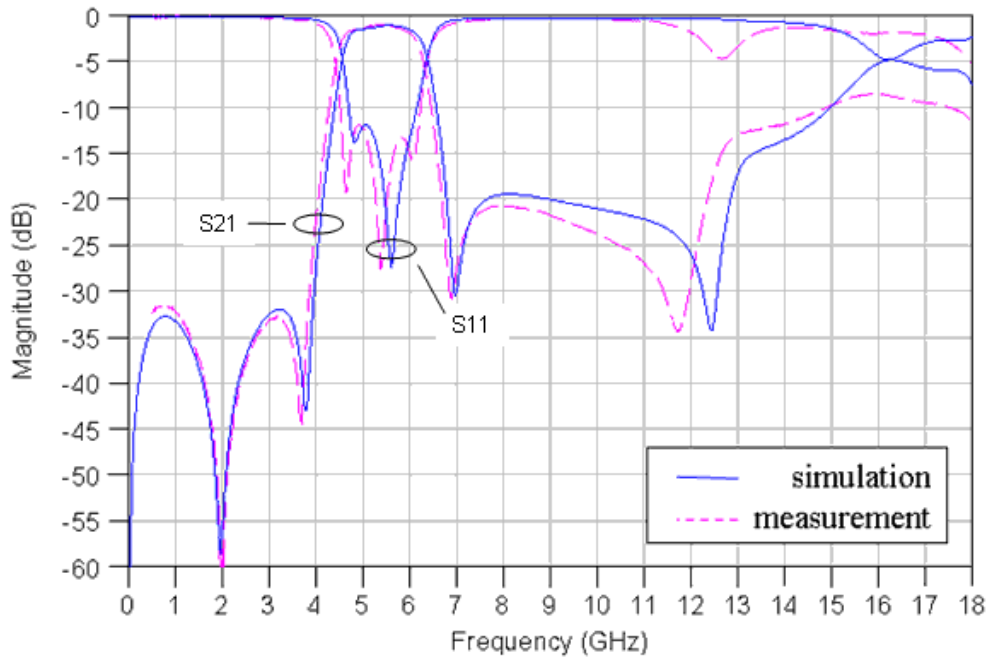
Figure 3.12: 3D view of the WLAN / WiMAX BPF (drawn using Sonnet [15])

3.5 Results on the Filter Design

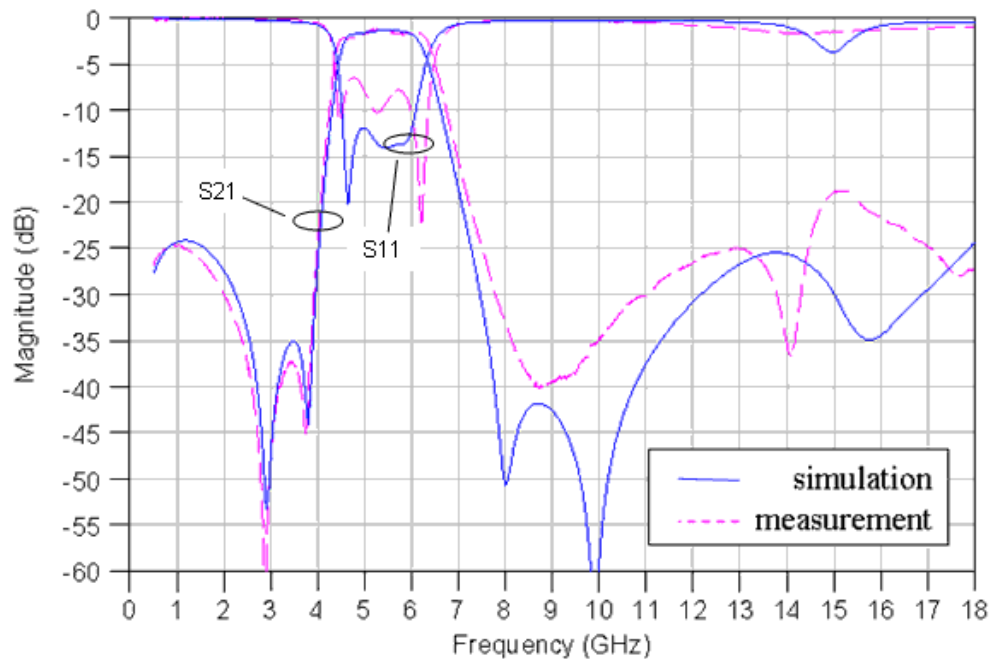
The new transversal / recursive filter conception has been presented. The filter avoids all problems of transversal filters realization using LTCC substrate. It is distinguished with its simplicity, absence of any active components and any large structures like a couplers or transmission lines. In comparison with the filter using directional current transmission, which looks similar, the proposed filter uses circular transmission that improves performance dramatically and utilizes the structure area much effective. The filter is very flexible and could be used in various implementations.

The filter provides low insertion loss with good enough suppression characteristics. The filter structure can be realized easily using multilayer LTCC substrate. For example, 5 GHz filter for WLAN is fitted in a package with size of $1.9 \times 1.0 \text{ mm}^2$. The characteristics are not worse than ones of standard resonator filters, sometimes even better.

The calculation method used in this part of the work can be implemented for all structures contained parallel interconnected chains. A common case could be filters with cross couplings, which synthesis procedure is based on iteration character. The method provides the straight forward synthesis procedure.



a) Type 1



b) Type 2

Figure 3.13: Simulation (using [15]) vs. measurements of the proposed transversal filter with different elements values (plotted using Microwave Office[14])

3.6 References to Chapter 3

- [1] C. Rauscher, "Microwave active filters based on transversal and recursive principles," *IEEE Transactions on Microwave Theory and Techniques*, vol. MTT-33, No.12, Dec. 1985, pp. 1350–1360.

- [2] W. Menzel and U. Vetter, "Passive and active microwave filter design using transversal filter principles," *Proceedings on European Microwave Conference*, Oct. 2000, pp. 1-4.
- [3] W. Mouzannar, L. Billonnet, B. Jarry and P. Guillon, "A new design concept for wideband frequency-tunable and high order MMIC microwave active recursive filters," *Microwave and Optical Technology Letters*, vol. 24, No. 6, Mar. 2005, pp. 380-385.
- [4] L. Billonnet, B. Jarry and P. Guillon, "Microwave recursive and transversal active filters using lange couplers," *Proceedings on European Microwave Conference*, Sept. 1992, pp. 5-9.
- [5] T. Hiratsuka and E. Ogawa, "A Ku-band transversal filter using directional couplers made of a multilayer ceramic," *IEICE Transactions on Electronics*, vol. E78-C, No. 8, Aug. 1995, pp. 1134-1138.
- [6] V. Pommier, D. Cros, P. Guillon, A. Carlier and E. Rogeaux, "Transversal filter using whispering gallery quarter cut resonators," *IEEE MTT-S International Microwave Symposium Digest*, vol. 3, Jun. 2000, pp. 1779 - 1782.
- [7] D. C. Rebenaque, F. Q. Pereira, J.L. Tornero, J. P. Garsia and A.A. Melcon, "Two simple implemetations of transversal filter with coupling between non-resonant nodes," *IEEE MTT-S International Microwave Symposium Digest*, vol. 2, Jun. 2005, pp. 957-960.
- [8] S. Jovanovich and A. Nesich, "New filter type suitable for miniature printed bandpass filters at RF and microwave frequencies," *Proceedings on European Microwave Conference*, Oct. 2005, 4 pp.
- [9] R. Kravchenko, D. Orlenko, et al., "Band-pass Filter," *Patent*, WO2006DE1695A, Sept. 2005.
- [10] C.-Y. Hsu, C.-Y. Chen and C. H. Huang, "The UWB filter using dual-mode ring resonator with spurious passbands suppression", *Proceedings on International Conference on Systems and Signals ICSS*, Apr. 2005.
- [11] A. Kundu and N. Mellen, "Miniaturized Multilayer Bandpass Filter with Multiple Transmission Zeros," *IEEE MTT-S International Microwave Symposium Digest*, pp. 760-763, Jun. 2006, pp. 760-763.
- [12] W. Wendel and M. Blind, "Bandstop filter (Bandsperre)," *Patent*, DE3304776, 1984.
- [13] D. K. Misra, "Radio-frequency and microwave communication circuits: Analysis and design," Ed. New York, NY: John Wiley & Sons Inc., 2001, p.288.
- [14] AWR Microwave Office Software Inc. v. 9.02r, 2010.
- [15] Sonnet Software Inc. v.12.52, 2010.

4. A New Ultra-Wideband Power Divider

A power divider is one of the important elements in RF systems. It's required in many applications using balanced power amplifiers, balanced mixers, data modulators, phase shifters and antenna systems. Regarding the phase difference between the output ports, power dividers can be classified into two types: the in-phase dividing splitter and the 180° out-of-phase one. Power dividers are subdivided by realization into types: resistive, transmission line, coupled lines, lumped element and mixed structures. The simplest power divider is resistive; unfortunately it possesses more losses than the other types. The transmission line splitters are easy to realize using different technologies, but require a space. The lumped element structures represent equivalent circuits of the transmission line dividers, but their characteristics are pared-down. The advantage of the splitter using coupled lines refers to the ability of controlling the working bandwidth by varying the circuit parameters.

A lot of work on splitters has been done already. The most famous power divider is Wilkinson divider due to its clear functionality and simple design. Basic design of the splitter is the described in [1]. It provides not enough wide passband in some applications, assuming narrowband performance of quarter-wave TL transformers. A large amount of investigations on the bandwidth of Wilkinson splitter is done and some typical of them can be observed in the following literature [2] - [10]. The power combiner has been also presented with lumped elements instead of TLs [11] - [13], but a relation between the bandwidth and the output ports isolation of these samples is unsuitable. Last jump in a splitter design considers hybrid of Wilkinson divider with tuning parallel stubs; this solution provides dramatically enlarging of the bandwidth and a decreasing number of sections in the power divider [14] – [17]. Unfortunately, some successful results achieved during the improvements provide either negligible passband extension or large and complicated component realization that makes it impossible for high level miniaturization. Moreover, Wilkinson divider is not compatible to be integrated using LTCC technology, because of the structure specific based on 2-dimensional representation.

Another type of widespread power dividers is the coupled-line splitters [18] – [20]. They provide wider passband characteristics in comparison with the common Wilkinson divider. Moreover, the passband width can be controlled with coupling coefficient, where increasing of the coupling corresponds to the bandwidth maximizing. It makes a big problem by miniaturization using LTCC technology, because of impossibility to achieve

very tight coupling. On the other hand, the miniaturization process results in narrowing the transmission characteristics that cancels the advantage of the splitter.

The new proposed in-phase power divider design [21], [22] represents new schematics based on a coupled-line structure that provides power division in a wide frequency band. It's not necessary to aspire for getting the most achievable tight coupling in order to get maximum of the bandwidth by using the new splitter. The condition providing the best function is the optimal coupling value.

4.1 Power Divider Concept

The proposed structure of the coupled-line power divider is based on a standard design of Marchand balun [23] shown in Fig. 4.1a (depicted ports 1 and 2, 3 represent the input and the outputs of the circuit correspondingly). CTL1 and CTL2 depicted in the figure – are the first and the second coupled transmission line sections terminated on open circuit (o.c.). It's clear that function of a balun is very similar to function of a splitter. Characteristics of a balun assume symmetrical (concerning two outputs) transmission – 3 dB insertion loss (dividing ratio by 2) with 180° phase difference between output signals (resides in a balun meaning). On the other hand, a splitter provides division of a signal into 2 parts that corresponds to the same 3 dB losses, while phase difference can be 0° or 180° depending on the power divider. Thus, a common balun could be observed as a power divider. However, there is one significant difference between a balun and a power combiner that lies in a balun function. As it's well known, 3-port lossless reciprocal network can't be perfectly matched with loads from all 3 ports simultaneously [24]. This issue doesn't disturb a balun function – the single-ended input port is perfectly matched, while the single-ended output ports are not matched. At the same time, the balanced port impedance measured between the ports 2 and 3 is also perfectly matched with the balanced load. To the contrary, every single-ended port of the power divider must be matched. A matching network with lossy elements must be used for this purpose. Therefore, the structure shown in Fig. 4.1b is just a basement for the splitter design, which suffers several add-ons defined below.

So getting back to the Marchand balun as a prototype for the new power divider, a new schematic of the basic structure for the splitter is derived. The task is to design an inphase (0° phase difference between the outputs) broadband power divider. In order to compensate 180° phase shift in the balun, the outputs positions were moved to opposite side and the open circuit was grounded to provide corresponding boundary conditions. A detailed analysis of the structure is described below.

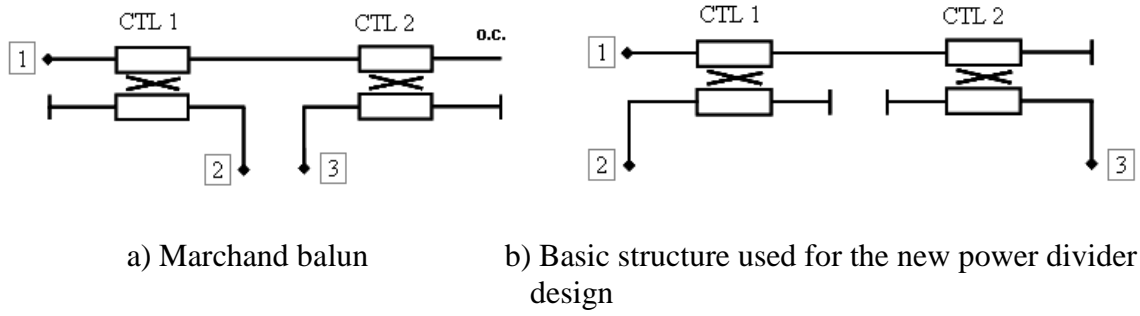


Figure 4.1: Structures based on coupled transmission lines

4.2 Implementation of the Splitter

The structure from Fig. 4.1b is comprised of two couplers connected with the primary line in series. It has been assumed for the analysis that we operate with the lossless elements and the couplers are backward-wave directional ones, the coupled lines are of the TEM type similar to striplines placed in a homogeneous dielectric medium and the even- and odd-mode characteristic impedances (Z_{0e} and Z_{0o}) of the lines as well as the phase constant (β) are properly chosen. Detailed schematic shown in Fig. 4.2 includes two couplers with the input / output ports (numbered from 1 to 8) and depicted incident (a) and reflected waves (b). The schematic is depicted in such a way that explains deriving the network S-parameters (4-1) from S-parameters of the single coupler (4-2) by using a principle of incident / reflected waves.

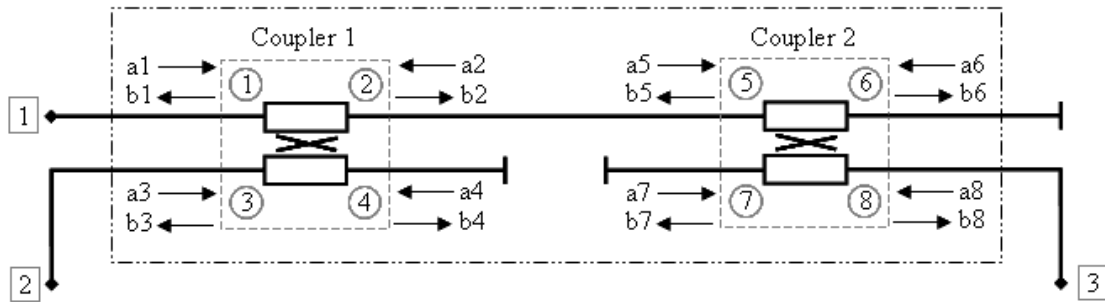


Figure 4.2: Detailed schematic of the basement for the splitter

$$[S]_{bPD} = \begin{bmatrix} S_{11}^{bPD} & S_{12}^{bPD} & S_{13}^{bPD} \\ S_{21}^{bPD} & S_{22}^{bPD} & S_{23}^{bPD} \\ S_{31}^{bPD} & S_{32}^{bPD} & S_{33}^{bPD} \end{bmatrix} \quad (4-1)$$

$$[S]_{Coupler} = \begin{bmatrix} S_{11}^C & S_{12}^C & S_{13}^C & S_{14}^C \\ S_{21}^C & S_{22}^C & S_{23}^C & S_{24}^C \\ S_{31}^C & S_{32}^C & S_{33}^C & S_{34}^C \\ S_{41}^C & S_{42}^C & S_{43}^C & S_{44}^C \end{bmatrix} \quad (4-2)$$

S-parameter matrix of the coupler given in [25]:

$$[S]_{\text{Coupler}} = \frac{j}{\sqrt{1-k^2} \cos \Theta + j \sin \Theta} \begin{bmatrix} 0 & -j\sqrt{1-k^2} & k \sin \Theta & 0 \\ -j\sqrt{1-k^2} & 0 & 0 & k \sin \Theta \\ k \sin \Theta & 0 & 0 & -j\sqrt{1-k^2} \\ 0 & k \sin \Theta & -j\sqrt{1-k^2} & 0 \end{bmatrix} \quad (4-3)$$

$$\text{where } k = \frac{Z_{0e} - Z_{0o}}{Z_{0e} + Z_{0o}} \text{ - coupling coefficient,} \quad (4-4)$$

$\Theta = \beta \cdot L$ (phase line length) and L - physical line length.

Taking into account a fact that maximum amount of coupling between the ports 1 and 3 (or between the ports 2 and 4, 5 and 7, 6 and 8) occurs if the couplers are comprised of the quarter-wave coupled sections:

$$L = \frac{\lambda_g}{4} \text{ or } \Theta = \frac{\pi}{2} \quad (4-5)$$

where λ_g denotes the guide wavelength in the medium of the TL.

Thus, at the center frequency, by substituting this value in (4-1), the scattering matrix of the coupler can be represented like the following:

$$[S]_{\lambda/4 \text{ Coupler}} = \begin{bmatrix} 0 & -j\sqrt{1-k^2} & k & 0 \\ -j\sqrt{1-k^2} & 0 & 0 & k \\ k & 0 & 0 & -j\sqrt{1-k^2} \\ 0 & k & -j\sqrt{1-k^2} & 0 \end{bmatrix} \quad (4-6)$$

Basing on this data, S-parameters of the basement can be calculated. The calculation is given in Appendix B. The result looks like the following:

$$[S]_{\text{bPD}} = \frac{1}{1+2k^2} \begin{bmatrix} 2k^2-1 & 2k & 2k \\ 2k & 1 & -2k^2 \\ 2k & -2k^2 & 1 \end{bmatrix} \quad (4-7)$$

Thus, the network performance shows a relation between S-parameters and the coupling coefficient. It's easy to examine that optimal functionality occurs with k_{opt} :

$$k_{\text{opt}} = 1/\sqrt{2} \quad (4-8)$$

and it has the form:

$$[S]_{\text{bPD opt}} = \begin{bmatrix} 0 & \frac{1}{\sqrt{2}} & \frac{1}{\sqrt{2}} \\ \frac{1}{\sqrt{2}} & \frac{1}{2} & -\frac{1}{2} \\ \frac{1}{\sqrt{2}} & -\frac{1}{2} & \frac{1}{2} \end{bmatrix} \quad (4-9)$$

Thus, the structure from (Fig. 4.1b) utilizing the quarter-wave lines and the optimal coupling coefficient is perfectly matched at the input port and provide in phase division of

the incoming signal into two equal parts. As it was mentioned above, the network is not able to match all 3 ports, and this issue is also depicted in the scattering matrix – the single-ended output return loss is only -6 dB. The fact that the power divider has to be matched from all ports forces us to apply some methods to realize this requirement.

4.2.1 Matching Procedure

The procedure of matching supposes implantation of lossy elements into the circuit. Let's implement the standard one used in Wilkinson divider – a parallel resistor between the outputs, like it depicted in Fig. 4.3.

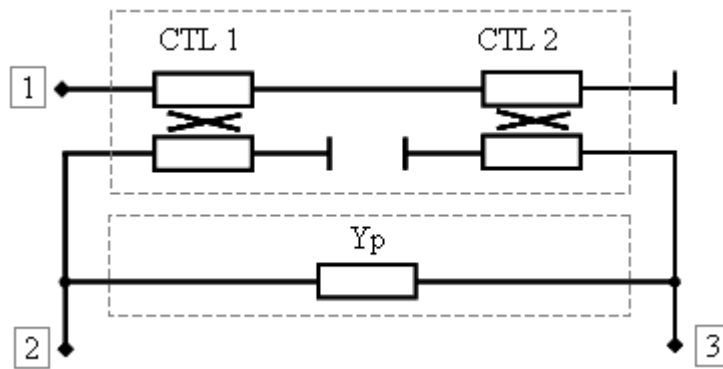


Figure 4.3: All ports matched power divider

The optimum solution would be to operate with Y-matrix, considering parallel interconnection between the basement and the matching resistor. In order to do this, the transformation equations of Y to S and S to Y matrix parameters will be used:

$$[Y] = [Y]_0 ([U] - [S]) \cdot ([U] + [S])^{-1} \quad (4-10)$$

$$[S] = ([Y]_0 [U] - [Y]) \cdot ([Y]_0 [U] + [Y])^{-1} \quad (4-11)$$

where

$$[U] = \begin{bmatrix} 1 & 0 & 0 \\ 0 & 1 & 0 \\ 0 & 0 & 1 \end{bmatrix} \text{ - unity matrix}$$

$$[Y]_0 = \begin{bmatrix} Y_0 & 0 & 0 \\ 0 & Y_0 & 0 \\ 0 & 0 & Y_0 \end{bmatrix} \text{ - Y-matrix of input / output impedance loads } Y_0$$

Taking into account that $[S]_{\text{bPD_opt}}$ is a singular matrix, the inverted matrix in (4-10) can not be calculated. We must use an approach to correct this issue. So, small losses have to be included in the network by correction of the matrix elements. The new S-parameters matrix with losses will be now:

$$[\mathbf{S}]_{\text{bPD opt L}} = \begin{bmatrix} S_{11L} & S_{12L} & S_{13L} \\ S_{21L} & S_{22L} & S_{23L} \\ S_{31L} & S_{32L} & S_{33L} \end{bmatrix} \quad (4-12)$$

The approach assumes including the losses in transmission without changes in matching and thus includes a small error, which will be corrected later.

$$S_{21L} = S_{12L} = S_{31L} = S_{13L} = 0.9S_{21 \text{ PD opt}} = 0.9S_{12 \text{ PD opt}} = 0.9S_{31 \text{ PFD opt}} = 0.9S_{13 \text{ PD opt}} \quad (4-13)$$

Finally the matrix (4-9) with losses will look like the following:

$$[\mathbf{S}]_{\text{bPD L}} = \begin{bmatrix} 0 & \sqrt{0.4} & \sqrt{0.4} \\ \sqrt{0.4} & \frac{1}{2} & -\frac{1}{2} \\ \sqrt{0.4} & -\frac{1}{2} & \frac{1}{2} \end{bmatrix} \quad (4-14)$$

Corresponding Y-matrix (using transformation equation (4-10)) will be:

$$[\mathbf{Y}]_{\text{bPD L}} = \mathbf{Y}_0 \begin{bmatrix} 9.5 & -6.7 & -6.7 \\ -6.7 & 4.8 & 4.8 \\ -6.7 & 4.8 & 4.8 \end{bmatrix} \quad (4-15)$$

The matrix will be converted after the parallel resistor (Y_p) connection (Fig. 4.3) into the following one:

$$[\mathbf{Y}]_{\text{PD L P}} = \mathbf{Y}_0 \begin{bmatrix} 9.5 & -6.7 & -6.7 \\ -6.7 & 4.8 + \frac{Y_p}{Y_0} & 4.8 - \frac{Y_p}{Y_0} \\ -6.7 & 4.8 - \frac{Y_p}{Y_0} & 4.8 + \frac{Y_p}{Y_0} \end{bmatrix} \quad (4-16)$$

And finally, using the equation (4-26), we've got the scattering parameters matrix of the power divider to be matched:

$$[\mathbf{S}]_{\text{PD L P}} = \begin{bmatrix} 0 & \sqrt{0.4} & \sqrt{0.4} \\ \sqrt{0.4} & \frac{Y_0 - 2Y_p}{2(Y_0 + Y_p)} & -\frac{Y_0 - 2Y_p}{2(Y_0 + Y_p)} \\ \sqrt{0.4} & -\frac{Y_0 - 2Y_p}{2(Y_0 + Y_p)} & \frac{Y_0 - 2Y_p}{2(Y_0 + Y_p)} \end{bmatrix} \quad (4-17)$$

Now implementing a vise-versa operation with the losses as in (4-28), we achieve S-parameters matrix without losses and this operation eliminates the error included by the losses before:

$$[S]_{PD} = \begin{bmatrix} 0 & \frac{1}{\sqrt{2}} & \frac{1}{\sqrt{2}} \\ \frac{1}{\sqrt{2}} & \frac{Y_0 - 2Y_p}{2(Y_0 + Y_p)} & -\frac{Y_0 - 2Y_p}{2(Y_0 + Y_p)} \\ \frac{1}{\sqrt{2}} & -\frac{Y_0 - 2Y_p}{2(Y_0 + Y_p)} & \frac{Y_0 - 2Y_p}{2(Y_0 + Y_p)} \end{bmatrix} \quad (4-18)$$

An optimal value of the matching resistor Y_p has to be found to match the network from all two outputs and this value is:

$$Y_p = \frac{Y_0}{2} \quad (4-19)$$

Thus S-matrix of the power divider matched in optimal way with the parallel resistor is:

$$[S]_{PD \text{ opt}} = \begin{bmatrix} 0 & \frac{1}{\sqrt{2}} & \frac{1}{\sqrt{2}} \\ \frac{1}{\sqrt{2}} & 0 & 0 \\ \frac{1}{\sqrt{2}} & 0 & 0 \end{bmatrix} \quad (4-20)$$

The splitter is matched from all ports and it provides equal in phase splitting. It should be noted that the output ports are perfect isolated at the same time.

4.2.2 Frequency Response

The previous calculations were done for the quarter-wave coupled sections splitter at the central working frequency under the condition (4-5). After the successful matching procedure we need to turn to our important target – the bandwidth. For this purpose, frequency dependent response of the coupler (4-3) will be used, where:

$$\begin{cases} b_1 = \frac{b_5 \sqrt{1-k^2} + a_3 jk \sin \Theta}{\sqrt{1-k^2} \cos \Theta + j \sin \Theta} \\ b_2 = \frac{a_1 \sqrt{1-k^2} - b_4 jk \sin \Theta}{\sqrt{1-k^2} \cos \Theta + j \sin \Theta} \\ b_3 = \frac{a_1 jk \sin \Theta - b_4 \sqrt{1-k^2}}{\sqrt{1-k^2} \cos \Theta + j \sin \Theta} \\ b_4 = \frac{b_5 jk \sin \Theta + a_3 \sqrt{1-k^2}}{\sqrt{1-k^2} \cos \Theta + j \sin \Theta} \end{cases} \quad \begin{cases} b_5 = \frac{-b_6 \sqrt{1-k^2} - b_7 jk \sin \Theta}{\sqrt{1-k^2} \cos \Theta + j \sin \Theta} \\ b_6 = \frac{b_2 \sqrt{1-k^2} + a_8 k j \sin \Theta}{\sqrt{1-k^2} \cos \Theta + j \sin \Theta} \\ b_7 = \frac{b_2 jk \sin \Theta + a_8 \sqrt{1-k^2}}{\sqrt{1-k^2} \cos \Theta + j \sin \Theta} \\ b_8 = \frac{b_6 jk \sin \Theta - b_7 \sqrt{1-k^2}}{\sqrt{1-k^2} \cos \Theta + j \sin \Theta} \end{cases} \quad (4-21)$$

The same calculation procedure, as the one carried out in the analysis part, was used, but taking already the optimal coupling from (4-8) at this time. The resulting scattering parameters, which have been got:

$$[\mathbf{S}]_{\text{bPD_opt}} = \begin{bmatrix} \mathbf{S}_{11}^{\text{bPD}} & \mathbf{S}_{12}^{\text{bPD}} & \mathbf{S}_{13}^{\text{bPD}} \\ \mathbf{S}_{21}^{\text{bPD}} & \mathbf{S}_{22}^{\text{bPD}} & \mathbf{S}_{23}^{\text{bPD}} \\ \mathbf{S}_{31}^{\text{bPD}} & \mathbf{S}_{32}^{\text{bPD}} & \mathbf{S}_{33}^{\text{bPD}} \end{bmatrix} \quad (4-22)$$

where

$$\mathbf{S}_{11}^{\text{bPD}} = -\frac{2 \cos^2[\Theta]}{jA}$$

$$\mathbf{S}_{12}^{\text{bPD}} = \mathbf{S}_{21}^{\text{bPD}} = \frac{2 \sin[\Theta](1 - \cos[2\Theta] + 2 \cos[4\Theta] - j\sqrt{2} \sin[2\Theta] + j3\sqrt{2}/2 \sin[4\Theta])}{A \cdot B}$$

$$\mathbf{S}_{13}^{\text{bPD}} = \mathbf{S}_{31}^{\text{bPD}} = \frac{2 \sin[\Theta](1 - 3 \cos[2\Theta] - j2\sqrt{2} \sin[2\Theta])}{A \cdot B}$$

$$\mathbf{S}_{22}^{\text{bPD}} = -\frac{1}{B^2} \left(1 + \frac{\sin^2[2\Theta]}{2jA} \right)$$

$$\mathbf{S}_{23}^{\text{bPD}} = \mathbf{S}_{32}^{\text{bPD}} = \frac{2 \sin^2[\Theta](-j + j3 \cos[2\Theta] - 2\sqrt{2} \sin[2\Theta])}{A \cdot B^2}$$

$$\mathbf{S}_{33}^{\text{bPD}} = \frac{-j(66 + 109 \cos[2\Theta] + 70 \cos[4\Theta] + 35 \cos[6\Theta] + 24 \cos[8\Theta]) - \sqrt{2}(40 \sin[2\Theta] + 42 \sin[4\Theta] - 24 \sin[6\Theta] - 17 \sin[8\Theta])}{8A \cdot B^4}$$

$$A = 3\sqrt{2} \sin[4\Theta] - 2\sqrt{2} \sin[2\Theta] - j(1 - j3 \cos[2\Theta] + 4j \cos[4\Theta])$$

$$B = \cos[\Theta] + j\sqrt{2} \sin[\Theta]$$

What is needed additionally, that is the use of the parallel output matching load $2Y_0$ as it was calculated before. The final power divider matched with the resistance provides the characteristics shown in Fig. 4.4. The splitter was simulated with the following parameters: $Z_0 = 50$ Ohm (port impedance), $Z_p = 100$ Ohm (matching resistance), $\varepsilon = 7.8$ (permittivity of the LTCC), $f_0 = 6.85$ GHz (center working frequency), $l = \frac{\lambda_g}{4} = \frac{c}{4f_0\sqrt{\varepsilon}} \approx 4$ mm (length of the coupled line section), λ_g - wavelength in the dielectric medium.

The even / odd-mode coupled line impedances must be satisfied with two equations (4-4) and the characteristic line impedance ([25]):

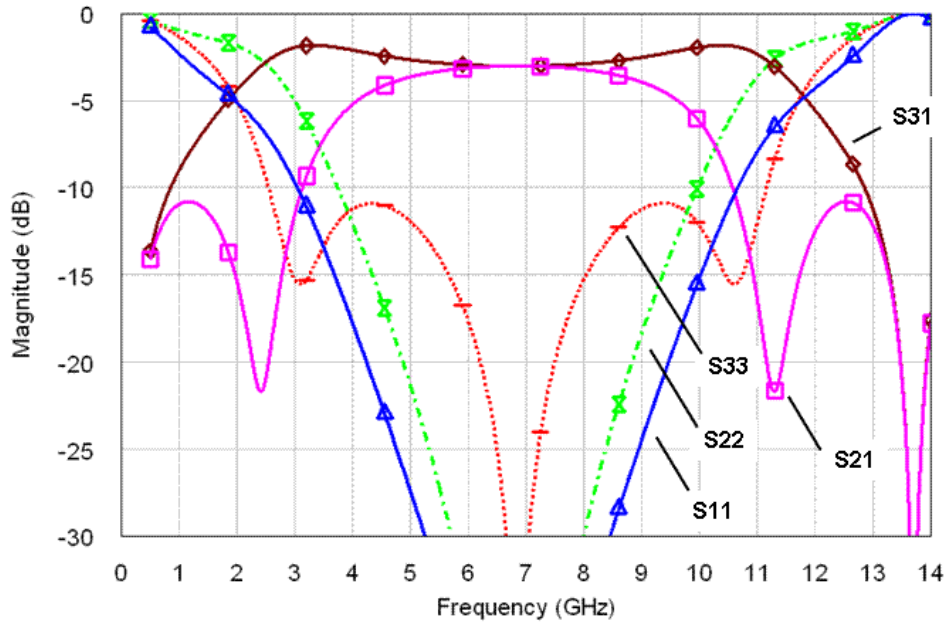
$$\begin{cases} k = \frac{Z_{0e} - Z_{0o}}{Z_{0e} + Z_{0o}} \\ Z_{0 \text{ CTL}} = \sqrt{Z_{0e} \cdot Z_{0o}} \end{cases} \quad (4-23)$$

where Z_{0e} and Z_{0o} - even- and odd-mode coupled lines impedance, $Z_{0 \text{ CTL}}$ - characteristic impedance of the coupled lines. Of course, the coupling coefficient has to be optimal, like the one (4-8) and the characteristic line impedance has to be equal to the port impedance:

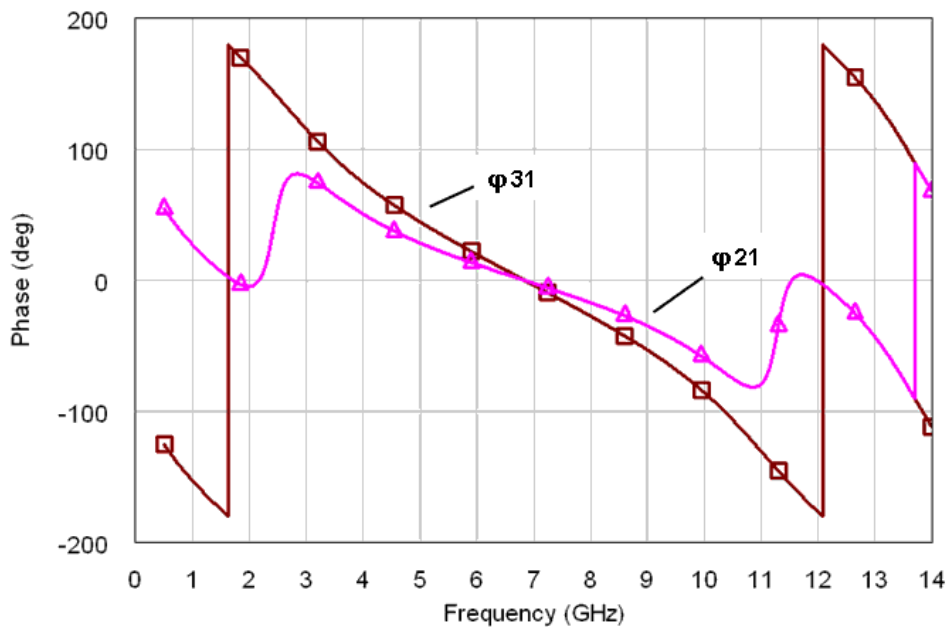
$$\begin{cases} k = k_{\text{opt}} \\ Z_{0 \text{ CTL}} = Z_0 \end{cases} \quad (4-24)$$

By substituting this equations system into (4-23), the conditions for the optimal matched power divider will be:

$$\begin{cases} \frac{1}{\sqrt{2}} = \frac{Z_{0e} - Z_{0o}}{Z_{0e} + Z_{0o}} \\ 50 = \sqrt{Z_{0e} \cdot Z_{0o}} \end{cases} \quad (4-25)$$



a) Amplitude characteristics



b) Phase characteristics

Figure 4.4: Characteristics of the optimal resistor loaded simple power divider (simulated using Microwave Office [29])

The even / odd-mode coupled lines impedances are derived by solving the equations system and they are optimal:

$$\begin{cases} Z_{0e \text{ opt}} = 120 \text{ Ohm} \\ Z_{0o \text{ opt}} = 21 \text{ Ohm} \end{cases} \quad (4-26)$$

The simulation was done using the ideal components without losses.

The structure is not full symmetrical (mainly because of termination of the line on zero impedance), therefore obvious differences exists in both transmission characteristics (S_{21} , S_{31}) and the output matching (S_{22} , S_{33}). The bandwidth estimated by the transmission with 0.1 dB of the amplitude balance is equal to 30 %. Actually, the splitter is matched in wider frequency band, but the amplitude balance arises as a restriction criterion in this case. By examining the phase characteristics depicted in Fig. 4.4b, phase imbalance was registered. The phase difference between the output phases varies from “-25°” to “+25°” in the passband. This issue could be investigated under each of the certain implementation in separate.

4.2.3 Increasing the Bandwidth

The solution proposed in the previous chapter is already accomplished and could be successfully used in some relative narrowband implementations, like Bluetooth and WLAN, because achieved bandwidth is already wide enough for these purposes. Thus, the optimal solution for the network depicted in Fig. 4.3 is achieved. Unfortunately, the transmission performance is confined with the phase jump from 0° to 180°, as it shown in Fig. 4.4b; as the result, two notches appear in the S_{21} characteristic. The reason of such phase behavior is that the splitter behaves like a TL balun at the lower frequencies, but without shorting capacitors, which is detailed described in [26], [27]. The higher frequency function is just a mirrored harmonic representation that makes limitation on passband from the right side. In order to improve the phase and the amplitude characteristics thus enlarging the transmission bandwidth, a parallel shorted capacitor is proposed in this work. The new basic network used for a wideband splitter design is shown in Fig. 4.5.

The network contains the circuit from Fig. 4.1b with capacitor parallel connected to the outputs. It can be easy analyzed using Y-parameters, assuming the parallel interconnection of two parts. The procedure consists of the following steps:

- 1) Transformation of S-parameters of the coupled line sections into Y-parameters;
- 2) summing of obtained Y-parameters with Y-parameters of the capacitor;
- 3) backward transformation of combined Y-parameters into S-parameters.

These three steps are described in details below performing all necessary calculations.

Ad. 1) The procedure is equal to the one used by calculation of the matching, but full frequency dependent S-parameters representation (4-22) has been got at this time. Y-matrix of the coupled line part is calculated with the equation (4-10) and is:

$$Y_{\text{bPD}} = \frac{1}{P_1} \begin{bmatrix} P_2 P_{12} & 2P_4 P_6 P_7 P_{10} & 2jP_6 P_7^3 P_{10} P_{17} \\ 2P_4 P_6 P_7 P_{10} & P_2 P_9 & 2P_5 P_6 P_7^4 P_{10} \\ 2jP_6 P_7^3 P_{10} P_{17} & 2P_5 P_6 P_7^4 P_{10} & P_2 P_8 \end{bmatrix} \quad (4-27)$$

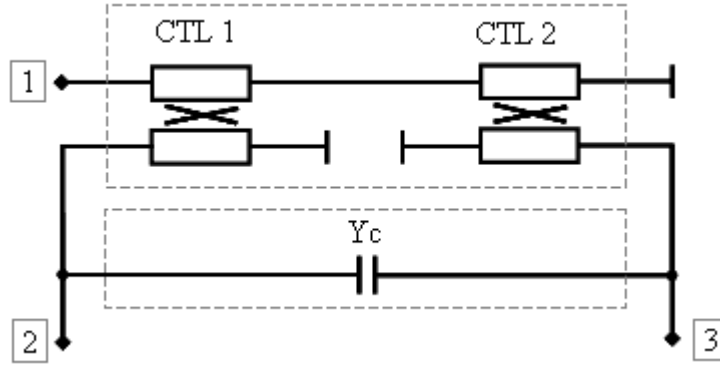


Figure 4.5: Basic structure with increased bandwidth used for the new power divider

The variables to be used for Y-parameters and for scattering parameters below are:

$$P_1 = 138\sqrt{2} + 72\sqrt{2} \cos[2\Theta] - 1924\sqrt{2} \cos[4\Theta] + 6837\sqrt{2} \cos[6\Theta] - 14290\sqrt{2} \cos[8\Theta] + 19389\sqrt{2} \cos[10\Theta] - 16436\sqrt{2} \cos[12\Theta] + 6726\sqrt{2} \cos[14\Theta] + 272j \sin[2\Theta] - 2748j \sin[4\Theta] + 9668j \sin[6\Theta] - 20208j \sin[8\Theta] + 27420j \sin[10\Theta] - 23244j \sin[12\Theta] + 9512j \sin[14\Theta]$$

$$P_2 = -\frac{jP_1}{\sqrt{2}}$$

$$P_3 = 30j \cos[\Theta] - 470j \cos[3\Theta] + 2022j \cos[5\Theta] - 4727j \cos[7\Theta] + 6945j \cos[9\Theta] - 6330j \cos[11\Theta] + 2786j \cos[13\Theta] + 54\sqrt{2} \sin[\Theta] + 310\sqrt{2} \sin[3\Theta] - 1428\sqrt{2} \sin[5\Theta] + 3343\sqrt{2} \sin[7\Theta] - 4911\sqrt{2} \sin[9\Theta] + 4476\sqrt{2} \sin[11\Theta] - 1970\sqrt{2} \sin[13\Theta]$$

$$P_4 = 35 \cos[\Theta] - 167 \cos[3\Theta] + 387 \cos[5\Theta] - 529 \cos[7\Theta] + 338 \cos[9\Theta] + 23j\sqrt{2} \sin[\Theta] - 115j\sqrt{2} \sin[3\Theta] + 273j\sqrt{2} \sin[5\Theta] - 374j\sqrt{2} \sin[7\Theta] + 239j\sqrt{2} \sin[9\Theta]$$

$$P_5 = -3 + 12 \cos[2\Theta] - 25 \cos[4\Theta] + 24 \cos[6\Theta] + 9j\sqrt{2} \sin[2\Theta] - 18j\sqrt{2} \sin[4\Theta] + 17j\sqrt{2} \sin[6\Theta]$$

$$P_6 = j - 3j \cos[2\Theta] + 4j \cos[4\Theta] + 2\sqrt{2} \sin[2\Theta] - 3\sqrt{2} \sin[4\Theta]$$

$$P_7 = \sqrt{2} \cos[\Theta] + 2j \sin[\Theta]$$

$$P_8 = Y_0 \csc[\Theta] \csc[2\Theta] \sin[3\Theta]$$

$$P_9 = Y_0 (1 + 2 \cos[2\Theta]) \csc[2\Theta]$$

$$P_{10} = 2Y_0 \csc[2\Theta]$$

$$P_{11} = Y_0 + Y_P - j \frac{P_8}{\sqrt{2}}$$

$$P_{12} = 2Y_0 \cot[2\Theta]$$

$$P_{13} = -Y_P + 4 \frac{P_5 P_6 P_7^4 P_{10}}{P_1}$$

$$P_{14} = Y_0 + Y_P - j \frac{P_9}{\sqrt{2}}$$

$$P_{15} = \frac{P_7}{P_1} (P_3 P_{10} P_{13} + 2P_4 P_6 P_{11} P_{12})$$

$$P_{16} = jP_6$$

$$P_{17} = -12j \cos[\Theta] + 41j \cos[3\Theta] - 71j \cos[5\Theta] + 58j \cos[7\Theta] + 9\sqrt{2} \sin[\Theta] - 28\sqrt{2} \sin[3\Theta] + 50\sqrt{2} \sin[5\Theta] - 41\sqrt{2} \sin[7\Theta]$$

$$P_{18} = \frac{P_7}{P_1} (4P_7^2 P_{10} P_{14} P_{16} P_{17} - P_3 P_{12} P_{13})$$

$$P_{19} = -j \frac{P_{12} P_{14}}{\sqrt{2}} - \left(\frac{P_3 P_7 P_{12}}{P_1} \right)^2$$

$$P_{20} = -j \frac{P_{11} P_{12}}{\sqrt{2}} - \left(\frac{P_3 P_7 P_{10}}{P_1} \right)^2$$

$$P_{21} = (Y_0 P_{14} + P_{19})(P_{11} P_{14} - P_{13}^2)$$

$$P_{22} = (Y_0 P_{11} + P_{20})(P_{11} P_{14} - P_{13}^2)$$

Ad. 2) Y-matrix of the whole network shown in Fig. 4.5 is:

$$Y_{\text{bPD}_C} = \frac{1}{P_1} \begin{bmatrix} P_2 P_{12} & 2P_4 P_6 P_7 P_{10} & 2jP_6 P_7^3 P_{10} P_{17} \\ 2P_4 P_6 P_7 P_{10} & P_2 P_9 + Y_C & 2P_5 P_6 P_7^4 P_{10} - Y_C \\ 2jP_6 P_7^3 P_{10} P_{17} & 2P_5 P_6 P_7^4 P_{10} - Y_C & P_2 P_8 + Y_C \end{bmatrix} \quad (4-28)$$

where $Y_C = j\omega C$ (conductivity of the parallel capacitor).

Ad. 3) The scattering parameters matrix can be computed using (4-11). A calculation problem occurs during the process, because of the equation complexity. The solution was found and it represents reduction of the 3 x 3 size Y-matrix to the 2 x 2 size one, in order to simplify the situation. By loading the port 2 and the port 3 alternately on the load impedance Y_0 and using the following equation from [24], two conductivity parameters matrices will be obtained for the ports 1 and 2 and for the ports 1 and 3 in separate:

$$Y_1 = \begin{bmatrix} Y_{11} & Y_{12} \\ Y_{21} & Y_{22} \end{bmatrix} - \begin{bmatrix} Y_{13} \\ Y_{23} \end{bmatrix} \cdot [Y_{33} + Y_0]^{-1} \cdot [Y_{31} \quad Y_{32}] \quad (4-29)$$

$$Y_2 = \begin{bmatrix} Y_{11} & Y_{13} \\ Y_{31} & Y_{33} \end{bmatrix} - \begin{bmatrix} Y_{12} \\ Y_{32} \end{bmatrix} \cdot [Y_{22} + Y_0]^{-1} \cdot [Y_{21} \quad Y_{23}] \quad (4-30)$$

Y_1 and Y_2 are matrices using the input / output ports 1/2 and 1/3 correspondingly. So, it is now to use the matrix transformation equation from Y to S parameters. By substituting the conductivity parameters from (4-28) to (4-29) and (4-30) with the following transformation using (4-26), the final transmission functions could be achieved:

$$S_{21}^{\text{bPD } C} = 2Y_0 \frac{P_{14}P_{18}}{(P_{18})^2 - P_{21}} \quad (4-31)$$

$$S_{31}^{\text{bPD } C} = 2Y_0 \frac{P_{11}P_{15}}{(P_{15})^2 - P_{22}} \quad (4-32)$$

An analytical analysis of the capacitors influence on the bandwidth is not easy due to the complicated constituents in the equations and limited computation ability, therefore a relation between the bandwidth and the capacitance values is not obvious. Nevertheless, this relation can be calculated using a numerical method (Fig. 4.6).

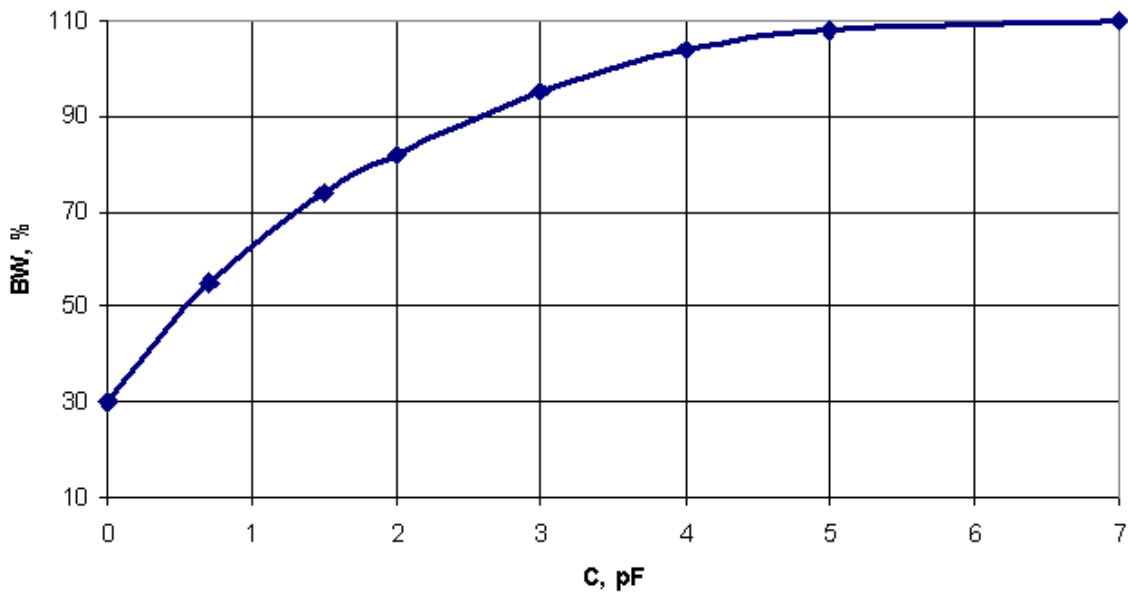


Figure 4.6: Relation: bandwidth vs. capacitance value

The relation is not linear; it begins with 30 % of the relative bandwidth (the circuit without capacitor: $C = 0$ pF), grows rapidly up to 109 % (with $C = 5$ pF) and afterwards tends slow to its maximum value, while further increasing of the capacitance value doesn't bring essential improvement in the passband, because the passband is confined with the transmission zeros (regarding constant length of the coupled line sections) and the phase flip-flap described above. Thus, a functional range of the capacitance values is limited with $C = 0 \dots 5$ pF, where the bandwidth could be effective controlled.

The target was to achieve the maximal bandwidth performance inside minimum area, therefore an optimal capacitance value assuming reasonable size would be $C = 5$ pF, which is realizable using LTCC technology.

On the other hand, the amplitude balance depends strongly on the capacitance value as well. The amplitude imbalance as the main criterion of the bandwidth constraining is a reason why the bandwidth extension occurs due to the capacitor increasing. For example, a typical relation between the amplitude balance and the capacitance for the maximal measured value in the passband for the ultra-wideband splitter with center frequency at

6.85 GHz is shown in Fig. 4.7. The balance is not symmetrical in the passband and the transmission performance suffers from the imbalance mostly at 3.1 GHz side. It's clear from the figure that the amplitude balance is lower 0.5 dB limit within the passband using selected capacitance value of 5 pF. Of course, the power divider will function with smaller capacitance values up to 2 pF but showing the worse performance – up to 1.5 dB imbalance, which is not applicable for most of applications. Further decreasing of the capacitor value leads to deterioration of the performance dramatically.

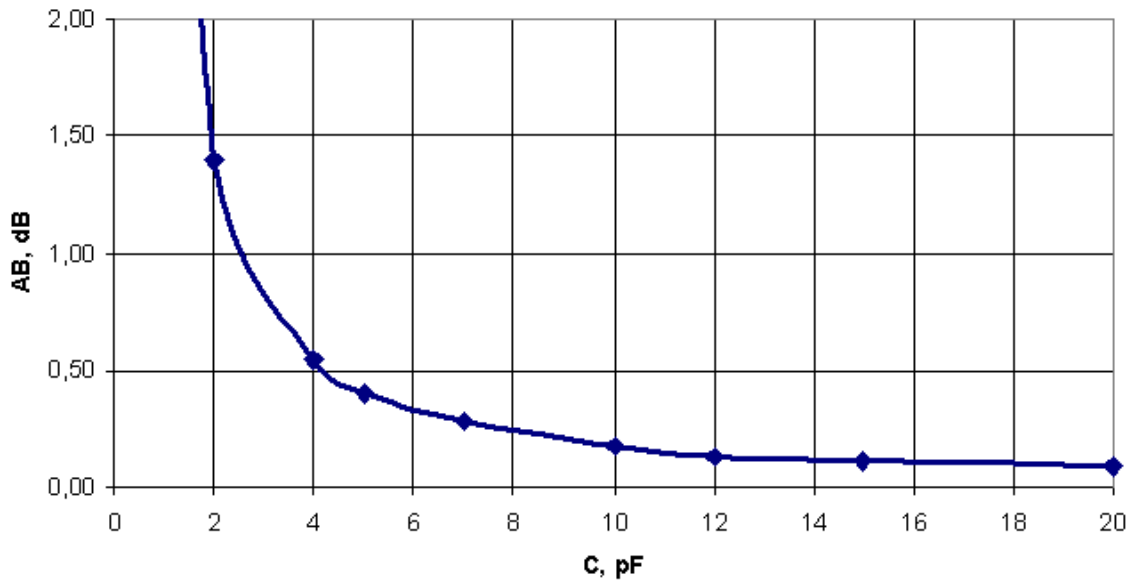


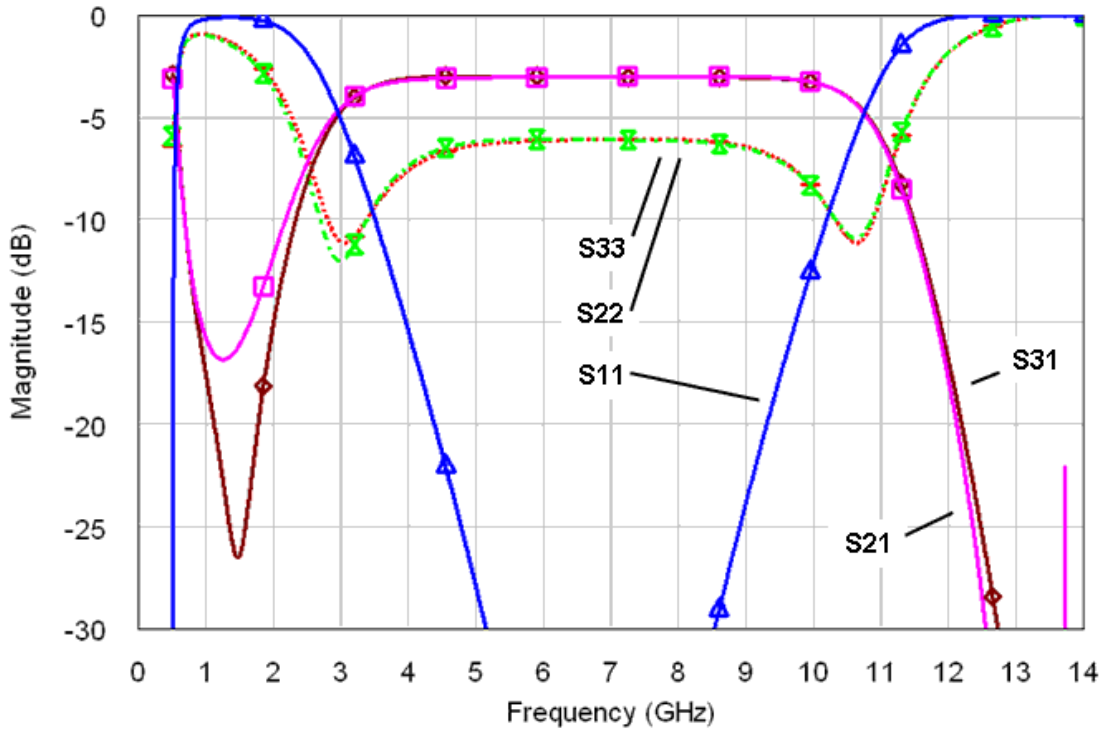
Figure 4.7: Relation: amplitude balance vs. capacitance value (at 3.1 GHz)

Though, the minimum required value is 5 pF, we will take the value of 20 pF in order to investigate a quasi-ideal case of the splitter with 0.1 dB imbalance. The resulting performance of the proposed network is shown in Fig. 4.8.

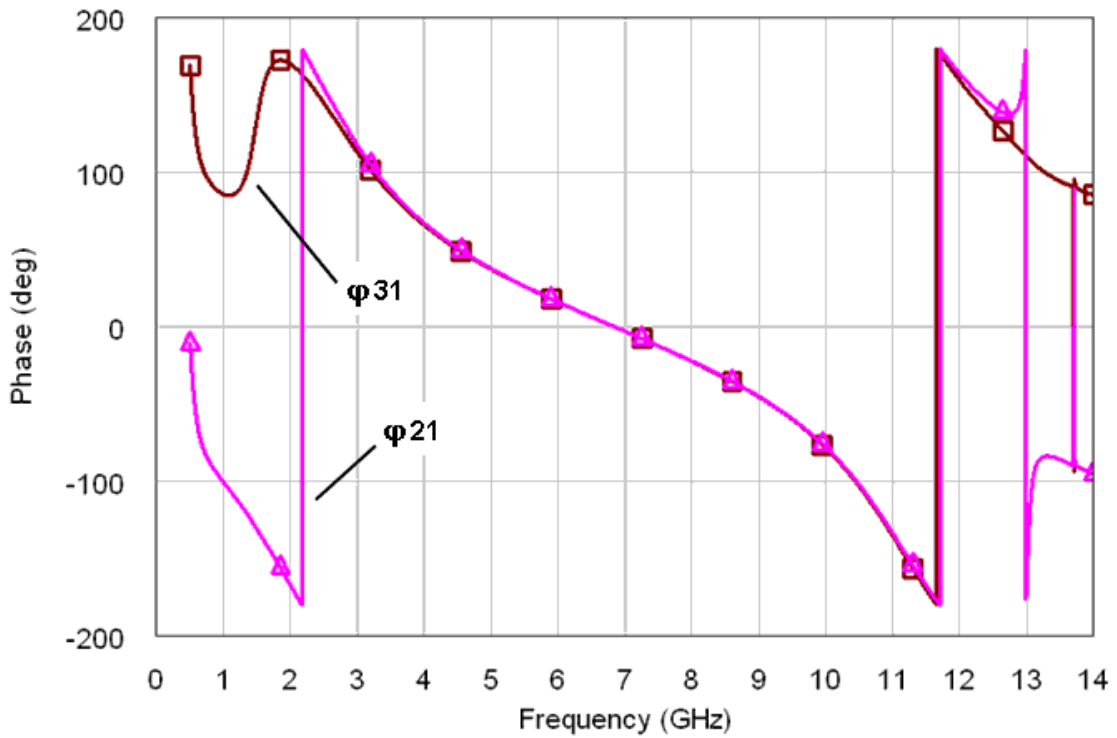
The network was simulated with the same parameters as the ones before: $Z_0 = 50$ Ohm - port impedance, $\varepsilon = 7.8$ - permittivity of the LTCC, $f_0 = 6.85$ GHz - center

working frequency, $L_{CTL} = \frac{\lambda_g}{4} = \frac{c}{4f_0\sqrt{\varepsilon}} \approx 4$ mm (length of the coupled line section). The even / odd-mode coupled line impedances are optimal and they were taken from (4-26).

The network provides the bandwidth of 110 % with the sufficient amplitude and phase balance. This issue shows essential improvement in comparison with the original circuit performance with 30 % bandwidth depicted in Fig. 4.4a. The analysis of the improved network has been done without matching procedure; therefore the circuit is not matched from the output side (ports 2 and 3), while the input is perfectly matched. Further step would be the matching procedure.



a) Amplitude characteristics



b) Phase characteristics

Figure 4.8: Characteristics of the basement for the power divider with improved bandwidth (simulated using Microwave Office [29])

4.2.4 Final Matching Procedure

Taking into account a fact that the improved network differs from the original one, the matching calculated already using the parallel resistance will be not compatible for this new case. A new matching circuit will be built at this time basing on the data from a smith diagram of the output impedances. Assuming that the input port 1 is matched and the ports 2 and 3 have to be matched; we will consider only two output ports 2 and 3, which scattering parameters are depicted in the smith chart in Fig. 4.9.

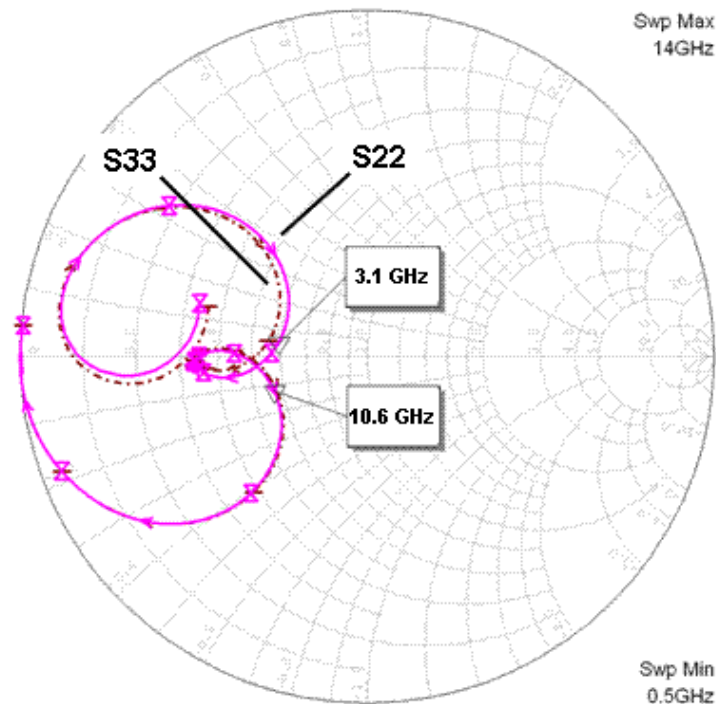


Figure 4.9: Smith chart: output S-parameters of the basement for the power divider with improved bandwidth (simulated using Microwave Office [29])

The working region is the standard UWB full frequency band (from 3.1 to 10.6 GHz), it's marked in the figure and it looks like the output impedances located inside the region are almost active and an average value in the passband is equal to 25 Ohm. Frequency response of the s-parameters introduces a coil form and all values are concentrated inside the small region that makes the matching procedure possible in the whole band. There are several ways to match such network and the matching circuits could be classified on three types depending on the methods:

- 1) Type 1: matching with implanted losses;
- 2) Type 2: lumped element matching;
- 3) Type 3: transmission line matching.

The matching types are arranged from the simplest one with the worst performance to the most complicated one with the best performance.

4.2.4.1 Matching with Implanted Losses

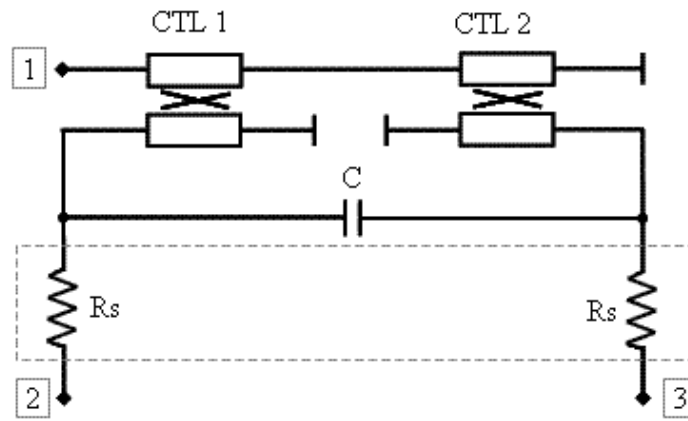
The first type of the matching is the simplest one, because it consists of minimum number of the components. Taking into account that the real output impedance (Z_{out}^b) of each port is smaller than the real environment impedance (Z_0), the method assumes including the losses in series to the outputs in order to get overall output impedances equal to Z_0 . Thus, the required series losses could be calculated like the following:

$$R_s = Z_0 - Z_{out}^b \quad (4-33)$$

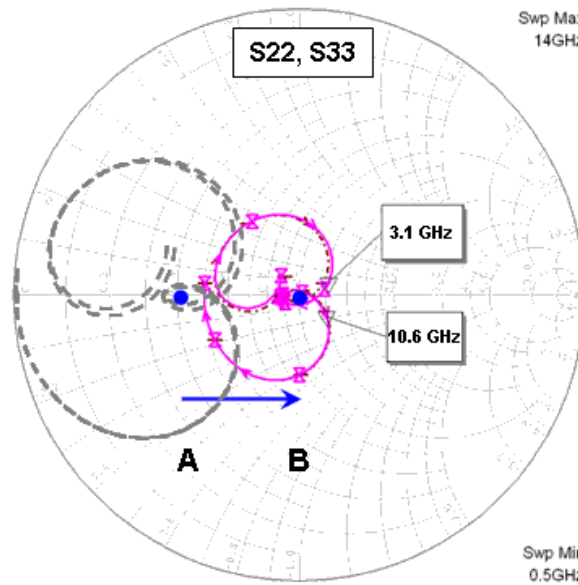
A realization of the method is shown in Fig. 4.10a. In the 50 Ohm environment and with the 25 Ohm average output impedance the resistance will be equal to $Z_R = 50 \text{ Ohm} - 25 \text{ Ohm} = 25 \text{ Ohm}$. As a result, the reflection coefficient curves on the smith chart suffer the right-hand shift into a region which corresponds to the reflection from 50 Ohm impedance, like it's shown in Fig. 4.10b. The original characteristics of the splitter without matching circuit are marked with gray color and dashed lines, while the matched characteristics are marked with colored solid lines; the arrow shows the matching direction. Matched amplitude characteristics of the splitter are shown in Fig. 4.10c. An influence on the input matching could be observed during the output matching procedure; nevertheless, all ports provide sufficient reflection coefficients. Though the main advantage of the power divider is minimal number of the elements, there is also a disadvantage, which causes in the insertion loss, because of the lossy components used in the circuit (the series resistors). The total minimal losses (assuming lossless circuit elements) are comprised of 3 dB division losses with 2 dB insertion losses and result 5 dB in sum (see Fig. 4.10c). Thus this simplest type of the splitter corresponds to low-cost high-loss solution.

4.2.4.2 Lumped Element Matching

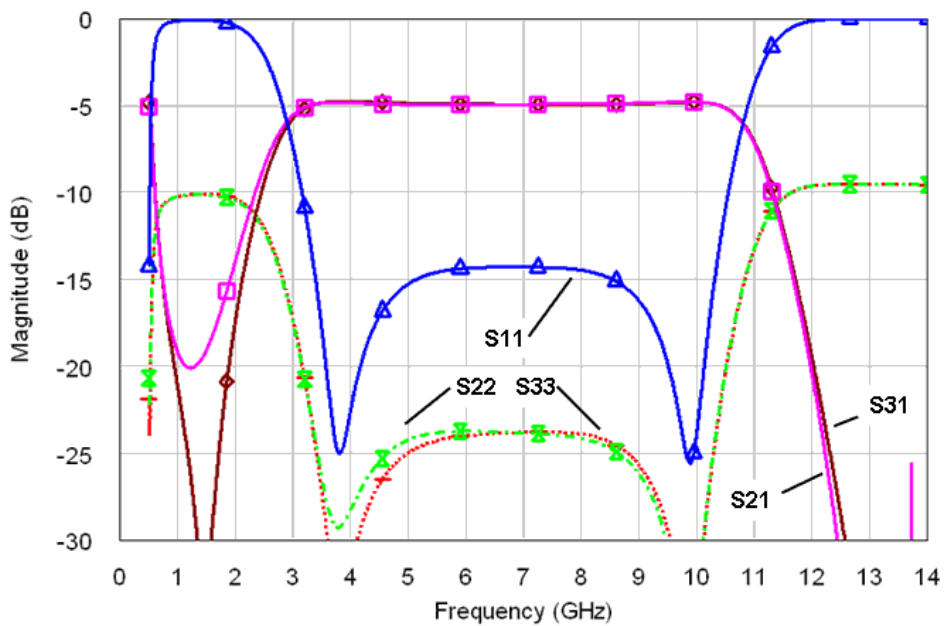
The main aim of the other matching procedures is to avoid additional 2 dB losses, which were presented using the first procedure. This can be achieved by refusing from resistors placed in series to current flow and implanting a resistor placed between the outputs, thus it appears in parallel. As it's well known, a resistor connected in parallel to



a) Schematic



b) Matching procedure (smith diagram)



c) Amplitude characteristics

Figure 4.10: Power divider with matching “type 1” (simulated using Microwave Office [29])

nodes decreases the total impedance measured at these nodes (in our case the outputs). The average output impedance of the basement is 25 Ohm that value is less than the environment impedance of 50 Ohm. Therefore, in order to achieve the final impedance equal to the environment impedance, firstly the output impedance must be increased up to the defined value of intermediate impedance Z_{in} and only afterwards it must be decreased to the environment value using the parallel resistor. The intermediate impedance value can be calculated from the equation for parallel interconnected resistors:

$$Z_{out} = \frac{R \cdot Z_{in}}{R + Z_{in}} \quad (4-34)$$

And it's equal to:

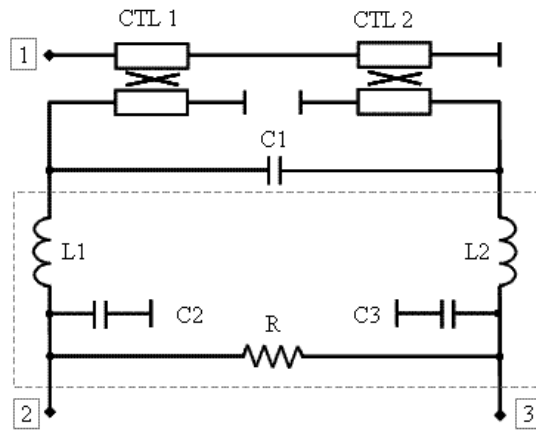
$$Z_{in} = \frac{R \cdot Z_{out}}{R - Z_{out}} = \frac{100 \cdot 50}{100 - 50} = 100 \text{ Ohm} \quad (4-35)$$

where $R = 100 \text{ Ohm}$ (the parallel resistor defined above for the matching procedure), $Z_{out} = Z_0 = 50 \text{ Ohm}$ (the output impedance that must be equal to the ports impedance).

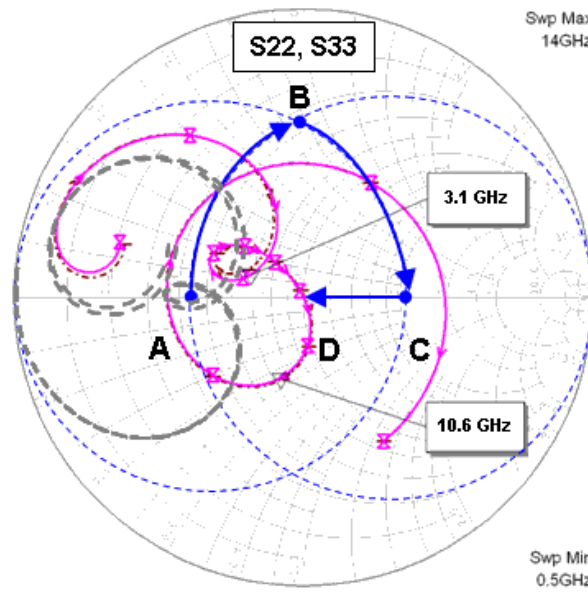
Transformation of the output impedance of the basement from the original value to the intermediate one could be done by different ways using both lumped elements and transmission lines. The power divider using a typical simple lumped element matching circuit is shown in Fig. 4.11a. The matching process depicted at the smith chart in Fig. 4.11b shows way from the point A to D step by step. The scattering parameters of the original basement are drawn with the dashed gray lines and fix the point A as the start one. We will take under consideration one path only, assuming circuit symmetry. The first series inductance moves the curve along the reactance circle clockwise (curve A-B). Afterwards, the characteristics will be moved along the susceptance circle clockwise (curve B-C), thus the point C is reached, which corresponds to the real impedance of 100 Ohm, defined above as the intermediate impedance.

The next step (C-D) shows lowering of the impedance value to the environment one by including the parallel resistor. The final matched curves are depicted in the smith chart using colored lines and the transmission performance is shown in Fig. 4.11c.

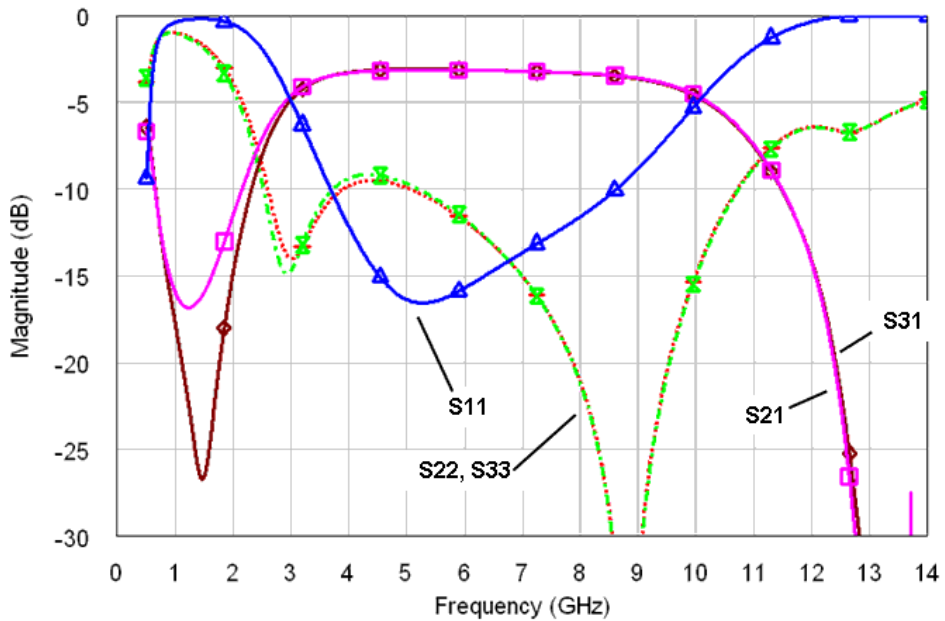
The proposed matching circuit has two disadvantages, which arise as a payment for the simplicity of the circuit. The first drawback is a narrowband function. The passband limits on the smith chart (Fig. 4.11b) are stretched out far away from each other, while the original performance depicted in Fig. 4.9 shows the bandwidth concentrated inside the small area. The splitter is perfectly matched only in the region around 9 GHz (Fig. 4.11c), nevertheless, the lower frequency band represents still good return loss values up to 10 dB that corresponds to the reflection value about 10 %.



a) Schematic



b) Matching procedure (smith diagram)



c) Amplitude characteristics

Figure 4.11: Power divider with matching “type 2” (simulated using Microwave Office [29])

The second weakness contributes to degradation of the input matching. It occurs due to differences in the input and the output impedances of the LC network, while the basement for the power divider was simulated using the standard port impedance of 50 Ohm, which corresponds to the output port impedance. Degradation of the input return loss confines the bandwidth dramatically (Fig. 4.11c). A solution for this problem would be the equalizing these input and output impedances. Only a fully symmetrical network can provide an equality of both impedances, therefore the following Pi-network (C-L-C) as it's shown in Fig. 4.12a was proposed. Of course, T-network (L-C-L) gives similar results, but the first network is more attractive due to the implementation of two C elements instead of two L elements that is significant issue by LTCC designing in the meaning of losses, because of much higher quality factor realized in capacitances in comparison with the one in inductances. The Pi-network used in transformation of the outputs impedances have to provide the following condition:

$$Z_{in}^{Pi} = Z_{out}^{Pi} = Z_0 = 50 \text{ Ohm} \quad (4-36)$$

The network with such parameters represents itself an equivalent circuit of a transmission line with characteristic impedance of 50 Ohm. Taking into account that the impedance transformation operates with real values, the line must be quarter-wave-long. Under these conditions, the element values can be calculated like the following [25]:

$$L = L_1 = L_2 = \frac{Z_0}{\omega} = \frac{50}{2\pi \cdot 6.85 \cdot 10^9} = 1.16 \text{ nH} \quad (4-37)$$

$$C = C_2 = C_3 = C_4 = C_5 = \frac{1}{Z_0 \omega} = \frac{1}{50 \cdot 2\pi \cdot 6.85 \cdot 10^9} = 0.47 \text{ pF} \quad (4-38)$$

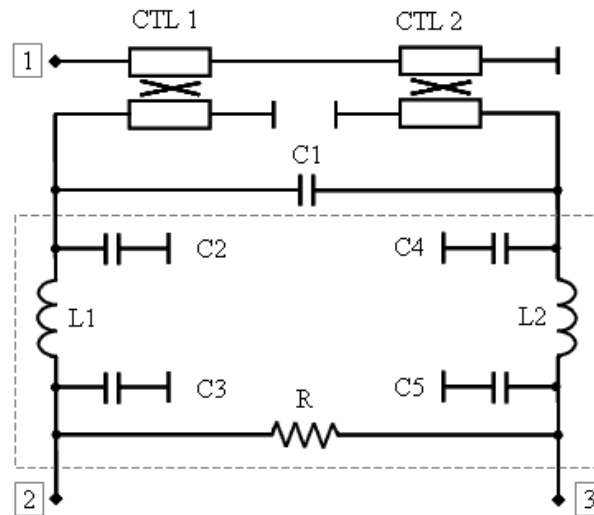
where $\omega = \omega_0 = 2\pi f_0 = 2\pi \cdot 6.85 \text{ GHz}$ (the central working frequency).

The network contained these elements will be perfect matched at the center frequency, but the bandwidth is not wide enough. An optimal circuit could be built using the following elements achieved iterative:

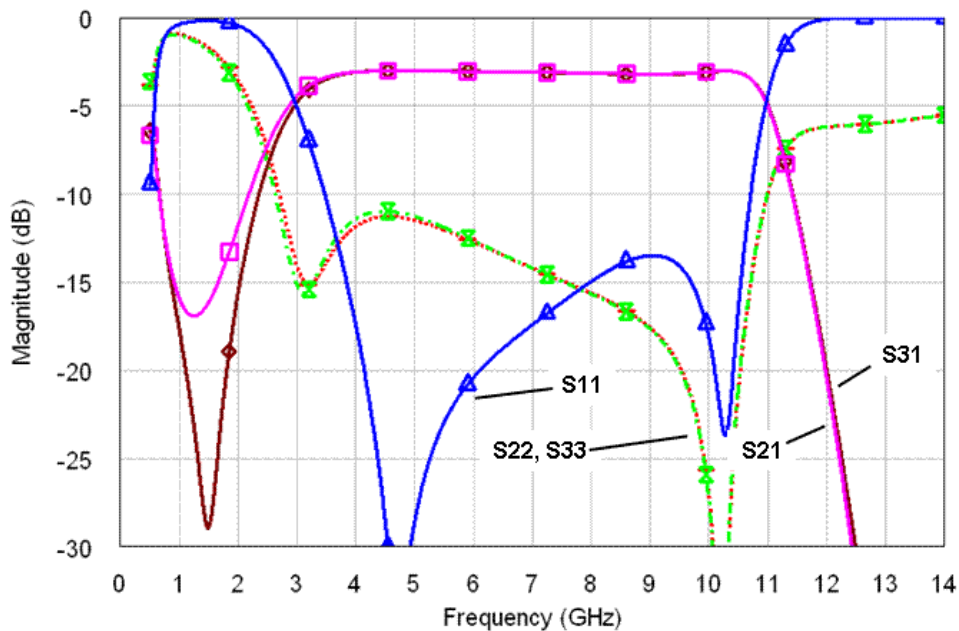
$$L_{opt} = L_1 = L_2 = 1.05 \text{ nH} \quad (4-39)$$

$$C_{opt} = C_2 = C_3 = C_4 = C_5 = 0.18 \text{ pF} \quad (4-40)$$

In this case, an optimum was selected between values of the bandwidth and the return loss. The input matching response shown in Fig. 4.12b is much better than the one in previous case, but still worse than the original performance shown in Fig. 4.8a. Unfortunately, the parameters of the Pi-network are frequency dependent, so it's impossible to realize the perfect wideband matching. Though, the worst value of the return loss is a little better than 10 dB, the circuit is already practical applicable.



a) Schematic



b) Amplitude characteristics

Figure 4.12: Power divider with improved matching “type 2” (simulated using Microwave Office [29])

4.2.4.3 Transmission Line Matching

The last type of the matching circuit avoids the frequency dependence of its input impedance in the ideal case and it shows more intelligent solution using transmission lines. The method doesn't use series resistors, which helps to save 2 dB insertion losses. A typical network is shown in Fig. 4.13a. The real transmission lines are used instead of their lumped element equivalents, as it was in the previous case. The method is based on the same principle as before - shifting the complex scattering parameters into the area

correspondingly to high impedance value with the following lowering of the impedance by its return into the target area using the parallel resistor. This procedure is depicted in Fig. 4.13b. The trace A-B implies the impedance transformation using the quarter-wave TLs.

The parameters of the matching lines can be calculated like the following: $L_{TL} = \frac{\lambda_g}{4} \approx 4$ mm (length of the TLs), $Z_{0_{TL}} = \sqrt{Z_{in} \cdot Z_{out}} = 50$ Ohm (characteristic impedance of TL), where $Z_{in} = 25$ Ohm (input impedance of the splitter without matching (point A)), $Z_{out} = 100$ Ohm (output impedance of the unmatched splitter with TLs (point B)). Afterwards, a way from point B to point C could be realized using the parallel resistor with the value $R = 100$ Ohm.

Unmatched scattering parameters of the splitter are marked with dashed gray curves and the parameters of the matched power divider are marked with colored lines, in the same manner as it was done in the previous chapter. The matched scattering parameters are concentrated closely to each other inside the matching region. Such broadband matching occurs due to the positioning of all frequency points along the circle line with equal conductivity after the quarter-wave transformation. Thus the final network is perfectly matched at the central frequency and it is broadband at the same time.

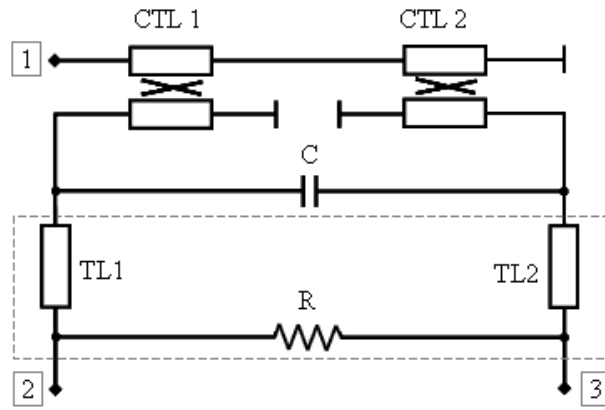
This time the outputs are matched but the input return loss arises as a limitation factor on the bandwidth. Let's turn to the smith chart again. Input matching of the circuit depicted in Fig. 4.13a is shown in Fig. 4.14a as a dashed gray curve. The optimization procedure was targeted on the best matching in the middle of the passband, thus the passband coil is placed so, that the center frequency cross a center of the smith chart, while other frequencies lie on the right-hand side from the center and the outermost values came out of the matching circle that corresponds to 10 dB limit. A logical step would be now to move the characteristics to the left-hand side improving the passband performance in such a way. A quasi-optimal input impedance value at the center frequency will be 40 Ohm.

The input impedance value is defined with even- and odd-mode parameters of the coupled transmission line, as it's shown in (4-23). Assuming that the coupling coefficient has to be optimal for the best transmission conditions, even- and odd-mode characteristic impedances can be found from equation system:

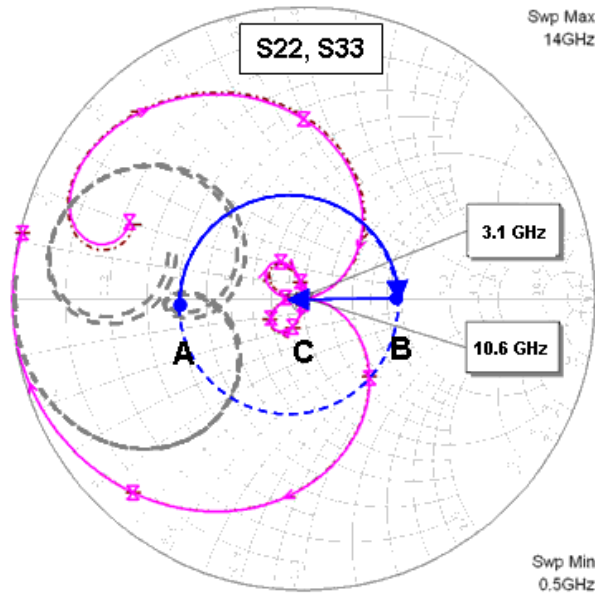
$$\begin{cases} k_{opt} = \frac{1}{\sqrt{2}} = \frac{Z_{0e} - Z_{0o}}{Z_{0e} + Z_{0o}} \\ Z_{0_{CTL}} = 40 = \sqrt{Z_{0e} \cdot Z_{0o}} \end{cases} \quad (4-41)$$

Finally we've got the quasi-optimal values of the impedances for the maximal bandwidth:

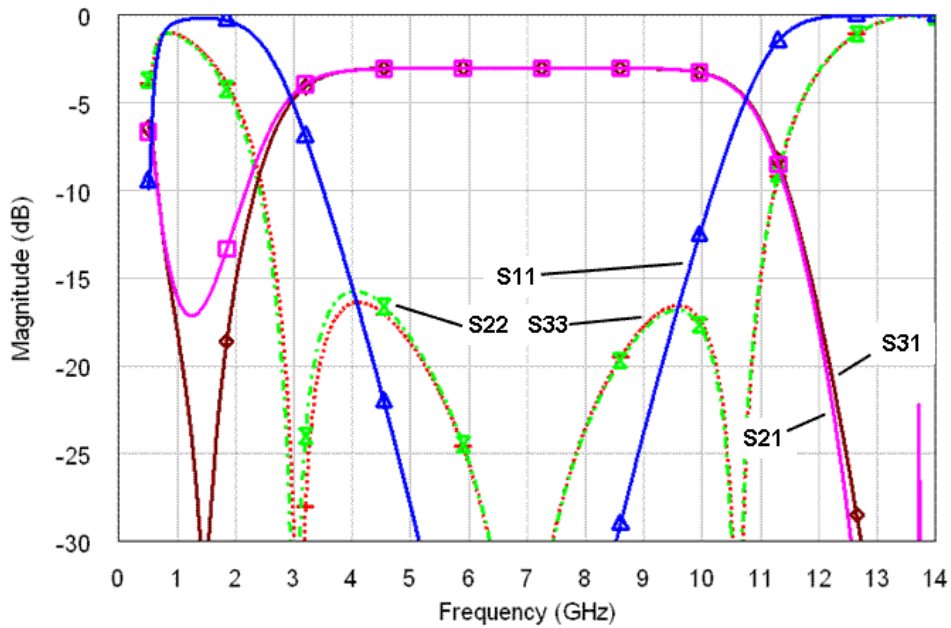
$$\begin{cases} Z_{0e} = 100 \text{ Ohm} \\ Z_{0o} = 15 \text{ Ohm} \end{cases} \quad (4-42)$$



a) Schematic



b) Matching procedure (smith diagram)



c) Amplitude characteristics

Figure 4.13: Power divider with matching “type 3” (simulated using Microwave Office [29])

The splitter built on these calculated values shows much better performance in the bandwidth, though the return loss is not optimal in the middle of the passband, where its input S-parameter curves are shown in Fig. 4.14a with colored line. The line from the point A to the point B shows this correction procedure. The overall transmission performance is depicted in Fig. 4.14b. The bandwidth is wider than in the last case and the return loss at all ports is below -10 dB.

Thus, the maximum achievable bandwidth has been reached and it covers UWB bandwidth luckily. In contrary to a coupled transmission line power divider described in [19], the proposed splitter meets 110 % bandwidth barrier with much smaller even- and odd-mode impedance values that corresponds with much smaller size of the structure (for more or less equal impedance values, the new power divider provides 110 % bandwidth, while the described one provides only 40 %). Moreover, the optimal values for the even- and odd-mode impedances exist as well as the coupling coefficient, while for the known power divider; these values have to be as high as possible to achieve the maximal bandwidth. From this point of view, the new proposed power divider is more attractive for miniaturization reasons.

4.3 Realization Using LTCC

LTCC technology has been used to realize the power divider described in the previous chapter. As a prototype for the realization, the best design is selected. It's the design utilizing transmission line matching depicted in Fig. 4.13a with the impedance values from (4-42) corresponded to the maximal bandwidth, which simulated characteristics are shown in Fig. 4.14b.

The problem of the realization implies a constraint of the design rules that define restrictions on physical structure implementation, e.g. the minimal line width, the minimal distance between elements, etc. Thus the main task is to reproduce physically the coupled lines with the even- and odd-mode impedances realized more closely to the calculated ones. We are going to operate with the following LTCC design rules:

- 1) K8 material (ceramic with dielectric permittivity of 7.8);
- 2) minimum width of the lines is equal to 50 microns;
- 3) minimum layer thickness is equal to 50 microns;
- 4) distance between lines in the same layer is 100 microns;
- 5) other parameters are standard and they are not critical for this type of design.

There are two types of the design that corresponds to different integration purposes:

- 1) a component for further integration in modules;
- 2) a single component (without the following high level integration).

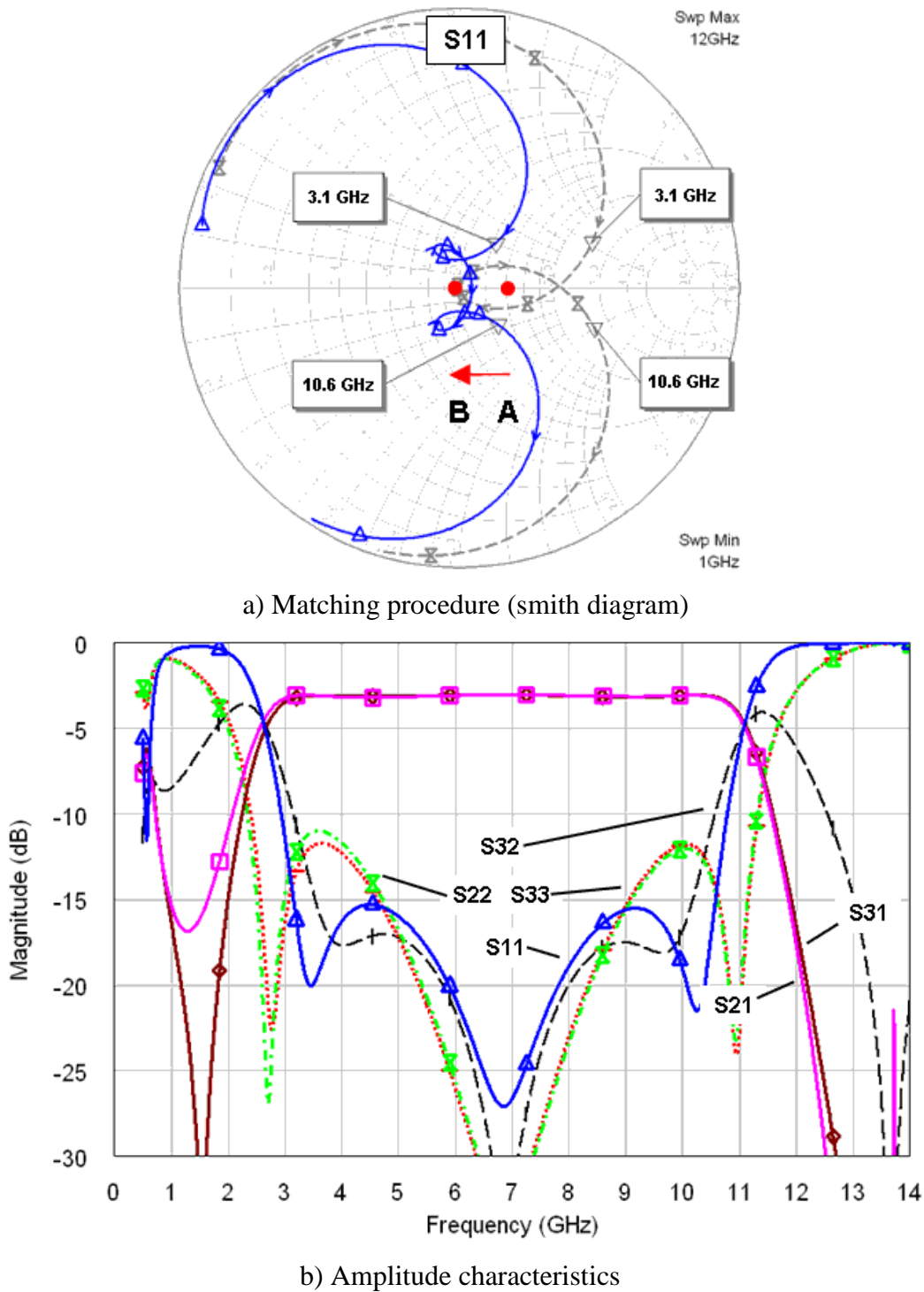


Figure 4.14: Power divider from Fig. 4.13 with quasi-optimal values of Z_{0e} , Z_{0o} (simulated using Microwave Office [29])

Difference between these two components lies in the maximum possible height. The top limit for any integrated component varies between 1.0 and 1.4 mm, accordingly to implementation requirements. This limit is applicable for both a module and separate component realization. Assuming that the module with high level integration includes some active components on the surface, the total height value has to be distributed between the components placed on the top and the passive structure inside LTCC. Thus, typical

requirement for the component to be placed in the module will be the maximal height of 0.8 mm, while this value for the separate component will assign the full available area.

Let's firstly investigate more complicated case – the first type of the component confined with 0.8 mm in height. Based on own height of the ceramic layer and the metallization thickness around 7 microns, overall possible number of the layers would be 14. Broadside-coupled striplines were selected for the splitter realization, because of its full symmetry and shield protection from all sides. 3D structure will have a look like it's shown in Fig. 4.15. The input and output lines shown with magenta color are situated inside the structure and they are ready to be implemented for interconnections within a module. Two magenta pads situated on the top of the LTCC module are meant for soldering an external SMD resistor. On the right hand side of the picture, the coupled striplines are confined within two ground layers, an internal capacitor is placed above. In order to minimize the size of the component, the coupled transmission lines are realized in form of spirals, which function was successfully proved on an example of the Marchand balun and its derivative designs [27]. The matching lines are also implemented using the spiral form, but they are microstrip lines, which characteristic impedance is equal to 50 Ohm, like it was simulated above. Due to the special form that is similar to a typical inductance design, these lines are not clearly transmission lines and they could be observed like a quasi-transmission lines or quasi-Pi-circuit shown in the Fig. 4.12a, taking into account self capacitance to ground. Assuming all approaches given above, the final characteristics are expected to be not ideal and slightly different to the ones shown in the Fig. 4.14b.

Special connectors named launchers depicted in Fig. 4.16 are used to measure the internal circuit. They are connected with the circuit from one side and the other side is situated on the bottom of a ceramic piece. Produced LTCC ceramic with a lot of structures inside shown in Fig. 4.17 is ready for the measurements. The power divider is zoomed out from the panel. Measurements will be provided using a probe device utilizing connectors, which are compatible with the launcher footprint, by turning upside-down and following testing the internal structures. The procedure allows us to measure components without cutting.

The power divider has been designed for 5 GHz WLAN / WiMAX band. Though the bandwidth is too narrow in comparison with UWB and almost any power divider could provide such function, an idea was to use the same splitter for 2 GHz WLAN / WiMAX and 3 GHz WiMAX bands. Therefore, working center frequency has been selected in the middle and it's equal to 4.5 GHz. This issue determines the line lengths of the coupled striplines and the matching lines; they are equal and must be:

$$L_{CTL} = L_{TL} = \frac{\lambda_g}{4} = \frac{c}{4f_0\sqrt{\epsilon}} = \frac{3 \cdot 10^8}{4 \cdot 4.5 \cdot 10^9 \sqrt{7.8}} = 5.967 \text{ mm} \approx 6 \text{ mm}$$

The capacitance value can be derived from the Fig. 4.6. In order to cover 55 % of the bandwidth, we need the capacitor with the value of 0.7 pF.

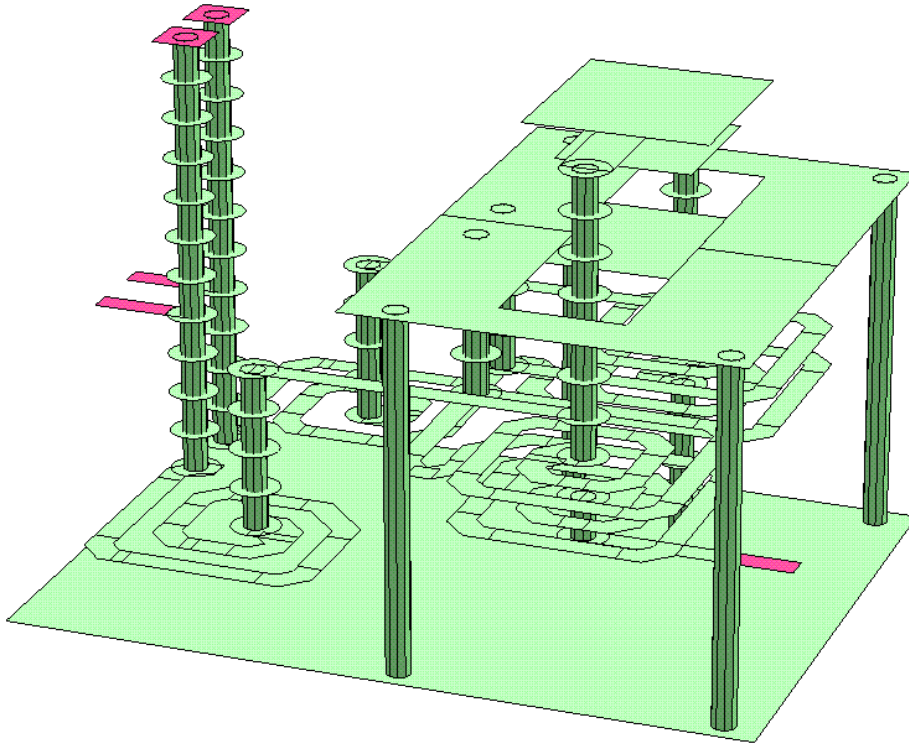


Figure 4.15: 3D view of the power divider realization using 14 layers (drawn using Sonnet [30])

The last step would be an estimation of the even- and odd-mode line impedances. The optimal values are given in (4-42) and this is the design target to be achieved. We have to operate with a number of layers and line widths given in the design rules above. Finally, due to optimization of the even- and odd-mode impedance values, the component will require all available 14 layers, while the coupled stripline section will occupy only 9 layers. The layers are collated in the following way: 4 layers are between each of the striplines and the ground, 1 layer is between the coupled striplines, and the others layers are occupied for the capacitance and the external shields. Using the method described in [28], the impedances result in the following values:

$$Z_{0e} = \frac{188.3/\sqrt{\epsilon_r}}{\frac{w/b}{1-s/b} + \frac{C'_{fe}}{\epsilon}} = 51 \text{ Ohm}$$

$$Z_{0o} = \frac{188.3/\sqrt{\epsilon_r}}{\frac{w/b}{1-s/b} + \frac{w}{s} + \frac{C'_{fo}}{\epsilon}} = 20 \text{ Ohm}$$

where $\epsilon_r = 7.8$ (relative dielectric constant), $w = 100 \mu\text{m}$ (line width), $b = 450 \mu\text{m}$ (distance between ground planes for the coupled striplines), $s = 50 \mu\text{m}$ (distance between

the coupled lines), $\frac{C'_{fe}}{\epsilon} = \frac{C'_{fo}}{\epsilon} = 0.88$ (even- and odd-mode fringing capacitances, graph values [28]).

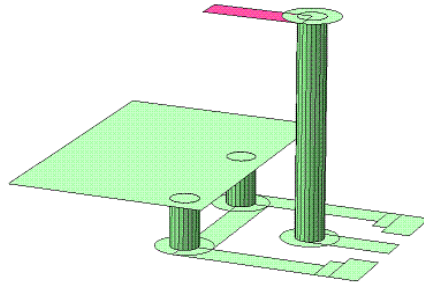


Figure 4.16: Launcher configuration (drawn using Sonnet [30])

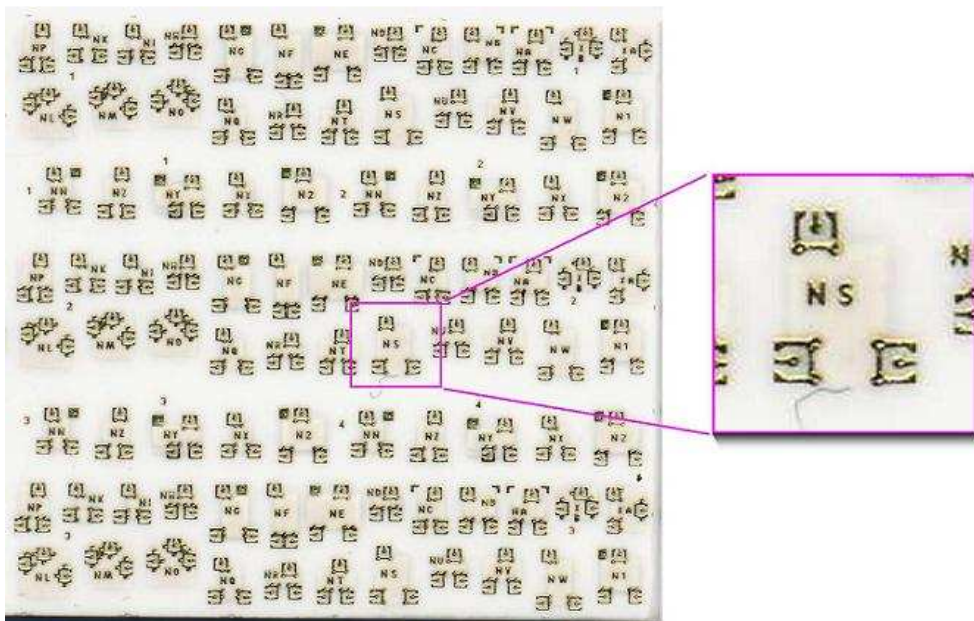


Figure 4.17: LTCC panel view

Due to the design rules restrictions, the values are not optimal. The odd-mode impedance value could not be reduced, because the minimal distance between the coupled lines is already used. The even-mode impedance has got its maximal value due to impossibility to increase the number of layers. Because of non-optimal impedance values, the input impedance and the coupling coefficient of the coupled lines are also not optimal. For a homogeneous dielectric with the quarter-wave coupled lines, their values are using an equation (4-23):

$$\begin{cases} k = 0.436 \\ Z_{0_CTL} = 32 \text{ Ohm} \end{cases}$$

The simulation results of the power divider with calculated parameters are depicted in Fig. 4.18. As expected, the matching is not optimal in the passband, but good enough (the return loss is less than 10 dB). The measurements in comparison with the simulations

are shown in Fig. 4.18 and they are pretty good correlated. As it's clear from the characteristics, the maximal potential bandwidth is 110 % and it corresponds to the value calculated before. The capacitance value increased minimum up to 5 pF (Fig. 4.6) will enlarge the bandwidth up to the maximal possible value. Thus, the passband will be covered from 2 to 7 GHz, because of the improvement of the amplitude balance at the left side of the power divider performance corresponding to the graph (Fig. 4.7).

Let us now consider the power divider as a single component, which is able to possess the total available height of 1.0 - 1.4 mm. The situation is now much better in case of design freedom, though we are still confined with the design rules and only discrete values of the impedances can be achieved, because of the discrete thicknesses of the layers. The goal values remain the same as before and they have been evaluated above in (4-42).

The power divider designed under these conditions is depicted in Fig. 4.19. The structure is similar to the one shown in the Fig. 4.15, excepting the values of the elements. The center working frequency is higher now and it's equal to 6.85 GHz, therefore the length of the coupled lines and the matching lines is:

$$L_{CTL} = L_{TL} = \frac{\lambda_g}{4} = \frac{c}{4f_0\sqrt{\epsilon}} = \frac{3 \cdot 10^8}{4 \cdot 6.85 \cdot 10^9 \sqrt{7.8}} = 3.92 \text{ mm} \approx 4 \text{ mm}$$

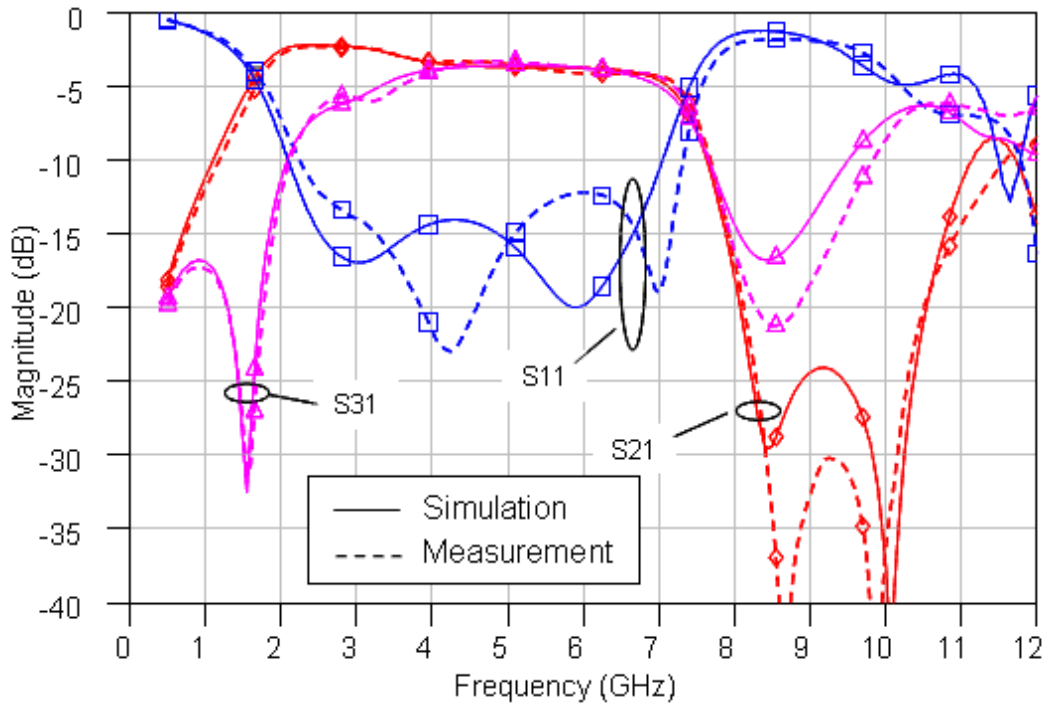
The capacitor is 5 pF that provides function of the power divider within a bandwidth, which is closely to the maximum achievable value. A number of the ceramic layers used for the design is set to 20 corresponding to both the optimal approach and fulfillment of the design rules. Thus, the impedance values are:

$$Z_{0e} = \frac{188.3/\sqrt{\epsilon_r}}{\frac{w/b}{1-s/b} + \frac{C'_{fe}}{\epsilon}} = 83 \text{ Ohm}$$

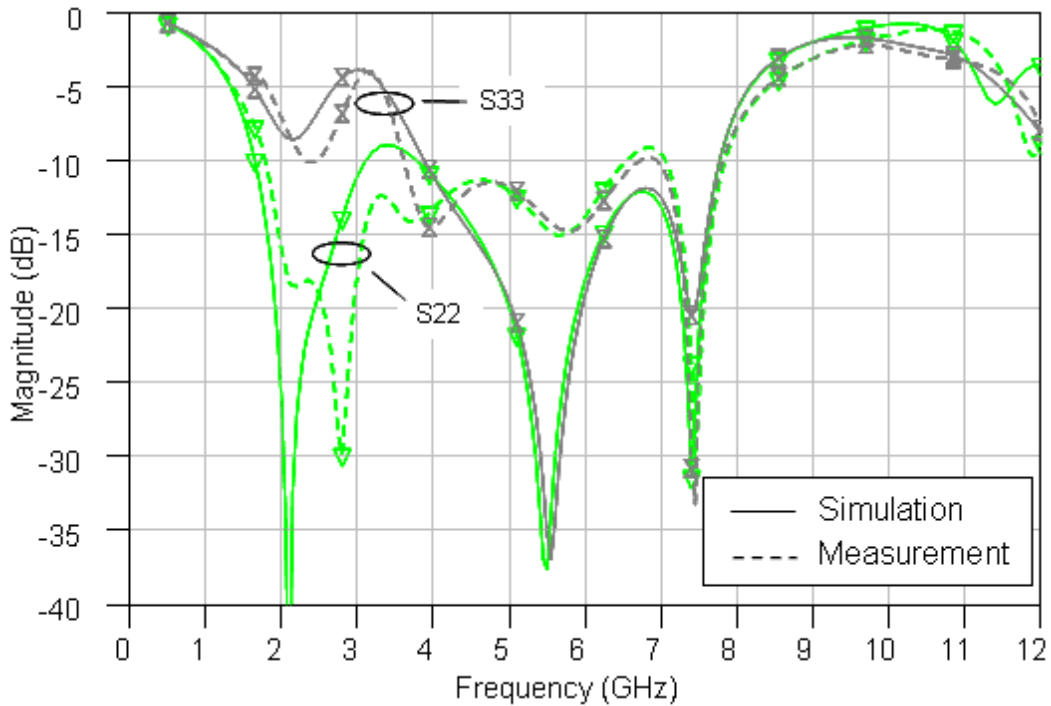
$$Z_{0o} = \frac{188.3/\sqrt{\epsilon_r}}{\frac{w/b}{1-s/b} + \frac{w}{s} + \frac{C'_{fo}}{\epsilon}} = 15 \text{ Ohm}$$

where $\epsilon_r = 7.8$ (relative dielectric constant), $w = 150 \mu\text{m}$ (line width), $b = 650 \mu\text{m}$ (distance between ground planes for the coupled striplines), $s = 50 \mu\text{m}$ (distance between the coupled lines), $\frac{C'_{fe}}{\epsilon} = 0.54$; $\frac{C'_{fo}}{\epsilon} = 1.2$ (even- and odd-mode fringing capacitances (from [28])). This time the even- and odd-mode impedances are much closer to the optimal values. Calculated coupling coefficient and input impedance are shown below:

$$\begin{cases} k = 0.7 \approx \frac{1}{\sqrt{2}} \\ Z_{0_{CTL}} = 35 \text{ Ohm} \end{cases}$$



a) Transmission and input return loss



b) Output return loss

Figure 4.18: Performance of the power divider (simulations using [30] vs. measurements) plotted in [29]

The coupling coefficient is almost equal to the optimal one, calculated in (4-41). The input impedance a little bit smaller than the expected one that results in the slightly worse matching. Simulated performance of the designed power divider is shown in Fig. 4.20.

Simulated characteristics of the splitter are expected to be the same as the ones calculated and shown in the Fig. 4.14b, unfortunately, several differences are obvious. Worsening of the matching is already explained with the input impedance discrepancy.

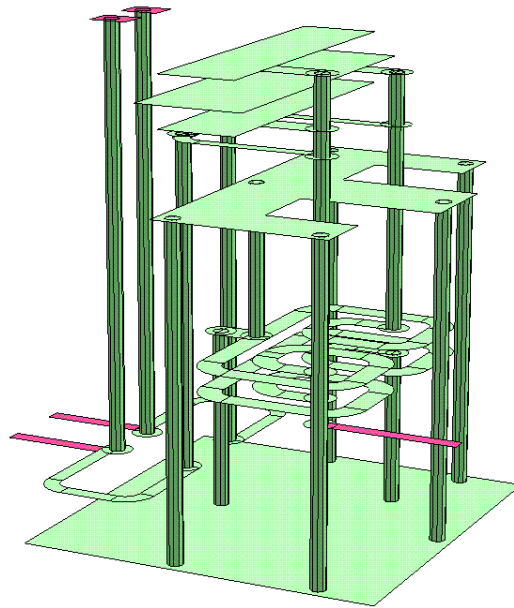


Figure 4.19: 3D view of the power divider realization using 20 layers (drawn using Sonnet [30])

What is about the bandwidth reduction? The results are unexpected, higher frequencies of the splitter are confined with 8.6 GHz instead of 10.6 GHz. How can such a difference of 2 GHz happen? The closer analysis of the structure realized that the performance is limited with the capacitor realization.

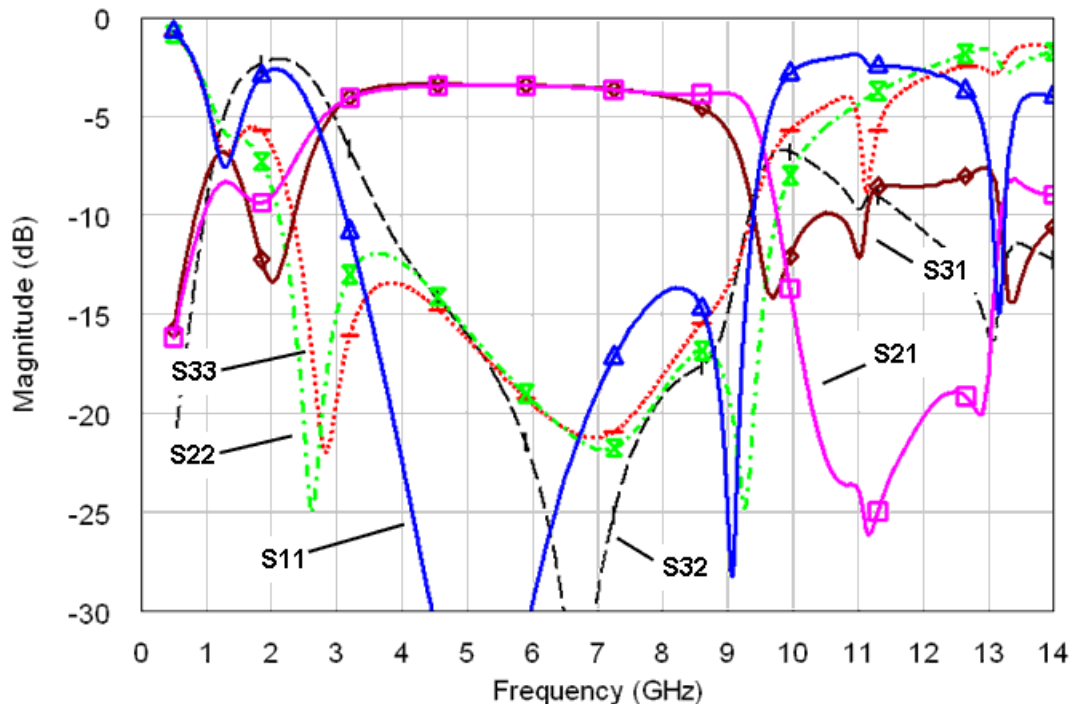


Figure 4.20: Simulated performance of the UWB power divider (using Sonnet [30])

The capacitor is too big in size and the first self resonance assuming parasitic inductances of connecting conductors lays about 9.6 GHz, which influences the function dramatically. Main contribution is made by the connection between the coupled transmission lines and the capacitor. A realization of the lines as half-wave sections could be helpful, but firstly the component size would be enormous and secondly these lines would bring self resonances decreasing the performance in such a way. Decreasing of the capacitance size doesn't help, because the passband will be reduced under the conditions described above and correspondingly to the graphic shown in the Fig. 4.6. Thus the performance is confined within these limits and the only solution would be eliminating the self resonances of the multilayer capacitor. SMD component could be used instead of the multilayer capacitor also, but all such components are limited with frequency as well and usually they don't function up to 10 GHz. So, the main challenge for the future work is to solve this high frequency problem.

4.4 Results on UWB Power Divider

The novel solution for the ultra-wideband power divider was proposed in this work. The theoretical investigations show an essential improvement of case size and bandwidth in comparison with the existing solutions. Most of the existing CTL solutions need enormous increasing of the even-mode impedance value in order to achieve wideband performance. Proposed power divider is able to operate with the same passband ranges up to 110 % of relative bandwidth but with much smaller even-mode impedance values, resulting in much smaller structure size. The even- and odd-mode impedances must be equal to the optimum values, which can be calculated using strict defined procedure. In contrary to the already known transmission line splitters, the described power divider can be realized in LTCC technology in a small size using spiral lines. Implementing other structures is not possible due to performance degradation. Unfortunately, its function at higher frequencies is confined with self resonance of the large capacitor based on parasitic effects, but it's normally for discrete components that function under defined frequency limit. Operation on such high frequencies assumes using the components with distributed parameters. Thus, the future work corresponds to finding the solution for this issue.

Assuming the fact that existing UWB system solutions function without using the total UWB frequency band, proposed power divider is already could be usable UWB solution. The power divider was successfully designed on base of the attached calculation process, produced using LTCC and measured. The measurements show good agreement with the simulations that proves applicability of the design.

4.5 References to Chapter 4

- [1] E. J. Wilkinson, "An N-way Hybrid Power Divider," *IRE Transactions on Microwave Theory and Techniques*, vol. 8, Jan. 1960, pp. 116-118.
- [2] N. Nagai, E. Maekawa and K. Ono, "New N-way Hybrid Power Dividers," *IEEE Transactions on Microwave Theory and Techniques*, vol. 25, Dec. 1977, pp. 1008-1012.
- [3] H. R. Mgombelo and H. Nielinger, "Broadband N-way, Equiphase, Equal-Power Wilkinson Dividers," *AMSE Modeling, Simulation and Control*, vol. 29. No. 3, 1990.
- [4] C. C. Franck and J. B. Franck, "Preliminary Study of the Admittance Diagram as a Useful Tool in the Design of Stripline Components at Microwave Frequencies," *Proceeding on SPIE*, vol. 1527, Dec. 1991, pp. 288-290.
- [5] C. C. Franck and J. B. Franck, "A Practical Example Using the MOT Method," *Microwave Journal*, Jul. 1995.
- [6] L. Fan and K. Chang, "A 180° Out-of-Phase Power Divider Using Asymmetrical Coplanar Stripline," *IEEE Microwave and Guided Letters*, vol. 6, No. 11, Nov 1996, pp. 404-406.
- [7] S. Tsitsos, N. Karamitsos, B. M. Dillon and A. A. P. Gibson, "Variational Solution of Microwave Circuits and Structures," *IEEE Transactions on Microwave Theory and Techniques*, vol. 44, No. 3, Mar. 1996, pp. 460-462.
- [8] Y. Sun and A. P. Freundorfer, "Broadband Folded Wilkinson Power Combiner/Splitter," *IEEE Microwave and Wireless Components Letters*, vol. 14, No. 6, Jun. 2004, pp. 295-297.
- [9] A. Wentzel, V. Subramanian, et al., "Novel Broadband Wilkinson Power Combiner," *Proceedings on European Microwave Conference*, Sept. 2006, pp. 212-215.
- [10] L. Yang and Q. Chu, "Design of a Compact UWB Wilkinson Power Divider," *Proceedings on International Conference on Microwave and Millimeter Wave Technology ICMMT*, vol.1, Apr. 2008, pp. 360-362.
- [11] J. Staudinger, "Wide Bandwidth MMIC Power Dividers: Implementation and a Practical Design Technique," *Microwave Journal*, Feb. 1990.
- [12] H. S. Nagi, "Miniature Lumped Element 180° Wilkinson Divider," *IEEE MTT-S International Microwave Symposium Digest*, vol. 1, Jun. 2003, pp. 55-58.
- [13] D. Kholodnyak, P. Kapitanova, et al., "Novel Wilkinson-Type Power Dividers Based on Metamaterial Transmission Lines," *Proceedings on European Microwave Conference*, Oct. 2008, pp. 341-344.

- [14] R. Pazoki, M. R. G. Fard and H. G. Fard, "A Modification in the Single-Stage Wilkinson Power Divider to Obtain Wider Bandwidth," *Proceedings on Asia-Pacific Microwave Conference*, Dec. 2007, pp. 1-4.
- [15] X. Qu and Q. Chu, "A Modified Two-section UWB Wilkinson Power Divider," *Proceedings on International Conference on Microwave and Millimeter Wave Technology ICMWT*, vol. 3, Apr. 2008, pp. 1258-1260.
- [16] Y. Zhu, X. Zhang, et al., "Novel Wilkinson Power Divider with Uniform Impedance Line," *Proceedings on Asia-Pacific Microwave Conference*, Dec. 2008, pp. 1-4.
- [17] O. Ahmed and A. R. Sebak, "A Modified Wilkinson Power Divider/Combiner for Ultrawideband Communications," *Antennas and Propagation Society International Symposium Digest*, Jun. 2009, pp. 1-4.
- [18] S. Y. London, "A New Broadband Coupled-Line N-Way Power Combiner/Splitter," *Applied Microwave and Wireless*, May 2001.
- [19] I. Kang and J. Park, "A Reduced-size Power Divider Using the Coupled Line Equivalent to a Lumped Inductor," *Microwave Journal*, Jul. 2003.
- [20] P. K. Singh, S. Basu and Y. Wang, "Coupled Line Power Divider with Compact Size and Bandpass Response," *IEEE Electronics Letters*, vol. 45, Aug. 2009, pp. 892-894.
- [21] R. Kravchenko, "Broadband RF Power Divider," *Patent application*, P2008,0588 DE.
- [22] R. Kravchenko, M. Stadler and E. Leitgeb, "A New UWB Coupled Transmission Line Power Divider," *IEEE MTT-S International Microwave Symposium Digest*, May 2010, pp. 1568-1571.
- [23] N. Marchand, "Transmission-Line Conversion Transformers," *Electronics*, vol. 17, Dec. 1944, pp. 142-146.
- [24] W. Klein, *Mehrtortheorie*, 3d ed., Ed. Berlin, Germany: Akademie-Verlag, 1976, pp. 60, 111.
- [25] R. Mongia, I. Bahl and P. Bhartia, *RF and Microwave Coupled-Line Circuits*, Ed. Boston, London: Artech House, 1999, p. 137-138, 258.
- [26] K. S. An, Y. C. Leong and C. H. Lee, "Analysis and Design of Miniaturized Lumped-Distributed Impedance-Transforming Baluns," *IEEE Transactions on Microwave Theory and Techniques*, vol. 51, Mar. 2003, pp. 1009-1017.
- [27] R. Kravchenko, K. Markov, et al., "Implementation of a Miniaturized Lumped-Distributed Balun in Balanced Filtering for Wireless Applications," *Proceedings on European Microwave Conference*, Oct. 2005, 4 pp.
- [28] G. L. Matthaei, L. Young and E. M. T. Jones, *Microwave Filters, Impedance-Matching Networks, and Coupling Structures*, Ed. Norwood, MA: Artech House Inc., 1980, pp. 180-181.
- [29] AWR Microwave Office Software Inc. v. 9.02r, 2010.
- [30] Sonnet Software Inc. v.12.52, 2010.

5. A New Multiplexing Circuit

A variety of the existing wireless communication standards provides a wide spectrum of service. Modern communication equipment supporting multi-functional operation tries to cover as much functions as possible. Additionally, requirements on the equipment demonstrate a tendency of system miniaturization leading in sum to the small and high-performance component base. A common multi-frequency transceiver supporting frequency division multiple access (FDMA) incorporates a front-end part comprised by a number of passive elements such as filters, baluns, multiplexers and different matching circuits. The main function of the high frequency front-end part is to separate / combine frequency channels, where the most challenging process belongs to operation with contiguous channels (located closely to each other). The present work assumes development of the components using multilayer LTCC technology, which makes the development process more complicated, because of the difficult or even not applicable existing solutions in the multilayer technology.

A lot of work has been done during a long time period on analyzing a problem of the contiguous bands being multiplexed and presenting different solutions for this. A basic theory of a channel multiplexing is given in [1], while some particular cases are described in [2] - [5]. There are four common used types of the multiplexers, such as manifold, using directional filters, series / parallel interconnection and the cascaded ones. The first type provides a contiguous multiplexing of the filters with very narrowband response. Its realization lies mostly on a waveguide technique due to specific of the structure consisting of a waveguide line with a propagating signal along and bandpass filters connected in parallel to the line. In order to obtain the optimal frequency division by filtering, additional components like matching circuit or delays have to be used in the structure, thus making the multiplexer design complicated and less compatible with the multilayer realization, additionally restricting the maximal bandwidth of each channel. A number of such contiguous multiplexers have been described in [6] - [14], where most of them function at higher frequencies and are intended for a satellite channel combining. An optimization algorithm for the multiplexers was developed in [15]. A solution for LTCC substrate presented in [16] shows good results with a relative large size making impossible the fact of using the multiplexer in small and compact devices. The next type of the multiplexers based on using the directional filters (described in [1]) is too enormous and complicated because of implementing two times more bandpass filters and two 90° hybrids for each of

the channels. Such issue doesn't give an opportunity to use these multiplexers in small portable hand-held devices. An attention should be paid for the third multiplexer type representing itself series / parallel filters interconnection. The main advantage of these multiplexers, that the filters and the interconnection point can be realized with any technology including the multilayer one. On the other hand, the structure is simpler and requires any additional components. A focus lies on connection principles of the filters inside the multiplexer. Basic theory and design procedure are depicted in [1] and [2], [3] correspondingly. The last type of the multiplexer is the simplest one and it represents itself cascaded blocks, which are either diplexers or lowpass and highpass filters. The channel multiplexing is provided with step by step frequencies separation by using the LPFs and HPFs, like it shown in [17] and [18]. The last two types are mostly useful for the realization of non-contiguous multiplexers, where the frequency bands are located relatively far from each other. In an opposite way, the contiguous band multiplexing is difficult to realize due to specific requirements on a contrabands reflection.

The idea of this work is to develop the simple multiplexer structure using contiguous channels that could be implemented with the multilayer technology, like LTCC. Manifold multiplexers and the ones using directional filters don't fit into the idea, because of their complexity and their size. The point of interests will be the multiplexers with parallel connected filters and it's focused on an optimal junction configuration providing a possibility of the filters with contiguous bandwidths interconnection. The practical methodology and the examples on production of typical multiplexers with parallel connected filters is described in [19] - [21] in detail. The filters assume to have low (zero Ohm, in ideal case) input impedance at contra-band frequencies. Such impedance behaviour is typical for a majority of filters being a result of schematics and it is much more attractive, because the zero Ohm impedance is much easier to obtain than an infinity high value needed for high level rejection characteristics. On the other hand, accordingly to the theory, the filters with high impedance values at the mentioned frequencies can be directly connected in parallel together taking into account some restrictions. Usually, series connected transmission lines are used for an impedance transformation (quarter-wave transformers) from negligible small values to the large ones in order to prepare the filters for the connection. This procedure alters a little bit the filter characteristics and makes passbands narrower. Other example utilizing TLs proposed in [22] presents ultra-wideband response and tries to triplex the contiguous channels. The concept shows drawbacks already in the simulations resulting in worse return loss (RL) values. Thus it's not possible to achieve the optimal performance by transformation of the input impedance. Another solution for the problem was proposed in [23], [24], where the filters having the high value of the input impedance's real part and specially defined imaginary parts of the impedance in the contra-band frequencies could be directly connected in parallel. During the design

procedure, the filters must be carefully selected using the conditions of the input impedance values and there is not a necessarily issue that the multiplexer built on these principles could provide a contiguous band function. One useful idea described in the patent [25] assumes separating channels on the even and the odd ones accordingly to their numbers, combining them into two parts and the following using two antennas for each part – even and odd, while the idea of the invention lies on matching the directional filters together inside the multiplexer. This multiplexer is applicable for three and more channels and needs two antennas, that issue is not practical for small applications. Instead of two antennas, one antenna in combination with a high quality contiguous diplexer can be implemented, thus returning to the question of the contiguous diplexing.

The present work contains investigations on a new junction solution for the filters with contiguous bands connected in parallel, thus forming a multiplexer using easy design procedure and avoiding an effect of worsening of the filters performance due to using the original filters possessing zero Ohm input impedance value for out-of-band rejection.

5.1 Multiplexer concept

One interesting conception of the contiguous multiplexer design providing high selectivity properties is presented in [26]. The idea is to multiple samples of the input signal using a power divider with the following frequency processing of each channel in separate by the filters. Such configuration helps to avoid interactions between the filters, thus improving the filtering characteristics and setting safe distance between the passbands to negligible small value. A price for the perfect multiplexing would be insertion loss (IL), where the more channels the higher losses are included. These losses, of course, are losses on the power division, beginning with 3 dB on division onto two channels. The second drawback is complexity resulting in necessarily using delays and especially Butler matrix.

The target of this work is to develop a multiplexer that avoids losses on the division. Let's take a common balun, for example, Marchand type described in [27]. As it's well known, the balun function is similar to a power divider. In order to convert a single-ended signal into the balanced one, the balun divides the input signal in two parts and rotate the phases, thus two output signals have equal amplitudes and are opposite in phase. The output signal is differential and can be loaded on a differential load, while the output nodes in separate are not matched with a single load. An out-of-phase power divider could be achieved by matching of the outputs with the single loads. Examples of a typical all ports matched balun are shown in [28] - [31]. Unfortunately, the situation remains the same as with the original in-phase power divider, because use of this balun type doesn't give an improvement in IL, that doesn't fit with the given task.

Let's look at the balun from the other side without any attempts to provide all port matching. Two solutions were proposed in [32] and [33], where a broadband slot balun was used as a junction point for the parallel interconnected filters which input impedances are high ("open" in terms of high frequencies) and low ("short") correspondingly. In the first reference, the input impedance of the filters must represent open network for optimal functionality and this fact doesn't meet the requirements put on the filters above, therefore, it's not reasonable to be considered. The second method contains the filters providing the short circuit input impedance and it provides more or less simple construction with high selectivity properties. A payment for this issue will be higher insertion losses due to a mismatch at the outputs. As it will be shown below, using the typical balun with the optimal characteristics gives not optimal performance in the multiplexing circuit.

Therefore, a new approach providing the optimal multiplexer function is presented in this work by connecting the filters to a special circuit, which will be named a quasi-balun. This circuit is based on the balun design but it couldn't be used as the typical balun any more due to modified properties. The input impedance values of the filters are strictly defined as the matched impedance in the transmission band and the short-circuit impedance out-of-passband that corresponds to properties of majority of the resonator filters. A typical view of the diplexer built using this principle is shown in Fig. 5.1a and the required input complex reflection coefficient of the filters is depicted at smith chart (Fig. 5.1b). The solution has been already patented in [34].

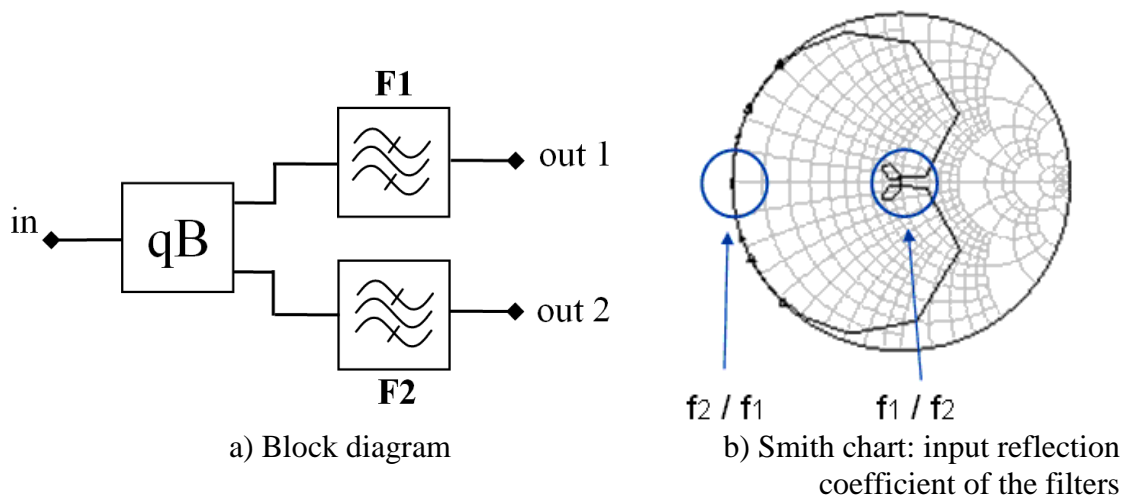


Figure 5.1: An example of the diplexer using new principles

There are following notations in the Fig. 5.1:

- qB: quasi-balun;
- in, out1, out2: input and outputs of the circuit;
- F1 and F2: filters for selected transmission bands;
- f1 and f2: center passband frequencies for corresponding filters.

Simply to say, the filters input impedances must follow the requirements:

$$\left\{ \begin{array}{l} \text{Passband F1:} \\ \text{Passband F2:} \end{array} \right. \begin{cases} Z_{in1} \rightarrow Z_0 \\ Z_{in2} \rightarrow 0 \\ Z_{in1} \rightarrow 0 \\ Z_{in2} \rightarrow Z_0 \end{cases} \quad (5-1)$$

where Z_0 – system impedance.

5.2 Multiplexing Using the Ideal Balun

Structure of the diplexer containing a common balun (B) is depicted in Fig. 5.2 and it's similar to the one shown in Fig. 5.1a. Requirements on the input impedance of the filters remain the same as the ones listed above (5-1). Let's investigate the structure on question, which performance could be expected from it. For the future analysis, all elements will be held as the ideal ones and lossless.

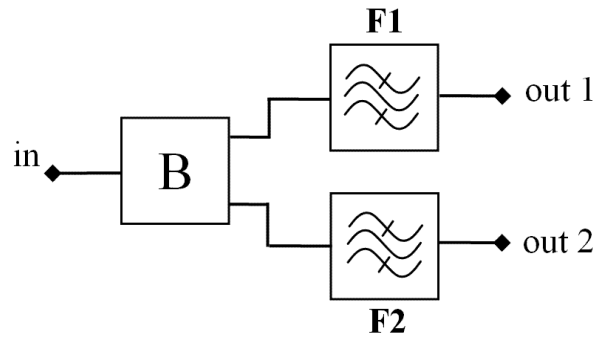


Figure 5.2: Block diagram of the diplexer using a balun

As it's well known, S-parameters of the optimal designed balun look like follow:

$$S_{\text{balun opt}} = \begin{bmatrix} 0 & j/\sqrt{2} & -j/\sqrt{2} \\ j/\sqrt{2} & 1/2 & 1/2 \\ -j/\sqrt{2} & 1/2 & 1/2 \end{bmatrix} \quad (5-2)$$

These S-parameters refer to the balun loaded on the equal load impedance ($Z_0 = 1/Y_0$) at all three nodes (the input and the outputs); normally this system impedance value is equal to 50 Ohm. Thus function is typical for the common balun. On the other hand, the balun functions inside the diplexer under other special conditions. In this case, it's connected to the filters and the output nodes are loaded on the inputs of the filters. The filters impedances are not constant over the whole frequency range, while they vary from zero to the system impedance values and could be even more, as it was shown already in Fig. 5.1b. Thus, the balun will provide different transmission characteristics depending on frequency. It's not necessary to investigate behaviour of the characteristics at all frequencies, as minimum, two typical cases would be enough. The first case corresponds to the frequencies on which the input impedances of the filters are very small or close to zero

and the second case corresponds to that one with the impedance close to Z_0 . These frequencies relate to the transmission bands and contra-band rejection of the filters – the point of interests.

Based on Fig. 5.1b and accordingly to the requirements on the filters (5-1), the input impedance of the filter F1 is close to Z_0 and the input impedance of the filter F2 is close to zero, while observing the passband of the filter F1, and the situation is vice-versa for the passband of the filter F2. Thus, assuming the ideal case, where the corresponding impedances are equal exactly to zero and Z_0 , an equivalent circuit for the loaded balun is shown in Fig. 5.3 for both passband frequencies.

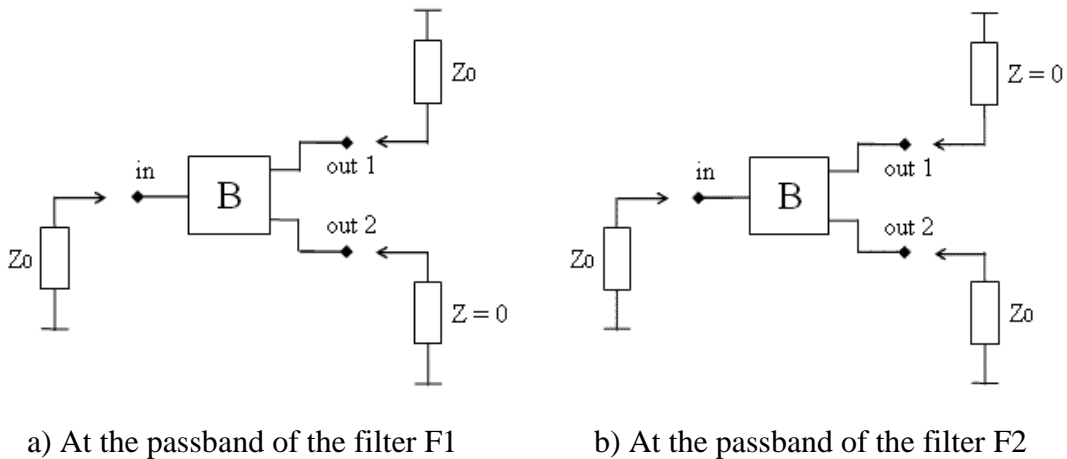


Figure 5.3: Equivalent block diagram of the balun loaded on ideal filters impedances

Assuming full reflection from the short loaded node, there is no sense to analyse the circuit on the transmission characteristics from all three ports. The node loaded on zero Ohm impedance can be terminated on ground and the circuit could be observed as a two-port network. Thus, these two equivalent block diagrams will be transformed into one equivalent circuit shown in Fig. 5.4 due to symmetrical function of the balun.

This equivalent circuit is the 2-port network, which contains the 3-port network with one port shorted on ground. Using the fact that both networks are terminated on the ports with the equal impedances $Z_0 = 1/Y_0$, S-parameters of the 2-port network could be obtained by transformation of S-parameters of the 3-port one. Taking into account an interconnection of the port named “out2” with ground, a rational way would be to transform S-parameters to Y-parameters applying required changes and transforming back to S-parameters. Y-parameters of the optimal designed balun, which correspond to S-parameters (5-1), are:

$$Y_{\text{balun opt}} = \frac{j \cdot Y_0}{\sqrt{2}} \begin{bmatrix} 0 & -1 & 1 \\ -1 & 0 & 0 \\ 1 & 0 & 0 \end{bmatrix} \quad (5-3)$$

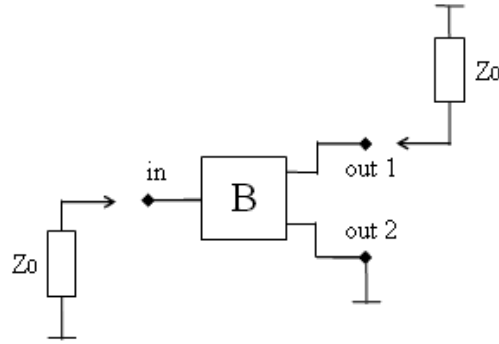


Figure 5.4: Equivalent two-port network of the balun terminated with one node on ground

Let's assign Y_S as an admittance connected to the port "out2". Thus, Y-matrix of such balun will look like follow:

$$Y_{BS} = \frac{j \cdot Y_0}{\sqrt{2}} \begin{bmatrix} 0 & -1 & 1 \\ -1 & 0 & 0 \\ 1 & 0 & Y_S \end{bmatrix} \quad (5-4)$$

Using the transformation equation from [35], the matrix Y_{BS} can be reduced to a matrix with size 2 x 2:

$$Y_{BS} = \frac{Y_0}{\sqrt{2}} \begin{bmatrix} Y_0 / \sqrt{2} Y_S & -j \\ -j & 0 \end{bmatrix} \quad (5-5)$$

This matrix corresponds already to the 2-port network shown in Fig. 5.4. Using the backward transformation, S-parameters matrix can be achieved like the following:

$$S_{BS} = \begin{bmatrix} \frac{Y_S - Y_0}{3Y_S + Y_0} & \frac{2j\sqrt{2}Y_S}{3Y_S + Y_0} \\ \frac{2j\sqrt{2}Y_S}{3Y_S + Y_0} & \frac{Y_S + Y_0}{3Y_S + Y_0} \end{bmatrix} \quad (5-6)$$

If port "out2" is connected to ground, then $Y_S \rightarrow \infty$ and S-parameters of the optimal balun with one port shorted on ground will be:

$$S_{BSG} = \begin{bmatrix} 1/3 & j2\sqrt{2}/3 \\ j2\sqrt{2}/3 & 1/3 \end{bmatrix} \quad (5-7)$$

Analysing these S-parameters matrix, a conclusion can be done that the 2-port network is not matched at the input and output nodes and a part of incident energy is transmitted through; other part of the energy is reflected back from the input. Physical meaning of this issue is the following - if two filters are connected to the optimal balun outputs, where one filter provides zero impedance value in the passband frequencies of the other one causing in reflection from corresponding node, then not all of the energy comes to the second filter and it will not be perfect matched with the balun inside the diplexer

structure, therefore the diplexer will not be perfectly matched, too. Moreover, it occurs in the ideal case, while the situation in the practice will be even worse assuming losses and mismatch.

5.3 New Approach

Finally, the optimal diplexing function using filters which meet the requirements (5-1) and the balun providing optimal function is not possible. So, the optimal balun is not a solution for the optimal diplexer. A new solution has to be found to fulfill the requirements of the optimal multiplexer. Marchand balun will be chosen as a prototype for a new multiplexing circuit. What are the parameters we can operate with? General Marchand balun is built of two coupled transmission line sections interconnected in manner shown in Fig. 5.5. Coupled lines are usually being described with even- (Z_{0e}) and odd-mode (Z_{0o}) impedance values due to propagation of the modes named correspondingly. By varying these modes, the characteristic impedance ($Z_{0\text{CTL}}$) of the CTL and the coupling coefficient (k) between the CTL can be controlled. This relation is given in [36]:

$$\begin{cases} k = \frac{Z_{0e} - Z_{0o}}{Z_{0e} + Z_{0o}} \\ Z_{0\text{CTL}} = \sqrt{Z_{0e} \cdot Z_{0o}} \end{cases} \quad (5-8)$$

CTL's characteristic impedance $Z_{0\text{CTL}}$ has to be matched with the system impedance Z_0 and this value is constant. The parameter, which gives a freedom, is the coupling coefficient k . Firstly, S-parameters of the balun have to be presented depending on the coupling coefficient. For this reason, the balun must be analysed basing on the single CTL parameters. The figure 5.5 shows Marchand balun separated on parts, which contain single couplers. Nodes of the coupler are denoted with the signs from 1 to 8, where incident (a) and reflected (b) wave directions are shown. The port 1 is assigned as the input one and the ports 2 and 3 as the output ones; the abbreviation "o.c." means open circuit; other outputs of the couplers are connected to ground.

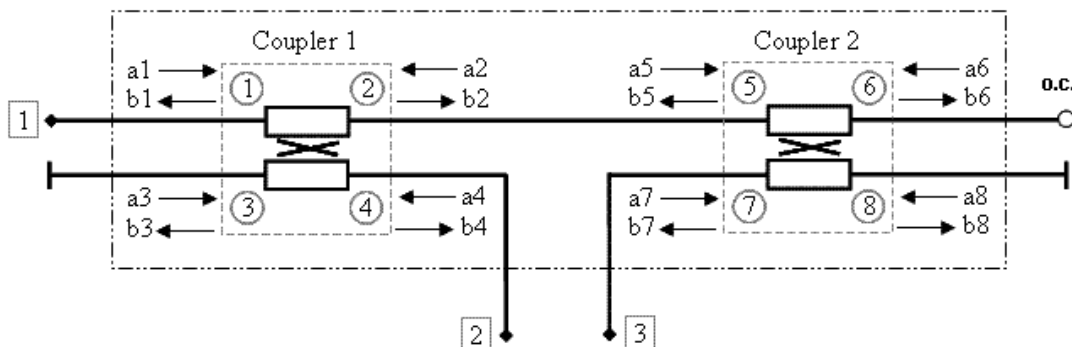


Figure 5.5: Marchand balun: detailed schematic of the basement for new multiplexer

S-parameters matrices of the basement for the new multiplexer and the single coupler will have following forms:

$$[S]_{\text{bM}} = \begin{bmatrix} S_{11}^{\text{bM}} & S_{12}^{\text{bM}} & S_{13}^{\text{bM}} \\ S_{21}^{\text{bM}} & S_{22}^{\text{bM}} & S_{23}^{\text{bM}} \\ S_{31}^{\text{bM}} & S_{32}^{\text{bM}} & S_{33}^{\text{bM}} \end{bmatrix} \quad (5-9)$$

$$[S]_{\text{Coupler}} = \begin{bmatrix} S_{11}^{\text{C}} & S_{12}^{\text{C}} & S_{13}^{\text{C}} & S_{14}^{\text{C}} \\ S_{21}^{\text{C}} & S_{22}^{\text{C}} & S_{23}^{\text{C}} & S_{24}^{\text{C}} \\ S_{31}^{\text{C}} & S_{32}^{\text{C}} & S_{33}^{\text{C}} & S_{34}^{\text{C}} \\ S_{41}^{\text{C}} & S_{42}^{\text{C}} & S_{43}^{\text{C}} & S_{44}^{\text{C}} \end{bmatrix} \quad (5-10)$$

The task is to obtain 3 x 3 S-matrix of the basement basing on the 4 x 4 S-matrix of the coupler. General S-parameter matrix of the lossless coupler is given in [36]:

$$[S]_{\text{Coupler}} = \frac{j}{\sqrt{1-k^2} \cos \Theta + j \sin \Theta} \begin{bmatrix} 0 & -j\sqrt{1-k^2} & k \sin \Theta & 0 \\ -j\sqrt{1-k^2} & 0 & 0 & k \sin \Theta \\ k \sin \Theta & 0 & 0 & -j\sqrt{1-k^2} \\ 0 & k \sin \Theta & -j\sqrt{1-k^2} & 0 \end{bmatrix} \quad (5-11)$$

where $\Theta = \beta \cdot L$ (phase length) of the CTL, L - physical length of the CTL.

Taking into account that the maximal amount of the coupling between the ports 1 and 3 (or between the ports 2 and 4, 5 and 7, 6 and 8) occurs if the couplers are comprised of the quarter-wave coupled line sections:

$$L = \frac{\lambda_g}{4} \text{ or } \Theta = \frac{\pi}{2} \quad (5-12)$$

where λ_g denotes the guide wavelength of the TL in the medium.

Thus, at the center frequency, by substituting this value in (5-12), the scattering matrix of the coupler can be presented like the following:

$$[S]_{\lambda/4 \text{ Coupler}} = \begin{bmatrix} 0 & -j\sqrt{1-k^2} & k & 0 \\ -j\sqrt{1-k^2} & 0 & 0 & k \\ k & 0 & 0 & -j\sqrt{1-k^2} \\ 0 & k & -j\sqrt{1-k^2} & 0 \end{bmatrix} \quad (5-13)$$

Using the calculations presented in Appendix C, S-parameters of the basement were achieved. Now, S-parameters matrix of the basement proceeds from the relations calculated above between b_1, b_4, b_7 and a_1, a_4, a_7 . It looks like the following:

$$[S]_{\text{bM}} = \frac{1}{1+k^2} \begin{bmatrix} 1-3k^2 & 2jk\sqrt{1-k^2} & -2jk\sqrt{1-k^2} \\ 2jk\sqrt{1-k^2} & 1-k^2 & 2k^2 \\ -2jk\sqrt{1-k^2} & 2k^2 & 1-k^2 \end{bmatrix} \quad (5-14)$$

The S-parameters are the function of the coupling factor or indirect relationship between the even- and odd-mode characteristic impedances of the coupled lines based on

the equation (5-8). This issue provides a relative freedom in control of the transmission characteristics only by changing the TL parameters. Thus, if the optimal function exists, than corresponding parameters of the multiplexer basement can be found. The analysis procedure will be similar to the one implemented above and it lies in the transformation of S-parameters into Y-parameters, the necessarily conversions and the backward transformation.

Y-parameters matrix of the basement would be:

$$[Y]_{bM} = \frac{jkY_0}{\sqrt{1-k^2}} \begin{bmatrix} 0 & -1 & 1 \\ -1 & 0 & 0 \\ 1 & 0 & 0 \end{bmatrix} \quad (5-15)$$

Y-parameters of the basement with the node “out2“ loaded on the admittance Y_S , as it was shown in Fig. 5.4, are:

$$[Y]_{bM} = \frac{jkY_0}{\sqrt{1-k^2}} \begin{bmatrix} 0 & -1 & 1 \\ -1 & 0 & 0 \\ 1 & 0 & -\frac{jY_S\sqrt{1-k^2}}{kY_0} \end{bmatrix} \quad (5-16)$$

The obtained matrix will be reduced to the 2 x 2 one:

$$[Y]_{bMS} = \frac{kY_0}{\sqrt{1-k^2}} \begin{bmatrix} \frac{kY_0}{Y_S\sqrt{1-k^2}} & -j \\ -j & 0 \end{bmatrix} \quad (5-17)$$

The backward transformation into S-parameters matrix follows in:

$$[S]_{bMS} = \frac{1}{Y_S + Y_0k^2} \begin{bmatrix} Y_S(1-2k^2) - Y_0k^2 & 2jkY_S\sqrt{1-k^2} \\ 2jkY_S\sqrt{1-k^2} & Y_S(1-2k^2) + Y_0k^2 \end{bmatrix} \quad (5-18)$$

By connecting the port 3 to ground, which step is equal to the statement $Y_S \rightarrow \infty$, the following matrix corresponded to 2-port circuit shown in Fig. 5.6 occurs:

$$[S]_{bMSG} = \begin{bmatrix} 1-2k^2 & 2jk\sqrt{1-k^2} \\ 2jk\sqrt{1-k^2} & 1-2k^2 \end{bmatrix} \quad (5-19)$$

So, this is 2 x 2 S-parameters matrix, which corresponds to the basement for the multiplexer with the one of the output port connected to ground. Optimal situation would be absence of the reflected from the inputs waves resulting in all-ports matching and the minimum insertion losses ($S_{11} = S_{22} = 0$, or $1 - 2k^2 = 0$). Solving this equation gives an optimal value for the coupling coefficient:

$$k_{bM \text{ opt}} = \frac{1}{\sqrt{2}} \quad (5-20)$$

By substituting this value into (5-19), S-matrix of the basement for the multiplexer will contain the optimal values:

$$[S]_{\text{bMSG opt}} = \begin{bmatrix} 0 & j \\ j & 0 \end{bmatrix} \quad (5-21)$$

So, this 2-port circuit shows perfect matching at both nodes and full transmission. By the way, the optimal coupling coefficient for the multiplexer basement provides the same value as the one for the ultra wideband power divider based also on the coupled transmission line sections and described in this work. In comparison, the optimal coupling coefficient for Marchand balun is equal to $\frac{1}{\sqrt{3}}$.

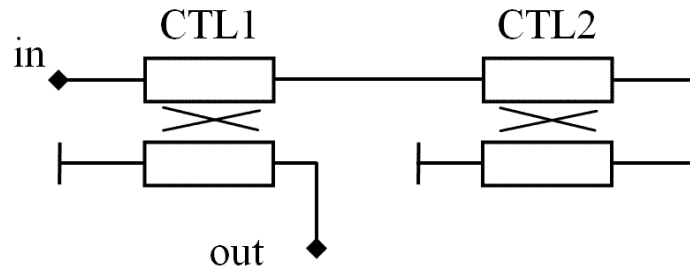


Figure 5.6: Two-port network: the basement terminated with one output on ground

Coming back to the 3-port network shown in the Fig. 5.5 and substituting the optimal coupling value into S-matrix (5-14) related to this circuit, optimal S-parameters matrix for the basement can be achieved:

$$S_{\text{bM opt}} = \begin{bmatrix} -1/3 & j2/3 & -j2/3 \\ j2/3 & 1/3 & 2/3 \\ -j2/3 & 2/3 & 1/3 \end{bmatrix} \quad (5-22)$$

These S-parameters possess now the strictly constant values without any variables. Any circuit (not only the presented above CTL basement) providing such S-parameters can be used as the basement for the proposed type of multiplexing. Usually, structures of another balun types could be taken as a prototype with the following tuning it's characteristics until the parameters required in (5-22) will be achieved.

Thus, using the proposed coupled line circuit providing S-parameters shown in (5-22) in combination with two passband filters providing characteristics correspondingly to (5-1), the optimal contiguous diplexer can be built and its schematic is shown in Fig. 5.7. The multiplexer design is based on this conception, where cascaded diplexers would be typical solutions as it's shown in Fig. 5.8.

The first type is the standard diplexer multiplication method. By increasing the number of the channels, the number of the diplexers (or the number of the basements in this case) grows in geometrical progression causing in high insertion loss. The coupled transmission line concept let to connect the basements in series, thus reducing the number

of that to $N/2$, where N – is a number of the channels. Unfortunately, by large number of the channels, insertion losses are not equal distributed among them.

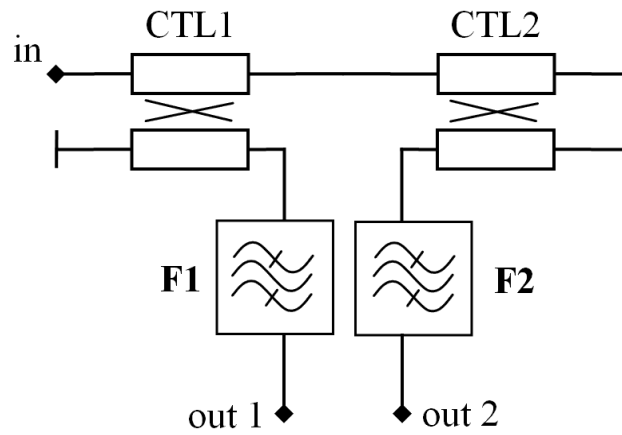


Figure 5.7: New diplexer circuit based on coupled transmission line basement

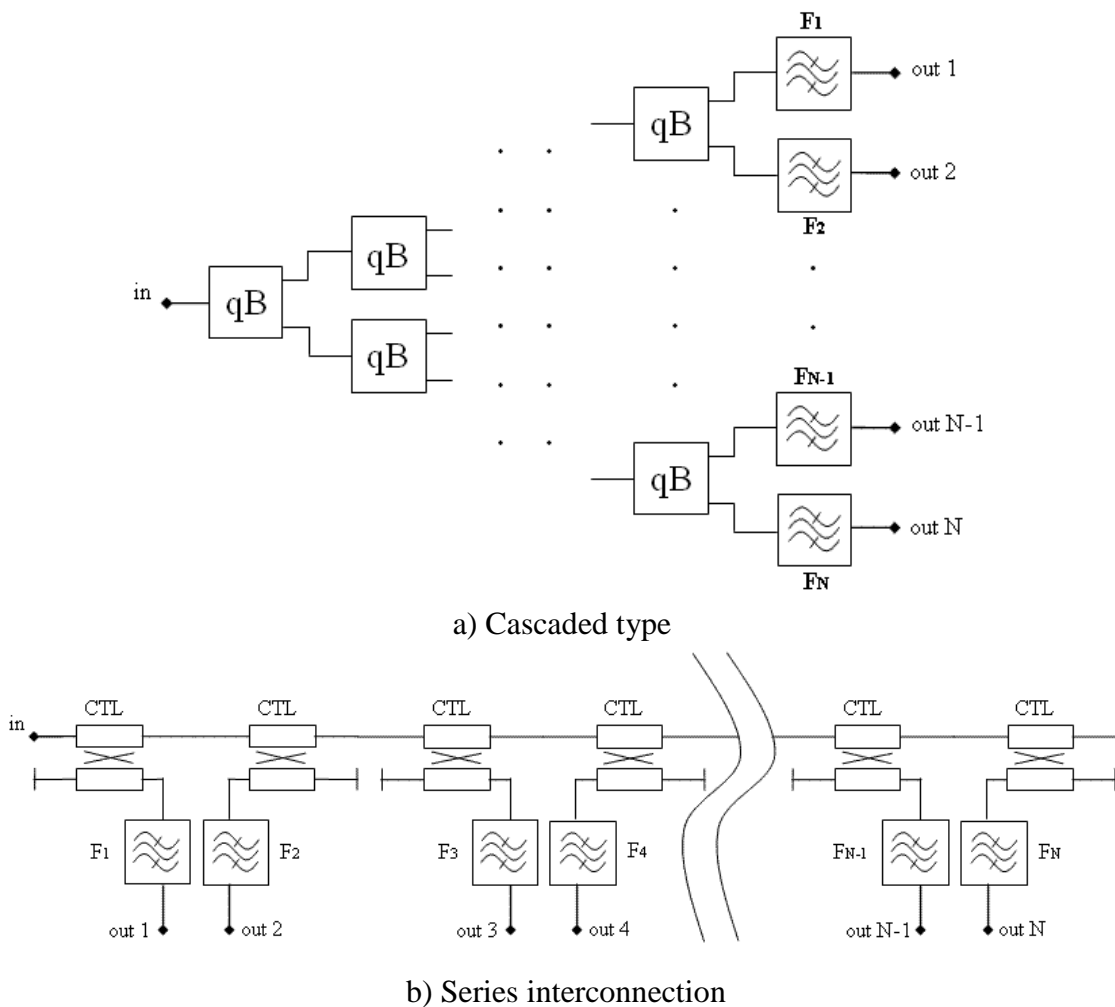


Figure 5.8: New diplexer circuit based on coupled transmission line basement

Another limitation factor is the working bandwidth. The transmission bandwidth of the basements must cover all frequency bands included in the multiplexing. Usually, the bandwidth of the basement is equal to the working bandwidth of the corresponding balun. Basically, the diplexer is intended for the applications working with contiguous bands; nevertheless, its function is extended to diplexing of arbitrary bands, which are situated inside the basement passband region. Function of the diplexer is confined only with its working bandwidth. A challenge of the future work lies in the development of an extra broadband basement design.

5.4 3D Implementation

The realization of the proposed basement for the multiplexing must be similar to the one for the ultra wideband power divider described in this work due to using the coupled line sections with equal coupling coefficients. The difference causes only in different interconnection principle between the coupled lines. Based on the calculated optimal coupling coefficient (5-20) and by solving the equations system (5-8), the values for even- and odd-mode coupled line impedances in the 50 Ohm environment ($Z_0 = 50$) will be:

$$\begin{cases} Z_{0e \text{ opt}} = 120 \text{ Ohm} \\ Z_{0o \text{ opt}} = 21 \text{ Ohm} \end{cases} \quad (5-23)$$

That corresponds to the optimal conditions:

$$\begin{cases} k_{\text{opt}} = 1/\sqrt{2} \\ Z_{0 \text{ opt}} = 50 \text{ Ohm} \end{cases} \quad (5-24)$$

Broadside-coupled striplines will be selected for the realization, like it was in case of the ultra wideband power divider. The values of optimal even- and odd-mode impedances are exactly the same as the ones for the power divider. This issue means that physical dimensions concerning the coupled line section will be exactly the same as the ones of the power divider.

3D configuration of the proposed structure is shown in Fig. 5.9. The CTL sections are comprised of coiled lines in order to occupy fewer places and they are placed between the ground planes. In the same manner as before, the input port is numbered with 1 and the output ports are 2 and 3.

Definition parameters for the structure would be the line width (w), the spacing between the ground plane and the lines (b) and the distance between the lines (s). Using the parameters given prior $\epsilon_r = 7.8$ (relative dielectric constant) with $w = 100\mu$ and the methods described in [1], parameters for the stripline configuration with the even- and odd-mode impedances from (5-23) can be found from the equation system:

$$\left\{ \begin{array}{l} Z_{0e} = \frac{188.3/\sqrt{\epsilon_r}}{\frac{w/b}{1-s/b} + \frac{C'_{fe}}{\epsilon}} \\ Z_{0o} = \frac{188.3/\sqrt{\epsilon_r}}{\frac{w/b}{1-s/b} + \frac{w}{s} + \frac{C'_{fo}}{\epsilon}} \end{array} \right. \quad (5-25)$$

where: $\frac{C'_{fe}}{\epsilon}$, $\frac{C'_{fo}}{\epsilon}$ - even- and odd- mode fringing capacitances.

As it was reported in the part of this work referencing to the power divider, the optimal values for the even- and odd-mode impedances were not achieved, due to the limitation of the structure height following to the limited number of the ceramic layers. This leads to the worsening of the matching characteristics, which is not a big problem for the power divider, because of the negligible reflections in the working passband from all input / output ports. This situation is other for the multiplexing. The channels function on the different frequency bands; therefore not all of the ports are matched simultaneously at the arbitrary selected frequency point. Thus, the requirements for the basement are a little bit stronger and the basement has to be as good as possible matched to the optimal parameters in order to avoid unwanted additional reflections causing in degradation of the multiplexer performance.

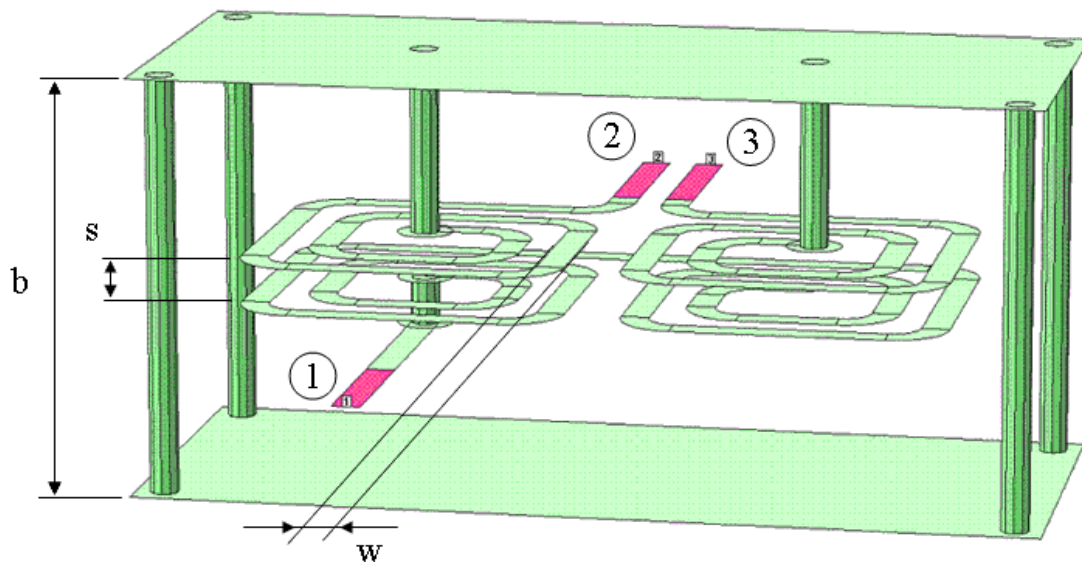


Figure 5.9: The basement for the multiplexer: broadside coupled striplines configuration (drawn using Sonnet [37])

The advantage of the basement in comparison with the power divider lies in the structure. The basement consists of the CTL section only, representing two coupled lines put into the box and confined with the ground planes from top and bottom sides. The

additional capacitor and the matching TLs are not needed, as it was in case of the power divider. Moreover, the use of the multiplexer circuit excludes implementation of such active components like switches, which have to be put on top of the LTCC component. Such simplification of the structure pushes up the top limit on the maximal height from 1 mm (as it was for the splitter) up to 1.4 mm depending on application. Free space between top and bottom sides of the component is given for the CTL realization only, providing more freedom for realization of the basement variants. Optimal 3D solution for the basement under this new limitation will be found in the following computations.

5.4.1 Structure Optimization

The system equation (5-25) contains three variables referencing to 3D realization of the component. They are: w, ε_r, b, s . The idea is to maximize approach of these parameters to the real ceramic parameters declared in the official design rules. The optimization procedure operating with four unknown parameters is too complicated. It's proposed in this work to confine the optimization with two parameters only. Which ones? It could be possible to refuse the parameters which at least have to be predicted, so we can say what will happen with the circuit performance if they would be altered. The relative dielectric permittivity belongs to that category. Accordingly to the equations (5-25), relation between the even- and odd-mode impedances and $1/\varepsilon_r$ are linear and therefore it could be easy predicted. It's a little bit difficult with the second parameter being declined; all of them provide more complicated influence on the final result. The line width is scarce in equations and will be taken as the second refused parameter. Thus, the relative dielectric constant and the line width will be set to defined constant values for the further analysis.

Taking into account, that the fringing capacitances are the functions of the ratio s/b (graph values from [1]) and therefore the even- and odd-mode impedances can't be directly calculated, the procedure of the equation solution will have iteration character. By setting up the values of s and b parameters, firstly the fringing capacitance values will be extracted from the given table and afterwards the corresponding impedances will be calculated. Finally, values of the coupling factor and the input impedance can be estimated. Decision on the further steps will be done after comparison between these values and set up ones (the optimal coupling factor and the environment impedance):

$$\begin{cases} \Delta Z = Z_0 - Z_{\text{calc}} \\ \Delta k = k_{\text{opt}} - k_{\text{calc}} \end{cases} \quad (5-26)$$

If the delta values are less then set iteration error ($\Delta k < \Delta k_{\text{set}}, \Delta Z < \Delta Z_{\text{set}}$) then the quasi-optimal solution is achieved. Otherwise, the input values of s and b have to be

changed and the next iteration step must be done. Such iterations could be repeated a lot of times until the optimal solution will be found, thus making the whole optimization procedure very complicated.

The following solution was proposed to solve the problem of complexity. To achieve full overview of behavior representation of the even-, odd-mode, input impedances and the coupling factor, the whole data massive will be used in the calculations. The final data representation will be depicted in 3D form: dependency from s and b values with constant set $w = 200 \mu\text{m}$ and $\epsilon_r = 7.8$ (standard values). The graphs contained these data are shown in Appendix D.1. They show physical possible realization limited within LTCC design rules. The graphs are colored separating in such a manner values within different levels.

These graphs have to be used for the coupled striplines synthesis. The physical dimensions can be derived from the 3D curves by setting up either the desired values of the even- and odd-mode impedances or the coupling factor and the characteristic impedance. This is the straight forward design procedure for such structures using the coupled striplines. In the presented case, the coupled striplines must correspond to the optimal conditions (5-24). It could be not easy to find an exact point at the graphs in the figures D.1.3 and D.1.4, where the geometry fulfills the requirements of the optimal values for the coupling coefficient and the characteristic impedance simultaneously. To simplify this task, an additional graph will be built containing the criterion characterizing absolute limits on the optimal values. This criterion is named the error minimization criterion and it's based on calculation of the absolute error, corresponding to the relative error set up in (5-26). The error minimization criterion will be calculated using the following equation:

$$C_{\text{abs}} = \frac{|Z_0 - Z_{\text{calc}}|}{Z_0} + \frac{|k_{\text{opt}} - k_{\text{calc}}|}{k_{\text{opt}}} \quad (5-27)$$

The criterion shows the maximal deviation between the realized and optimal values of both examined parameters in sum. 3D representation of a relation between the criterion values and the physical parameters of the structure is shown in Fig. 5.10.

It's obviously, that the smaller criterion values the closer the solution to the optimal one. Basing on the graph, the following conclusion can be done: the optimal solution using LTCC structure is localized in the area confined with the values of $s = 60 \dots 90 \mu\text{m}$ and $b = 1200 \dots 1700 \mu\text{m}$, where the optimal values are $s = 75 \mu\text{m}$ and $b = 1400 \mu\text{m}$.

This analysis was done assuming a constant value of the line width. It's also interesting to investigate behavior of the characteristics depending on the line width. The same 3D analysis as the previous one will be proposed this time. The question is only, which parameter should be the second one, s or b ? Maybe it would be a relation s/b . In such a way both variables will be related, moreover the equations (5-25) contain the relation s/b and the fringing capacitances in this equation are also functions from s/b . Thus,

the relation s/b can be observed as the second parameter. This relation must provide a value in range of 0.04 ... 0.075 (optimal 0.05) in order to achieve the optimal overall performance accordingly to the first analysis. The first parameter will be also a relation such w/b .

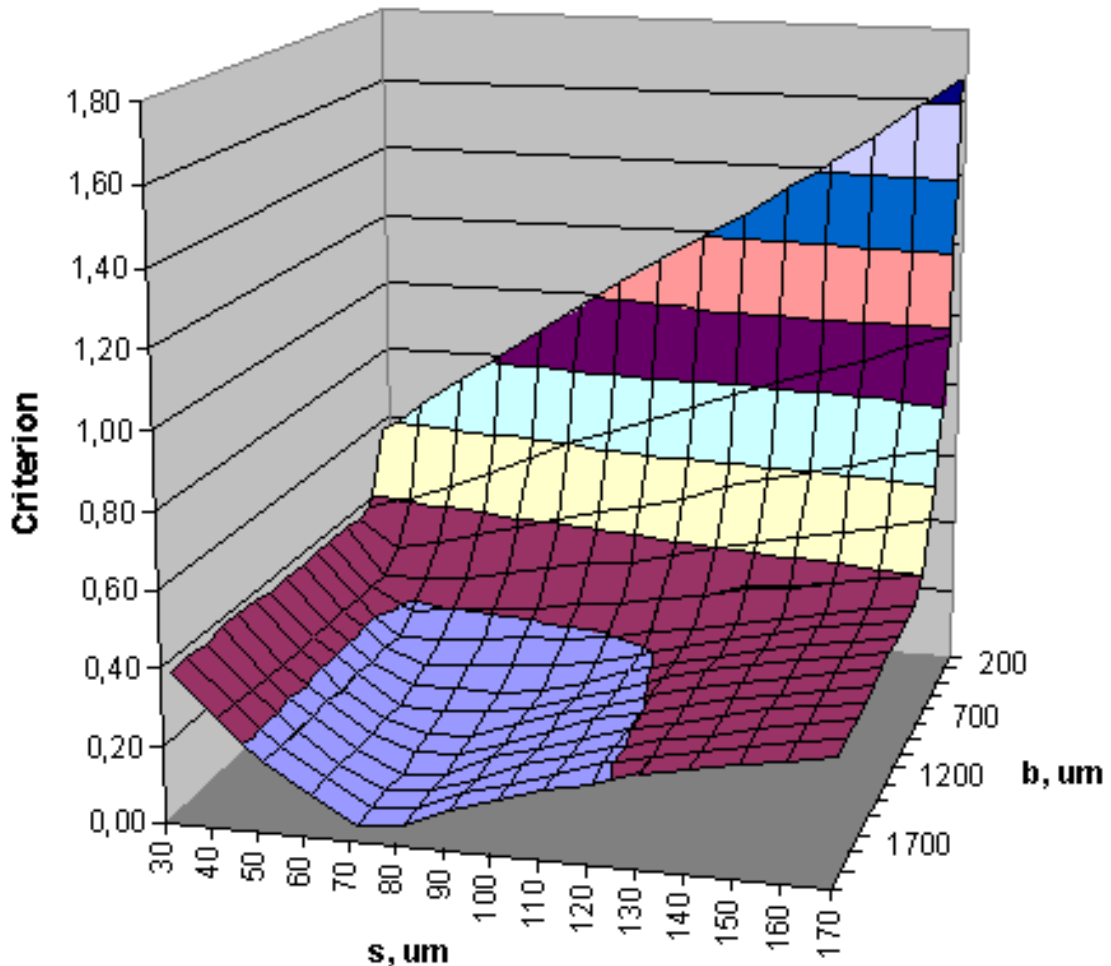


Figure 5.10: Error minimization criterion from (5-39)

The value of b will be set to 1.4 mm (optimum achieved in previous analysis) and the relation s/b will be varied from 0.02 to 0.86 with a step of 0.06. S/b variation are confined with the values presented in [1] in the table showing dependency of the fringing capacitors from this relation. The other values are not possible to be calculated due to absence in the fringing capacitances in the defined table related to the source. The calculated results are shown in 3D form in the figures in Appendix D.2.

As it was seen from these pictures, the line width plays not the last role in forming of the characteristics. The pictures showed above include a variation of all three variables (w , s and b) already. As it was in the previous analysis, the error minimization criterion (5-27) will be observed in order to get the optimum result. The calculated values are combined in 3D representation (Fig. 5.11). The graph shows a complicated performance, where is clear

that the smaller values of w/b and s/b the smaller is the criterion. The first minimum corresponds to $w/b = 0.02$ (or $w = 30 \mu\text{m}$) and $s/b = 0.02$. This is not our case, because the line width of $30 \mu\text{m}$ is not realizable in LTCC technology and the relation $s/b = 0.02$ was not optimal, as in the previous calculations. The second minimum lies in a range of the optimum relation value of $s/b = 0.05$ and corresponds to the value of $w/b = 0.08$ (or $w = 110 \mu\text{m}$). These values are already realistic.

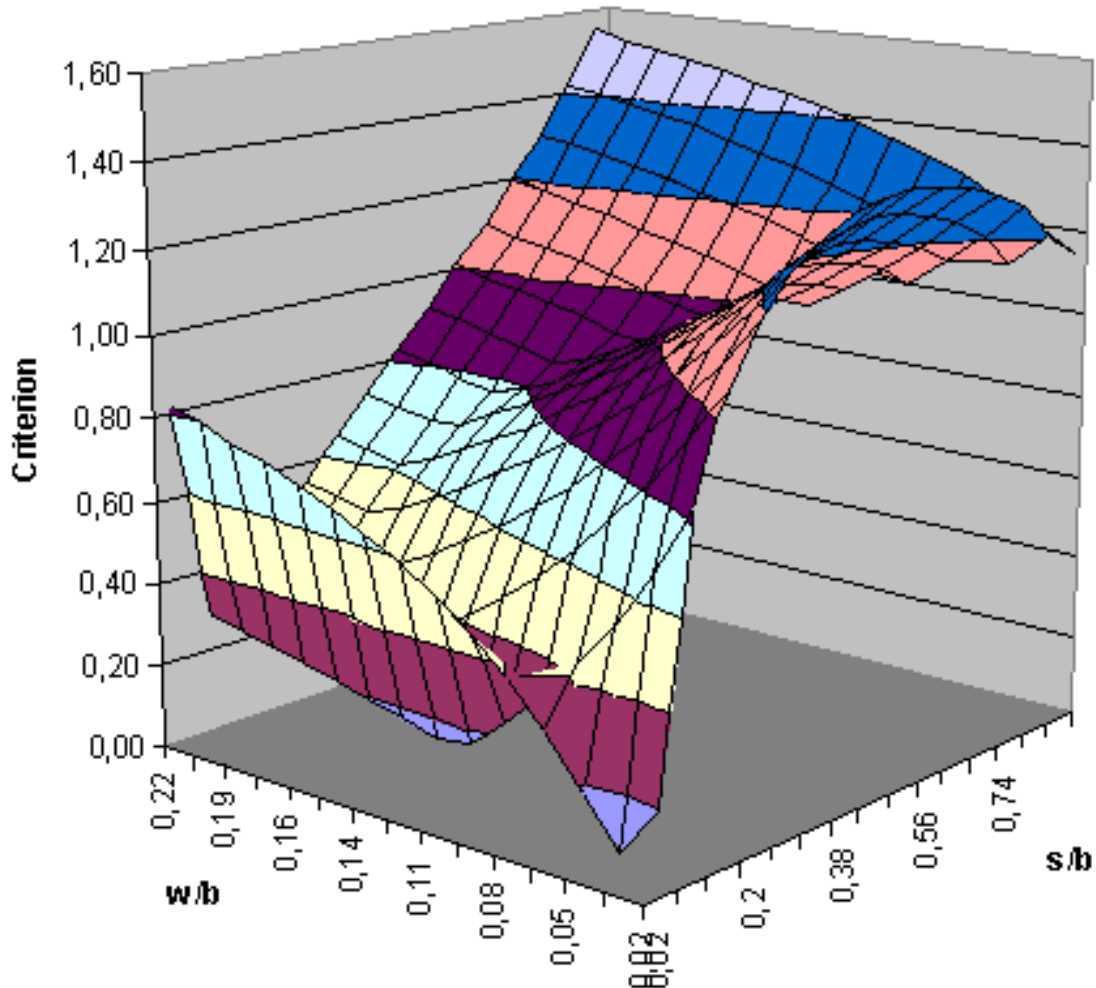


Figure 5.11: Error minimization criterion from (5-39)

Using these two steps of the analysis let us to find the optimal solution for the coupled striplines operating with three variables (w , s and b) and this optimum is absolute for this type of investigations. Thus, in order to build the optimal basement for the multiplexing, the requirements (5-24) have to be fulfilled. The practical realization of this basement using the coupled striplines must provide the transmission line properties shown in (5-23). Corresponding to these properties, the physical dimensions are:

$$\begin{cases} w = 110 \mu\text{m} \\ s = 75 \mu\text{m} \\ b = 1400 \mu\text{m} \end{cases} \quad (5-28)$$

5.4.2 Performance Using the Ideal Basement

Taking into account the discrepancy between optimal parameters defined in (5-28) and the official design rules for components produced using LTCC technology, in order to have the whole overview, firstly a diplexer using ideal basement will be calculated and afterwards a diplexer using the real basement. Thus, achievable potential of the proposed basement will be estimated. It would be possible to approach the optimal circuit parameters using other technology.

Let's take into consideration satellite channels down-converted by LNB (low-noise block converter) and forwarded to a digital receiver (this application is presented in the chapter 6.1). A typical frequency range of such signals is 950 – 2150 MHz. Using several LNBs, the sub bands have to be combined together, before they will be forwarded to the tuner. This is a common task of multiplexing using contiguous bands. As an example, combination of two sub bands will be observed with corresponding frequencies: 959 – 1192 MHz and 1265 – 1501 MHz. A distance between the sub bands is only 73 MHz, which is smaller than each bandwidth and it corresponds to about 30 % of the relative bandwidth. The relative distance between the sub bands is 6 %, while the relative bandwidths of the sub bands are 21.7 % and 17 % correspondingly. Both narrowband and high rejection filters must be used in this situation for the channels separation; moreover the diplexer circuit must properly operate with such a small gap between the channels.

This task is only demonstrative and main goal is to show the diplexer function, therefore requirements on contra band rejection of the designed filters will be simplified. Transmission line resonator type filters are selected for this purpose. 3D view of the filters realized using LTCC is shown in Fig. 5.12a and corresponding simulated transmission characteristics are depicted in Fig. 5.12b. Coupled stripline resonators shown in the Fig. 5.12a use shorting capacitors in order both to minimize size of the filters and to make tuning of the filters more flexible. Performance of the filters shows typical Butterworth BPF response without any additional notches from both sides of the passband.

These filters will be connected together using both the ideal quarter-wave transmission line sections and the proposed ideal basement. Thus, the proposed solution could be compared with the standard one. Block-schematic simulations will use ideal schematic of the corresponding components (the TLs or the quasi-balun basement) and real simulation results of the filters shown in Fig. 5.12b. The simulation schema is shown in Fig. 5.13, where F1 and F2 are real simulated parameters of the corresponding filters. The input 3-port sub-circuit contains either a standard transmission line section or a new quasi-balun basement depending on the simulation as it's shown in the same figure.

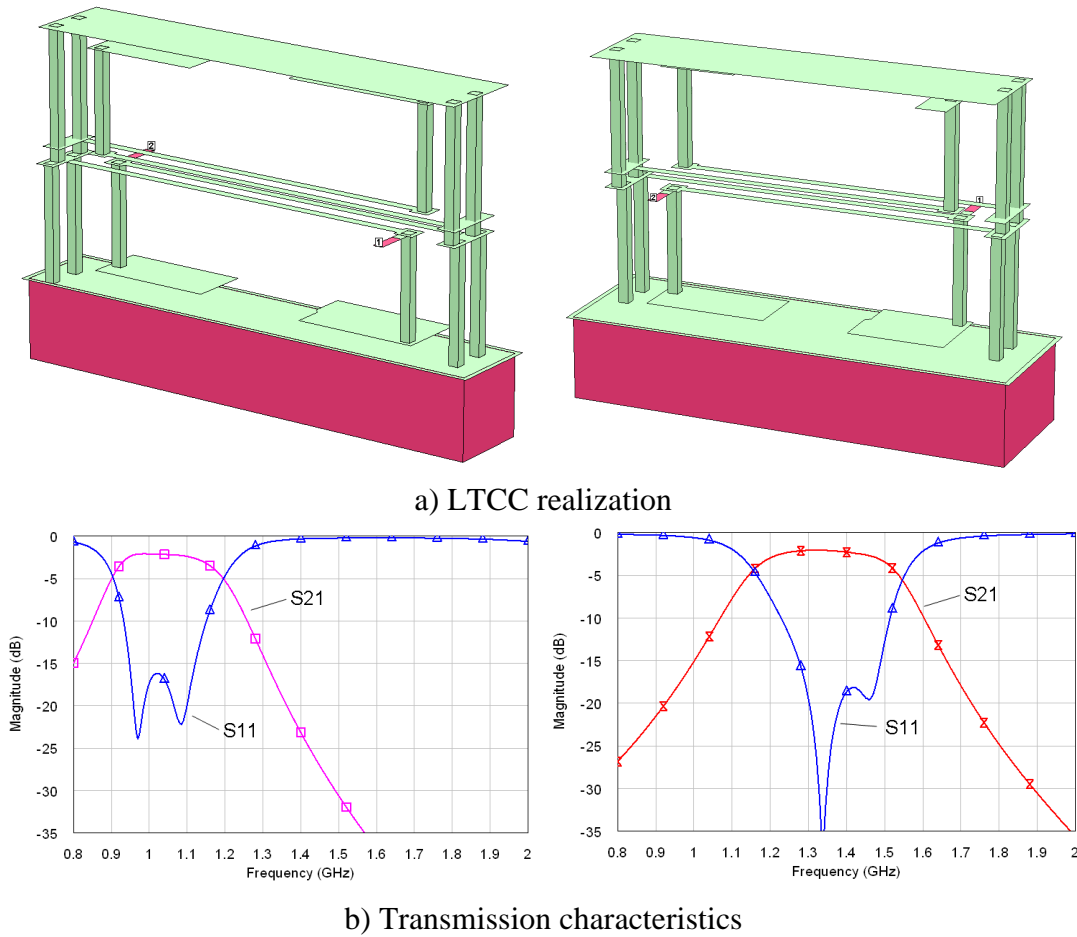


Figure 5.12: TL bandpass filters used for diplexing (simulated using Sonnet [37])

The simulation results of these two diplexing circuits are depicted in Fig. 5.14. It's clear that using the ideal basements, there are no changes in the passband in comparison with the original filters, depicted in Fig. 5.12. Though, there are differences in matching depending on which type of the basement is taken.

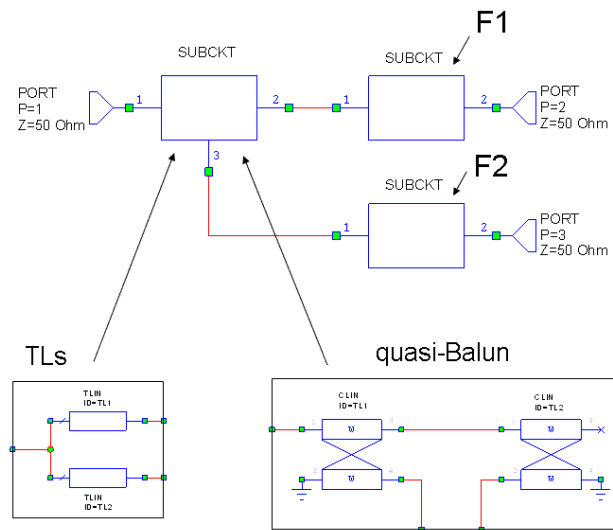
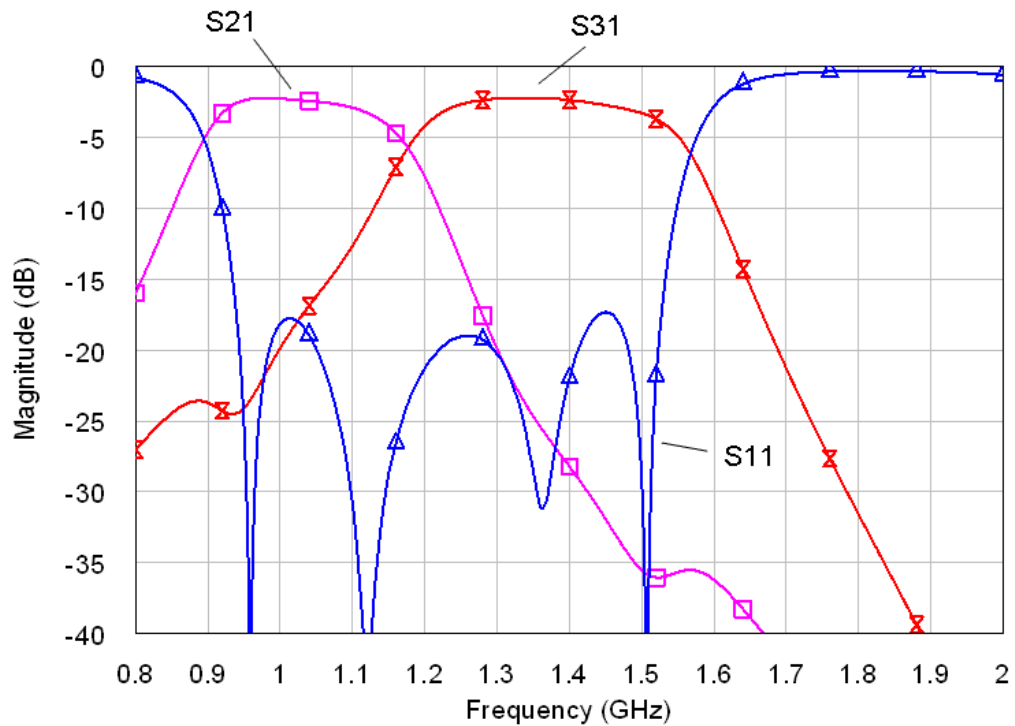
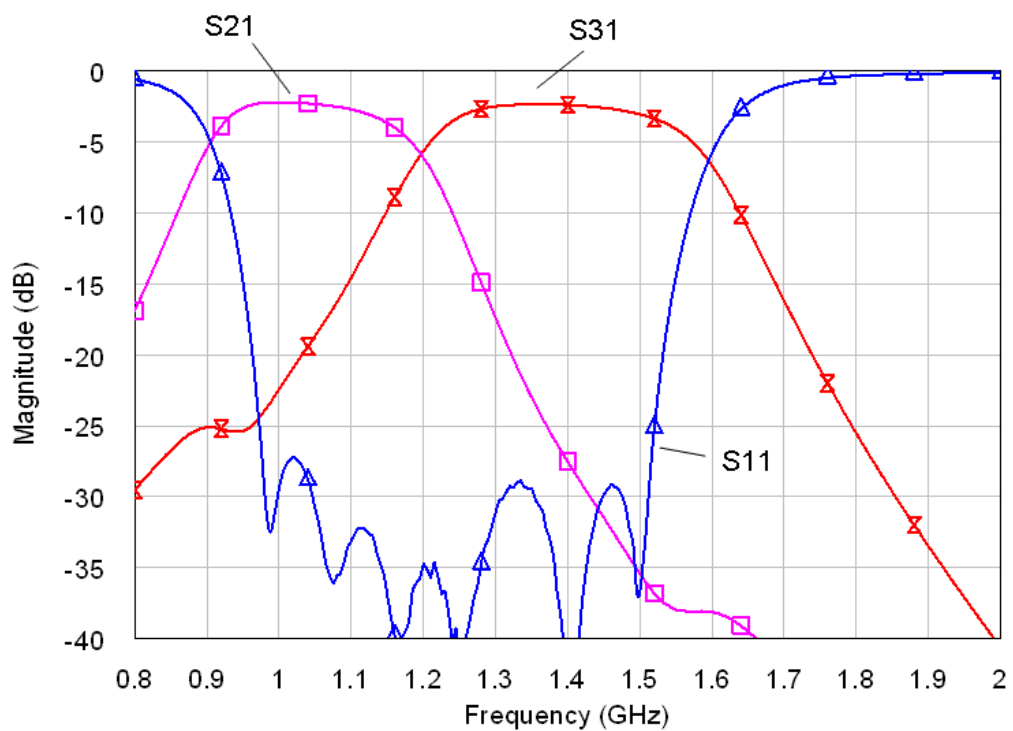


Figure 5.13: Block diagram using ideal diplexing with real filters (drawn using Microwave Office [38])

The common transmission line diplexing shows pure performance in comparison with the proposed solution based on the quasi-balun (17 dB return loss vs. 27 dB). The diplexer based on the quasi-balun basement provides less internal and therefore less external unwanted reflections.



a) Common TL basement



b) New proposed quasi-balun basement

Figure 5.14: Performance of the diplexers using ideal basements (simulated using Microwave Office [38])

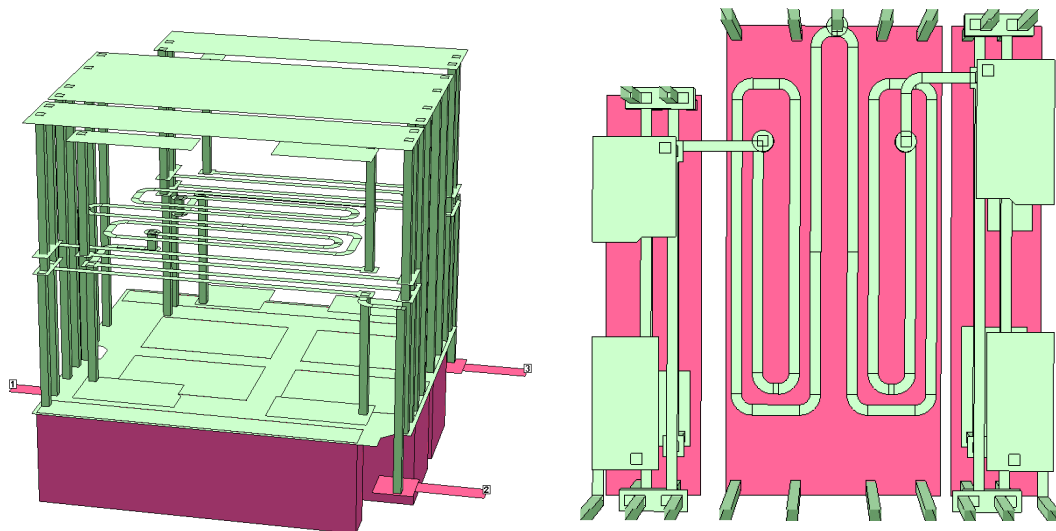
Both matching circuits are good enough for the circuit terminating with 50 Ohm loads; nevertheless, it's only the ideal simulations which don't take into account parasitic effects occurring during full 3D simulation and moreover standard tolerances during production of the hardware. The final values of the return loss the same as the passband characteristics could be much worse than the simulation ones, therefore, it's very important to achieve the simulation values as good as possible. The new proposed quasi-balun basement gives such opportunity. Let's do the following step – practical realization.

5.4.3 LTCC Realization

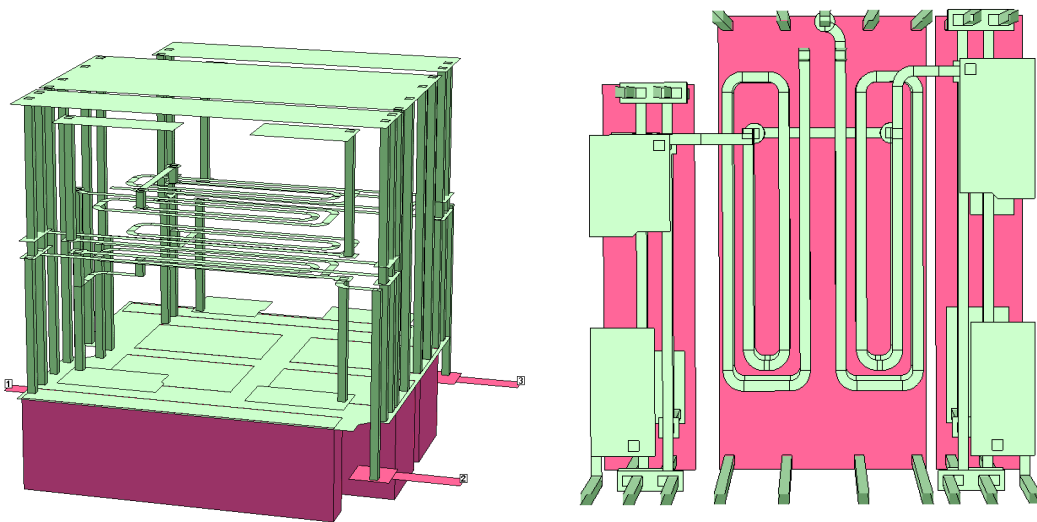
The optimal geometrical values achieved (5-28) for the quasi-balun above are close to the values defined by design rules for LTCC technology. LTCC realization lets us operate with the following quasi-optimal values: $w = 100 \mu\text{m}$, $s = 100 \mu\text{m}$ and $b = 1400 \mu\text{m}$. In contrary, the transmission line realization is simpler in this case, because it's almost always possible to achieve either microstrip line or stripline with impedance close to 50 Ohm. But a simple solution brings best results not always. In the same way, as in the previous simulations, both diplexer types were realized to be compared. Full 3D realization of the diplexers including the basements and the filters in a single package are shown in Fig. 5.15.

Both diplexers have equal sizes of $5.1 \times 4.8 \times 1.0 \text{ mm}^3$. Side view is not informative; therefore front cut is added. Two filters are situated from the sides and the basement is placed in the middle of the structure. Additional technological advantage of the new quasi-balun proposal is that it doesn't require more space than the common transmission line solution. This occurs, because both the single ended transmission lines and the coupled transmission lines are equal in length (they are quarter wavelength). Moreover, the broadside-coupled lines are stacked in z-direction. Thus, four lines compounding the quasi-balun shown in Fig. 5.12 are equal in size to two lines compounding the TL basement in the same picture.

Characteristics of both diplexers are shown in Fig. 5.16. The standard solution provides spread transmission characteristics with worsening of out-of-band rejections. In contrary, the new solution does almost no changes in performance of the filters, remaining the bandwidth and the attenuations in the same range. Regarding to the return loss, the real simulations of both solutions of course show worse performance. Though the real realization of the diplexer using the quasi-balun basement doesn't provide the optimal structure parameters defined in (5-28), it is still better, than the optimal solution for the diplexer using the transmission line basement. Thus, the new proposed diplexer is more attractive for mass production, assuming worsening characteristics based on the production tolerances.



a) Common basement using TLs

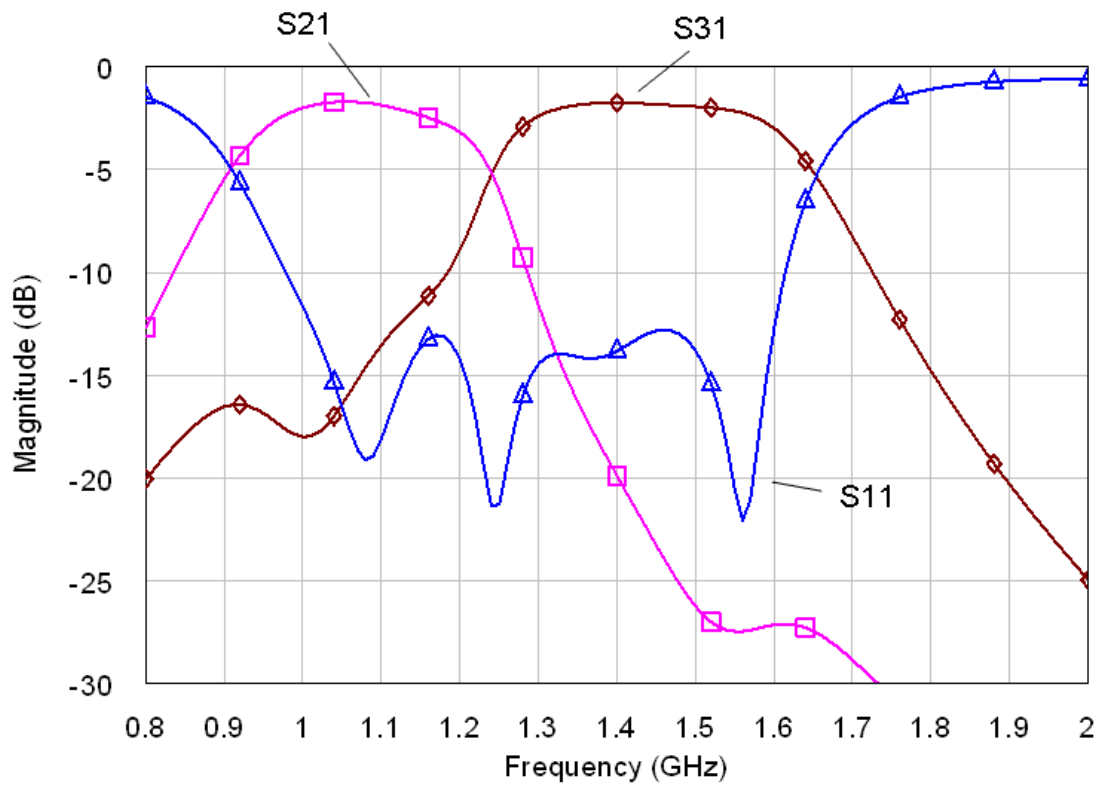


b) New proposed basement using quasi-balun

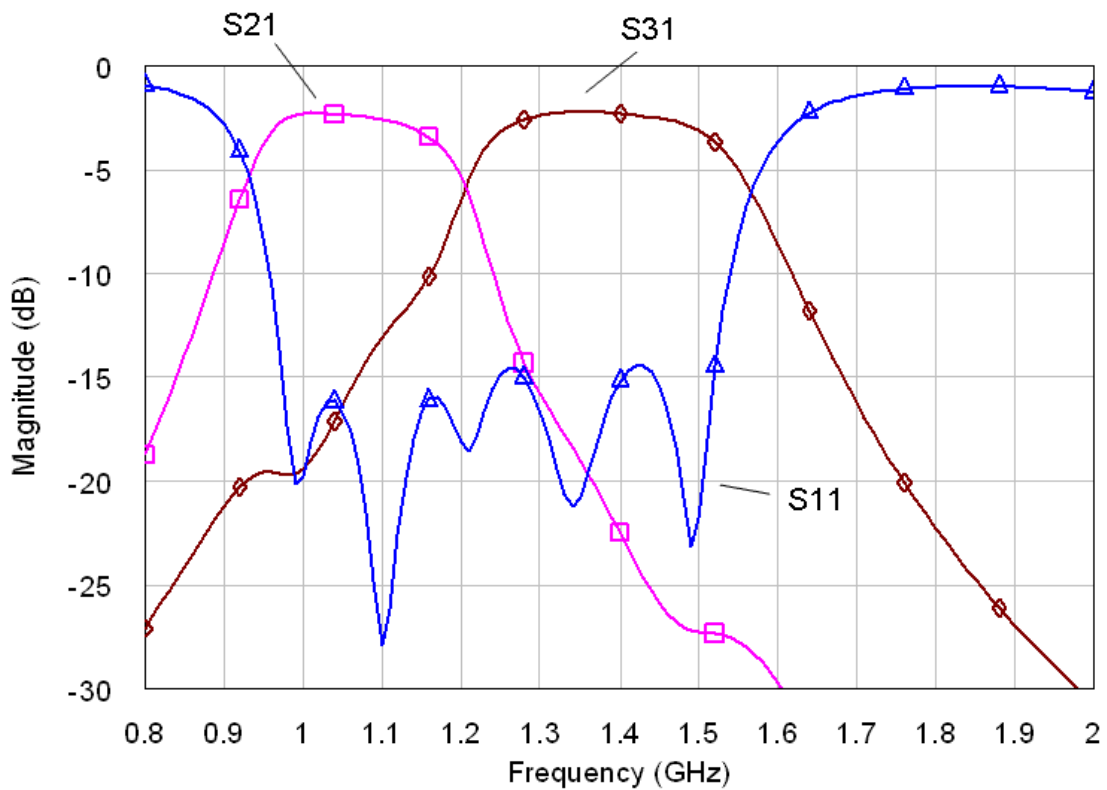
Figure 5.15: 3D view of the diplexers (drawn using Sonnet [37])

Of course, the proposed diplexer is not a universal component, which could solve all tasks. Function of the diplexer is confined logically with the bandwidth of the quasi-balun; the component can't operate with signals out of its bandwidth. This issue makes the diplexer special oriented on diplexing of the contiguous bands, which task is very difficult for the other types of diplexer. Frequency bands situating far away from each other can be also combined without problems taking into account the bandwidth of the basement.

For example, it's not possible to cover all down-converted frequency sub-bands for satellite application within 950 – 2150 MHz because of the bandwidth limitations for the basement. Though this task could be solved using a combination of the new UWB power divider (tuned on required frequency band) described in this work and the quasi-balun basements. The second solution would be development of the broadband basement using the quasi-balun like in case of the UWB power divider.



a) Diplexer using common TL basement



b) Diplexer using new proposed quasi-balun basement

Figure 5.24: Performance of the real diplexers (simulated using Sonnet [37])

5.5 Results on the Multiplexing Circuit

The new solution for multiplexing procedure was proposed in this work. The multiplexer is specialized for operating with contiguous bands as well as with the arbitrary ones. The basement for the multiplexing lets filters to be connected together and it's implemented using the quasi-balun concept realized by the coupled transmission lines. In comparison with the existing solutions, such multiplexer configuration provides much better performance, because the filters characteristics will not be changed and much less reflections occur during the multiplexing. Moreover, the majority of the existing common filters, which input impedance behaviour lies under the special conditions corresponding to the Fig. 5.1 b, can be connected with the proposed basement. The filters passbands have to be situated inside the working bandwidth of the basement, which is the limitation factor of the design. Of course, the bandwidth of the basement is similar to the bandwidth of Marchand balun, which relative value could be realized in LTCC up to 70 %. The future steps would be the investigations on potential enlarging of the bandwidth.

The attached calculation procedure proves an optimum of the solution. As an example, the diplexer was calculated and optimized for function with 50 Ohm impedance environment. Additionally, the optimization procedure is shown making it possible to rebuild the diplexer for function with different environment impedances by changing the even- and odd-mode impedance values.

5.6 References to Chapter 5

- [1] G. L. Matthaei, L. Young and E. M. T. Jones, *Microwave Filters, Impedance-Matching Networks, and Coupling Structures*, Ed. Norwood, MA: Artech House Inc., 1980, pp. 180-181, 965-1000.
- [2] E. G. Cristal and G. L. Matthaei, "A Technique for the Design of Multiplexers Having Contiguous Channels," *IEEE Transaction on Microwave Theory and Techniques*, vol. 12, Jan. 1964, pp. 88-93.
- [3] J. D. Rhodes and R. Levy, "A Generalized Multiplexer Theory and Design of Manifold Multiplexers," *IEEE MTT-S International Microwave Symposium Digest*, vol. 78, June 1978, pp. 211-213.
- [4] R. Levy, "Analytical Design of Contiguous Multiplexers," *IEEE MTT-S International Microwave Symposium Digest*, vol. 3, Jun. 1999, pp. 899-902.

- [5] J. W. Bandler, S. Daijavad and Qi-Jun Zhang, "Exact Simulation and Sensitivity Analysis of Multiplexing Networks," *IEEE Transaction on Microwave Theory and Techniques*, vol. 34, Jan. 2003, pp. 93-102.
- [6] R. J. Wenzel and W. G. Erlinger, "Narrowband Contiguous Multiplexing Filters with Arbitrary Amplitude and Delay Response," *IEEE MTT-S International Microwave Symposium Digest*, vol. 76, Jun. 1976, pp. 116-118.
- [7] M. H. Chen, "A 12-channel Contiguous Band Multiplexer at Ku-band," *IEEE MTT-S International Microwave Symposium Digest*, vol. 83, May 1983, pp. 77-79.
- [8] R. Tong and D. Smith, "A 12-channel Contiguous Band Multiplexer for Satellite Application," *IEEE MTT-S International Microwave Symposium Digest*, vol. 84, May 1984, pp. 297-298.
- [9] R. R. Bonetti and A. E. Williams, "A Quadruple-mode Contiguous-band Multiplexer for Communications Satellites," *Proceedings on European Microwave Conference*, Sept. 1989, pp. 687-691.
- [10] C. Rauscher, "Logarithmic-periodic Contiguous-channel Microwave Multiplexers," *IEEE MTT-S International Microwave Symposium Digest*, vol. 2, Jun. 1989, pp. 675-678.
- [11] G. G. Connor and M. J. Perren, "Design and Performance of a Ku-band 8 Channel Contiguous OMUX for Satellite Applications," *IEEE Colloquium on Microwave Filters and Multiplexers*, vol. 12, Nov. 1990, pp. 1-5.
- [12] G. Tanne, S. Toutain at al., "Optimal Design of Contiguous-band Output Multiplexers (COMUX)," *Electronic Letters*, vol. 29, Sept. 1993, pp. 2050-2052.
- [13] M. K. Chahine and G. Carrer, "Optimal Design of Contiguous Band Multiplexers," *Electronic Letters*, vol. 30, Nov. 1994, pp. 2050-2052.
- [14] M. K. Chahine and G. Carrer, "Novel Approach to Contiguous Band Multiplexer Design for Satellite Applications," *Microwave and Optical Technology Letters*, vol. 8, Feb. 1995, pp. 164-170.
- [15] J. W. Bandler, W. Kellermann and K. Madsen, "A Nonlinear 11 Optimization Algorithm for Design, Modeling, and Diagnosis of Networks," *IEEE Transactions on Circuits and Systems*, vol. 34, Feb. 1987, pp. 174-181.
- [16] Y. Rong, K. A. Zaki at al., "Low Temperature Cofired Ceramic (LTCC) Ridge Waveguide Multiplexers," *IEEE MTT-S International Microwave Symposium Digest*, vol. 2, Jun. 2000, pp. 1169-1172.
- [17] C.-W. Tang, J.-W. Wu, C.-C. Hu, et al., "The Multilayered Triplexer with Low Insertion Loss," *Proceedings on Asia-Pacific Microwave Conference*, Dec. 2006, pp. 1224-1227.

- [18] A. Simine, V. Piatnitsa, A. Lapshin, et al., "Design of Quasi-Lumped-Element LTCC Filters and Duplexers for Wireless Communications," *Proceedings on European Microwave Conference*, Oct. 2003, pp. 911-914.
- [19] C. W. Tang and S. F. You, "Design Methodologies of LTCC Bandpass Filters, Diplexer, and Triplexer with Transmission Zeros," *IEEE Transaction on Microwave Theory and Techniques*, vol. 54, Feb. 2006, pp. 717-723.
- [20] T. Ohno, K. Wada, and O. Hashimoto, "Design Methodologies of Planar Duplexers and Triplexers by Manipulating Attenuation Poles," *IEEE Transaction on Microwave Theory and Techniques*, vol. 53, Jun. 2006, pp. 2088-2095.
- [21] H. Joshi, H. H. Sigmarsson, S. Moonet, et al., "Tunable High Q Narrow-Band Triplexer," *IEEE MTT-S International Microwave Symposium Digest*, Jun. 2009, pp. 1477-1480.
- [22] M. Karlsson, P. Hakansson and S. Gong, "A Frequency Triplexer for Ultra-Wideband Systems Utilizing Combined Broadside- and Edge-Coupled Filters," *IEEE Transactions on Advanced Packaging*, vol. 31, No. 4, Nov. 2008, pp. 794-801.
- [23] D. Orlenko, K. Markov at al., "Novel High-Rejection LTCC Duplexers for Dual-Band WLAN Applications," *IEEE MTT-S International Microwave Symposium Digest*, Jun. 2005, pp. 727-730.
- [24] S. Sakhnenko, D. Orlenko at al., "Ultra-Low-Profile Small-Size LTCC Front-End Module (FEM) for WLAN Applications Based on a Novel Diplexer Design Approach," *IEEE MTT-S International Microwave Symposium Digest*, Jun. 2009, pp. 609-612.
- [25] H. Clark Bell, Harold A. Rosen, "Contiguous Channel Multiplexer," *Patent*, US4029902A, Jun. 1977.
- [26] R. M. Rudish, S. F. Hall, "Contiguous Channel Multiplexer/Demultiplexer," *Patent*, US4839894, Jun. 1989.
- [27] N. Marchand, "Transmission-Line Conversion Transformers," *Electronics*, vol. 17, Dec. 1944, pp. 142-146.
- [28] M. Chongcheawchamnan, C. Ng and I. Robertson, "Miniaturised and Multilayer Wilkinson Divider and Balun for Microwave and Millimeter-wave Applications," *IEEE Postgraduate Student Colloquium on High Frequency*, Sept. 2001, pp. 174-179.
- [29] M. Chongcheawchamnan, C. Ng at al., "On Miniaturization Isolation Network of an All- Ports Matched Impedance-Transforming Marchand Balun," *IEEE Transactions on Microwave and Wireless Component Letters*, vol. 13, Jul. 2003, pp. 281-283.
- [30] J.-S. Lim, H.-S. Yang at al., "E-band Wilkinson Balun Using CPW MMIC Technology," *Electronic Letters*, vol. 40, Jul. 2004, pp. 879-881.
- [31] Y. Guo, Z. Zhang and L. Ong, "LTCC Full-Matching Marchand Balun," *Proceedings on European Microwave Conference*, Sept. 2006, pp. 76-78.

- [32]H. Mandai, et al., “Duplexer and Mobile Communication Device Using the Same,” *Patent*, US6525626B2, Feb. 2003.
- [33]R. A. Gilbert, “Reconfigurable Diplexer for Communications Applications,” *Patent*, US2001/0035801A1, Nov. 2001.
- [34]R. Kravchenko, “Multiplexer,” *Patent*, DE102009003884A1, Jan. 2009.
- [35]W. Klein, *Mehrtortheorie*, 3d ed., Ed. Berlin, Germany: Akademie-Verlag, 1976, p.60.
- [36]R. Mongia, I. Bahl and P. Bhartia, *RF and Microwave Coupled-Line Circuits*, Ed. Boston, London: Artech House, 1999, pp. 137-138.
- [37]Sonnet Software Inc. v.12.52, 2010.
- [38]AWR Microwave Office Software Inc. v. 9.02r, 2010.

6. Several Applications of the Designed Components

The high frequency components described in this work carry out the main functions of frequency processing in receive / transmit front-end part, such as frequency filtering and frequency / power division of the RF signals. A lot of applications based on wireless communications mainly require these components. The components are universal in case of frequency range; they could be tuned on arbitrary working frequency bands. As an example, a project “Satellite (SAT) Channel Combiner” is shown below, where some LTCC components take part in realization of an equipment for Digital Broadcast Satellite (DBS) communication. Another project is going on in corporation with Technical University of Graz (Institut fuer Signalverarbeitung und Sprachkommunikation) and partners (XERXES Electronics GmbH and xFace e.U.), which is named “Noncoherent orthogonal frequency division multiplexing (NOFDM) ultra-wideband (UWB) receiver”.

6.1 Single Cable Distribution

Since satellite broadcasting turns from analog to digital signal processing, interest on it has been increasing due to improved quality, a number of translated channels and additional service functions. High Ku-band was appended in addition to low Ku-band used for analog systems and both polarizations (vertical and horizontal). Moreover, digital signals occupy much less frequency space, than the analog ones. Thus, potential advantages of DBS were possible to be realized. Taking into account a number of the existing satellites, the number of channels can be increased just by simultaneous receiving the signals from different satellites. Of course, such system improving leads to complication of the realization.

Former installation techniques of a DBS receive station utilizing multiple satellite reception is shown in Fig. 6.1a, which is taken from [1]. A multiple LNB system assumes using multiple cable distribution corresponding to the number of the satellites. Such system installation provides direct access of each SAT receiver to all of LNBS making the receive procedure as simple as possible. Unfortunately, the proposed solution requires an enormous place for the cables violating ergonomic view. More beautiful technical solution would be refusing from all these cables and using only a single cable to provide the same function. The picture presented in Fig. 6.1b (it's also taken from [1]) shows the single

cable solution. This solution became possible under the new industry standard for the single-cable satellite reception and distribution - CENELEC EN50494 [2]. A short description of the standard challenges can be found in [3], [4]. Accordingly to it, several users have a possibility to receive radio and television channels from several satellites via single cable.

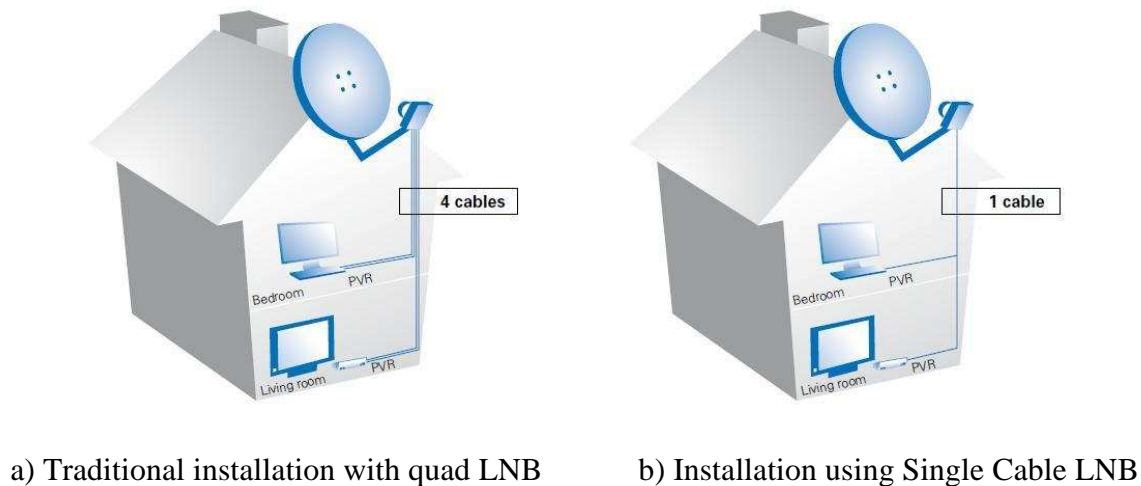


Figure 6.1: SAT installation (from [1])

Technical background of the single cable distribution (SCD) technology is described in details in [5]. The technology is also well known in different sources like the satellite channel router (SCR) [6], [7] and the channel stacking switch (CSS) one [8] – [11]. A lot of ready to use products specified on this area like routers and switches have been produced by several suppliers [12] – [22]. RF part of the routers provides frequency division multiple access. A typical block diagram of the RF part supporting quad LNB system is shown in Fig. 6.2. It contains two integrated circuits (ICs) RF5210 [23], which are marked with blue color; the other components are external. This system configuration provides allocation of six channels inside the working frequency band of 950 – 1500 MHz. Normally, ICs are universal and they function in the total frequency band allocated for the satellite communication, such as 950 – 2150 MHz (sometimes the upper B-band is also used: 2250 – 3000 MHz). The operating frequency band for each IC in the system contains three sub-bands and they are separated by Surface Acoustic Wave (SAW) filters included parallel into each of three passes inside the IC. At the output of the IC, the sub-bands suffer level equalization and they are combined together forming a compound balanced signal. By combining several ICs together, a balanced multiplexer (BalMPX) is needed. The BalMPX is located inside a region confined with a red rectangle in the Fig. 6.2 and contains baluns and a power divider (PD). A frequency allocation of the band 950 – 2150 MHz is shown in Fig. 6.3. The whole band is divided into four bands (B I – B IV), while each of these bands is subdivided into three sub-bands (sB1 – sB12) mentioned above.

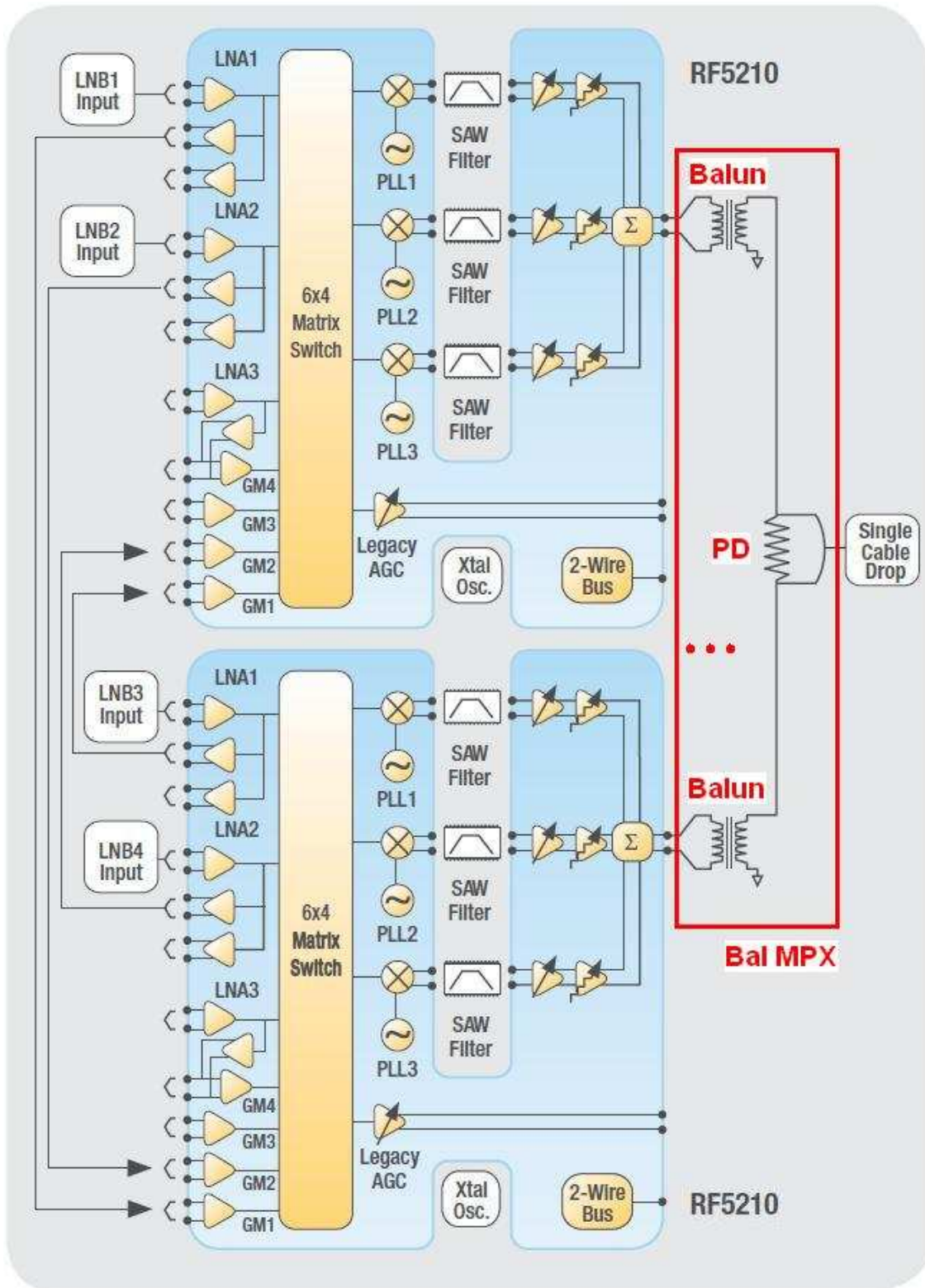


Figure 6.2: CSS: functional block diagram (from [23])

Logically, the single IC depicted in Fig. 6.2 supports one of the bands: B I – B IV, where SAW filters are responsible for the sub-bands. It's clear, that, in order to cover the whole DBS frequency band, four ICs are necessary. Typically, such broadband response is not needed and some suppliers (for example, DirecTV [24]) use only frequency band from 950 MHz to 1800 MHz. A system supporting operation with this band will contain three

ICs RF5210 and the balanced triplexer (BalTPX) correspondingly. Realization of this BalTPX based on LTCC technology will be shown below.

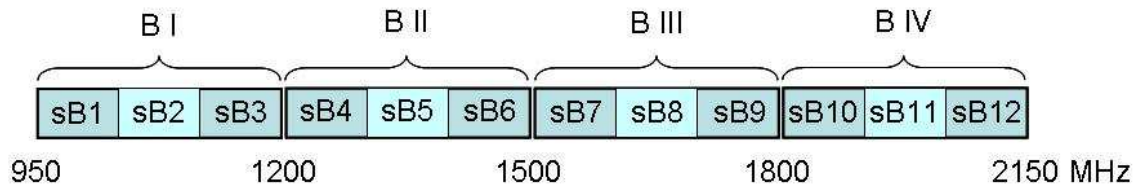


Figure 6.3: Frequency allocation for DBS

The figure 6.2 represents a multiplexer circuit roughly. Such circuit doesn't provide frequency selectivity and includes additional not necessarily losses due to using the power divider. The losses on division of a signal into three parts are 4.77 dB. An alternative circuit shown in Fig. 6.4 is proposed in order to avoid the disadvantages mentioned above.

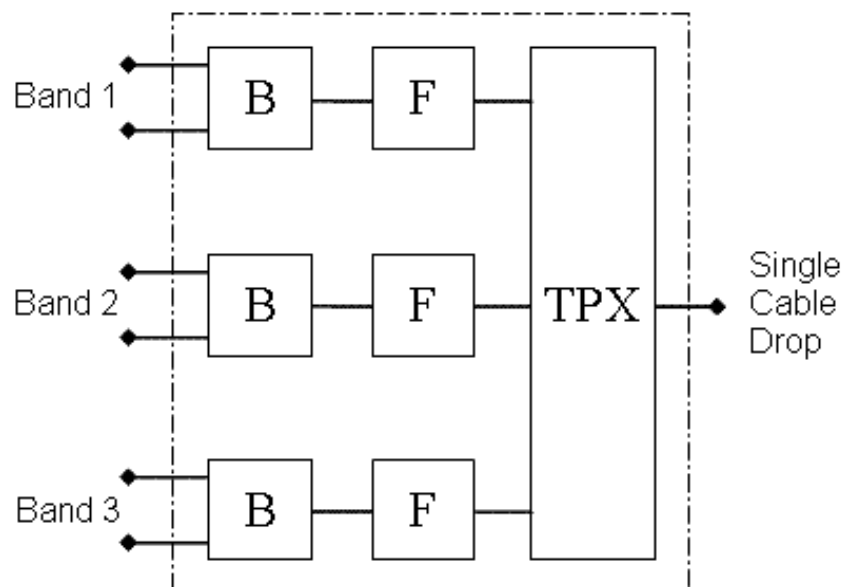


Figure 6.4: Balanced triplexer: block diagram

The circuit is a little bit complicated than the proposed one, but implies the better performance. In order to reduce the transmission losses, a triplexer (TPX) have to be used instead of the power divider. Frequency selectivity is provided using the filters (F) included in each pass. Finally, baluns convert single-ended signal into the balanced one.

The elements used in the realization could be the transversal / recursive filter and the multiplexing circuit described in this work. The broadband PD shown in the work can be useful also if the original circuit proposed above would be implemented.

The triplexer with contiguous bands proposed in this work would be the best solution for the task. Unfortunately, relative bandwidth ($\approx 62\%$) is too broadband for the triplexer function. Thus, future work on the triplexer design has to be put on enlarging of the working frequency band. Instead of it, a typical combination of lowpass-highpass filters

was used for the channels separation. Regarding the filters, there are no limitations on using the transversal / recursive filter type. Finally, common Marchand transmission line baluns [25] was involved in module design.

3D view of the designed module is shown in Fig. 6.5, which is fitted into a size of $7.2 \times 6.2 \text{ mm}^2$ and comprised of 20 ceramic layers with dielectric permittivity of 18 and thickness of $38 \mu\text{m}$ each. The single-ended output is situated on the left-hand side of the module, while the balanced inputs are on the right-hand side. The inner structure is marked with green color, while the pinout – with the magenta one.

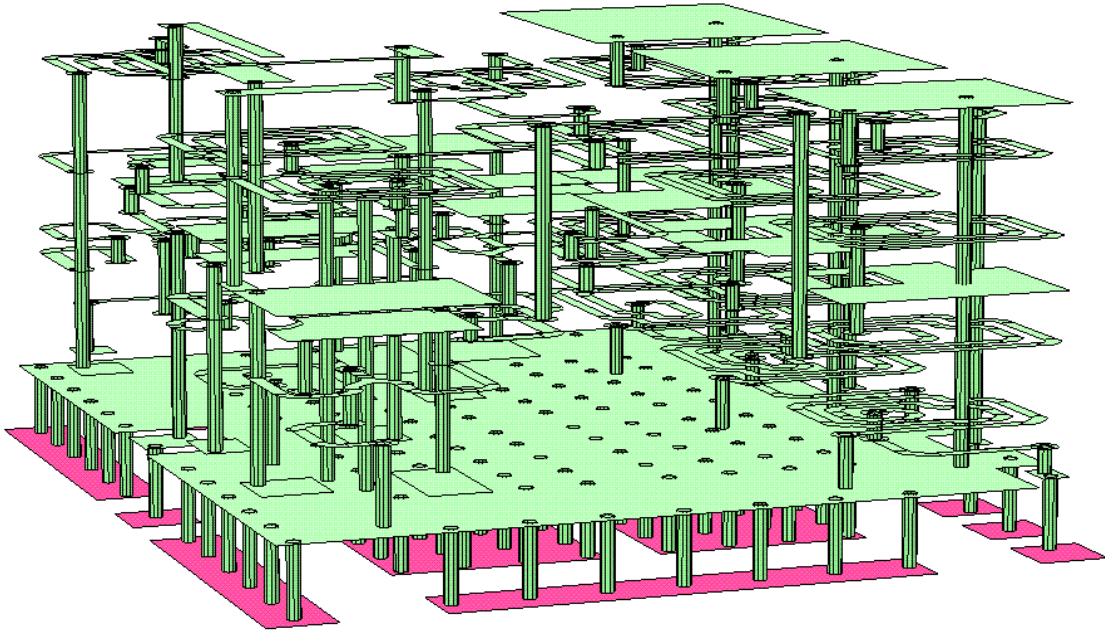


Figure 6.5: Design of the balanced triplexer: 3D view (drawn using Sonnet [40])

A real prototype of the LTCC component was produced and successfully tested. A typical view of the BalTPX samples is shown in Fig. 6.6.

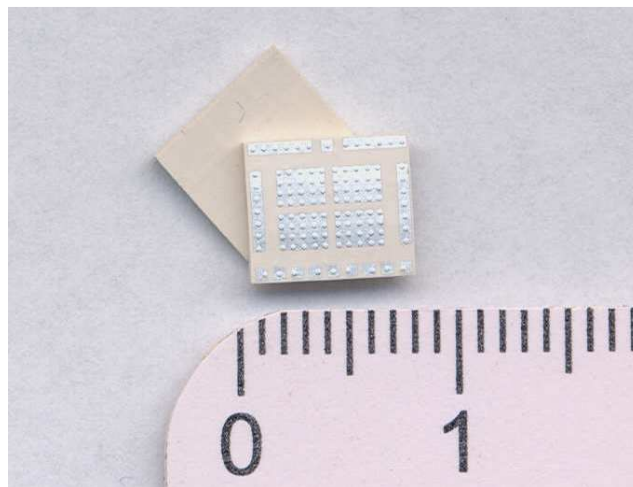


Figure 6.6: Balanced triplexer samples

It's easy to recognize signal pins (small metal plates) and ground plates (the large ones). Performance of the triplexer is shown in Fig. 6.7, where simulation curves are solid and the measured ones are dotted, the output is marked with port 1 and the balanced inputs are marked with ports 2, 3 and 4.

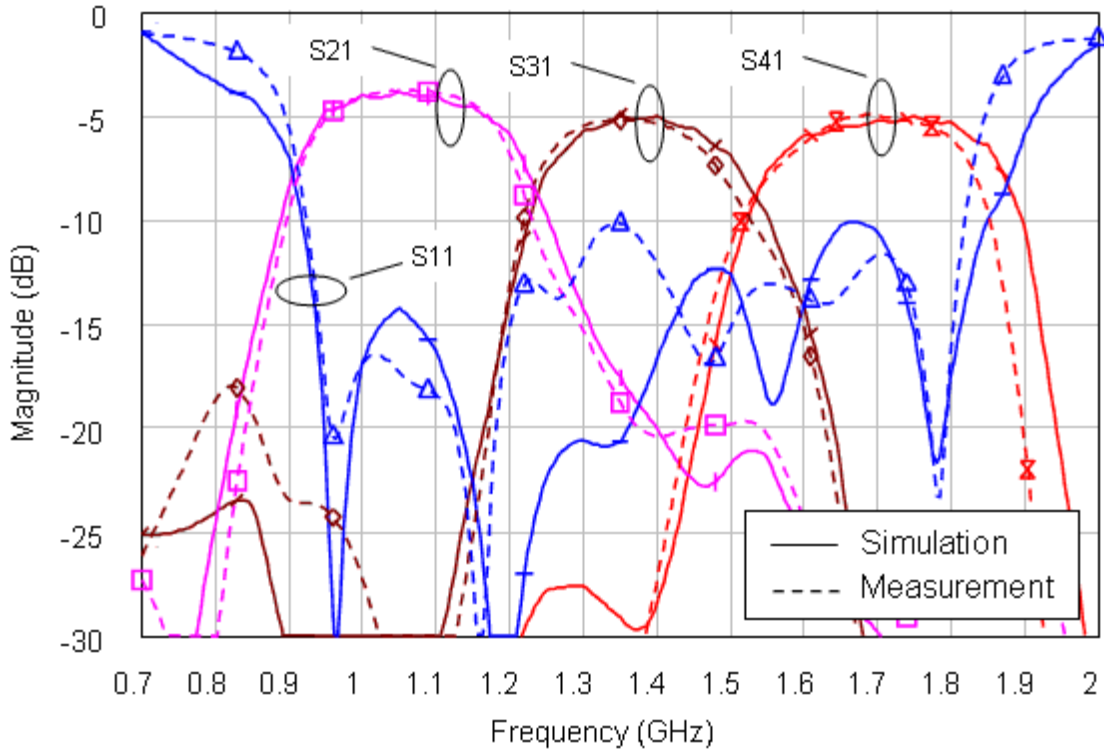


Figure 6.7: Characteristics of the balanced triplexer (simulated using Sonnet [40])

The measurements show good agreement with the simulations. Return loss in both corresponding curves is not less than 10 dB. This value would be enough for single-band components, but it can be critical in case of multiplexing, because a reflected signal affects on contraband passes and causes on transmission characteristics. Thus, the transmission inside the passbands is not constant and presents a form of sin. There are no interactions between neighbor bands in the middle of the passbands due to the triplexing function, while the boundaries suffer strong impact of the reflections from the neighbor. Total amplitude imbalance inside the passbands varies from 1.5 to 2.0 dB.

There are two ways of the flatness improving: using the better multiplexing circuit or using the filter with higher steep slope in order to increase the channel isolation. The first opportunity lies in the following investigations on proposed in this work multiplexing circuit by increasing of the working passband. The second variant assumes using the high rejection transmission line filters and it will be examined right now. 3D-view of the balanced triplexer prototype with the TL filters is shown in Fig. 6.8. The high selectivity filters possess of 6 coupled resonators and occupy much larger size than the transversal /

recursive filters, therefore the total size of the BalTPX is equal to $8.4 \times 7.4 \text{ mm}^2$ and it's around 14 mm^2 bigger than the size of the previous triplexer.

The filters with a specific transmission function were used in order to improve the amplitude imbalance in the passbands. The resonators are so coupled that a pre-correction on the transmission characteristics is formed as it shown in Fig. 6.9a providing form of the passband closely to the sin-function with opposite sign. Thus by connecting such filters together inside the triplexer, the sin-form of the characteristics came from the multiplexing sums with the anti-sin form of the filters transmission and will result in the flat transmission characteristics. The final performance of the triplexer is shown in Fig. 6.9b.

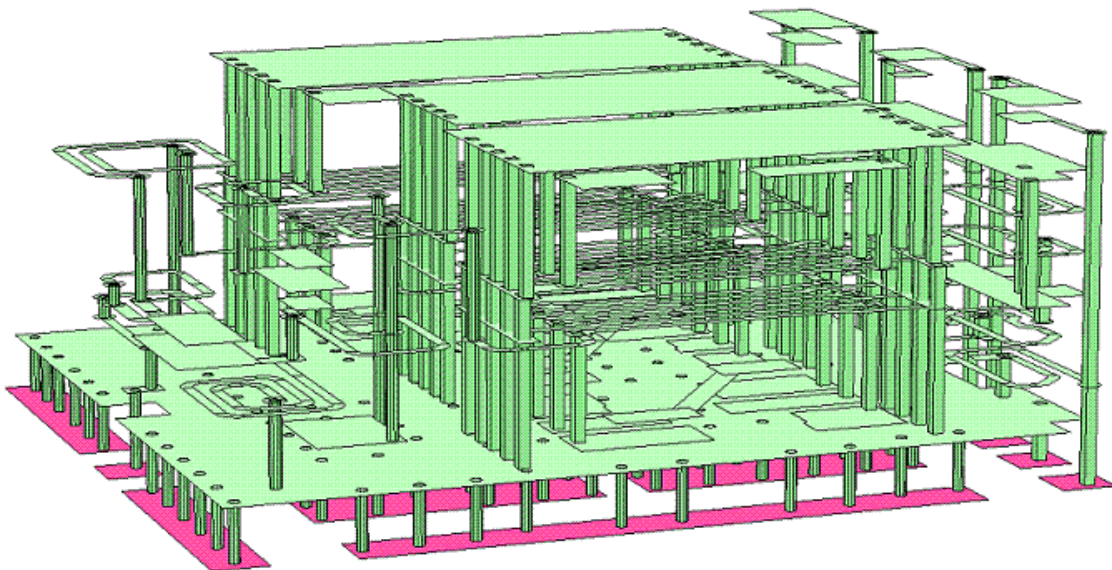
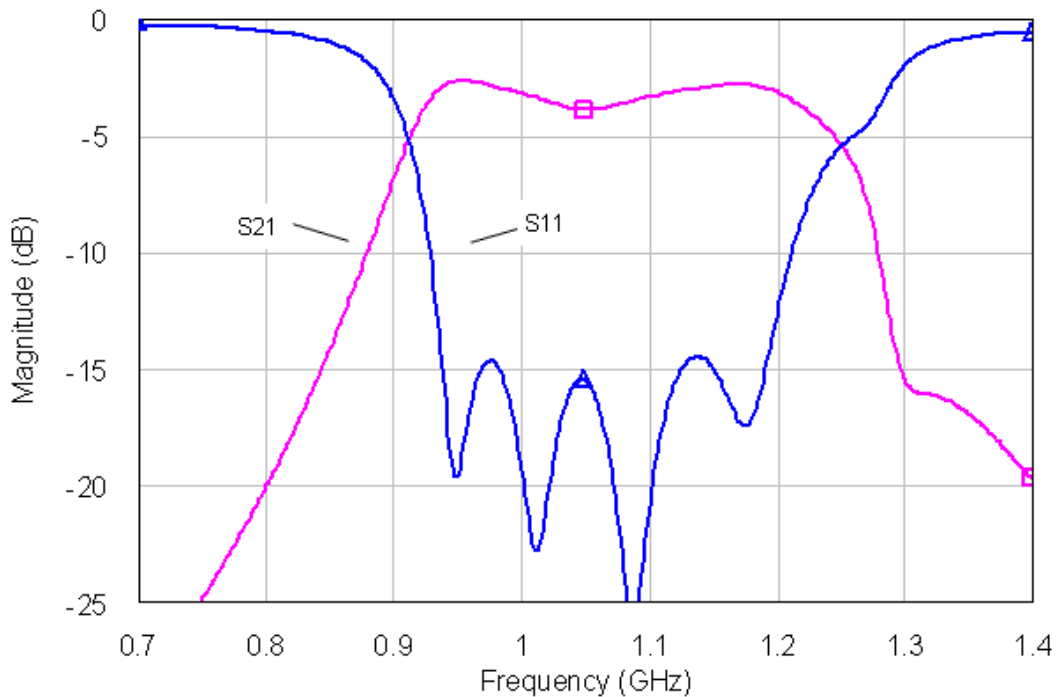


Figure 6.8: Design of the balanced triplexer with TL filters: 3D view (drawn using Sonnet [40])

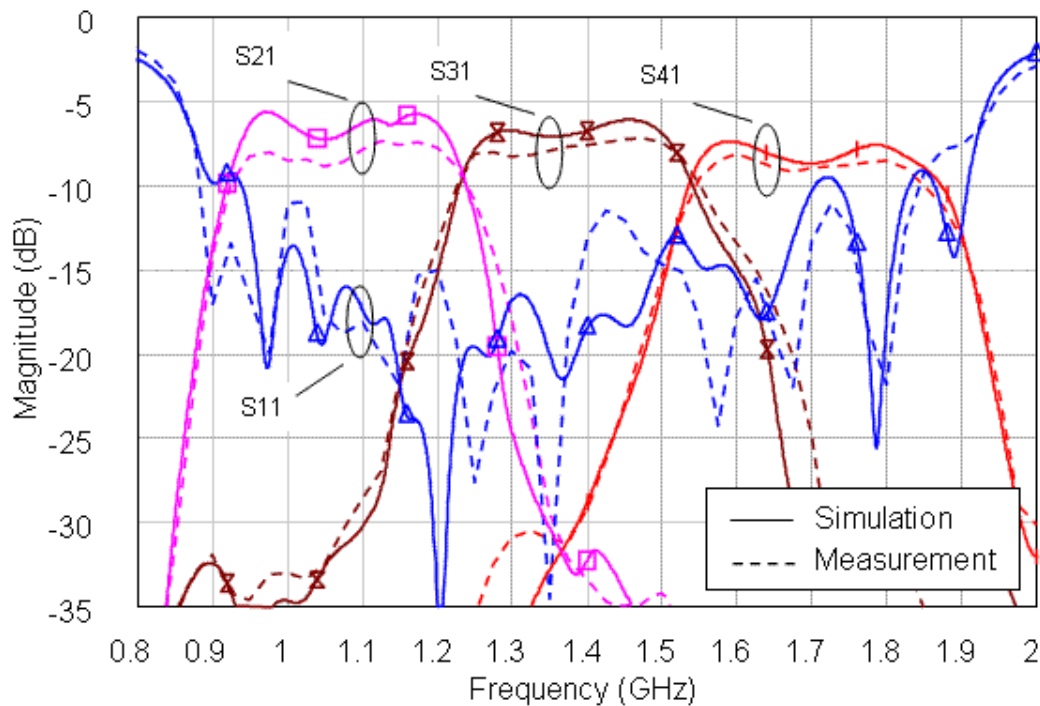
As it was already defined, the solid curves depict the simulation data and the dotted ones show the measurement results, where the port numbers remain the same as in the previous case. In comparison with the results shown in the Fig. 6.7, the passband transmission is more flat. Payment for this issue is an increase of the component size, complexity and insertion loss. Additional IL of 4 dB rises as a result of the flatness improvement of 0.5 dB, which lies now in the range of 1.0 – 1.5 dB. The following steps to improve the flatness would be based on selection of the optimal profile of the TL filter's transmission characteristics. The use of the same multiplexing procedure doesn't give a possibility to improve the output matching; therefore the worst values remain on the same level. A solution for this issue will be the use of the multiplexing circuit proposed in this work, which is optimal for function with contiguous channels and that must be still optimized for broadband function.

3D-view of the fabricated triplexer is shown in Fig. 6.10, where pin locations and their destinations are the same as the ones in the Fig. 6.6.

Thus, two types of the balanced triplexers were proposed for this project with an open way for the future investigations on the multiplexing circuit proposed in this work. The first triplexer is a low cost solution using the transversal / recursive filter described in this work, while the second one is improved in case of the flatness and is worse assuming the insertion loss.



a) Performance of the TL filter for B I



b) Transmission characteristics of the BalTPX

Figure 6.9: BalTPX using TL filters with pre-correction (simulated using Sonnet [40])

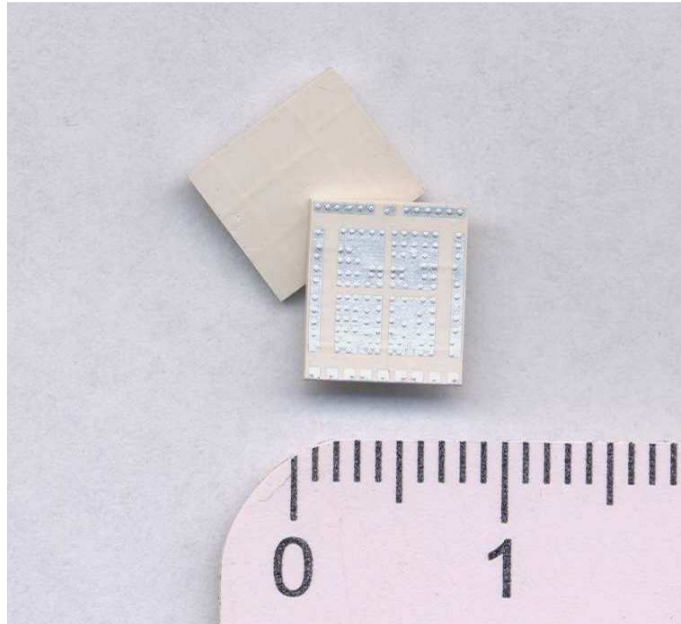


Figure 6.10: Samples: Balanced triplexer with improved flatness in passband

6.2 NOFDM UWB Receiver

Wireless standard IEEE 802.15.3a for a high-data-rate wireless personal area network (WPAN) assumes use of UWB signals for short range and high speed communication. UWB technology serves mainly for either transmission of huge amounts of data or objects localization, therefore, doesn't replace neither cellular nor wireless local area network (WLAN) connection technology. Frequency band occupied by UWB signal is situated in the range of 3.1 to 10.6 GHz. It is a big challenge to build a simple, high performance and low cost UWB receiver supporting high transmission speed. Present project "Noncoherent orthogonal frequency division multiplexing (NOFDM) ultra-wideband (UWB) receiver" focuses on development of a novel noncoherent receiver for wireless multicarrier transmission scheme of UWB signal and described in [26]. The idea was developed by Prof. Klaus Witrisal from TU Graz. Detailed information can be found in [27] – [30]. General block diagram of the receiver is shown in Fig. 6.11.

Front-end part of the receiver is standard and it consists of an antenna, bandpass filter (BPF), low-noise and variable gain amplifiers (LNA and VGA). Conventional digital receivers need high-speed analog-to-digital converters (ADC) and fast digital signal processors. This issue results in high power consumption level. In contrary to this, the proposed receiver uses autocorrelators connected in parallel, thus parallelize the process and reduce ADC processing speed. The autocorrelators consist of delays, mixers and integrators and they all are combined together in the block diagram and will be realized in

a single module. All passive structures will be integrated in LTCC substrate, while active elements will be mounted on the top side. The last step would be analog-to-digital conversion with the following digital processing.

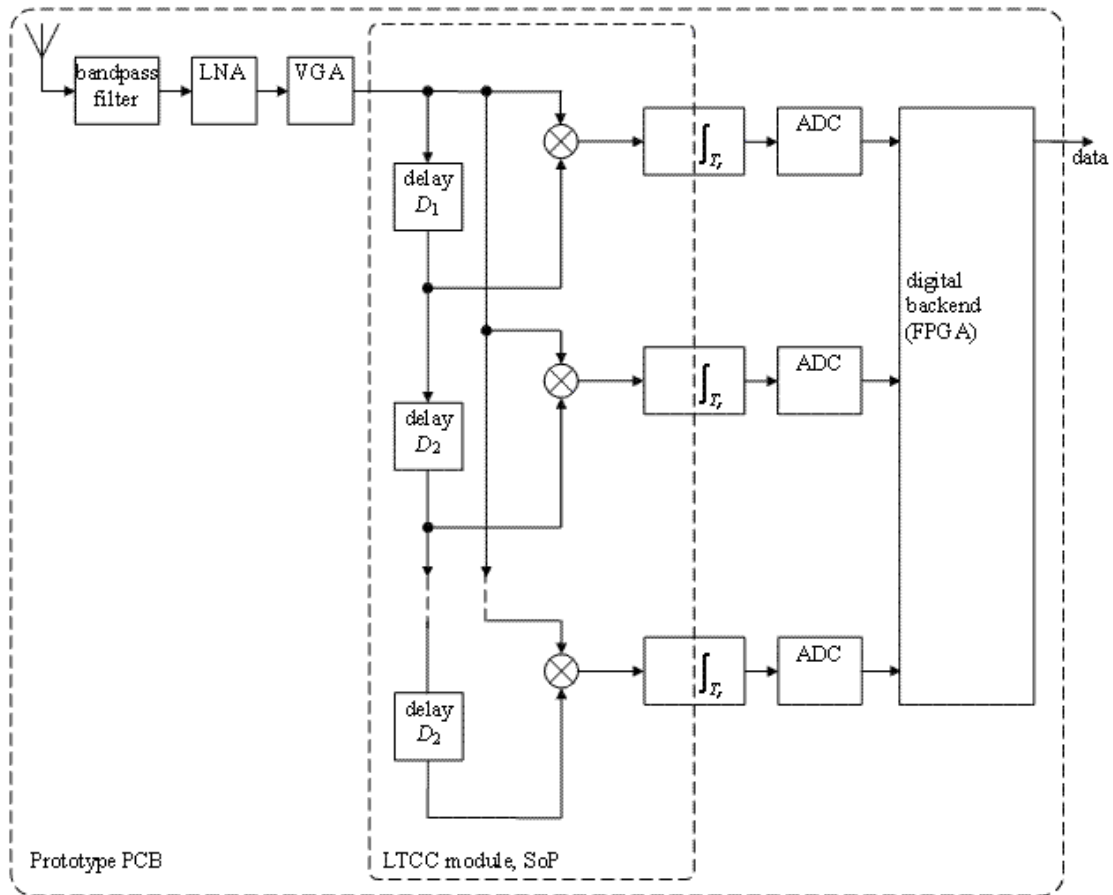


Figure 6.11: Functional block diagram (from [26])

A common noncoherent receiver exploits instantaneous power of a signal, while a coherent receiver operates with absolute phase information. Thus the noncoherent architecture is robust due to its simplicity and power efficient assuming operation with impulse signals. On the other hand, an energy detector suffers from a signal-to-noise ratio (SNR) loss compared with the coherent receiver and it's much less robust with respect to interfering signals, reducing in such a way data rate.

The proposed receiver architecture possesses all advantages of the noncoherent receivers. Additionally, the autocorrelators have been chosen instead of common used energy detectors (ED), thus to be able to discriminate signals at different frequencies. Moreover, it's able to mitigate narrowband interferences and it allows high-rate multicarrier transmission and frequency tuning.

The point of interests regarding the realization of the receiver is concentrated on the passive components that could be realized using LTCC. The receiver architecture shown in Fig. 6.11 is simplified for better understanding of its function. In general, the meaning of the joint points depicted in the figure is a power division that could be realized either using

power dividers or couplers that depends on required division ratio. For example, a typical autocorrelator is physically realized using the following blocks shown in Fig. 6.12, where PD - 3 dB power divider, D – delay line. Original signal and the delayed one are mixed and integrated. This would be a realization of the first autocorrelator shown in Fig. 6.11. The other autocorrelators connected in parallel and separated by delay lines use couplers for joint point's realization in order to equalize the signal level among the autocorrelators.

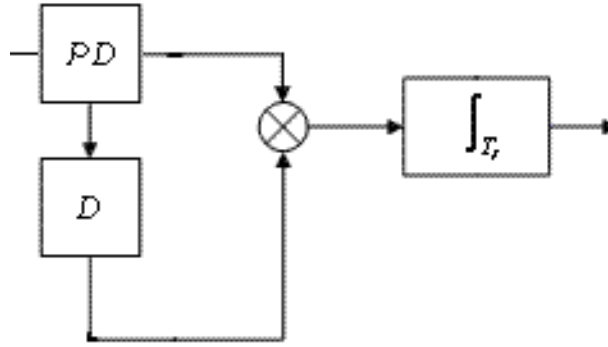


Figure 6.12: Autocorrelator: detailed block diagram

The power divider described in this work is a good candidate to be implemented in the receiver. The first receiver prototype, which is going to be designed, will not use the whole UWB frequency band and will be confined with the band from 3 to 5 GHz, because of the challenges on a design of the delay lines and couplers. Nevertheless, the receiver will provide high speed communication (with calculated speed above 500 Mbit/s) over limited distance (less than 5 m), already. A single power divider realized using LTCC with internal ports is shown in Fig. 6.13.

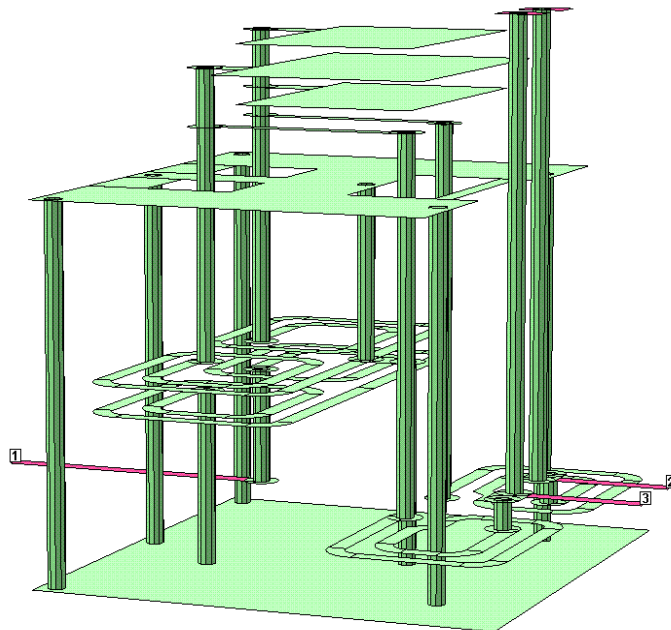


Figure 6.13: 3D view of the PD realized using LTCC (drawn using Sonnet [40])

The power divider has been optimized for the receiver. This LTCC component is comprised of 20 ceramic layers with dielectric permittivity of 7.8 and thickness of 55 microns each. The size of the component is $2.8 \times 2.65 \text{ mm}^2$.

Simulated performance of the splitter is depicted in Fig. 6.14. For S-parameters representation, port 1 is denoted as the input one and ports 2 and 3 as the output ones. The power divider is matched inside the working band (return loss is less than 12 dB) with corresponding low losses (3 dB on division onto two parts plus 1.5 dB on transmission loss). Isolation between the channels is more than 12 dB within the band.

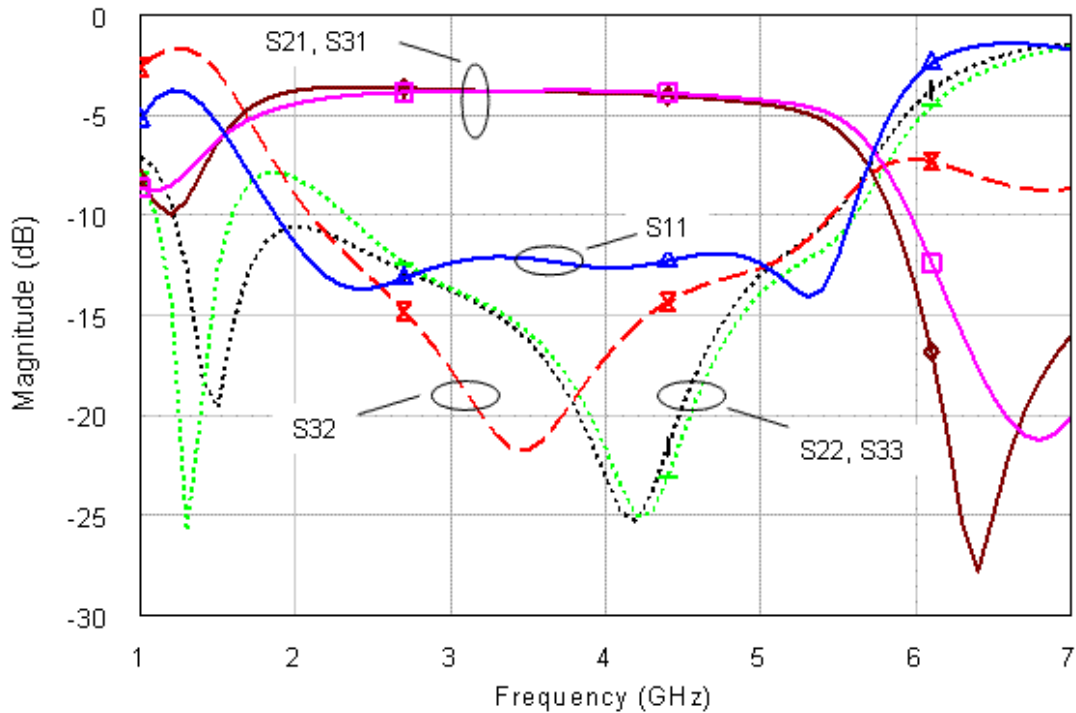


Figure 6.14: Performance of the power divider (simulated using Sonnet [40])

Measurements of the power divider are not available at the moment, because the splitter is a part of the future LTCC module incorporating the autocorrelators connected in parallel as it's shown in Fig. 6.11. But it's not necessary taking into account the fact that feasibility of the splitter was already proved in this work, where the measurements correlate very good with the simulations. So, we can trust in these simulations.

6.3 Universal Balun

Most of the components developed in the present work, like the power divider and the multiplexer, are based on the modified Marchand balun design. It seems that the balun is a universal structure, which modifications bring new properties. This issue can lead to the unification of a design process and therefore to decreasing of time needed for

development of passive components and modules. For example, a block diagram of a typical receive front-end part supporting multi-frequency operation is shown in Fig. 6.15. It contains baluns (B), filters (F) and diplexers (DPX). Minimal number of the components to be designed is 8, assuming a fact that each of the baluns functions at the whole frequency range for both channels. In case when frequencies for receive channels (RX) situate close to each other, contiguous diplexing is necessary.

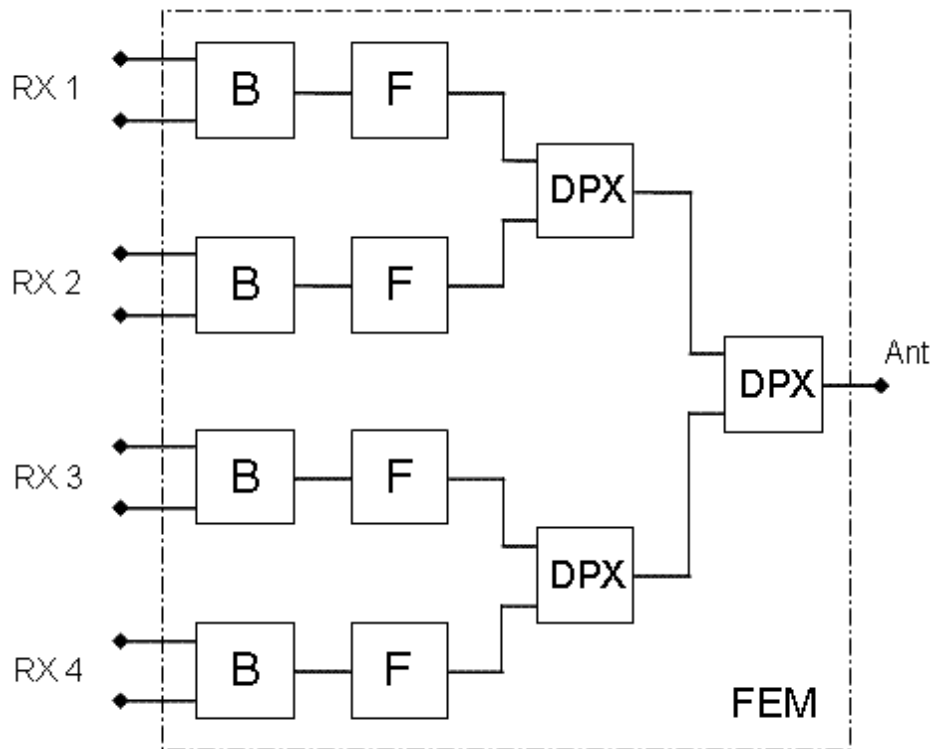


Figure 6.15: A common receive front-end part: functional block diagram

An alternative front-end part based on designs proposed in this work is shown in Fig. 6.16. The module provides the same functionality as the one shown in Fig. 6.15a and it's comprised of baluns and quasi-baluns (qB) only. The first vertical line with the baluns situated on the left-hand side of the block-diagram remains the same as in the common module. The next baluns pairs provide a filter function, where each pair contains equal baluns. The filters can be both either step-impedance resonator (SIR) type or the transversal one. Finally, the diplexers are exchanged with quasi-baluns, which are equal due to their functionality. Thus, in order to realize such module, six basic designs must be done instead of eight ones as it was in the previous case. The quasi-baluns are the same as four first baluns, but with altered the even- and odd-mode coupled transmission line impedances. Procedure of such module design is much easier and therefore quicker, because the realization assumes a design of the single balun type for different frequencies.

The next proposed structure of the module is shown in Fig. 6.17. This module consists of even less components. There are no filters inside, because the baluns take both

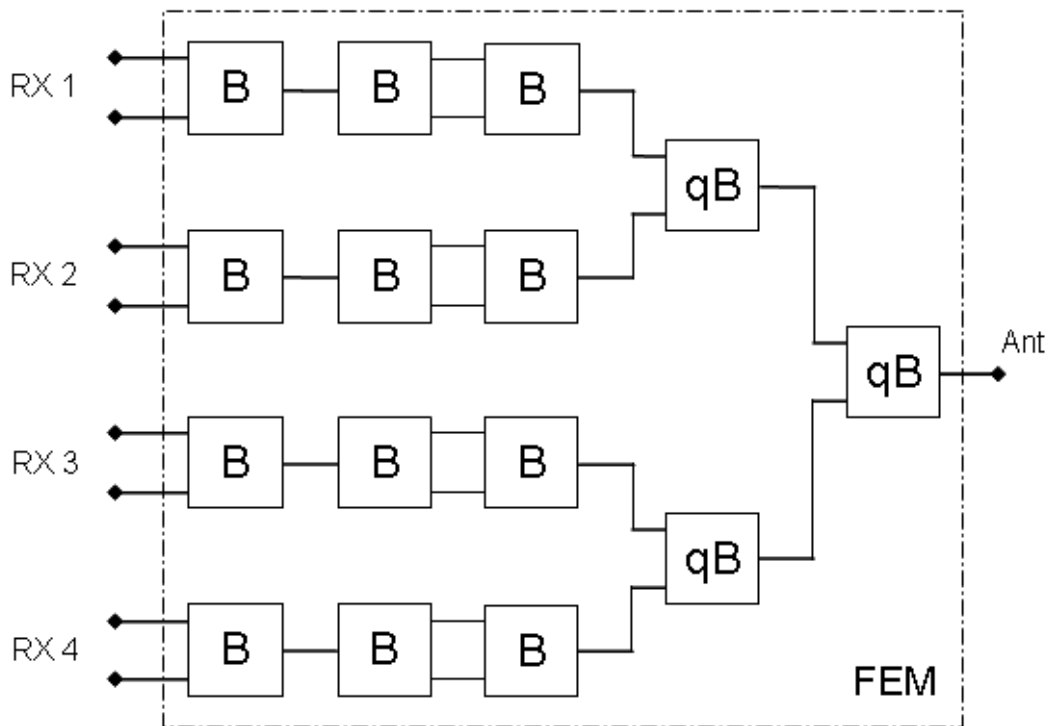


Figure 6.16: Balun-based receive front-end part

balancing and filtering functions as it was shown in [31]. Such design procedure provides miniaturization in addition to the unification. The quasi-baluns remain the same as in the previous balun-based module, while the baluns are tuned onto different frequencies corresponding to the channels. A number of the components to be realized is less than in the previous module, as well as a number of the basic designs – five.

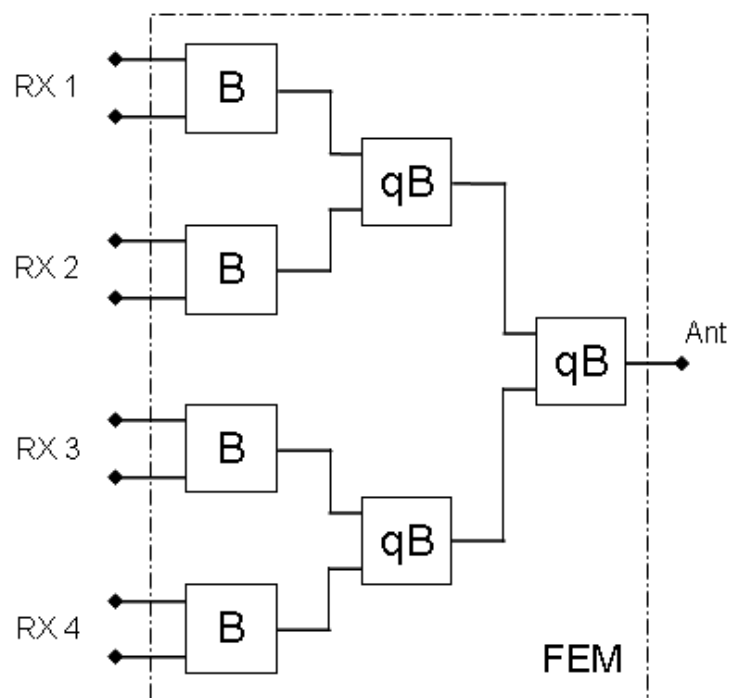
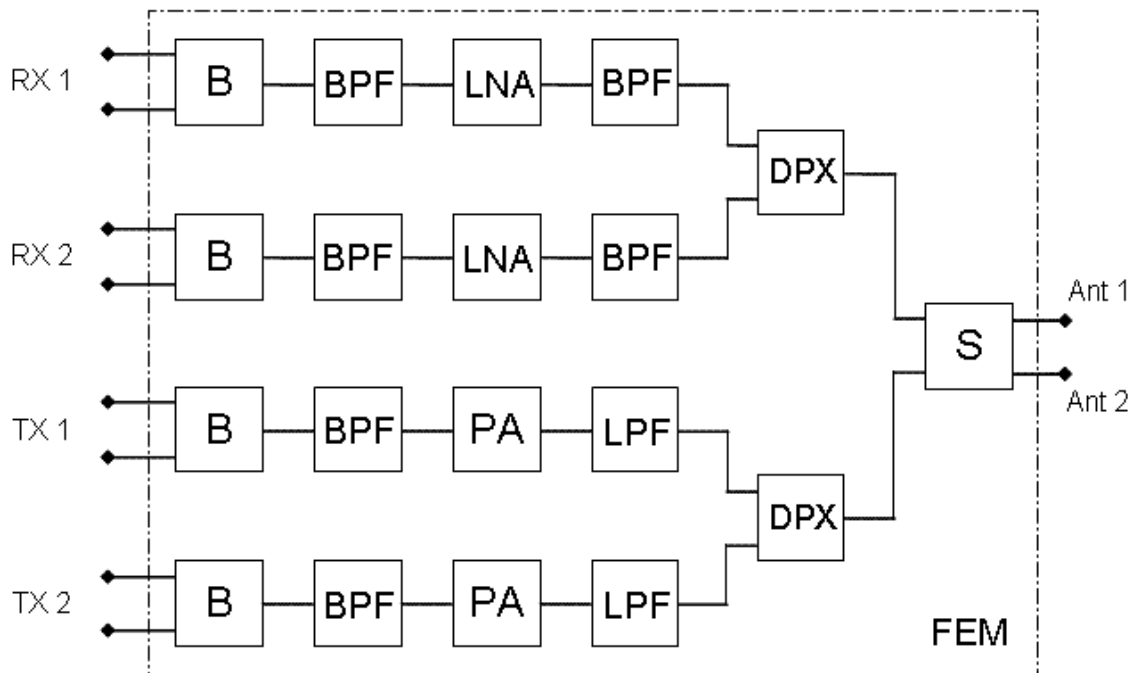
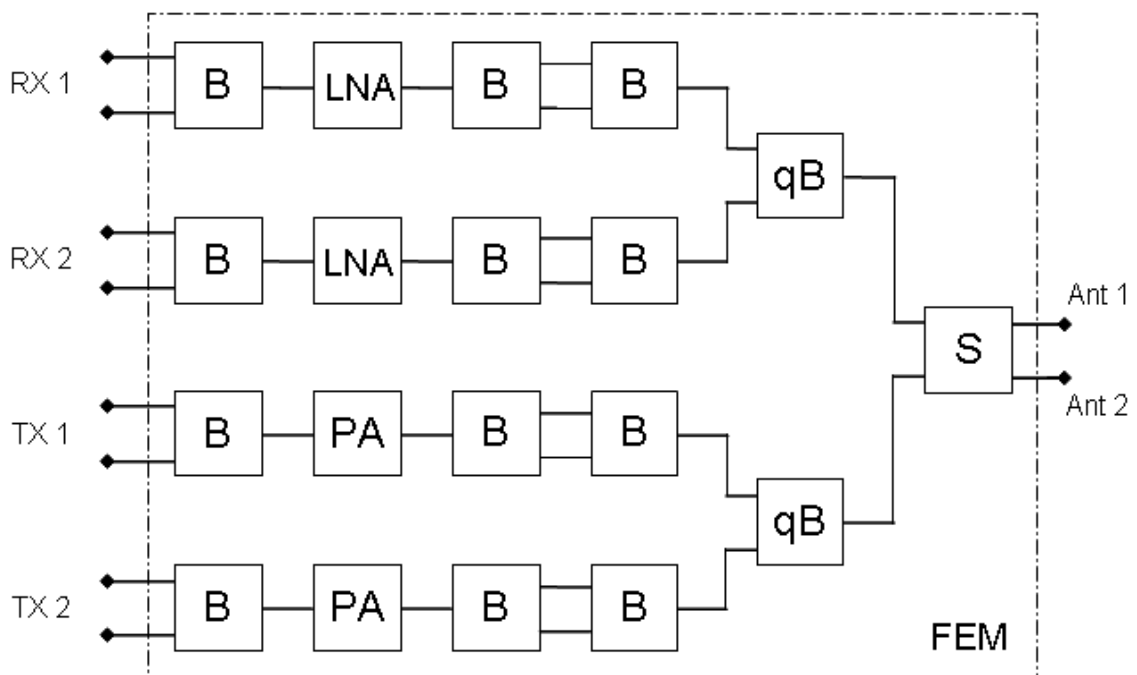


Figure 6.17: The simplest balun-based FEM

The same procedure can be done, for example, with a standard receive / transmit (RX / TX) module operating with two frequency bands. An original simplified architecture (power monitor, electro static device protection and antenna matching are not depicted) is shown in Fig. 6.18a. It contains switch (S), diplexers (DPXs), bandpass filters (BPFs), lowpass filters (LPFs), baluns (Bs), low-noise and power amplifiers (LNAs and PAs). A lot of modules based on this block diagram have been done already, some of them are described in [32] – [36].



a) Original block diagram



b) Balun-based block diagram

Figure 6.18: A typical RX / TX FEM

Unificated balun-based architecture is depicted in Fig. 6.18b. Eleven different passive components are replaced now by six unificated balun designs. The proposed above FEM structures (Fig. 6.16, 6.17 and 6.18b) can be used like references for the future module designs. The design procedure is uniform and simple. There are only technical restrictions based on the functional bandwidth of the baluns. Using this method, I designed RX module for WiMAX (worldwide interoperability for microwave access) applications [37]. As the result, a size of the module is almost twice smaller than sizes of the analogue modules ([38] – [40]). This fact proves applicability of the methods.

This part of the work has shown some tasks where the components described above found practical implementation. Of course, these components are not ideal or universal, but in some cases, they provide either performance improvement or essential miniaturization of a structure. The components were realized within the modules using LTCC technology, though any technology could be used for the realization as well as single components production.

6.4 References to Chapter 6

- [1] “Single Cable Distribution. The industry standard for single-cable satellite reception and distribution,” Astra. [Online]. Available: http://www.ses-astra.com/resources/pdf/en-shared/products_services/0_Single_Cable_Distribution_brochure.pdf
- [2] *Satellite signal distribution over a single coaxial cable in single dwelling installations*, CENELEC Std. EN50494, 2007.
- [3] Astra website. [Online]. Available: <http://www.ses-astra.com/business/en/solutions/media/single-cable/index.php>
- [4] TV-netcom website. [Online]. Available: http://tv-netcom.de/inlineframe_unicable_einkabeltechnik.htm
- [5] “Changing DBS Delivery – The Single Wire Solution,” Entropic Communications, 2008.
- [6] *Satellite Channel Router (SaTCR-1)*, STMicroelectronics, 2004.
- [7] “Einfach Umsteigen, Weg von Kabel - aber wie?,” INFOSAT, No. 233, Aug. 2007.
- [8] “Channel Stacking Switch Technology for Residential DBS Reduces Cabling and STBs,” Entropic Communications, 2007.
- [9] “New channel-stacking switch RF ICs from Entropic Communications,” Entropic Communications, 2007.
- [10] “CSS and MoCA Combine to Deliver Competitive Advantages to DBS Operators,” Entropic Communications, 2008.

- [11]“Digital Broadcast Satellite Systems: The Benefits of Channel Stacking Switch Technology,” Entropic Communications, 2009.
- [12]“Satellitenempfang trotz Baumverteilung,” Axing, 2009.
- [13]Axing website. [Online]. Available: http://www.axing.com/katalog_de/Multischalter57.html
- [14]*Unicable Multiswitch (SDUC 502/902)*, Grundig SAT Systems.
- [15]*Kaskadierter Unicable Multischalter für 2 Satelliten (IDL-UPSS200-CU10-8PP)*, Inverto.
- [16]*Sat-ZF-Verteilssystem Einkabel-Multischalter (EXR 1942/2942)*, Kathrein.
- [17]EMP-Centauri website. [Online]. Available: <http://www.emp-centauri.cz/products.php?page=products>
- [18]*Satellite Multiswitch (MS 13(17)/XXPIU-6)*, EMP-Centauri.
- [19]*Profi Line Combiners (P.1XX-W)*, EMP-Centauri.
- [20]BELSAT website. [Online]. Available: <http://www.belsat.ch/Service+Support/Tech-Infos/Beispiel-4.htm>
- [21]*Sat Channel Router (WCR41P)*, Elcon.
- [22]DIRECTV website. [Online]. Available: <http://www.lcdtv2010.com/Bestsellers-in-directv-wnc-multi-satellite-dish-with-integrated-triple-lnb-built-in-multi-switching.html>
- [23]*Satellite Channel Stacking Switch IC (RF5210)*, Entropic Communications.
- [24]Satellite Television. [Online]. Available: http://en.wikipedia.org/wiki/Satellite_television.
- [25]N. Marchand, “Transmission-Line Conversion Transformers,” *Electronics*, vol. 17, Dec. 1944, pp. 142-146.
- [26]SPSC Lab TU Graz website. [Online]. Available: <http://www.spssc.tugraz.at/research/projects/nofdm-noncoherent-orthogonal-frequency-division-multiplexing>
- [27]K. Witrisal, “Noncoherent Autocorrelation Detection of Orthogonal Multicarrier UWB Signals,” *Proceedings on IEEE International Conference on Ultra-Wideband*, Sept. 2008, pp. 161-164.
- [28]K. Witrisal, “A Noncoherent Multiband Receiver for IEEE802.12.4a UWB Signals,” *in COST 2100 Managem. Comm. Meeting*, Trondheim, Norway, Jun. 2008.
- [29]K. Witrisal, G. Leus et al., “Noncoherent Ultra-Wideband Systems,” *IEEE Signal Processing Magazine*, Jul. 2009, pp. 48-66.
- [30]P. Meissner and K. Witrisal, “Analysis of a Noncoherent UWB Receiver for Multichannel Signals,” *Proceedings on IEEE Vehicular Technology Conference*, May 2010, pp. 1-5.

- [31] R. Kravchenko, K. Markov, et al., "Implementation of a Miniaturized Lumped-Distributed Balun in Balanced Filtering for Wireless Applications," *Proceedings on European Microwave Conference*, Oct. 2005, pp. 1303-1306.
- [32] A. Chernyakov, K. Markov, et al., "Novel small-size LTCC-based WLAN frontend-modules with integrated power amplifiers," *IEEE MTT-S International Microwave Symposium Digest*, Jun. 2004, pp. 559-562.
- [33] A. Chernyakov, K. Markov, D. Orlenko, P. Heide and C. Ruppel, "Miniature Fully-integrated WLAN Frontend-Modules based on LTCC Technology," *IEEE Radio and Wireless Symposium Digest*, Sept. 2004, pp. 139-142.
- [34] A. Yatsenko, J. Heyen, et al., "Highly-Integrated Dual-Band Front-End Module for WLAN and WiMAX applications based on LTCC technology," *IEEE MTT-S International Microwave Symposium Digest*, Jun. 2008, pp. 13-16.
- [35] A. Yatsenko, W. S. Wong, et al., "System-in-Package solutions for WiMAX applications based on LTCC technology," *IEEE Radio and Wireless Symposium Digest*, Jan. 2009, pp. 470-473.
- [36] S. Sakhnenko, D. Orlenko, et al., "Ultra-Low-Profile Small-Size LTCC Front-End Module (FEM) for WLAN Applications Based on a Novel Diplexer Design Approach," *IEEE MTT-S International Microwave Symposium Digest*, Jun. 2009, pp. 609-612.
- [37] R. Kravchenko, M. Stadler and E. Leitgeb, "Extra-highly Integrated LTCC Balanced Triplexer for WiMAX Applications," *Proceedings on European Microwave Conference*, Sept. 2010, pp. 1-4.
- [38] D. Orlenko, G. Sevskiy, T. Kerssenbrock, and P. Heide, "LTCC Triplexer for WiMAX Applications," *Proceedings on European Microwave Conference*, Oct. 2005, pp. 97-100.
- [39] D. Kim, D. H. Kim, et al., "LTCC-based Triplexers for WiMAX Front-end Modules," *Electrical Design of Advanced Packaging and Systems Symposium Digest*, Dec. 2008, pp. 190-193.
- [40] D. Kim, D. H. Kim, J. I. Ryu, and J. C. Kim, "Highly Integrated Triplexers for WiMAX Applications," *IEEE MTT-S International Microwave Symposium Digest*, Jun. 2008, pp. 1091-1094.
- [41] Sonnet Software Inc. v.12.52, 2010.

7. Conclusion

The present work showed the development process of the key components (filters, power dividers and multiplexers) with improved characteristics for microwave front-end applications. New solutions on improvement of technical and mechanical characteristics of the components were presented. The thesis contains descriptions of the components implementation and real applications using them.

7.1 Summary

In this work, new design ideas for inner structure of some microwave passive components have been presented. The main principle assumes decreasing a number of elements in the structure that provide better technical parameters of the structure and gives substantial miniaturization effect together with the advantages of LTCC technology. The investigations were focused on the key components in the front-end part of the devices supporting wireless communications: filters and frequency / power dividers.

First of all, the new transversal / recursive filter concept has been presented. The filter is a lumped element equivalent circuit of a ring resonator with perturbations and it avoids all problems of common transversal filters realization using LTCC substrate. The filter is distinguished with its simple structure without any active components and any large structures like couplers or transmission lines. As an example, 5 GHz filter for WLAN with a size of $1.9 \times 1.0 \text{ mm}^2$ was realized. The filter provides low transmission loss with good enough suppression characteristics.

The next novel solution presented in this work is UWB power divider. Theoretical investigations show essential improvements on the component size and performance in comparison with the existing solutions. The proposed power divider is able to operate with 110 % relative bandwidth using small even-mode impedance values of the coupled stripline, therefore, resulting in small structure size. A prototype of the power divider based on the attached calculation process was successfully designed, produced using LTCC technology and measured. The measurements show good agreement with the simulation results and this fact proves applicability of the design.

A new solution was proposed for the multiplexer operating with contiguous bands. The basement for the multiplexer lets the filters with specific defined input impedance characteristics to be connected together without enormous signal reflections. A design of the multiplexer is based on the quasi-balun concept realized by coupled striplines. In

comparison with the existing solutions, such multiplexer provides much better performance, because the filters characteristics suffer any changes and much less reflections occur at the interconnection node during the multiplexing. The attached calculation procedure has found an optimal solution. As an example, the diplexer was calculated and optimized for function with the 50 Ohm environment. Additionally, the presented optimization procedure shows a possibility to rebuild the diplexer for function with different environment impedances by changing the even- and odd-mode coupled stripline impedances, only.

Finally, the practical implementations prove applicability of the developed structures. These simple structures allow refusing from difficult and big circuit solutions. Of course, these components are not ideal or universal, but they provide either performance improvement or essential miniaturization of a structure in some cases. The components were realized both integrated in modules and like single. An implementation of the components is not confined only with LTCC technology. Any other technology, which can provide realization of the circuits, could be used as well.

7.2 Future work

Nothing can be investigated thoroughly and this case is not exclusion. Some tips are given below regarding my activities on future investigations of the components.

The transversal / recursive filter examined above presents a simple structure that is built of two parallel paths. The next step would be to carry out detailed investigation of the filter containing higher number of the parallel passes. Geometrically, such filter will have a form of a framework for 3D sphere. Such structure is much more complicated in analysis and design, but performance of the filter is promised to meet the most overparticular specifications. This filter type could be a good candidate for the next filter generation.

Regarding UWB power divider, the performance at high frequencies has to be improved. Function of the splitter at the high frequencies is confined with a self resonance of the large capacitor and the interconnection lines. On the other hand, the same capacitor enlarges the bandwidth and this issue leads to a collision. My future work considers development of the appropriate 3D solution optimized for the high frequency function.

One important restriction is put on the use of the proposed multiplexer operating with contiguous bands. It functions strictly within the bandwidth of the basement, which relative value realized in LTCC is about 70 %. My research work on potential improvement of the bandwidth is planed for the nearest future taking into account significance of contiguous channels multiplexing in modern equipment.

Appendices

The appendixes are split into four parts, where more detailed information about several aspects in this work is placed. The first part contains some general information about LTCC design and manufacturing; next two parts present calculations made for the power divider and the multiplexer circuit in details. Finally, calculated and organized parameters of the coupled striplines configuration used for multiplexer design are placed to the last part.

Appendix A: LTCC Components

Appendix A.1: Design Process

All of the HF components described in this work were implemented in 3D structure using design flow algorithm, which is shown in Fig. A. 1.1.

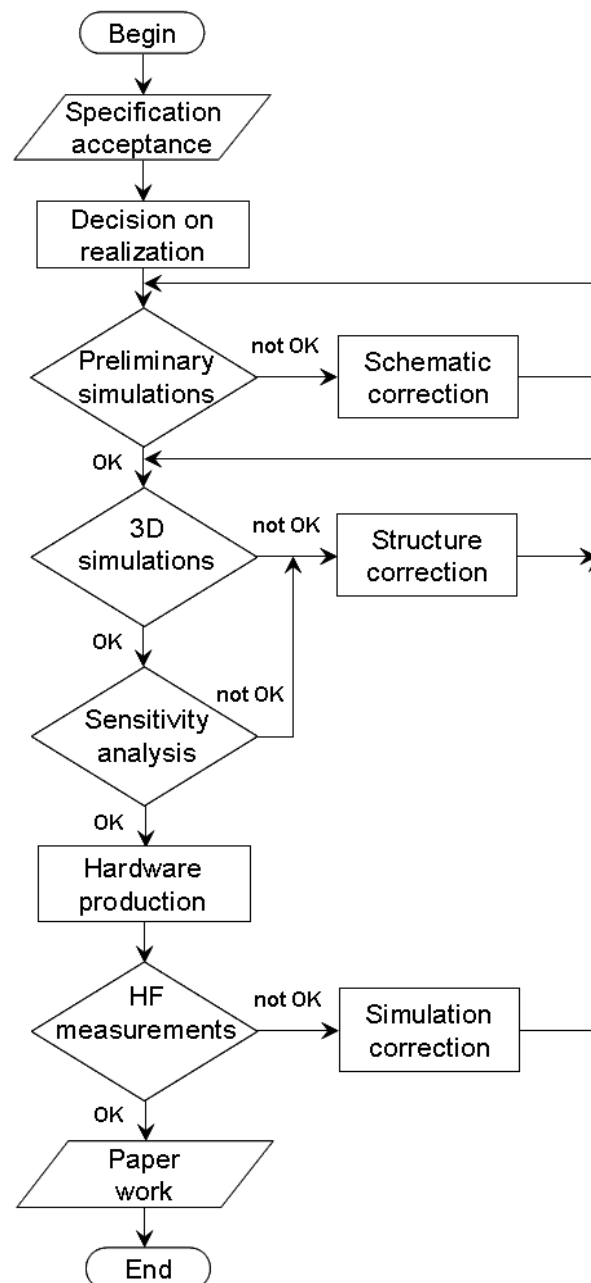


Figure A.1.1: Design flow algorithm

Design of each component begins with specification overview and acceptance of realization possibility. Afterwards, the following decisions have to be met, how the component will be realized (using either lumped elements or elements with distributive

parameters). Preliminary simulations using ideal circuit elements realization must be done before the component will be realized in 3D structure in order to prove and fix preliminary component performance. At this stage, an optimization procedure is included in the process and it is named “schematic correction”. After the calculation of the elements parameters has been done, the structure has to be realized in LTCC with corresponding tuning and optimization procedure. A sensitivity analysis has to be provided with the final structure in order to test its functional stability dependent on production tolerances, where additional corrections on the designed structure have to be done if needed. If the design phase is finalized, the component must be produced, measured and verified. The verification procedure assumes comparison of measured and simulated, mostly. A decision has to be done, if the component meets specified requirements or not. In case of negative answer, redesign procedure must be started, which includes analysis (why the measurements don't agree the simulations) and correction (re-simulation) phases. A paper work finalizes the design process, where all necessary documentation must be done.

Appendix A.2: Production

In this appendix, a typical view of LTCC components is shown. Appearance of the components within the sintered panel is depicted in Fig. A. 2.1. Perspective view on the components as well as cut sections of the component is presented in Fig. A. 2.2.

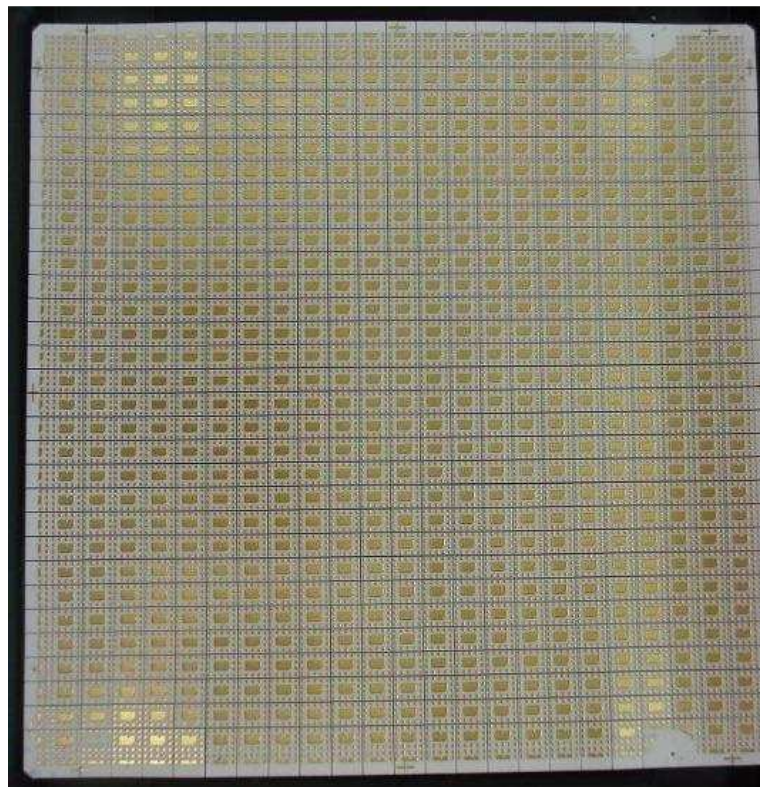
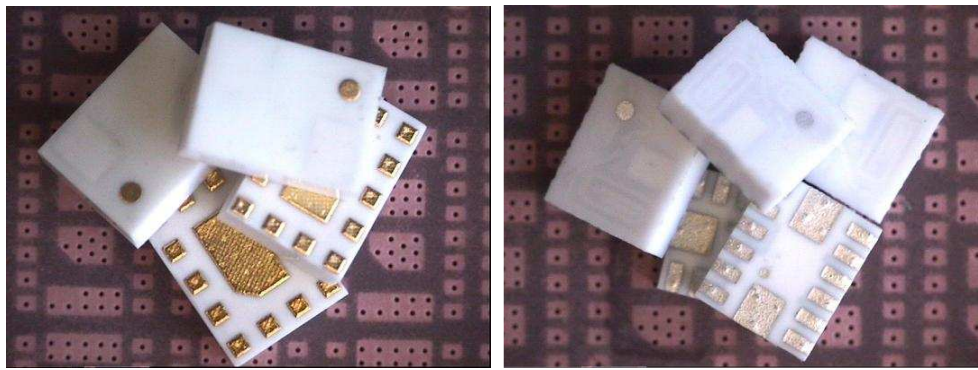
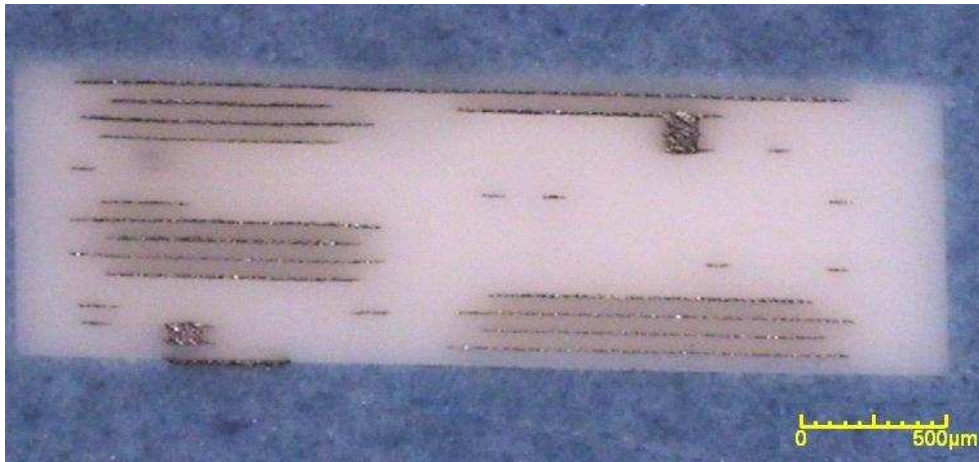


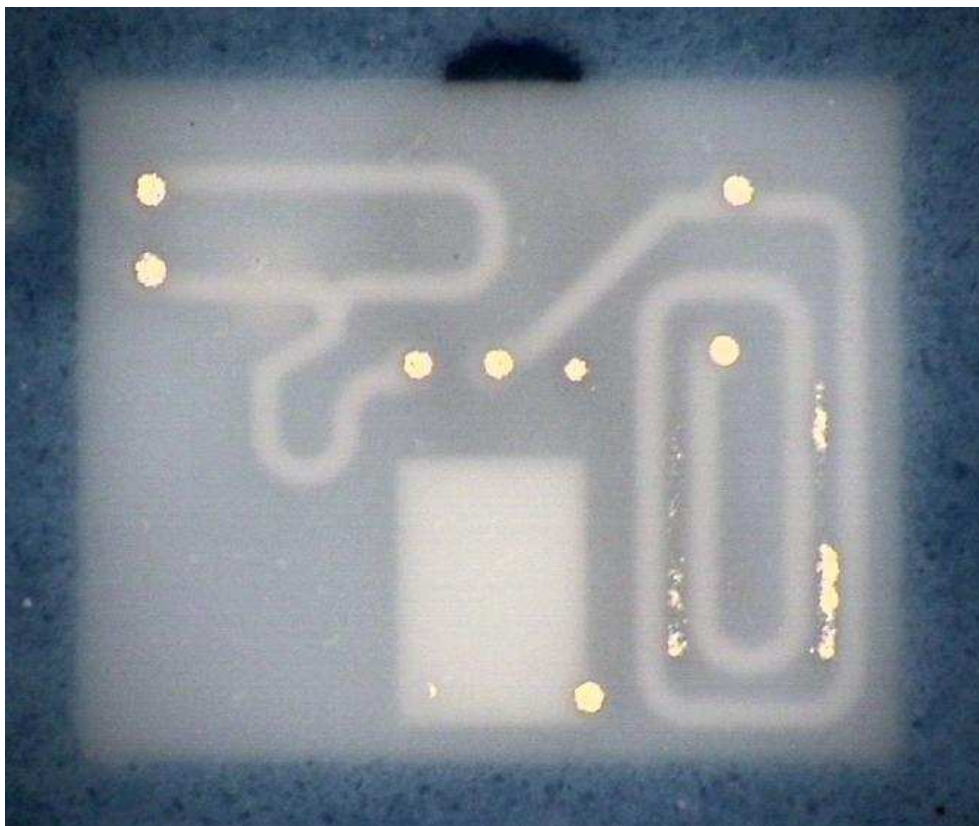
Figure A.2.1: LTCC components – sintered und cut LTCC panel



a) Perspective view



b) Side cut plane

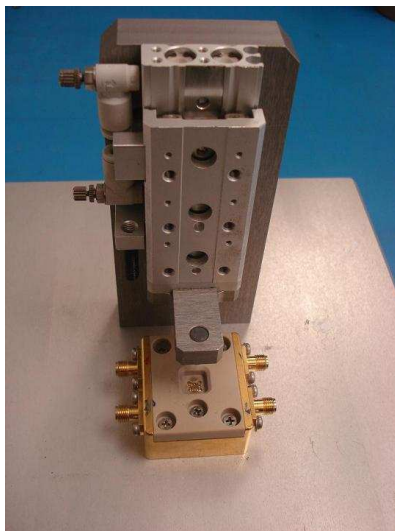


c) Top cut plane

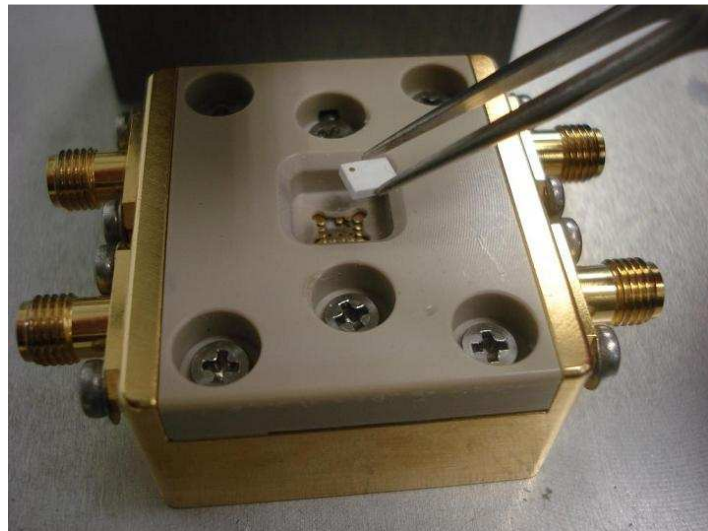
Figure A.2.2: LTCC components

Appendix A.3: Measurements

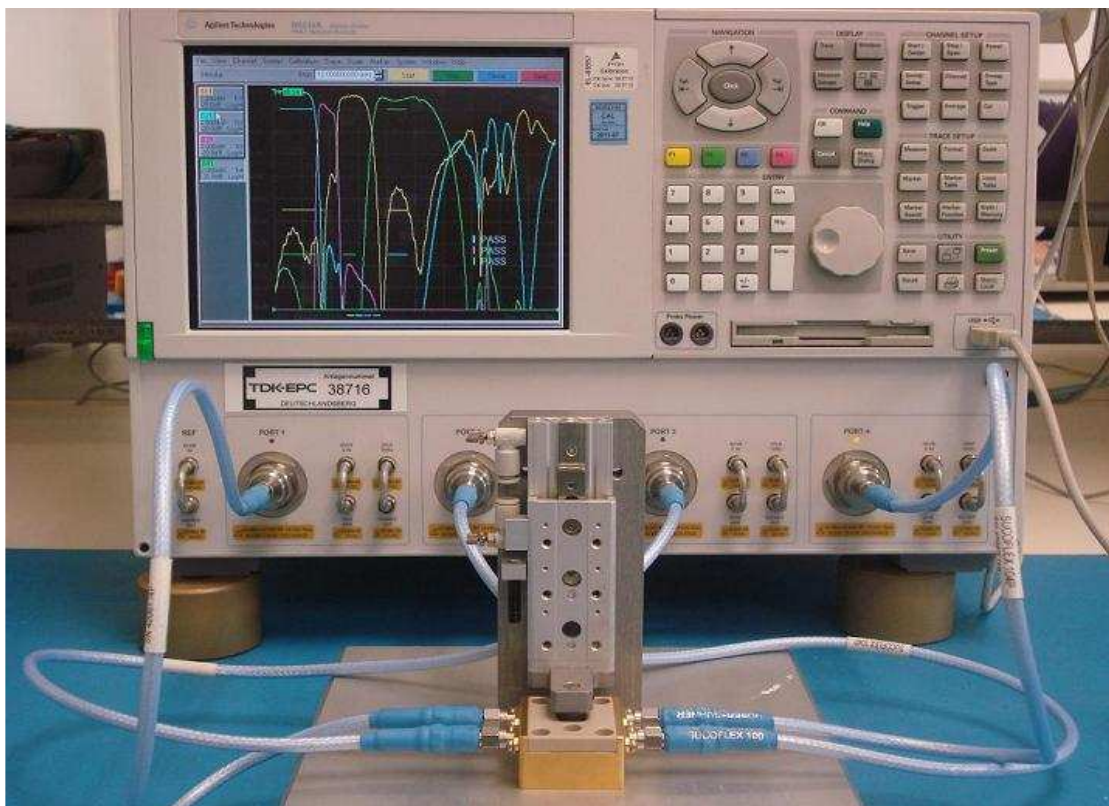
Measurements of LTCC components could be done either using a test jig (Fig. A. 3.1) or PCB (Fig. A. 3.2). The first measurement procedure is used in case of quick and mass measurements, while the second one is more precise and used for verification of the components.



a) Press machine

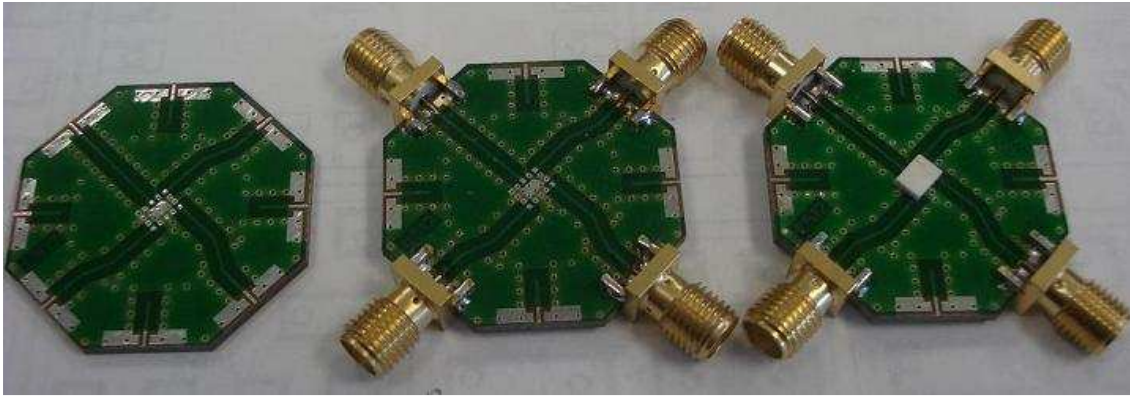


b) Test jig

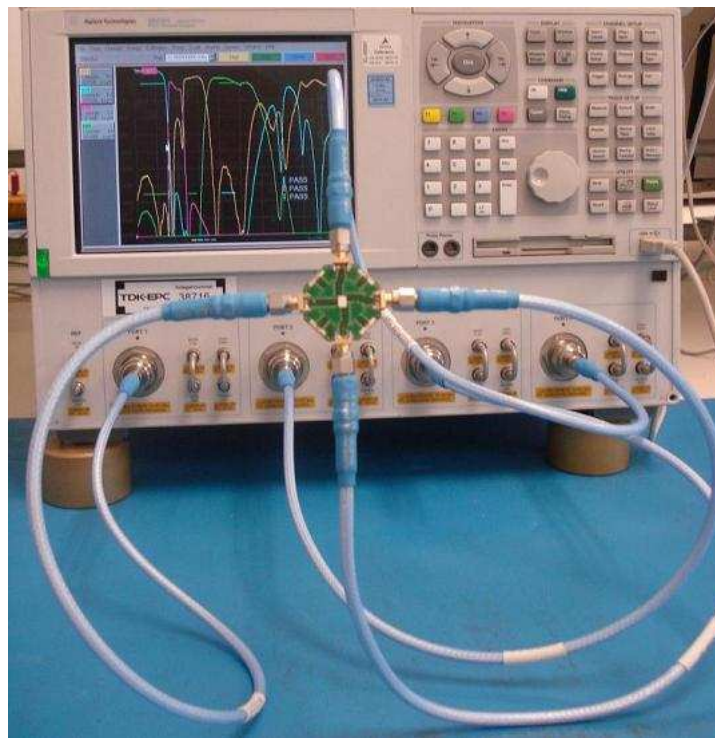


c) Measurement equipment

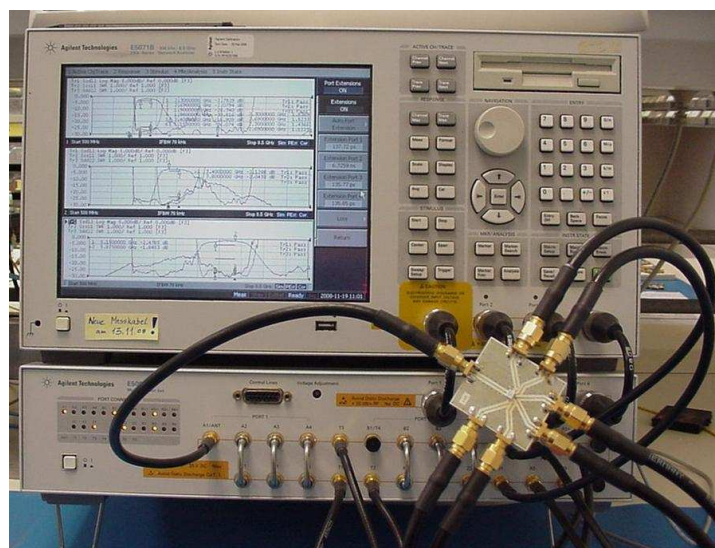
Figure A.3.1: Measurement of a component using test jig



a) PCBs



b) Single-ended triplexer



c) Balanced triplexer

Figure A.3.2: Measurements of components using PCB

Appendix B: S-parameters for the Power Divider

This appendix contains calculations of the basement S-parameters for the power divider shown in Fig. 4.2. The basement consists of two series connected quarter-wave broadside-coupled striplines (couplers). The calculations are based on S-parameters of the single quarter-wave coupler. Taking into account connection method of the couplers inside the basement and considering the scattering parameters like a relation between reflected and incident waves, the calculation can be carried out as it's shown below. S-parameters of the quarter-wave coupler are:

$$[S]_{\lambda/4 \text{ Coupler}} = \begin{bmatrix} 0 & -j\sqrt{1-k^2} & k & 0 \\ -j\sqrt{1-k^2} & 0 & 0 & k \\ k & 0 & 0 & -j\sqrt{1-k^2} \\ 0 & k & -j\sqrt{1-k^2} & 0 \end{bmatrix} \quad (\text{B-1})$$

Relationships between the incident and reflected waves for the splitter basement and the coupler are given like the following:

$$\begin{cases} b_1 = a_1 S_{11}^{\text{bPD}} + a_3 S_{12}^{\text{bPD}} + a_8 S_{13}^{\text{bPD}} \\ b_3 = a_1 S_{21}^{\text{bPD}} + a_3 S_{22}^{\text{bPD}} + a_8 S_{33}^{\text{bPD}} \\ b_8 = a_1 S_{31}^{\text{bPD}} + a_3 S_{32}^{\text{bPD}} + a_8 S_{33}^{\text{bPD}} \end{cases} \quad (\text{B-2})$$

$$\begin{cases} b_1 = a_1 S_{11}^{\text{C}} + a_2 S_{12}^{\text{C}} + a_3 S_{13}^{\text{C}} + a_4 S_{14}^{\text{C}} \\ b_2 = a_1 S_{21}^{\text{C}} + a_2 S_{22}^{\text{C}} + a_3 S_{23}^{\text{C}} + a_4 S_{24}^{\text{C}} \\ b_3 = a_1 S_{31}^{\text{C}} + a_2 S_{32}^{\text{C}} + a_3 S_{33}^{\text{C}} + a_4 S_{34}^{\text{C}} \\ b_4 = a_1 S_{41}^{\text{C}} + a_2 S_{42}^{\text{C}} + a_3 S_{43}^{\text{C}} + a_4 S_{44}^{\text{C}} \\ b_5 = a_5 S_{11}^{\text{C}} + a_6 S_{12}^{\text{C}} + a_7 S_{13}^{\text{C}} + a_8 S_{14}^{\text{C}} \\ b_6 = a_5 S_{21}^{\text{C}} + a_6 S_{22}^{\text{C}} + a_7 S_{23}^{\text{C}} + a_8 S_{24}^{\text{C}} \\ b_7 = a_5 S_{31}^{\text{C}} + a_6 S_{32}^{\text{C}} + a_7 S_{33}^{\text{C}} + a_8 S_{34}^{\text{C}} \\ b_8 = a_5 S_{41}^{\text{C}} + a_6 S_{42}^{\text{C}} + a_7 S_{43}^{\text{C}} + a_8 S_{44}^{\text{C}} \end{cases} \quad (\text{B-3})$$

So, the task is to find the unknown coefficients a_i, b_i from (B-3) and by putting those into (B-2) to get desired S-parameters matrix of the basement for the power divider.

Considering schematic of the basement network (Fig. 4.2) the following relationships are derived:

$$\begin{cases} a_2 = b_5 \\ a_4 = -b_4 \\ a_5 = b_2 \\ a_6 = -b_6 \\ a_7 = -b_7 \end{cases} \quad (\text{B-4})$$

Therefore the equations (B-3) became simpler view:

$$\begin{cases} b_1 = a_1 S_{11}^C + b_5 S_{12}^C + a_3 S_{13}^C - b_4 S_{14}^C \\ b_2 = a_1 S_{21}^C + b_5 S_{22}^C + a_3 S_{23}^C - b_4 S_{24}^C \\ b_3 = a_1 S_{31}^C + b_5 S_{32}^C + a_3 S_{33}^C - b_4 S_{34}^C \\ b_4 = a_1 S_{41}^C + b_5 S_{42}^C + a_3 S_{43}^C - b_4 S_{44}^C \\ b_5 = b_2 S_{11}^C - b_6 S_{12}^C - b_7 S_{13}^C + a_8 S_{14}^C \\ b_6 = b_2 S_{21}^C - b_6 S_{22}^C - b_7 S_{23}^C + a_8 S_{24}^C \\ b_7 = b_2 S_{31}^C - b_6 S_{32}^C - b_7 S_{33}^C + a_8 S_{34}^C \\ b_8 = b_2 S_{41}^C - b_6 S_{42}^C - b_7 S_{43}^C + a_8 S_{44}^C \end{cases} \quad (\text{B-5})$$

By substituting the scattering parameters from (B-1) into (B-5), we achieve the following equation system:

$$\begin{cases} b_1 = -jb_5 \sqrt{1-k^2} + a_3 k \\ b_2 = -ja_1 \sqrt{1-k^2} - b_4 k \\ b_3 = a_1 k + jb_4 \sqrt{1-k^2} \\ b_4 = b_5 k - ja_3 \sqrt{1-k^2} \\ b_5 = jb_6 \sqrt{1-k^2} - b_7 k \\ b_6 = -jb_2 \sqrt{1-k^2} + a_8 k \\ b_7 = b_2 k - ja_8 \sqrt{1-k^2} \\ b_8 = -b_6 k + jb_7 \sqrt{1-k^2} \end{cases} \quad (\text{B-6})$$

To get the final solution the next steps using substitutions were done:

1) b_6 and $b_7 \rightarrow$ in b_5 :

$$b_5 = b_2(1-2k^2) + 2ja_8 k \sqrt{1-k^2} \quad (\text{B-7})$$

$b_4 \rightarrow$ in b_2 :

$$b_2 = -ja_1 \sqrt{1-k^2} - b_5 k^2 + ja_3 k \sqrt{1-k^2} \quad (\text{B-8})$$

$b_2 \rightarrow$ in b_5 :

$$b_5 = \frac{1}{1+k^2(1-2k^2)} [j\sqrt{1-k^2}(a_3 k - a_1) + 2ja_8 k \sqrt{1-k^2}] \quad (\text{B-9})$$

$b_5 \rightarrow$ in b_1 :

$$b_1 = a_1 \frac{2k^2-1}{1+2k^2} + a_3 \frac{2k}{1+2k^2} + a_8 \frac{2k}{1+2k^2} \quad (\text{B-10})$$

2) $b_5 \rightarrow$ in b_4 :

$$b_4 = a_1 \frac{jk\sqrt{1-k^2}(1-2k^2)}{-1-k^2+2k^4} + a_3 \frac{j\sqrt{1-k^2}}{-1-k^2+2k^4} - a_8 \frac{2jk^2\sqrt{1-k^2}}{-1-k^2+2k^4} \quad (\text{B-11})$$

$b_4 \rightarrow$ in b_3 :

$$b_3 = a_1 \frac{2k}{1+2k^2} + a_3 \frac{1}{1+2k^2} - a_8 \frac{2k^2}{1+2k^2} \quad (\text{B-12})$$

3) $b_4 \rightarrow$ in b_2 :

$$b_4 = -a_1 \frac{j\sqrt{1-k^2}}{1+k^2-2k^4} + a_3 \frac{jk\sqrt{1-k^2}}{1+k^2-2k^4} - a_8 \frac{2jk^3\sqrt{1-k^2}}{1+k^2-2k^4} \quad (\text{B-13})$$

$b_2 \rightarrow$ in b_6 and b_7 :

$$b_6 = -a_1 \frac{1-k^2}{1+k^2-2k^4} + a_3 \frac{k(1-k^2)}{1+k^2-2k^4} + a_8 \frac{-2k^3(1-k^2) + k(1+k^2-2k^4)}{1+k^2-2k^4} \quad (\text{B-14})$$

$$b_7 = -a_1 \frac{jk\sqrt{1-k^2}}{1+k^2-2k^4} + a_3 \frac{jk^2\sqrt{1-k^2}}{1+k^2-2k^4} - a_8 \frac{j\sqrt{1-k^2}(1-k^2)}{1+k^2-2k^4} \quad (\text{B-15})$$

b_6 and $b_7 \rightarrow$ in b_8 :

$$b_8 = a_1 \frac{2k}{1+2k^2} - a_3 \frac{2k^2}{1+2k^2} + a_8 \frac{1}{1+2k^2} \quad (\text{B-16})$$

Now we've got the relationships (B-10), (B-12) and (B-16) that can be substituted into (B-2). Afterwards the S-parameter matrix of the basement for the power divider is achieved and looks like following:

$$[S]_{\text{bPD}} = \frac{1}{1+2k^2} \begin{bmatrix} 2k^2-1 & 2k & 2k \\ 2k & 1 & -2k^2 \\ 2k & -2k^2 & 1 \end{bmatrix} \quad (\text{B-17})$$

Appendix C: S-parameters for the Multiplexing Circuit

Calculations of S-parameters of a basement for the multiplexing circuit shown in Fig. 5.5 are provided in this appendix. The basement consists of two series connected quarter-wave broadside coupled striplines (couplers). The calculations are based on S-parameters of the single quarter-wave coupler and relations between reflected and incident waves, like in case of the power divider. There is only one difference - connection method of the couplers. S-parameters of the quarter-wave coupler are given in appendix B (B-1). Relationships between the incident and reflected waves for the basement and the couplers are given below:

$$\begin{cases} b_1 = a_1 S_{11}^{bM} + a_4 S_{12}^{bM} + a_7 S_{13}^{bM} \\ b_4 = a_1 S_{21}^{bM} + a_4 S_{22}^{bM} + a_7 S_{33}^{bM} \\ b_7 = a_1 S_{31}^{bM} + a_4 S_{32}^{bM} + a_7 S_{33}^{bM} \end{cases} \quad (C-1)$$

$$\begin{cases} b_1 = a_1 S_{11}^C + a_2 S_{12}^C + a_3 S_{13}^C + a_4 S_{14}^C \\ b_2 = a_1 S_{21}^C + a_2 S_{22}^C + a_3 S_{23}^C + a_4 S_{24}^C \\ b_3 = a_1 S_{31}^C + a_2 S_{32}^C + a_3 S_{33}^C + a_4 S_{34}^C \\ b_4 = a_1 S_{41}^C + a_2 S_{42}^C + a_3 S_{43}^C + a_4 S_{44}^C \\ b_5 = a_5 S_{11}^C + a_6 S_{12}^C + a_7 S_{13}^C + a_8 S_{14}^C \\ b_6 = a_5 S_{21}^C + a_6 S_{22}^C + a_7 S_{23}^C + a_8 S_{24}^C \\ b_7 = a_5 S_{31}^C + a_6 S_{32}^C + a_7 S_{33}^C + a_8 S_{34}^C \\ b_8 = a_5 S_{41}^C + a_6 S_{42}^C + a_7 S_{43}^C + a_8 S_{44}^C \end{cases} \quad (C-2)$$

A general S-parameters model of the basemen for the new multiplexer can achieved from the coupler's parameters, assuming interconnection properties, where:

$$\begin{cases} a_2 = b_5 \\ a_3 = -b_3 \\ a_5 = b_2 \\ a_6 = b_6 \\ a_8 = -b_8 \end{cases} \quad (C-3)$$

Assuming (C-3), the equations (C-2) can be transformed into the following one:

$$\begin{cases} b_1 = a_1 S_{11}^C + b_5 S_{12}^C - b_3 S_{13}^C + a_4 S_{14}^C \\ b_2 = a_1 S_{21}^C + b_5 S_{22}^C - b_3 S_{23}^C + a_4 S_{24}^C \\ b_3 = a_1 S_{31}^C + b_5 S_{32}^C - b_3 S_{33}^C + a_4 S_{34}^C \\ b_4 = a_1 S_{41}^C + b_5 S_{42}^C - b_3 S_{43}^C + a_4 S_{44}^C \\ b_5 = b_2 S_{11}^C + b_6 S_{12}^C + a_7 S_{13}^C - b_8 S_{14}^C \\ b_6 = b_2 S_{21}^C + b_6 S_{22}^C + a_7 S_{23}^C - b_8 S_{24}^C \\ b_7 = b_2 S_{31}^C + b_6 S_{32}^C + a_7 S_{33}^C - b_8 S_{34}^C \\ b_8 = b_2 S_{41}^C + b_6 S_{42}^C + a_7 S_{43}^C - b_8 S_{44}^C \end{cases} \quad (C-4)$$

After substituting scattering parameters of the coupler from (B-1) into (C-4):

$$\begin{cases} b_1 = -jb_5\sqrt{1-k^2} - b_3k \\ b_2 = -ja_1\sqrt{1-k^2} + a_4k \\ b_3 = a_1k - ja_4\sqrt{1-k^2} \\ b_4 = b_5k + jb_3\sqrt{1-k^2} \\ b_5 = -jb_6\sqrt{1-k^2} + a_7k \\ b_6 = -jb_2\sqrt{1-k^2} - b_8k \\ b_7 = b_2k + jb_8\sqrt{1-k^2} \\ b_8 = b_6k - ja_7\sqrt{1-k^2} \end{cases} \quad (C-5)$$

To get final solution the next steps using the substitutions were done:

1) $b_2 \rightarrow$ in b_6 :

$$b_6 = -a_1(1-k^2) - ja_4k\sqrt{1-k^2} - b_8k \quad (C-6)$$

$b_6 \rightarrow$ in b_8 :

$$b_8 = -a_1 \frac{k(1-k^2)}{1+k^2} - a_4 \frac{jk^2\sqrt{1-k^2}}{1+k^2} - a_7 \frac{j\sqrt{1-k^2}}{1+k^2} \quad (C-7)$$

b_2 and $b_8 \rightarrow$ in b_7 :

$$b_7 = -a_1 \frac{2jk\sqrt{1-k^2}}{1+k^2} + a_4 \frac{2k^2}{1+k^2} + a_7 \frac{1-k^2}{1+k^2} \quad (C-8)$$

2) $b_8 \rightarrow$ in b_6 :

$$b_6 = -a_1 \frac{1-k^2}{1+k^2} - a_4 \frac{jk\sqrt{1-k^2}}{1+k^2} + a_7 \frac{jk\sqrt{1-k^2}}{1+k^2} \quad (C-9)$$

$b_6 \rightarrow$ in b_5 :

$$b_5 = a_1 \frac{j\sqrt{1-k^2}(1-k^2)}{1+k^2} - a_4 \frac{k(1-k^2)}{1+k^2} + a_7 \frac{2k}{1+k^2} \quad (C-10)$$

b_3 and $b_5 \rightarrow$ in b_1 :

$$b_1 = a_1 \frac{1-3k^2}{1+k^2} + a_4 \frac{2jk\sqrt{1-k^2}}{1+k^2} - a_7 \frac{2jk\sqrt{1-k^2}}{1+k^2} \quad (C-11)$$

3) $b_5 \rightarrow$ in b_4 :

$$b_4 = a_1 \frac{2jk\sqrt{1-k^2}}{1+k^2} + a_4 \frac{1-k^2}{1+k^2} + a_7 \frac{2k^2}{1+k^2} \quad (C-12)$$

Now, S-parameters matrix of the basement proceeds from the relations calculated above between b_1, b_4, b_7 and a_1, a_4, a_7 . It looks like the following:

$$[S]_{bM} = \frac{1}{1+k^2} \begin{bmatrix} 1-3k^2 & 2jk\sqrt{1-k^2} & -2jk\sqrt{1-k^2} \\ 2jk\sqrt{1-k^2} & 1-k^2 & 2k^2 \\ -2jk\sqrt{1-k^2} & 2k^2 & 1-k^2 \end{bmatrix} \quad (C-13)$$

Appendix D: Broadside-Coupled Striplines

A broadside-coupled striplines are used both in power divider and in multiplexing circuit designs. Optimal values for even- and odd-mode line impedances calculated for both designs have to be implemented in real multilayer structure. It means that these values must be transform into geometric parameters of the coupled lines. Taking into account the design rules restrictions applied to designed LTCC components, an optimization procedure executed in chapter 5.4.1 has to be done in order to find the best compatible geometric solution. Some intermediate results are shown in this appendix, like even- and odd-mode impedances, the coupling factor and the characteristic impedance of the coupled striplines vs. geometrical parameters. The presented calculations are done for the coupled stripline configuration shown in Fig. 5.9.

Appendix D.1: Absolute Relations

In this part of the appendix, the graphs show relations between the broadside-coupled stripline parameters and absolute values s , b (from Fig. 5.9).

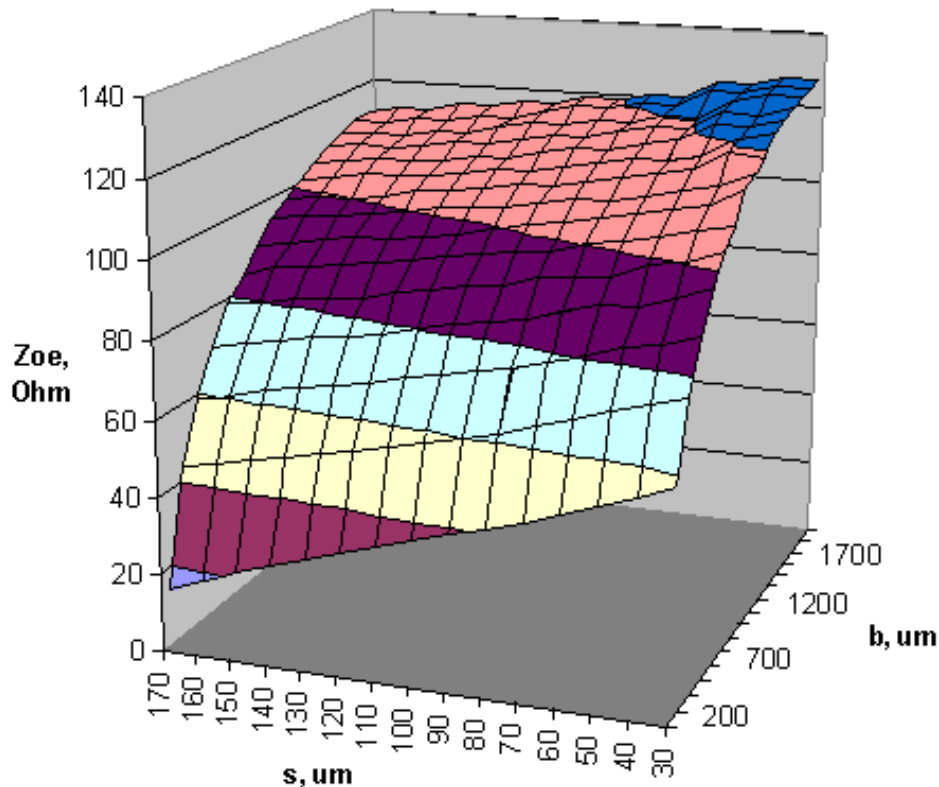


Figure D.1.1: Even-mode impedance of the coupled striplines

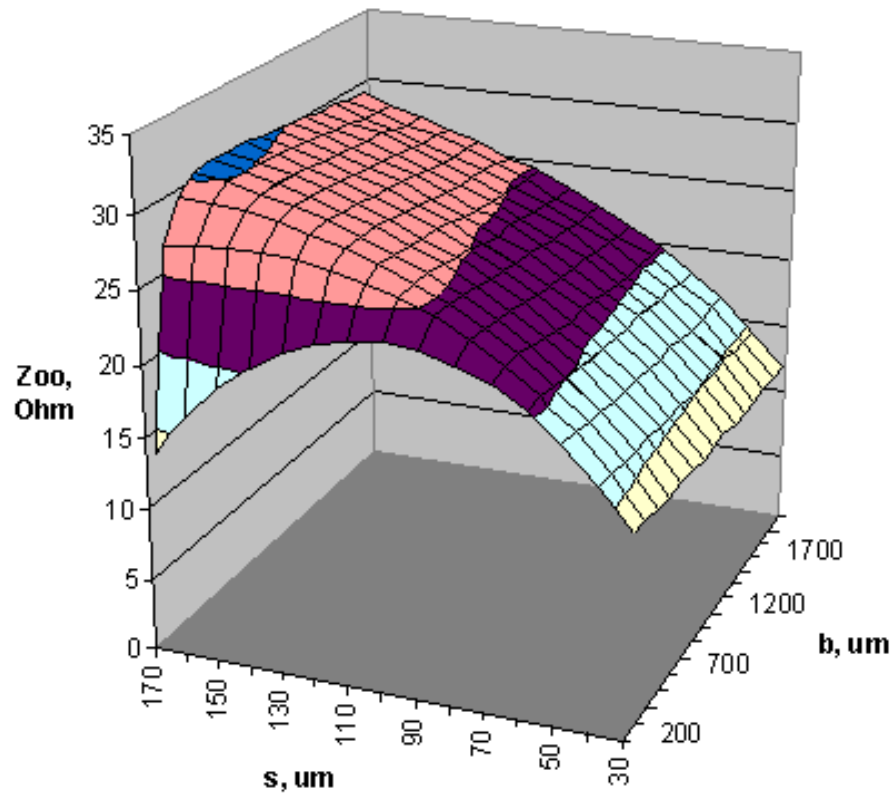


Figure D.1.2: Odd-mode impedance of the coupled striplines

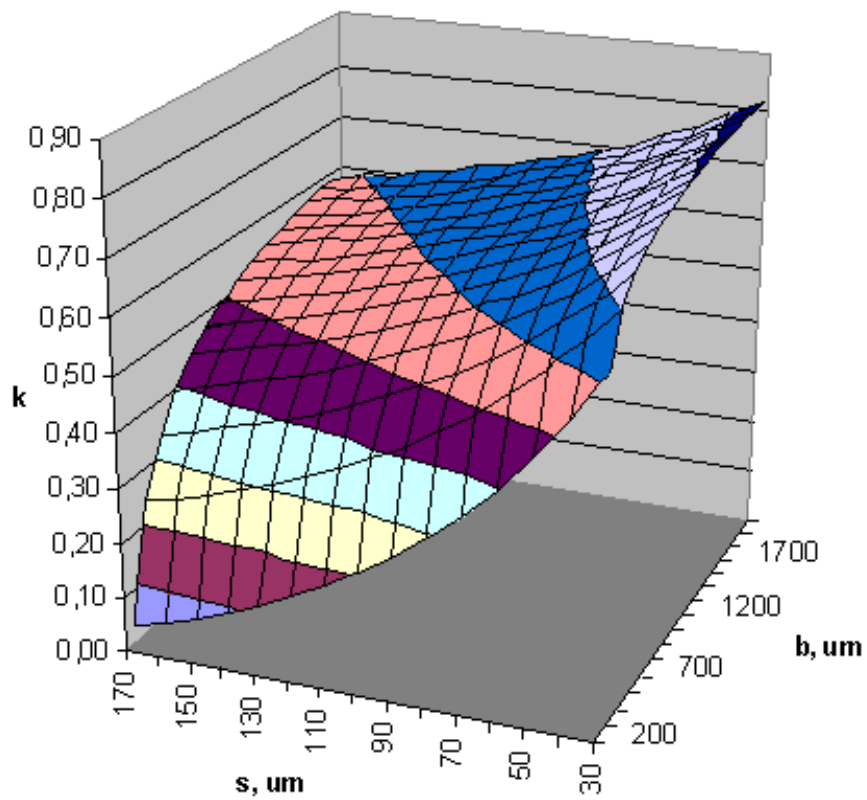


Figure D.1.3: Coupling factor of the coupled striplines

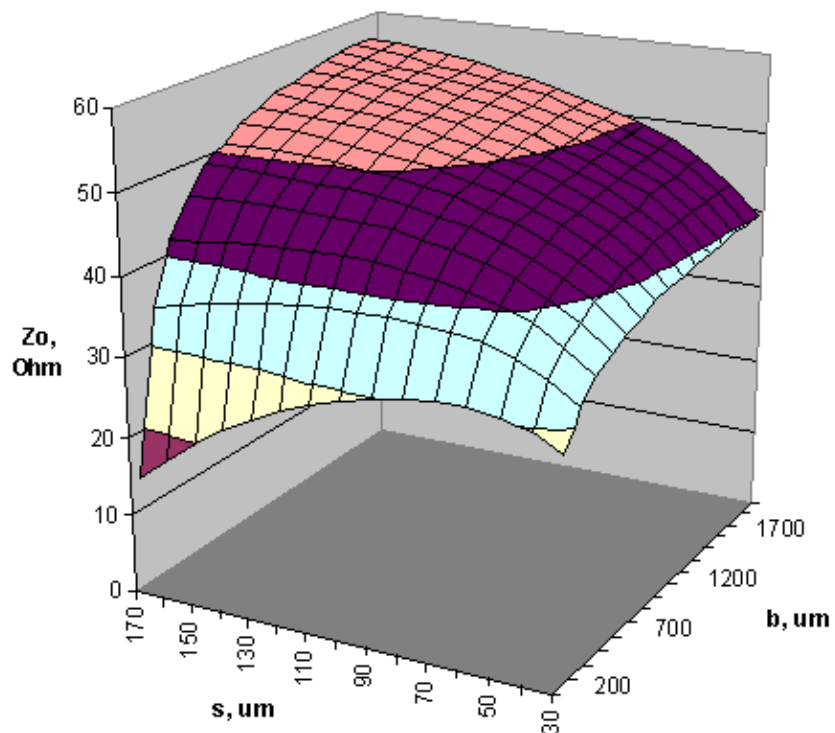


Figure D.1.4: Characteristic impedance of the coupled striplines

Appendix D.2: Relative Relations

This second part of the appendix contains the graphs, which show relations between the broadside-coupled stripline parameters and relative values s/w , b/w (from Fig. 5.9).

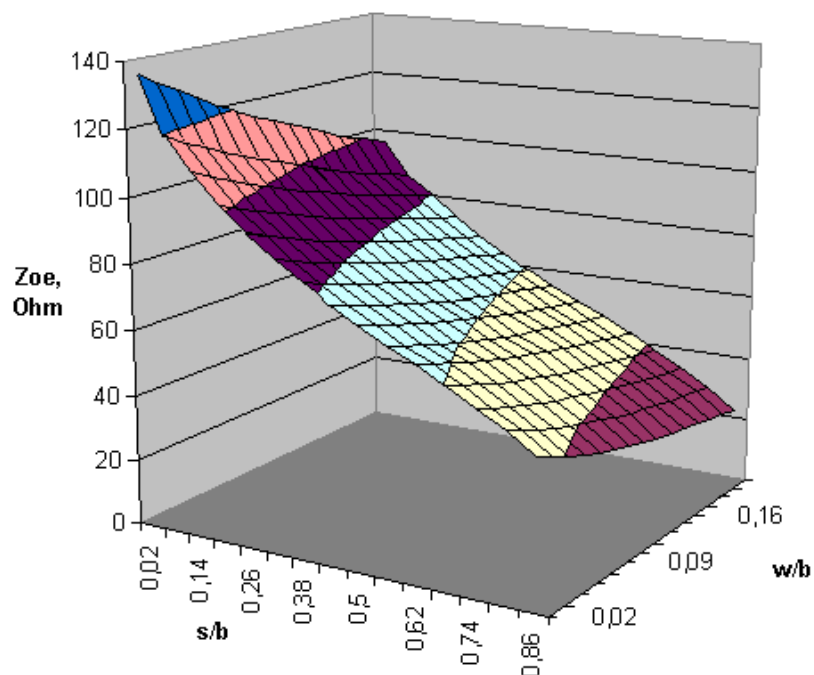


Figure D.2.1: Even-mode impedance of the coupled striplines

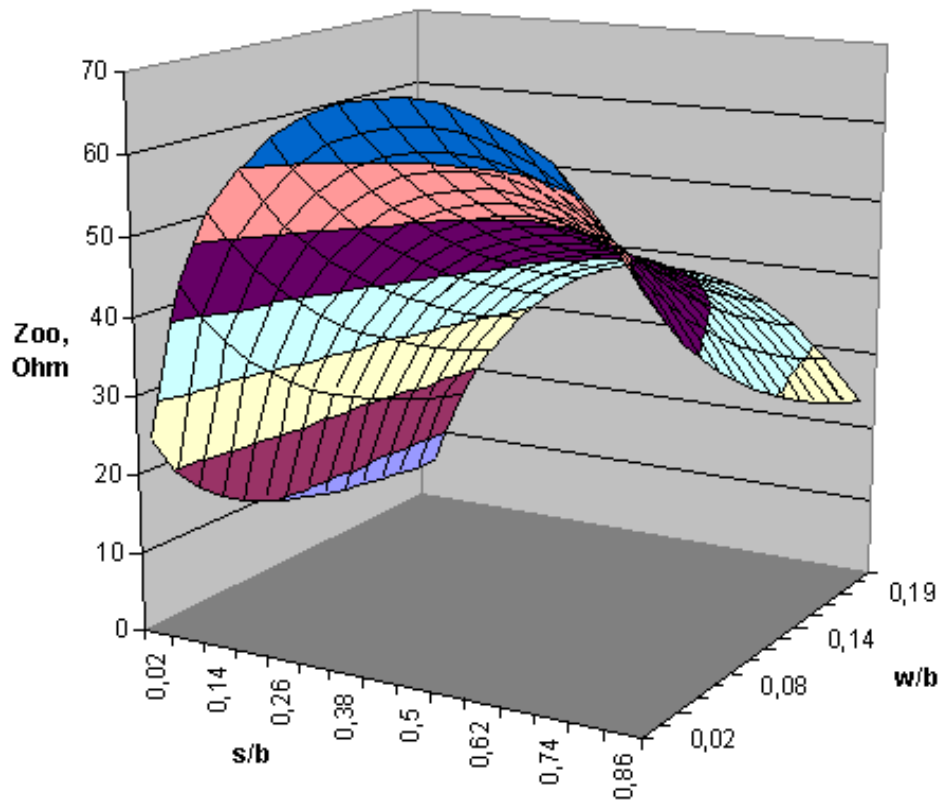


Figure D.2.2: Odd-mode impedance of the coupled striplines

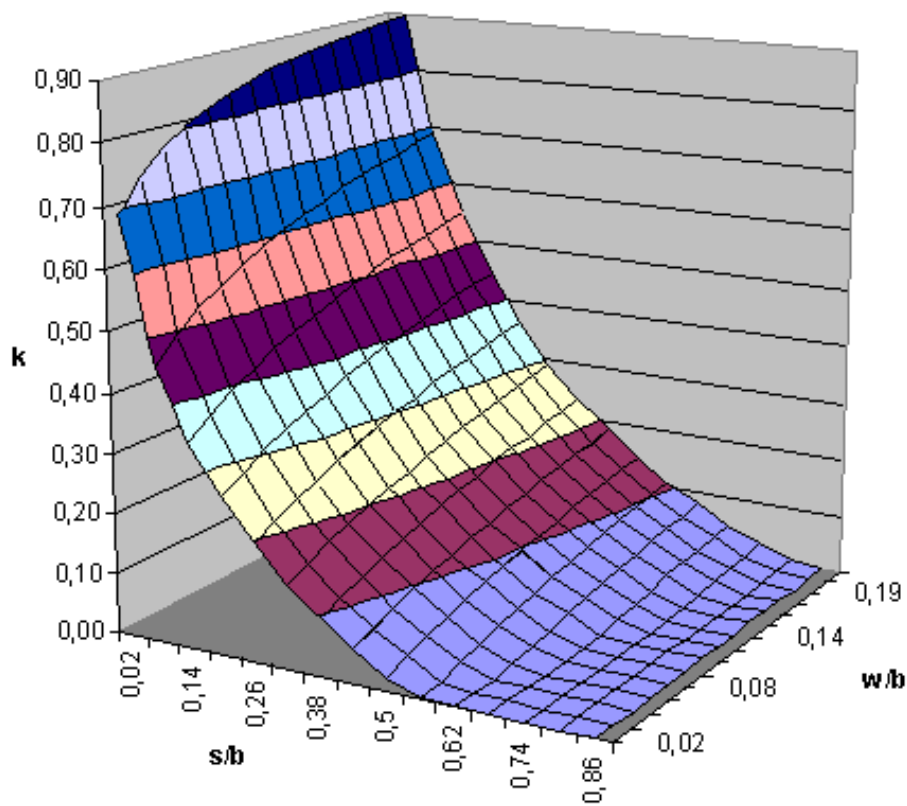


Figure D.2.3: Coupling coefficient of the coupled striplines

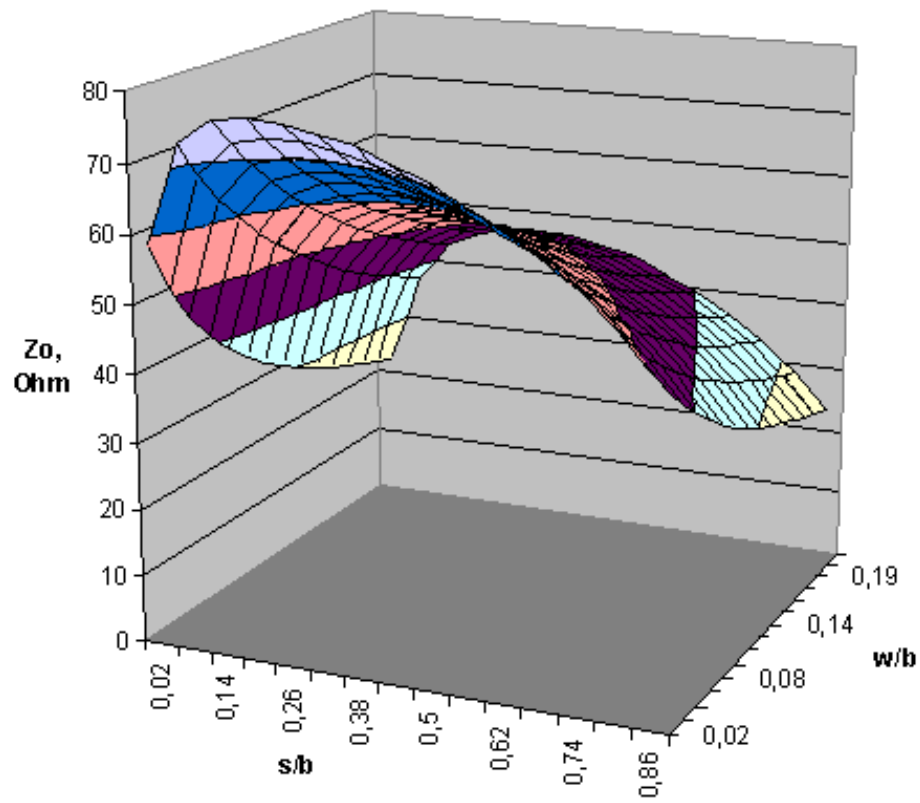


Figure D.2.4: Characteristic impedance of the coupled striplines.